AD_____

Award Number: DAMD17-01-1-0689

TITLE: The BESCT Lung Cancer Program (Biology, Education, Screening, Chemoprevention, and Treatment)

PRINCIPAL INVESTIGATOR: Waun Ki Hong, M.D.
Fadlo R. Khuri, M.D.

CONTRACTING ORGANIZATION: The University of Texas
M.D. Anderson Cancer Center
Houston, TX 77030

REPORT DATE: March 2005

TYPE OF REPORT: Annual

PREPARED FOR: U.S. Army Medical Research and Materiel Command
Fort Detrick, Maryland 21702-5012

DISTRIBUTION STATEMENT: Approved for Public Release;
Distribution Unlimited

The views, opinions and/or findings contained in this report are those of the author(s) and should not be construed as an official Department of the Army position, policy or decision unless so designated by other documentation.

20060525046

REPORT DOCUMENTATION PAGE

Form Approved
OMB No. 074-0188

Public reporting burden for this collection of information is estimated to average 1 hour per response, including the time for reviewing instructions, searching existing data sources, gathering and maintaining the data needed, and completing and reviewing this collection of information. Send comments regarding this burden estimate or any other aspect of this collection of information, including suggestions for reducing this burden to Washington Headquarters Services, Directorate for Information Operations and Reports, 1215 Jefferson Davis Highway, Suite 1204, Arlington, VA 22202-4302, and to the Office of Management and Budget, Paperwork Reduction Project (0704-0188), Washington, DC 20503

1. AGENCY USE ONLY	2. REPORT DATE	3. REPORT TYPE AND DATES COVERED
	March 2005	Annual (16 Feb 2004 - 15 Feb 2005)

4. TITLE AND SUBTITLE
The BESCT Lung Cancer Program (Biology, Education, Screening, Chemoprevention, and Treatment)

5. FUNDING NUMBERS
DAMD17-01-1-0689

6. AUTHOR(S)
Waun Ki Hong, M.D.
Fadlo R. Khuri, M.D.

7. PERFORMING ORGANIZATION NAME(S) AND ADDRESS(ES)
The University of Texas
M.D. Anderson Cancer Center
Houston, TX 77030

E-Mail: whong@mdanderson.org

8. PERFORMING ORGANIZATION REPORT NUMBER

9. SPONSORING / MONITORING AGENCY NAME(S) AND ADDRESS(ES)
U.S. Army Medical Research and Materiel Command
Fort Detrick, Maryland 21702-5012

10. SPONSORING / MONITORING AGENCY REPORT NUMBER

11. SUPPLEMENTARY NOTES

12a. DISTRIBUTION / AVAILABILITY STATEMENT
Approved for Public Release; Distribution Unlimited

12b. DISTRIBUTION CODE

13. ABSTRACT (Maximum 200 Words)

Our long-term objectives are to define the molecular processes contributing to lung cancer development and progression to recognize genetic and phenotypic changes early enough to be reversed with molecular targeted therapy and to develop innovative therapeutic approaches to lung cancer. Thus, the specific aims are to understand molecular alterations, develop prevention strategies, and implement experimental molecular approaches to lung cancer. In the past year, we identified that hypermethylation of $p16^{INK4a}$ and *RASSF1A* was associated with clinical outcomes in patients with respectable NSCLC; hypermethylated DAP kinase attenuated TRAIL-induced apoptosis of NSCLC cells; tumor-dominant *DNMT3B* variants was strongly associated with methylation status of $p16^{INK4a}$ and *RASSF1A*, and clinical outcomes. Also growth inhibition and apoptosis induction by the combination of Celecoxib and 4HPR were mediated by both activated mitochondrial apoptosis pathway and inhibited PI3K/Akt survival pathway. We demonstrated that SCH66336 inhibited angiogenic activities of NSCLC and HNSCC cells partly by inhibiting hypoxia- or IGF-stimulated HIF-1a and thus VEGF production *via* blocking the interaction HIF-1 and Hsp90 and inducing proteasomal degradation of HIF-1. Moreover, a mouse lung cancer model that develops lung carcinomas has been successfully developed and will be used for various studies including drug test and mechanistic studies of lung carcinogenesis.

14. SUBJECT TERMS
Lung cancer, genetic alterations, chemoprevention, molecular therapy

15. NUMBER OF PAGES
172

16. PRICE CODE

17. SECURITY CLASSIFICATION OF REPORT	18. SECURITY CLASSIFICATION OF THIS PAGE	19. SECURITY CLASSIFICATION OF ABSTRACT	20. LIMITATION OF ABSTRACT
Unclassified	Unclassified	Unclassified	Unlimited

TABLE OF CONTENTS

COVER....1

SF 298....2

INTRODUCTION....4

PROGRESS REPORT....4

Project 1....4

Project 2....12

Project 3....15

KEY RESEARCH ACCOMPLISHMENTS....20

REPORTABLE OUTCOMES....21

CONCLUSIONS....23

DEVELOPMENTAL RESEARCH PROGRAM....23

APPENDIX....26

Journal Articles

Best Available Copy

INTRODUCTION

Lung cancer is a devastating worldwide public health hazard. Advances in surgery, radiation therapy, and chemotherapy of non-small cell lung cancer (NSCLC) have only led to a marginal improvement in five-year survival. To reduce lung cancer incidence and mortality, it is imperative to develop effective therapeutic and preventive strategies targeting smokers and lung cancer patients. Our long-term objectives are to define the molecular processes contributing to lung cancer development and progression in order to recognize genetic and phenotypic changes early enough to be reversed with molecular targeted therapy and to develop innovative therapeutic approaches to lung cancer. The objectives can be achieved only by understanding the biology of lung cancer through molecular studies and preclinical experimental molecular therapeutic research. Therefore, the specific goals of this program are to understand molecular alterations in lung cancer, develop lung cancer prevention strategies, and implement experimental molecular approaches to lung cancer.

PROGRESS REPORT

Project 1: Mechanisms of Molecular Alterations in Lung Cancer

(Project Leader: Li Mao, M.D.)

Specific Aim 1 ***To determine the mRNA complex responsible for C-CAM1 splicing and identify factor(s) regulating exon 7 splicing.***

We have shown differential patterns of hnRNP proteins between cells with distinct *CEACAM1* splicing patterns. In light of this finding, we have developed Specific Aim 5 to determine hnRNP variants in these tumor cells and their role in regulating *CEACAM1* splicing.

Specific Aim 2 ***To determine function of identified splicing factor(s) in regulation of CEACAM1 and its potential alterations in lung cancer***

We have identified PTB and shown that it can regulate splicing of *CEACMA1* by increasing the short form *CEACAM1*. We also show that PTB expression was increased in most of primary lung tumors that exhibited predominant short form *CEACAM1* when compared with matched normal lung tissues. A manuscript is in the final stage of preparation for publication.

Specific Aim 3 ***To determine function of DNA methyltransferases and their role in controlling methylation and expression of critical tumor suppressor genes and tumor antigen genes.***

- We have shown that promoter hypermethylation in $p16^{INK4a}$ and *RASSF1A* tumor suppressor genes is frequently and strongly associated with clinical outcomes in patients with resectable non-small cell lung cancer. This study has been published in *Clinical Cancer Research*, 2004 (Wang J et al, *Clinical Cancer Research* 10:6119-25, 2004).

- We have demonstrated that hypermethylation of the death-associated protein kinase promoter attenuates the sensitivity of human NSCLC cells to TRAIL-induced apoptosis.

Death-associated protein (DAP) kinase plays an important role in IFN-gamma, tumor necrosis factor (TNF)-alpha, or Fas-ligand induced apoptosis. TNF-related apoptosis-inducing ligand (TRAIL) is a member of the TNF ligand family and can induce caspase-dependent apoptosis in cancer cells while sparing most of the normal cells. However, some of the cancer cell lines are insensitive to TRAIL, and such resistance cannot be explained by the dysfunction of TRAIL

receptors or their known downstream targets. We reported previously that DAP kinase promoter is frequently methylated in non-small cell lung cancer (NSCLC), and such methylation is associated with a poor clinical outcome. To determine whether DAP kinase promoter methylation contributes to TRAIL resistance in NSCLC cells, we measured DAP kinase promoter methylation and its gene expression status in 11 NSCLC cell lines and correlated the methylation/expression status with the sensitivity of cells to TRAIL. Of the 11 cell lines, 1 had a completely methylated DAP kinase promoter and no detectable DAP kinase expression, 4 exhibited partial promoter methylation and substantially decreased gene expression, and the other 6 cell lines showed no methylation in the promoter and normal DAP kinase expression. Therefore, the amount of DAP kinase expression amount was negatively correlated to its promoter methylation ($r = -0.77$; $P = 0.003$). Interestingly, the cell lines without the DAP kinase promoter methylation underwent substantial apoptosis even in the low doses of TRAIL, whereas those with DAP kinase promoter methylation were resistant to the treatment. The resistance to TRAIL was reciprocally correlated to DAP kinase expression in 10 of the 11 cell lines at 10 ng/mL concentration ($r = 0.91$; $P = 0.001$). We treated cells resistant to TRAIL with 5-aza-2'-deoxycytidine, a demethylating reagent, and found that these cells expressed DAP kinase and became sensitive to TRAIL. These results suggest that DAP kinase is involved in TRAIL-mediated cell apoptosis and that a demethylating agent may have a role in enhancing TRAIL-mediated apoptosis in some NSCLC cells by reactivation of DAP kinase. (Tang X, et al. *Molecular Cancer Research*, 2:685-691, 2004)

Specific Aim 4 ***To determine expression profiles and abnormalities of DNMT3B isoforms in lung tumorigenesis and their association with de novo DNA methylation patterns, and clinical applications.***

- We have revealed that expression of ΔDNMT3B variants in non-small cell lung cancer is associated with patients' clinical outcomes

DNMT3B is important in regulation of *de novo* DNA methylation and often overexpressed in human cancers. However, an association between the overexpression and promoter DNA methylation status in cancers is weak. Recent studies have shown that DNMT3B consists of multiple variants due to alternative splicing. These variants may have distinct biological functions in the regulation of DNA methylation. In this study, we determined expression of seven splicing variants of DNMT3B in 119 primary non-small cell lung cancer (NSCLC) specimens and their corresponding non-malignant lung tissues using specific primer sets. We analyzed the association between the expression and patients' clinical parameters including survivals. We further analyzed an association between expression patterns of the variants and the promoter methylation status of the $p16^{INK4a}$ and *RASSF1A* in these tumors. We found that *DNMT3B* variants were detectable in 94 (80%) of the 119 NSCLC tumors and 22 (20%) of the corresponding non-malignant lung tissues ($P = 0.001$). *DNMT3B1*, *DNMT3B2*, and *DNMT3B4* were the most frequently detected transcripts in the tumor tissues (61%, 74%, and 45%, respectively) whereas *DNMT3B5, DNMT3B6,* and *DNMT3B7* were less frequent and only detectable in the tumor tissues. We observed strong association between expression of DNMT3B variants and promoter methylation of $p16^{INK4a}$ and *RASSF1A*, particularly *DNMT3B4* expression and *RASSF1A* ($P<0.0001$). The expression of any of the low frequent *DNMT3B* variants (*DNMT3B5-7*) was strongly associated with poor survivals in patients with stage I/II or stage IIIa disease (P values between 0.002 and 0.0003). In patients with stage IIIa disease, the expression of *DNMT3B4* was found strongly associated with poor overall, disease-free, and disease-specific survivals ($P<0.0001$, $P=0.0007$, and $P<0.0001$, respectively). These data suggest that *DNMT3B* variants are involved in differential regulation of promoter methylation in lung tumorigenesis and may serve as biomarkers in lung cancer early detection and molecular classification. (Accepted for presentation in 2005 Annual Meeting, American Society of Clinical Oncology).

- We have demonstrated that *ΔDNMT3B4* plays a critical role in cell-type-dependent promoter-specific DNA methylation in NSCLC

We designed a small interference RNA (siRNA) and an antisense RNA to specifically target the junction of exon 5 and exon 7 of *ΔDNMT3B*. Because both *ΔDNMT3B4* and *ΔDNMT3B2* lack exon 6 (Fig. **1A**), these strategies are expected to trigger degradation of both the *ΔDNMT3B4* and the *ΔDNMT3B2* transcripts. We used the NSCLC cell line H1299 in this experiment because it shows promoter methylation of both *p16* and *RASSF1A*, lacks *p16* and *RASSF1A* gene expression, and expresses a high level of *ΔDNMT3B4* but no detectable *DNMT3B* expression (**Fig. 1B and C**).

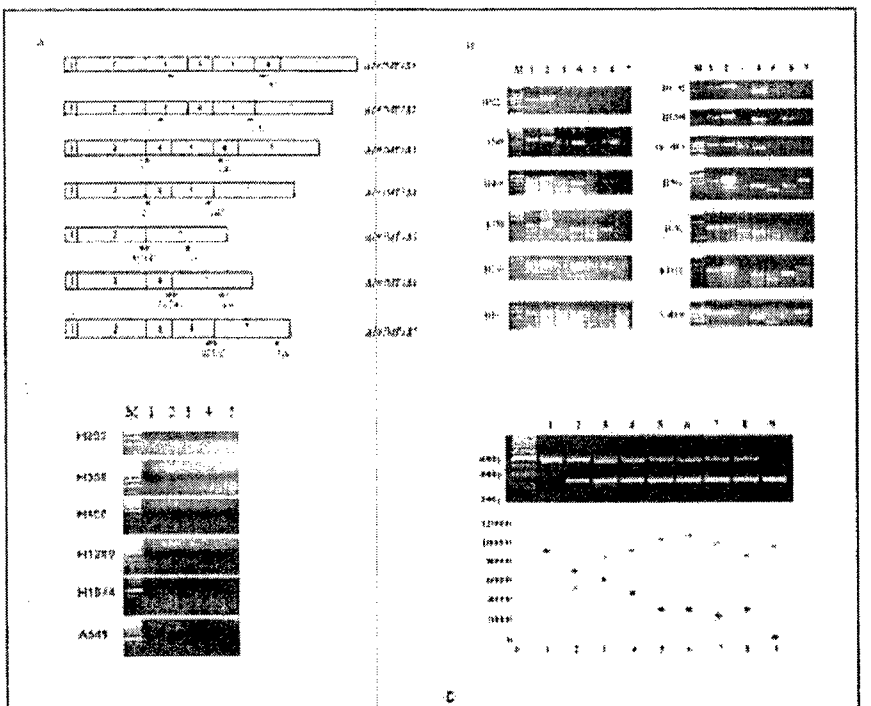


Fig. 1. Alternative or aberrant splicing variants of Δ*DNMT3B* subfamily. ***A***, Location of the primers used to amplify individual Δ*DNMT3B* variants in this study. ***B***, Expression patterns of Δ*DNMT3B* variants in NSCLC cell lines; 1–7 represent Δ*DNMT3B1–7*, respectively. ***C***, Expression patterns of *DNMT3B*s. with more proximal exons corresponding to *DNMT3B1–4* and Δ*DNMT3B6*. ***D***, Multiplex PCR using primer sets for *DNMT3B1* and Δ*DNMT3B1* with different ratios in concentration (concentration of *DNMT3B1* primer set was serially diluted from 1–9 and serially increased from 1–9; 1, *DNMT3B1* primer set alone; 9, Δ*DNMT3B1* primer set alone; 5, equal concentrations for both primer sets). The upper band represents the *DNMT3B1* product and the lower band represents the Δ*DNMT3B1* product. The lower panel shows relative intensity of the product bands.

The siRNA or the antisense RNA successfully eliminated transcripts of *ΔDNMT3B2* and *ΔDNMT3B4* in H1299 cells in a dose- and time-dependent manner but had no effect on *ΔDNMT3B1* (Fig. 2A). The effect was specific because the expression levels of the three transcripts in cells treated with medium, lipofectamine alone, lipofectamine plus scramble siRNA, or lipofectamine plus siRNA-*GAPDH* did not change (**Fig. 2A**). We then analyzed the effect of a *ΔDNMT3B4/2* knockout in the promoter methylation of *p16* and *RASSF1A*. The *RASSF1A* promoter became partially unmethylated in the cells treated with 20 nM siRNA-*ΔDNMT3B4/2* and

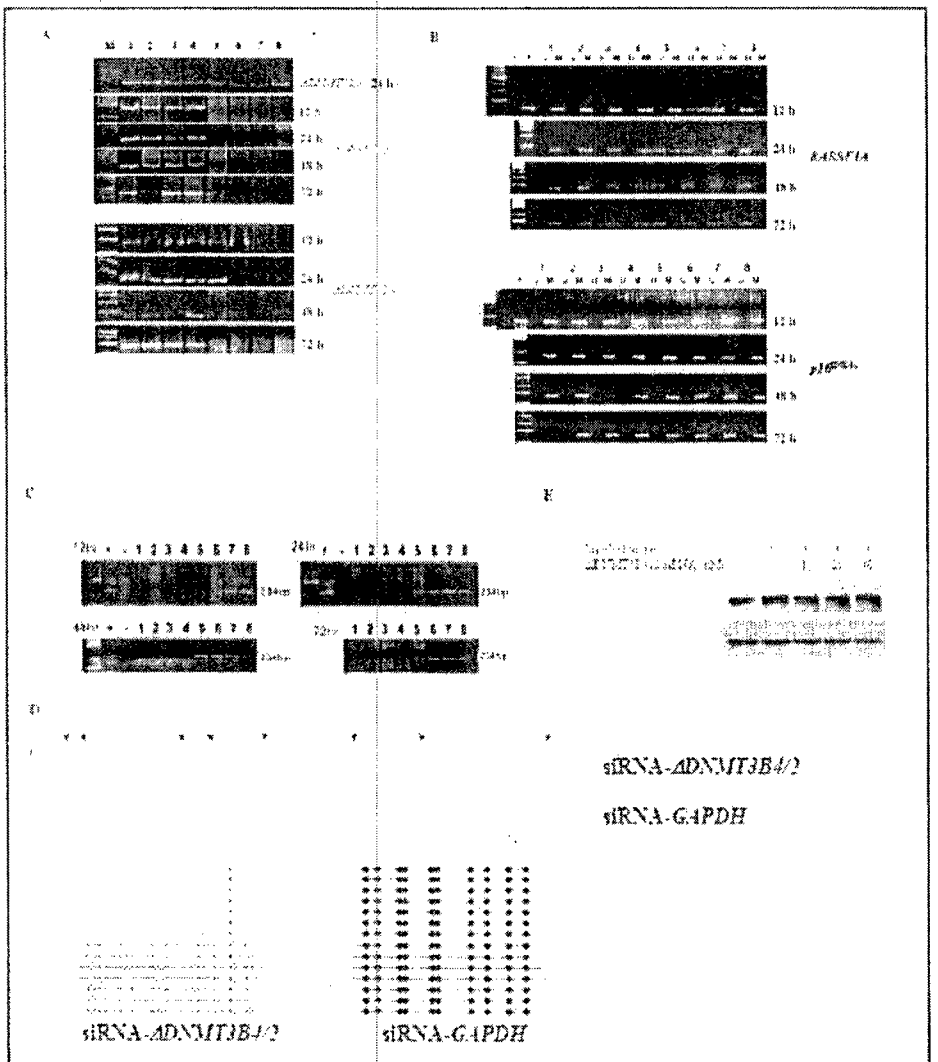


Fig. 2. Effects of *ΔDNMT3B4/2* knockout on H1299 cells. ***A***, Expression of *ΔDNMT3B1*, *ΔDNMT3B2*, and *ΔDNMT3B4* at different time points after treatment measured by RT-PCR. ***B***, Promoter methylation status of *p16INK4a* and *RASSF1A* at different time points after treatment measured by MSP. ***C***, RASSF1A gene expression status at different time points after treatment measured by RT-PCR. For ***A***, ***B***, and ***C***, M indicates size marker; 1, treated with medium alone; 2, treated with lipofectamine alone; 3, treated with lipofectamine plus 40 nM GAPDH-specific siRNA; 4, treated with lipofectamine plus 40 nM scramble siRNA; 5, treated with lipofectamine plus 10 nM *ΔDNMT3B4/2*-specific siRNA; 6, treated with 20 nM *ΔDNMT3B4/2*-specific siRNA; 7, treated with 40 nM *ΔDNMT3B4/2*-specific siRNA; 8, treated with 40 nM *ΔDNMT3B4/2* antisense RNA; -, negative control; +, positive control. ***D***, DNMT1 protein level in cells treated with or without *ΔDNMT3B4/2*-specific siRNA at the 48-h time point measured by Western blot analysis. ***E***, methylation status of individual CpG sites in a RASSF1A promoter region from cells treated with or without *ΔDNMT3B4/2*-specific siRNA. The open circles indicate unmethylated cytosine residuals, and the solid circles indicate methylated cytosine residuals in the CpG sites. Each line represents DNA from a single clone.

completely unmethylated (defined as no detectable methylated PCR product in by methylation-specific PCR studies) in the cells treated with 40 nM siRNA at 12 h (**Fig. 2B**). At 24 h, the promoter was completely unmethylated in the cells treated with 20 nM siRNA or 40 nM antisense RNA, whereas it was completely demethylated at 48 h in the cells treated with 10 nM siRNA (**Fig. 2B**). These results were consistent with the dose-dependent reduction of *ΔDNMT3B4* expression resulting from the siRNA or antisense RNA treatment (**Fig. 2A**).

In contrast, promoter methylation of *p16* was not affected by the knockout (**Fig. 2B**). Interestingly, *RASSF1A* remained completely unmethylated 72 h after the short-term siRNA or antisense RNA treatment (**Fig. 2B**).

We then analyzed the expression status of *RASSF1A* using RT-PCR. Expression of *RASSF1A* was restored in cells treated with 40 nM siRNA-*ΔDNMT3B4/2* or 40 nM antisense RNA at 12 h, with 20 nM siRNA at 24 h, and with 10 nM siRNA at 48 h (**Fig. 2C**). *RASSF1A* continued to express at least at 72 h after the treatment (**Fig. 2C**). This result was again consistent with the dose-dependent reduction of *ΔDNMT3B4* resulting from the siRNA or antisense treatment (**Fig. 2A**).

To provide more quantitative assessment of the extent of the demethylation, we performed bisulfite sequencing of the MSP products from cells treated with or without siRNA-*ΔDNMT3B4/2*. The fragment sequenced was part of the *RASSF1A* promoter and contained 10 CpG sites in addition to those within the primer sequences. None of the cytosine residuals at the 10 CpG sites was converted to uracil (recognized as thymidine in PCR products) by the bisulfite in any of the 14 clones derived from the cells 12 h after treatment with 40 nM siRNA-GAPDH, indicating a complete methylation status of the DNA fragment, whereas the cytosine residuals at all 10 CpG sites were converted to uracil by the bisulfite in all 14 clones derived from the cells 12 h after treatment with 40 nM siRNA-*ΔDNMT3B4/2* (**Fig. 2D**), an indication of complete unmethylated status of the DNA fragment. These data verified the finding that the *ΔDNMT3B4/2* knockout resulted in a complete reversal of the methylated *RASSF1A* promoter region.

To exclude the possibility that the treatment might affect DNMT1, the major enzyme responsible for maintaining DNA methylation, we analyzed DNMT1 protein expression in H1299 cells treated with siRNA and found no reduction in protein level (**Fig. 2E**), suggesting that DNMT1 was not the contributing factor to the observed promoter demethylation. We then analyzed H358 cells, another NSCLC cell line with *p16* and *RASSF1A* promoter methylation and *ΔDNMT3B4/2* expression (**Fig. 1B**). As with H1299, the treatment knocked out *ΔDNMT3B4/2* expression and resulted in the demethylation of the *RASSF1A* promoter but not of the *p16* promoter.

We used a microelectronic cell sensor system (ACEA Biosciences, Inc., San Diego, CA) to determine the dynamic change in cell growth affected by the *ΔDNMT3B4/2* knockout (measured every 30 min). In the H1299 cells, growth was inhibited at about 10 h after treatment with the siRNA-*ΔDNMT3B4/2* in a dose-dependent manner or the antisense RNA (**Fig. 3A**). To determine the potential mechanism for inhibiting the growth of the *ΔDNMT3B4/2* knockout, we examined the cell cycle distribution of the H1299 cells 24 h after treatment using flow cytometry. We observed a dose-dependent increase of the sub-G1 fraction in the cells treated with the siRNA-*ΔDNMT3B4/2* or the antisense RNA (**Fig. 3B**). This increase indicated that the treatment had induced cell death.

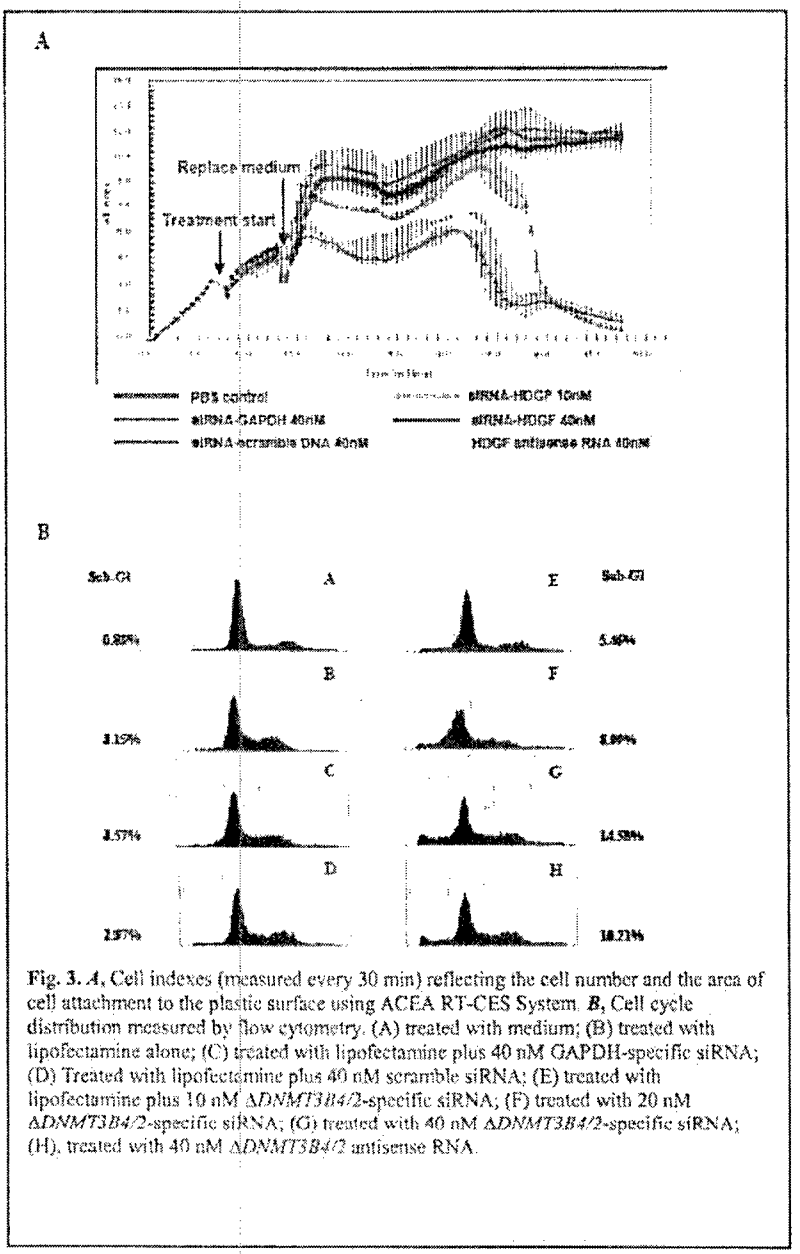


Fig. 3. *A*, Cell indexes (measured every 30 min) reflecting the cell number and the area of cell attachment to the plastic surface using ACEA RT-CES System. *B*, Cell cycle distribution measured by flow cytometry. (A) treated with medium; (B) treated with lipofectamine alone; (C) treated with lipofectamine plus 40 nM GAPDH-specific siRNA; (D) Treated with lipofectamine plus 40 nM scramble siRNA; (E) treated with lipofectamine plus 10 nM *ΔDNMT3B4/2*-specific siRNA; (F) treated with 20 nM *ΔDNMT3B4/2*-specific siRNA; (G) treated with 40 nM *ΔDNMT3B4/2*-specific siRNA; (H), treated with 40 nM *ΔDNMT3B4/2* antisense RNA.

By screening other promoters commonly methylated in lung cancers, we found about a 50% methylated death-associated protein (DAP)-kinase promoter in the H1299 cells; such methylation was completely eliminated after the siRNA-*ΔDNMT3B4/2* treatment (**Table 1**). Then, using pyrosequencing, we analyzed the effect of the siRNA-*ΔDNMT3B4/2* in repeat DNA sequences (Alu and LINE). This analysis indicated a more global DNA methylation status. In the H1299 cells, the treatment resulted in reduced DNA methylation in the LINE and Alu sequences but not in the H358 cells (**Table 1**). We analyzed two colorectal cancer cell lines (SW48 and RKO) to determine whether the effect of the siRNA-*ΔDNMT3B4/2* observed in the NSCLC cell lines also occurred in

other tumor types. DNA methylation occurred in these cell lines in more promoters (**Table 1**), and numerous *ΔDNMT3B4/2* transcripts were expressed (data not shown). Interestingly, none of these promoters, including *RASSF1A* or the repeat sequences, were demethylated after *ΔDNMT3B4/2* was knocked out by the siRNA-*ΔDNMT3B4/2* (**Table 1**).

Table 1. Modification of DNA methylation in promoters and repeat sequences

Method	MSP	MSP	MSP	MSP	MSP	MSP	MSP	Pyrosequencing	Pyrosequencing
Sequence name	RIZ	p14	MLH1	ECAD	RASSF1A	DAPK	p16	LINE methylation (%)	Alu methylation (%)
H1299 control					M	M&U	M	50.9	31.9
H1299 lipo					M	M&U	M	54.9	28.4
H1299 siRNA					U	U	M	35	23.6
H358 control					M		M	41.2	25.9
H358 lipo					M		M	40.3	26.4
H358 siRNA					U		M	39	25.3
RKO control	M	M	M	M	M		M	41	29.8
RKO lipo	M	M	M	M	M		M	46.4	30.8
RKO siRNA	M	M	M	M	M		M	44.6	30.5
SW48 control	M	M	M&U		M		M	56.3	30.1
SW48 lipo	M	M	M&U		M		M	61.8	32.6
SW48 siRNA	M	M	M&U		M		M	64.2	31.5

M: methylated promoter; U: unmethylated promoter; M&U: mixed with both methylated and unmethylated promoters; control: treated with medium alone, lipo: treated with lipofectamine alone; siRNA: treated with ΔDNMT3B4/2-specific siRNA

Specific Aim 5 ***To determine expression of hnRNP-A1 variants in lung cancer cells and their role in regulation pre-mRNA splicing.***

We have shown that CEACAM1 splicing patterns are associated with hnRNP protein variants. Two cell lines (A549 and H1944) with predominant long form of CEACAM1 possess predominantly full size nuclear hnRNP-A1 and hnRNP-A2/B1, whereas cell lines H460 and UMSCC17B with predominantly short form of CEACAM1 possess a number of truncated hnRNP-A1 and hnRNP-A2/B1 (**Fig. 4**). We initially thought that the expression of truncated hnRNP proteins was the result of alternative splicing of the corresponding genes, which contributes to the regulation of CEACAM1 splicing. To determine whether it is the case, we performed RT-PCR to analyze the gene expression patterns of hnRNP-A1 and hnRNP-A2/B1 using the four cancer cell lines described in **Fig. 4**. Our initial analysis failed to reveal obvious splicing variants of both hnRNPs (**Fig. 5**). When several different primer sets were used, some alternatively spliced forms were observed in the cell lines but the appearance of these variants was neither closely associated with the CEACAM1 splicing patterns nor the hnRNP protein patterns (**Fig. 4**). These results suggest the alternative

splicing may not be the major mechanism of generating the truncated hnRNPs. More complicated posttranslational processing may be involved in the protein modifications.

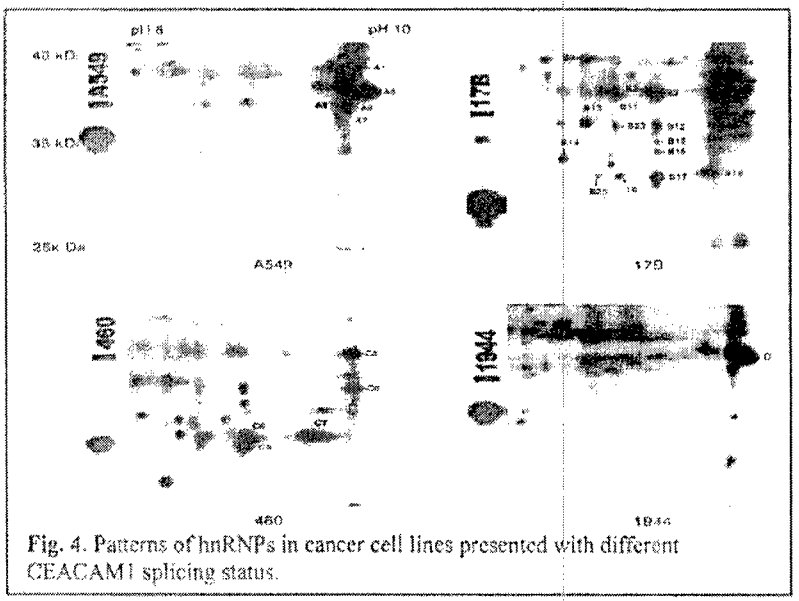


Fig. 4. Patterns of hnRNPs in cancer cell lines presented with different CEACAM1 splicing status.

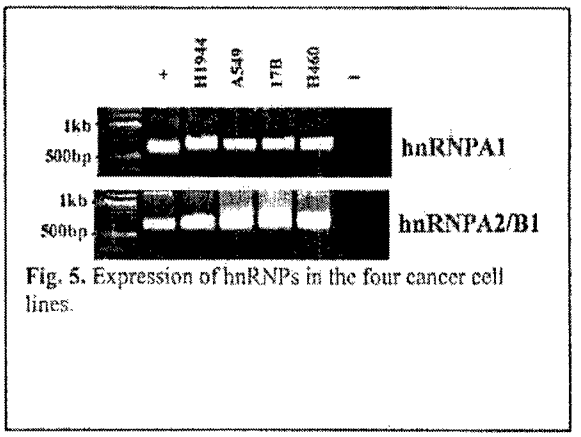


Fig. 5. Expression of hnRNPs in the four cancer cell lines.

Additional task not specified in the previous report:

Hepatoma-derived growth factor (HDGF), which is unrelated to hepatocyte growth factor, can stimulate DNA synthesis and cell proliferation on entering the nucleus. We hypothesize that HDGF plays an important role in biologic behavior of early-stage non-small-cell lung cancer (NSCLC). Ninety-eight patients with pathologic stage I NSCLC who underwent curative surgery were studied. Immunohistochemistry was used to determine the expression level of HDGF in the tumor specimens. The intensity of the protein staining and percentage of stained tumor cells were used to determine a labeling index. Statistical analyses, all two-sided, were performed to determine the prognostic effect of HDGF expression levels on clinical parameters and outcomes. The mean +/- standard deviation HDGF labeling index in the 98 tumors was 185 +/- 41. Patients whose tumors had higher HDGF indexes (>/= 185) had a significantly poorer probability of overall survival at 5 years after surgery than did those with lower HDGF indexes (0.26 v 0.82; P <.0001). Similarly, the 5-year disease-specific and disease-free survival probabilities were lower in those with higher HDGF indexes (0.42 v 0.92, and 0.34 v 0.71; P <.0001 and P =.0008; respectively). Multivariate analysis indicated that HDGF level was an independent predictor of overall, disease-specific, and disease-free survivals. We conclude that overexpression of HDGF is common in early-stage NSCLC. The expression level in tumor cells is strongly correlated with poor overall, disease-specific, and disease-free survivals, suggesting HDGF may be a powerful prognostic marker for patients with early-stage NSCLC. (Ren H et al, Journal of Clinical Oncology, 22:3230-3237, 2004)

Future research plan:

We will continue to study biologic effects of ΔDNMT3B variants in lung tumorigenesis. We will determine the role of ΔDNMT3B variants in early lung tumorigenesis by analyzing their expression

in bronchial epithelial cells from individuals with high-risk to develop lung cancer. We will construct vectors containing various forms of the variants including those with or without enzymatic motifs of DNA methyltransferase. We will determine the biological roles of each variant in regulation of DNA methylation and gene expression using immortalized normal bronchial epithelial cell lines and NSCLC cell lines. We will pay particular attention to ΔDNMT3B4 because our current data suggest this variant is the most influential factor in promoter methylation of RASSF1A which appears important in lung cancer progression. We will also plan to determine the mechanism of ΔDNMT3B2/4 mediated RASSF1A promoter methylation. We will further determine the role of HDGF in lung cancer progression and mechanism of HDGF associated aggressive biologic behaviors of NSCLC cells. We plan to design more primers to reveal rare splicing variant of hnRNP-A1 and A2/B1 and to determine a potential splicing pattern change of CEACAM1 by knocking down the hnRNP variants.

Project 2: Novel Strategies for Lung Cancer Chemoprevention
Project Leader: Fadlo Khuri, M.D.

Specific Aim 2.1 ***To evaluate the effects of oral bexarotene delivered to former smokers by inhalation alone or in combination with celecoxib.***

(Leader: Fadlo Khuri, M.D)

As reported in 2004, we were unable to conduct the clinical trial proposed in the original Specific Aim - *To evaluate the effects of aerosolized 13cRA delivered to former smokers by inhalation alone or in combination with Celecoxib* - due to excessive toxicity with aerosolized delivery. Thus, we have proposed another clinical trial, a phase I/II study of the combination of bexarotene/celecoxib in solid tumors, which is pending for HSRRB review and approval. The rationale for the trial is as follows:

Initial clinical studies have indicated that retinoids decrease the incidence of second primary tumors in patients who have previously undergone resection for NSCLC or head and neck cancer. However, subsequent large-scale chemoprevention trials have demonstrated that retinoids induce substantial toxicity and are of minimal benefit to individuals at high-risk for lung cancer, illustrating the need for more effective lung cancer chemoprevention strategies. The objective of this project is to evaluate the chemopreventive potential of bexarotene (Targretin®) and non-steroidal anti-inflammatory agents (NSAIDs) (e.g., celecoxib) using preclinical *in vitro* and animal model studies and clinical trials combining bexarotene and celecoxib. NSAIDs exhibit chemopreventive effects in animal models including lung carcinogenesis and familial adenomatous polyposis. This project will test whether the combination of bexarotene and celecoxib appears tolerable and promising in lung cancer patients, which would be taken forward into high-risk chemopreventive strategies.

Data to date with bexarotene in non-small cell lung cancer. Bexarotene is a non-classic retinoid or rexinoid, developed in the early 1990s, and tested extensively now in multiple solid tumor trials. Phase I trials of bexarotene by Miller and Rizvi (**Table 2**) indicated that approximately 30%-35% of all treated patients had disease stabilization for a minimum of 3 months while other trials showed that no NSCLC patients had demonstrated responses to bexarotene. Preliminary data showed that this agent was synergistic with cisplatin in squamous cell xenograft, which led to an enhanced de-differentiation of the tumor and enhanced sensitivity to cisplatin. Thus, several trials were conducted combining bexarotene with cytotoxic chemotherapy (**Table 2**). These trials, while failing to demonstrate an enhanced tumor response rate, showed improved survival over historical controls. Particularly prominent was our phase I/II combination of cisplatin and vinorelbine with bexarotene, which showed a median survival in stage IIIb-IV NSCLC of 14 months,

and 1, 2, and 3-year survivals of 61%, 32%, and 18% despite the modest response rate of 25%. Two other multicenter trials and a trial from the University of Maryland indicated that this agent had significant promise in NSCLC. Therefore, two phase III trials were launched, which we helped to oversee. These trials completed accrual of over 600 patients and used different combinations of chemotherapy with bexarotene compared with the chemotherapy of choice. The final analysis of these data is anticipated by the end of March 2005.

Table 2. Bexarotene Phase I/II Trials Completed NSCLC Studies

Study	No. Pts.	Author
Ph I in various cancers	20*	Miller, 1997
Ph I/II in various cancers	16*	Rizvi, 1999
Ph I/II, CisP-Navelbine, 1st line	43	Khuri, 2001
Ph II, maintenance after 1st line	52	Rizvi, 2001
Ph I/II, Carbo-Taxol, 1st line	43	Rizvi, 2002
Ph II, Carbo-Gem, 1st line	48	Edelman, 2004
*Patients with NSCLC	N = 222	

NSAIDs in Lung Cancer Chemoprevention. Two types of enzymes mediate arachidonic acid metabolism: cyclooxygenases (COXs) that generate prostaglandins and lipoxygenases (LOXs) that generate HETEs and leukotrienes. These metabolites enhance cell growth and survival. Increased activities of COX-2 and 5-LOX have been noted during carcinogenesis. The ability of various NSAIDs to suppress carcinogenesis in a variety of animal models of carcinogenesis including lung has indicated the potential clinical application of these compounds. This potential has been demonstrated in humans, especially in the prevention of gastrointestinal cancers. However, it is unknown whether NSAIDS could also be useful for lung cancer prevention. Inhibitors of COX-2 and 5-LOX among the NSAIDs affect the growth and apoptosis of various tumor cell lines including non-small cell lung cancer (NSCLC) cells, and celecoxib is shown to be effective on prevention of colon carcinogenesis in APC patients. Moreover, Mestre et al have demonstrated that retinoids (9-cis-retinoic acid, 13-cis-retinoic acid, and retinyl acetate) suppress both a basal level of COX-2 and EGF-mediated induction of COX-2. These results establish a rationale for combining COX-2 inhibitors with retinoids.

Therefore, we selected the combination of bexarotene with celecoxib in a dose-escalation schema shown in **Table 3**.

Table 3. Phase I Bexarotene-Celecoxib Dose Escalation Schema

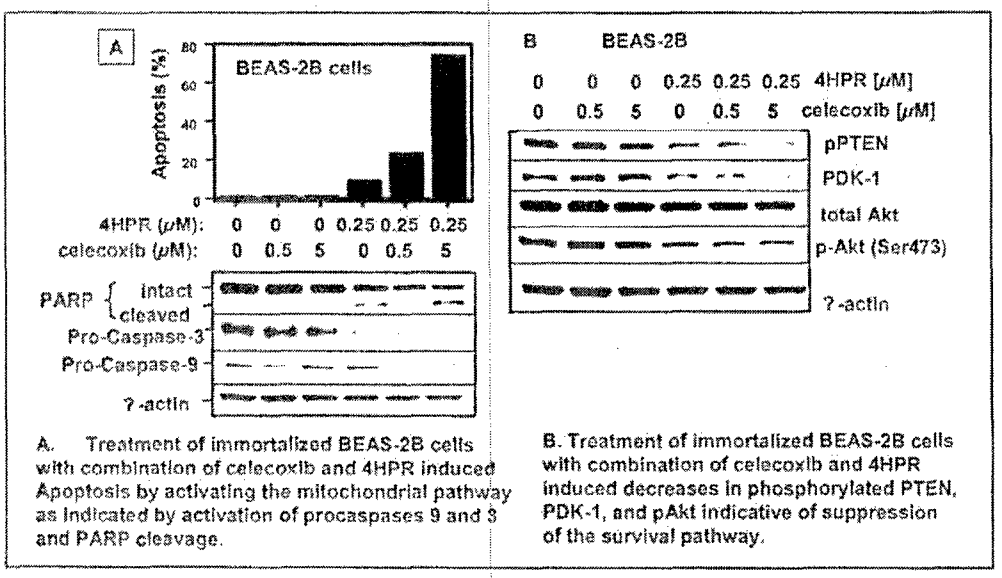
Dose Level	Bexarotene (mg/m^2 daily)	Celecoxib (mg bid)
0	200	200
1	300	200
2	300	400
3	400	400
4	600	400

Specific Aim 2.2. ***To evaluate effects of NSAIDs and 13cRA as single agents and in combinations on growth, apoptosis, and carcinogenesis using an in vitro cell system and an animal model.***

(Leader: Reuben Lotan, Ph. D.)

The purpose of the study is to evaluate effects of non-steroidal anti-inflammatory agents (NSAIDs) (e.g. celecoxib) and retinoic acids as single agents or in combinations on lung cancer growth, apoptosis, and lung carcinogenesis using an *in vitro* cell system and an animal model. In the first year of funding, we determined the efficacy and mechanisms of inhibitors of arachidonic acid metabolizing enzymes including cyclooxygenase 2 (COX-2) and lipoxygenase (e.g., 5-LOX) used as single agents, in combination with each other, or with retinoic acids on suppression of cell growth and induction of apoptosis of normal, immortalized, premalignant, transformed, and tumorigenic lung cells *in vitro*. We found that these effects were not related to the expression of the target enzymes, suggesting their COX-2-independent functions. Because the retinoid 13cRA shows enhancement of lung cancer among smokers in a clinical trial and has side effects whereas the synthetic retinoid fenretinide [*N*-(4-hydroxyphenyl) retinamide, 4HPR] is more potent and shows less side effects and has additive effects with celecoxib, we have replaced 13cRA with 4HPR for later studies.

Recently, we have demonstrated that treatment with the combination of the COX-2 inhibitor celecoxib and 4HPR was more effective on inhibition of growth and induction of apoptosis in premalignant and malignant lung cell lines than that with either agent alone. During the past year, we further investigated the pro-apoptotic mechanism of action of the celecoxib/4HPR combination in immortalized human bronchial epithelial cell line BEAS-2B, which does not express COX-2. As shown in the figure below, we found that simultaneous treatment of the cells with clinically



A. Treatment of immortalized BEAS-2B cells with combination of celecoxib and 4HPR induced Apoptosis by activating the mitochondrial pathway as indicated by activation of procaspases 9 and 3 and PARP cleavage.

B. Treatment of immortalized BEAS-2B cells with combination of celecoxib and 4HPR induced decreases in phosphorylated PTEN, PDK-1, and pAkt indicative of suppression of the survival pathway.

achievable concentrations of celecoxib (1 and 5 μM, respectively) and 4HPR (0.25 μM) for 3 days induced a marked apoptosis in a dose-dependent manner. The effects were associated with a sustained activation of mitochondrial membrane permeability transition detected by fluorescent MitoProbe™ assay and corresponding changes in members of the Bcl-2 family identified by western immunoblotting. Specifically, the release of cytochrome C from mitochondria to cytoplasm

increased, caspases 9 and 3 were activated, and the level of the antiapoptotic protein Bcl2 decreased. In addition, the celecoxib/4HPR combination inhibited the survival pathway, as evidenced by suppression of Akt phosphorylation, at concentrations such that each agent alone had no or low effects without altering the levels of PTEN phosphatase.

Specific Aim 2.4. ***To analyze differential gene expression between untreated NSCLC cells and celecoxib-treated NSCLC cells using affymetrix oligonucleotide microarrays and characterize genes that may be implicated in mediating apoptosis induction***

(Leader: Reuben Lotan, Ph.D.)

We have also begun to analyze the effects of celecoxib, 4HPR, and their combination on the expression of genes involved in apoptosis using the Affymetrix gene expression platform. The data are still being collected and analyzed in collaboration with bioinformatics support.

Specific Aim 2.3. ***To investigate whether genetic approaches to inhibit PI3K activity decrease lung tumor size and number in k-ras mutant mice.***

This Aim has been dropped as reported in the 2004 Annual Report.

Project 3: Experimental Molecular Therapeutic Approaches to Lung Cancer
Project Leader: Fadlo Khuri, M.D.

Specific Aim 3.1 ***To develop a relatively faithful murine model of lung cancer by crossing the k-ras mutant mouse (T. Jacks) with our p53 mutant missense mouse (G. Lozano) such that we can study the evolution of non-small cell lung cancer in primary lung tumor model with metastatic potential, as well as the effectiveness of these molecularly targeted strategies in that model.***

(Leader: Guillermina Lozano, Ph.D.)

We have developed a mouse lung cancer model that develops lung carcinomas due to an inherited mutation in the p53 tumor suppressor ($p53^{R172H\Delta g/+}$) and somatic inactivation of the *ras* oncogene ($K\text{-}Ras^{LA1/+}$). 84% of these mice develop lung adenocarcinomas by one year of age (**Table 4**). 30% of these mice have also developed metastases to intrathoracic and extrathoracic regions (**Table 5**). Extrathoracic metastases have occurred to many organs and include the mesentery lymph node, liver, adrenal gland, kidney and eye. Thus, the initial aim to generate and characterize the model has been accomplished. Dr. Adel El-Naggar performed pathology analysis.

Table 4. Tumor spectra of $p53^{R172H\Delta g/+}$; $K\text{-}Ras^{LA1/+}$ and $p53^{+/+}$; $K\text{-}Ras^{LA1/+}$ mice

Tumor Types	$p53^{R172H\Delta g/+}$; $K\text{-}Ras^{LA1/+}$ Incidence	Metastasis	$p53^{+/+}$; $K\text{-}Ras^{LA1/+}$ Incidence	Metastasis
Lung adenocarcinomas (AC)	48/57	14/48	22/32	0/22
Lung mesothelioma	2/57	2/2	0/32	-
Lung AC/mesothelioma	5/57	5/5	3/32	1/3
Lung adenoma	1/57	-	7/32	-
Lymphoma	6/57	-	7/32	-
Sarcomatoid carcinoma	9/57	-	0/32	-
Sarcoma			1/32	-
Papilloma	4/57	-	6/32	-

Table 5. The frequency of Metastases at different sites in $p53^{R172H\Delta g/+}$;$K\text{-}Ras^{LA1/+}$ mice

Metastatic sites	Lung adenocarcinoma	Lung mesothelioma
Intrathoracic		
Mediastinal lymph node	8/12	4/5
Heart	6/12	2/5
Parietal/diaphragmatic pleura	3/12	N/A
Extrathoracic		
Mesentery/lymph node	3/12	2/5
Liver	2/12	1/5
Adrenal gland	2/12	1/5
Subcutaneous tissue	2/12	2/5
Kidney	1/12	0/5
Eye tissue	1/12	0/5

Specific Aim 3.5 ***To study the in vivo and in vitro effects of farnesyl transferase inhibitors and tyrosine kinase inhibitors in mouse models and, ultimately, in humans with lung cancer***

(Leader: Guillermina Lozano, Ph.D.)

While the initial studies were designed to treat *$p53^{R172H\Delta g/+}$; $K\text{-}Ras^{LA1/+}$* mice with IRESSA and FTI, a new anti-cancer drug, Erlotinib (Tarceva), has more clinical promise. Therefore, we will use Erlotinib in this new mouse model of lung cancer. Erlotinib will be administrated orally by gavage every day at a concentration of 0.1mg/g body weight. The treatment will be started at three months of age when lung adenomas and a few small lung carcinomas are visible. After 30 days of treatment, mice will be sacrificed for pathological analysis. Before and after the treatment period, live mice will be scanned by micro-CT imaging to monitor lung tumor growth.

Specific Aim 3.6 ***To measure differences in gene expression between lung tumors that do or do not show metastasis, and in metastatic lesions themselves using the Affymetrix gene chip system***

(Leader: Guillermina Lozano, Ph.D.)

We have collected samples and have begun these studies. The samples collected are shown in **Table 6**. We have isolated mRNA from 6 different *p53*$^{R172H\Delta g/+}$; *K-Ras*$^{LA1/+}$ mice with primary adenocarcinomas and their metastases. Additionally we have isolated mRNA from three mice with *K-Ras*$^{LA1/+}$ mutation alone as controls. The quality of the mRNA was measured and the cRNA generated and hybridized to Affymetrix chips. We are currently evaluating the data with a bioinformatician.

Table 6. Samples Used for Expression Microarray Analysis

Genotype	Primary lung cancer	*Metastasis*
p53$^{R172H\Delta g/+}$; K-Ras$^{LA1/+}$	Adenocarcinoma	s.c. metastasis
p53$^{R172H\Delta g/+}$; K-Ras$^{LA1/+}$	Adenocarcinoma	Liver metastasis Inguinal metastasis s.c. metastasis
p53$^{R172H\Delta g/+}$; K-Ras$^{LA1/+}$	Adenocarcinoma	Liver metastasis
p53$^{R172H\Delta g/+}$; K-Ras$^{LA1/+}$	Adenocarcinoma	Mediastinal LN metastasis Heart metastasis s.c. metastasis
p53$^{R172H\Delta g/+}$; K-Ras$^{LA1/+}$	Adenocarcinoma	Mediastinal LN metastasis
p53$^{R172H\Delta g/+}$; K-Ras$^{LA1/+}$	Adenocarcinoma	Mediastinal LN metastasis Parietal pleural metastasis
p53$^{+/+}$; K-Ras$^{LA1/+}$	Adenocarcinoma	-
p53$^{+/+}$; K-Ras$^{LA1/+}$	Adenocarcinoma	-
p53$^{+/+}$; K-Ras$^{LA1/+}$	Adenocarcinoma	-

Specific Aim 3.7 ***To perform array CGH experiments to determine if other genomic changes have occurred***

Specific Aim 3.8 ***To perform LOH studies at specific loci (if warranted from the data obtained in Specific Aim 3.7)***

(Leader: Guillermina Lozano, Ph.D.)

The two proposed studies above have not been started and may begin sometime this year after the array analysis is completed in *Specific Aim 3.6*.

Specific Aim 3.2 ***To evaluate novel signal transduction inhibitors, both alone and in combination with one another and with cytotoxic agents, in the treatment of these mouse lung cancer models and, ultimately, in the treatment of human lung cancers.***

(Leader: Fadlo Khuri, M.D.)

In the past few years, we have studied farnesyltransferase inhibitors (FTIs) including Lonafarnib, which is a novel class of anticancer agents that show promise in suppressing the growth of tumors both in preclinical studies and in clinical trials. Although FTIs were originally designed to inactivate Ras by inhibiting Ras farnesylation, many studies have indicated that they may inhibit cell growth and induce apoptosis independent of Ras mutation. Alternatively, the PI3 kinase/Akt pathway has been proposed as a potential target for the FTIs' actions. Our studies have indicated that Akt is

unlikely to be a target for Lonafarnib's effect on growth arrest or apoptosis induction in human NSCLC cells.

FTIs are, however, known to potently synergize with paclitaxel (PTX) and other microtubule-stabilizing drugs, but the mechanism of this synergistic interaction remains elusive. Here we have shown that lonafarnib-treated cells display microtubule bundles, increase tubulin acetylation and polymerization, and decrease microtubule dynamics. Notably, treatment with the combination of low doses of LNF with PTX markedly enhances tubulin acetylation (a marker of microtubule stability) as compared to either drug alone and inhibits the *in vitro* deacetylating activity of the only known tubulin deacetylase, HDAC6. Taken together, the studies suggest a relationship between FT inhibition, HDAC6 function, and cell death, providing insight into the putative molecular basis of the LNF/taxane synergistic anti-proliferative combination. Thus, these successful preclinical studies supported by DoD have conceptually helped develop a phase I trial of Lonafarnib with paclitaxel funded by other financial sources.

We have evaluated safety, tolerability and efficacy of treatment using lonafarnib in combination with paclitaxel in patients with metastatic (stages IIIB/V), taxane-refractory/resistant NSCLC. Patients with NSCLC who experienced disease progression without prior taxane therapy or relapsed within 3 months following taxane therapy cessation were treated with continuous lonafarnib 100 mg PO BID beginning on Day 1 and paclitaxel 175 mg/m2 IV over 3 hours on Day 8 of each 21-day cycle. A total of 33 patients were enrolled, of which 29 patients were evaluated for response. Partial responses or disease stabilization was observed in 3 (10%) or 11 patients (38%), respectively; thus, 14/29 (48%) experienced clinical benefit (partial response and disease stabilization). Median overall survival time was 41.3 weeks and median progression-free survival time was 10.6 weeks. The combination of lonafarnib and paclitaxel was well tolerated with minimal toxicity. Grade 3 toxicities included fatigue (9%), diarrhea (6%), and dyspnea (6%). Grade 3 neutropenia occurred in only 1 patient (3%). Grade 4 adverse events included respiratory insufficiency in 2 patients (6%) and acute respiratory failure in 1 patient (3%). Lonafarnib plus paclitaxel have, thus, demonstrated clinical activities in patients with taxane-refractory/resistant metastatic NSCLC. In addition, the combination of lonafarnib and paclitaxel was well tolerated with minimal toxicity. Evaluation of this combination therapy in additional clinical trials is warranted.

Studies of FTI combinations using the mouse model will be incorporated in *Specific Aim 3.5.*

Specific Aim 3.3 ***To produce and test a liposomal gene-therapeutic strategy targeted to a novel tumor suppressor gene located on chromosome 3p, both in the mouse model and in human patients with advanced non-small cell lung cancer***

(Leader: Charlie Lu, M.D)

Previously, we reported that systemically delivered FUS1-lipoplex suppressed tumor growth in experimental lung metastasis mouse model and demonstrated the feasibility of the DOTAP:cholesterol-DNA vector for systemic therapy. Further, we tested its toxicity in mice and monkey and found a well-tolerated non-lethal dose. These preclinical data have thus conceptually helped develop a phase I trial of DOTAP:cholesterol-FUS1 liposome complex supported by independent financial resources.

Based in part upon these pre-clinical studies, we have started a Phase I clinical trial (Human Gene Transfer Protocol #0201-513) in advanced NSCLC patients at M.D. Anderson Cancer Center. Patients are treated by intravenous administration of the DOTAP:cholesterol-FUS1 liposome complex. Between 05/2003 and 09/2003, six patients were enrolled and received a total of 15

treatment cycles (range 1 to 6 cycles). One patient completed protocol therapy (6 cycles). Three patients discontinued therapy for disease progression. One patient developed hemoptysis in the setting of grade 1 thrombocytopenia. One patient discontinued therapy due to the study being placed on clinical hold. Grade 3 toxicities included lymphopenia (12 cycles), hypokalemia (1 cycle), and hyperkalemia (1 cycle). The grade 3 lymphopenia appeared to be of limited clinical significance. In all 12 cases lymphopenia improved to ≤ grade 2 after 24 hours. Determination of the cause of lymphopenia is confounded by the receipt of steroids by all subjects. It remains unclear whether the transient grade 3 lymphopenia was due to steroid use or the study drug. The single episode of grade 3 hypokalemia (2.9 mEq/L) occurred in patient #2 who was on chronic potassium supplementation due to prior platinum-based chemotherapy. The potassium corrected to normal in 24 hours (3.5 mEq/L) without any change in medications, and was interpreted to be of limited clinical significance. The same patient received another cycle of treatment without further hypokalemia. The single episode of grade 3 hyperkalemia (6.1 mEq/L) occurred in patient #1 on day 7 of cycle 3 without other metabolic or renal abnormalities and resolved without any noted clinical symptoms when laboratory tests were repeated. There was a single episode of grade 2 fever within 3 hours after the first drug infusion in subject #1. This was not accompanied by any other toxicity. Patient #1 was treated with steroids, and we treated the subsequent 5 patients with steroid premedications. Among the 6 patients who received 14 treatment cycles that were administered with steroid and diphenhydramine premedications, the highest observed fever was grade 1, which occurred in 3 patients with 4 cycles. A total of 6 patients were treated with a total of 15 treatment cycles at dose levels of 0.2 mg/Kg (3 patients) and 0.3 mg/Kg (3 patients).

Between 11/2003 and 2/2004, the trial was placed on a clinical hold for FDA review. After reopening the protocol, the first cohort of 3 patients was enrolled between 8/2004 and 1/2005 and was treated at a reduced starting dose level of 0.01 mg/Kg without the use of premedications. 2 of 3 patients developed evidence of an inflammatory response characterized by fever (grade 3), chills, and hypotension (grades 2 and 3). After consulting with the FDA, the protocol will be amended to require steroid premedication. Treatment with premedication will begin at the same initial dose level of 0.01 mg/Kg.

Specific Aim 3.4 ***To develop specific vascularly targeted strategies to the vascular epithelium of lung cancer cells in order to decrease the toxicity to normal cells and enhance the therapeutic index.***

(Leader: Ho-Young Lee, Ph.D)

Previously, we reported several lines of evidence showing that FTI SCH66336 has an antiangiogenic activity in aerodigestive tract cancer. In the past year, we have further investigated mechanisms that mediate the antiangiogenic activity of SCH66336 in NSCLC and HNSCC cells. We found that SCH66336 decreased VEGF and HIF-1 expression in hypoxic, normoxic insulin growth factor 1(IGF)-stimulated, unstimulated aerodigestive tract cancer, and endothelial cells. SCH66336 reduced the half-life of the HIF-1 protein, but ubiquitin inhibitors protected the hypoxia- or IGF–stimulated HIF-1 protein from SCH66336-mediated degradation. SCH66336 inhibited the interaction between HIF-1 and Hsp90, and overexpression of Hsp90, but not constitutive Akt or constitutive MEK, restored HIF-1 expression in IGF–stimulated or hypoxic cells, but not in unstimulated cells, which were pretreated with SCH66336. Thus, we have concluded that SCH66336 inhibits angiogenic activities of NSCLC and HNSCC cells partly by inhibiting hypoxia- or IGF-stimulated HIF-1a and thus VEGF production *via* blocking the interaction of HIF-1 and Hsp90 and inducing proteasomal degradation of HIF-1. These findings provide the rationale for clinical application of FTIs for antiangiogenic treatment targeting HIF-1 in aerodigestive tract cancers. The manuscript is in revision (JNCI, 2005)

Specific Aim 3.9 ***To evaluate GFE-1 peptide effects on blocking lung metastases in a rat model***

(Previous leader: Dr. Yun W Oh, M.D)

Dr. Yun Oh led the above aim in past years. Due to his duty change to a full-time clinical position, he discontinued participation in the BESCT program as noted in an official letter to Dr. Julie Wilberding on December 8, 2003. Thus, the aim is discontinued. A summary of his findings follows which was not included in the last report. The study led to a manuscript which has been accepted by *Chest*.

Efforts to target therapeutics and imaging agents to blood vessels in an organ- specific or disease-specific manner have led to the development of a technique by which small peptides that target receptors on endothelial cells can be identified. This approach, using large random peptide libraries displayed on the surface of bacteriophage, has been termed *in vivo* phage display. *In vivo* phage display is a screening method in which peptides homing to specific vascular beds are selected after intravenous administration of a random peptide library. This strategy has revealed a vascular address system that allows tissue-specific targeting of normal blood vessels and angiogenesis-related targeting of tumor blood vessels by selected peptides. Many vascular receptors or "addresses" targeted by homing peptides have been identified. One such vascular receptor of normal lung endothelium is membrane dipeptidase (MDP), which was found by *in vivo* phage display to bind the tripeptide motif Gly-Phe-Glu (GFE). Our studies with GFE peptide and lung vasculature suggest that MDP mediates cancer cell adhesion to lung vasculature and development of lung metastases, but that MDP is not present in vasculature of lung metastases. MDP appears to occupy a vascular distribution similar to the pulmonary artery circulation. These results demonstrate the promise of defining critical functional and anatomic characteristics of endothelial cells in lung and other organs by *in vivo* phage display.

KEY RESEARCH ACCOMPLISHMENTS

- Promoter hypermethylation in $p16^{INK4a}$ and *RASSF1A* tumor suppressors is frequently and strongly associated with clinical outcomes in patients with resectable non-small cell lung cancer
- Hypermethylation of the death-associated protein kinase promoter attenuates the sensitivity to TRAIL-induced apoptosis in human non-small cell lung cancer cells
- Expression of ΔDNMT3B variants in non-small cell lung cancer is associated with patients' clinical outcomes
- *ΔDNMT3B4* plays a critical role in cell-type-dependent promoter-specific DNA methylation in non-small cell lung cancer
- Combination of celecoxib and 4HPR exerts greater effect on apoptosis in premalignant lung cells than each agent alone through the induction of mitochondria-mediated apoptosis pathway and inhibition of Akt survival pathway
- SCH66336 inhibited angiogenic activities of NSCLC and HNSCC cells partly by inhibiting hypoxia- or IGF-stimulated HIF-1a and thus VEGF production *via* blocking the interaction HIF-1 and Hsp90 and inducing proteasomal degradation of HIF-1.
- A mouse lung cancer model that develops lung carcinomas has been established and will be used for a variety of proposed studies

REPORTABLE OUTCOMES

Peer reviewed publications

Hening Ren, Ximing Tang, J. Jack Lee, Lei Feng, Allen D. Everett, Waun Ki Hong, Fadlo R. Khuri, Li Mao. Expression of Hepatoma-Derived Growth Factor Is a Strong Prognostic Predictor for Patients with Early-Stage Non-Small Cell Lung Cancer. *Journal of Clinical Oncology*, 22:3230-3237, 2004.

Charles Lu, Jean-Charles Soria, Ximing Tang, Xiao-Chun Xu, Luo Wang, Li Mao, Reuben Lotan, Bonnie Kemp, B. Nebiyou Bekele, Lei Feng, Waun K. Hong, and Fadlo R. Khuri. Prognostic Factors in Resected Stage I Non-Small Cell Lung Cancer (NSCLC): A Multivariate Analysis of Six Molecular Markers. *Journal of Clinical Oncology*, 22:4575-4583, 2004.

Jie Wang, J. Jack Lee, Luo Wang, Diane D. Liu, Charles Lu, You-Hong Fan, Waun Ki Hong, Li Mao. Value of $p16^{INK4a}$ and *RASSF1A* promoter hypermethylation in prognosis of patients with resectable non-small cell lung cancer. *Clinical Cancer Research*, 10:6119-6125, 2004.

Ximing Tang, Weiguo Wu, Shi-yong Sun, Ignacio I. Wistuba, Waun Ki Hong, and Li Mao. Hypermethylation of the Death-Associated Protein-Kinase Promoter Attenuates the Sensitivity to Tumor Necrosis Factor-Related Apoptosis-Inducing Ligand-Induced Apoptosis in Human Non-Small-Cell Lung Cancer Cells. *Molecular Cancer Research*, 2:685-691, 2004.

Qingyi Wei Li-E Wang, Erich M. Sturgis, Li Mao. Lymphocytic Expression of Nucleotide Excision Repair Proteins as a Marker for Cancer Susceptibility: A Pilot of Study of Head and Neck Cancer. *Cancer Epidemiology Biomarkers and Prevention*, in press, 2005.

Khuri FR, Glisson BS, Kim ES, Statkevich P, Thall PF, Meyers ML, Herbst RS, Munden RF, Zaknoen S, Tendler C, Zhu Y, Bangert S, Thompson E, Lu C, Wang X-M, Shin DM, Kies MS, Papadimitrakopoulou V, Fossella FV, Kirschmeier P, Bishop WR, Hong WK. Phase I study of farnesyl transferase inhibitor (FTI) SCH66336 with paclitaxel in solid tumors. *Clinical Cancer Research* 10: 2968-76, 2004.

Marcus AI, Zhou J, Hamel E, Nivens M, El-Naggar A, Khuri FR, Giannakakou P. Novel target for the farnesyl transferase inhibitor, lonafarnib: increased microtubule acetylation underlies synergy with taxanes. *Cancer Research*, In press, 2005.

Schroeder CP, Yang P, Newman RA, Lotan R. Eicosanoid Metabolism in Squamous Cell Carcinoma Cell Lines Derived from Primary and Metastatic Head and Neck Cancer and its Modulation by Celecoxib. *Cancer Biol Ther.* 3: 847-852, 2004

Sun SY, Schroeder CP, Yue P, Lotan D, Hong WK, Lotan R. Enhanced Growth Inhibition and Apoptosis Induction in NSCLC Cell Lines by Combination of Celecoxib and 4HPR at Clinically Relevant Concentrations. *Cancer Biol & Ther.*, in press, 2005

Schroeder CP, Kadara H, Lotan R. Combination of Celecoxib and 4HPR Exhibits Enhanced Apoptosis by Increasing Mitochondrial Membrane Permeability and Suppressing PI3K/AKT-signaling Pathway in BEAS-2B Immortalized Human Bronchial Epithelial Cells (in preparation)

Han JY, Oh SH, Kim E, Hong WK, Lee HY. Implication of hypoxia-inducible factor-1α in antiangiogenic activity of farnesyl transferase inhibitor SCH66336 in human aerodigestive tract cancer. *J. Natl. Cancer Institute*, 2005 (revised)

Yun Oh, Mohiuddin I, Sun C, Putnam JB Jr., Hong WK, Arap W, Pasqualini R. Phenotypic Diversity of the Lung Vasculature in Experimental Models of Metastases. *Chest*, in press 2005.

Abstracts and Presentations

Marcus A, Hamel E, Nivens MD, Iaconelli J, Khuri FR, Giannakakou P. Farnesyl transferase inhibitors affect microtubule stability and function. *American Association for Cancer Research*, 2004.

Fadlo Khuri. The treatment of lung cancer as an emerging paradigm for translational research. 2004 Cancer Research Conference, Braselton, GA, May 2004.

Fadlo Khuri. Update of retinoid studies in NSCLC, Fifth International Lung Cancer Congress, Kauai, HI, July 2004.

Fadlo Khuri. Non-small cell lung cancer therapeutics as a model for translational research, Future Directions in Hematology and Oncology, Sea Island, GA, July 2004.

Fadlo Khuri. From Prevention to Proteomics and Beyond, Lung Cancer Symposium, Mayo Clinic, Rochester, MN, August 2004.

Fadlo Khuri. Molecularly Targeted Approaches to the Chemoprevention of Lung Cancer, 10th World Conference on Lung Cancer, Lisbon, Portugal, September 2004.

Fadlo Khuri. Update of retinoid studies in NSCLC, The Future of Lung Cancer: A Translational Focus, Las Vegas, NV, September 2004.

Fadlo Khuri. Molecularly Targeted Approaches to Lung Cancer, Grand Rounds at the University of Maryland, Baltimore, MD, January 2005.

Project Generated Resources

NIH U01 (Mouse Models of Human Cancers Consortium)
(Baylor College of Medicine and U.T. M.D. Anderson Cancer Center)
Program: Modeling Airway Lung Cancer and the Role of Inflammation
Role: Project 2 and 5
Leader: Lin Ji
Duration: 4/1/2004-3/31/2009

PATENTS

Mao L, Wang J, and Wang L. A method of treating a cancer. Reference number: UTXC:875USP1.

CONCLUSIONS

Over the past year, the three projects have made considerable progress. Ten research articles have been published in peer-reviewed journals and two are in preparation. We have discovered that hypermethylated *p16* and *RASSF1A* tumor suppressor genes are strongly associated with poor clinical outcomes in patients with resectable NSCLC; hypermethylated DAPK attenuates TRAIL-induced apoptosis of NSCLC cells; the expression of *DNMT3B4* is significantly associated with poor overall, disease-free, and disease-specific survival in patients with stage IIIa NSCLC. These findings will help to identify prognostic predictors or biomarkers in early detection and molecular classification of lung cancer. Enhanced apoptosis in premalignant lung cells, by combination of celecoxib and 4HPR, is mediated through the induction of mitochondria-mediated apoptosis pathway and inhibition of Akt survival pathway. Also, FTI SCH66336 inhibits angiogenic activities of NSCLC and HNSCC cells partly by inhibiting hypoxia- or IGF-stimulated HIF-1a and thus VEGF production *via* blocking the interaction of HIF-1 and Hsp90 and inducing proteasomal degradation of HIF-1. These mechanistic studies have elucidated how these agents work on tumor cells. A successful, established mouse lung cancer model that develops lung carcinomas provides a powerful tool to study lung carcinogenesis and test promising drugs.

DEVELOPMENTAL RESEARCH PROGRAM

A Genetic/Combinatorial Algorithmic Strategy for Anticancer Therapy Development
(Project Leader: Ralph Zinner, M.D)

Targeted therapeutic agents are highly promising in combination because they are both well-tolerated and interact with the targets that cause cancer. We propose a direct functional screen of combinations as a complement to the molecular insight-based approach. However, with new drugs added to the list, the number of possible combinations rises exponentially that is beyond the capacity of any foreseeable technology to fully screen. We propose the MACS (Medicinal Algorithmic Combinatorial Screen) to identify promising combinations that would be otherwise impossible to be found through a simple screen alone. The foundation of MACS is a genetic algorithm. The study adopts a preclinical screen that assesses anticancer efficacies of combinations with cell proliferation assays.

In the last several months, we have conducted functional screens of all possible combinations derived from two NSCLC cell lines treated with six drugs and obtained some preliminary results. The studies are the first steps in the development of MACS.

Specific Aim 1: ***To determine feasibility (robots, cell death assays, combining drugs) of screening process***

We first tested whether we could add drug combinations to two different cell lines, A549 and H226. After determining an optimal cell density of 2×10^3 cells/well in 96-well plates for a three-day assay, we proceeded to identify drugs that are active against these cell lines as single agents and define their dose response curves. We selected drugs that had sufficiently gentle grades (at least a log difference in dose between near maximum and minimum inhibition) to allow reasonable reproducibility and a minimal DMSO (less than 0.2 % when diluted to final volume). Inhibition was detected 66 hrs after treatment by the WST-1 proliferation assay (Roche). Six drugs were selected for any given experiment. They were combined in all 64 possible combinations (6 singles, 15 doublets, 20 triplets, 15 four -tuples, 6 five-tuples, one 6-tuple, and one without treatment at a fixed dose (IC20). We also used DMSO alone controls. Each experiment was done in triplicate.

Originally we proposed six drugs, Herceptin, Iressa, Gleevec, C225, Docetaxel, and Velcade. Because four of the drugs (Herceptin, Iressa, C226, Docetaxol) tested in A549 either had no efficacy or required the addition of ethanol, which showed some inhibitory effect, and Velcade was not available at this time, we instead tested two other sets of drugs. These drug changes did not affect the ability to test the principles of the proposal.

The first set of drugs included LY294002 (PI-3-kinase inhibitor), Anisomycin (JNK/SAPK activator), Rapamycin (cdk inhibitor), SP600125 (JNK inhibitor), Indirubin-3'-oxime (CDKs inhibitor), and Bortezomib (Velcade) (proteasome inhibitor). The second set was gemcitabine, PD 168393 (MEK inhibitor), Indirubin-3-oxime, Gleevec (PDGFR and c-kit inhibitor), Anisomyci, and Bortezomib. A549 cells were tested with both sets of drugs. We found that standard deviations across triplets were 1% to 5%. Thus, our data indicated a good feasibility (reproducibility) among the experiments. A similar reproducibility was observed in the single experiment done in triplicate using the second set of drugs in H226.

Experiments using 7 or more drugs in all possible combinations (128 combinations for 7) will require the use of a robot. Initial experiments using a Tecan robot are under way. In addition, we have established a stable GFP-expressing A549 clone in order to reach a better resolution on effective combinations that kill all cells by day 3. Currently, we are evaluating combinations using the GFP cells.

Specific Aim 2: ***To determine the range of outcomes and patterns of cellular response from an initial screening of combinations of drugs***

One of the requirements for MACS will be the presence of some degree of linearity or higher order relationships among combinations. This means that knowing the behavior of some combinations formed from a set of drugs enables prediction of the behavior of other combinations formed from the same drugs. If there were perfect linearity, knowing the behavior of all the single agents will allow prediction of the behavior of all larger drug combinations that are formed from them. On the opposite extreme, if there were no linearity, it would not be possible to improve from one generation to the next, a requirement of a MACS. At present, little is known of the degree of relatedness of larger combinations of anticancer agents have. However, we have analyzed the data extensively from the first set of drugs.

One of the sets of 64 combinations was repeated 5 times in A549 in triplicate each time at the same intended doses and experimental conditions. We averaged the replications, normalized data to the condition with no drugs, and performed a simple regression analysis across all of the data using the presence or absence of a given drug as independent variables (this is equivalent to a type of ANOVA). We found that 75% of the variance was explained by the regression and the drugs had a significant, negative effect on normalized fitness. This result indicates a fair amount of linearity in the system. We also analyzed the data more directly and found that there were, at least in the six-drug world, some nonlinear effects. This would make generating good predictions about large combinations from smaller ones unpredictable.

Thus, our preliminary evidence indicates that knowledge of some of the combinations is modestly predictive of others, not enough to avoid a screen, but enough to make a MACS possible. Analyses of the second set of drugs in A549 and the first set of drugs in H226 cells are being conducted now.

Specific Aim 3: ***To develop genetic algorithm to guide selection and identification of promising combinations of drugs***

We have developed an algorithm that can be used to run larger experiments. The algorithm has been tested on some toy problems with 16 drugs (where the first six drugs have two levels of use (a given dose or no dose), the next four have three levels, and the last six have four levels, giving 21,233,664 possible combinations). The design was tied to the 96-well plate with three replications each and it basically runs two cell populations of experiments simultaneously. The first two plates, each allowing thirty two experiments (32x3=96), seed the two populations, and after that, each plate runs two sets of sixteen experiments for twenty four additional generations. The current version of the algorithm takes 832 experiments (26 plates) and 13 steps in a sequence (since the experiments are done 2 plates at a time). On these toy problems, the algorithm performs well and comes up with sensible answers.

Thus, we are in a good position to use algorithmic search to find new therapies. We will take twenty drugs at a single dose for each drug. We will limit the combination size to 8 or fewer drugs to avoid identifying the trivial solution that larger combinations are more toxic (there are about 120,000 possible combinations of 8-tuples from a pool of 20 drugs). All combinations will have the same concentration of DMSO to avoid the trivial observation that the combinations with the most DMSO will be most potent. To differentiate combinations that kill all cells by 72 hours, earlier time points will also be obtained. In as few as 5-7 steps entailing a total of about 300 assays in triplicate, we have a high probability of showing improved performance through an algorithm. Each step will be done in close collaboration with a mathematician. We anticipate we will have the first results within a few months.

Abstract:

RG Zinner, BL Barrett, AY Volgin, JG Gelovani, J Huang, HT Tran, GB Mills, WK Hong, Y Fu, L Mao. Higher Order Relationships and the Medicinal Algorithmic Combinatorial Screen (MACS). 2005. (ASCO)

APPENDIX

Higher Order Relationships and the Medicinal Algorithmic Combinatorial Screen (MACS)

R. G. Zinner, B. L. Barrett, A. Y. Volgin, J. G. Gelovani, J. Huang, H. T. Tran, G. B. Mills, W. K. Hong, Y. Fu, L. Mao; MD Anderson Cancer Center, Houston, TX; MD Anderson Cancer Center, Houston, TX; UT School of Public Health Houston, Houston, TX; MD Anderson Cancer Center, Houston, TX

Background: Targeted therapeutics are highly promising in combination because they are both well tolerated and interact with the signals that cause cancer. We propose a direct functional screen of combinations in the lab as a complement to the molecular insight based approach. However, with each drug added to the list, the number of possible combinations rises exponentially quickly beyond the capacity of any foreseeable technology to fully screen. We propose the MACS to identify combinations otherwise impossible to be found through a simple screen alone. The foundation of MACS is a genetic algorithm. One of the requirements for MACS will be the presence of some degree of higher order relationships among combinations. This means that knowing the behavior of some combinations formed from a set of drugs enables prediction of the behavior of other combinations formed from the same drugs. However, little is known of the degree of relatedness larger combinations of anticancer agents have. We performed experiments to evaluate this. **Methods:** A549 cells were plated at 2000/well and incubated in 96-well plates with drug for 66 hours before being read using the WST-1 proliferative assay (Roche). The agents were LY294002, PI-3-kinase inhibitor (Tocris); Anisomycin, activator JNK/SAPK activator (Tocris), Rapamycin, cdk inhibitor (Tocris); SP600125, JNK inhibitor (Tocris), Indirubin-3'-oxime, inhibits CDKs (Tocris); Bortezomib, proteasome inhibitor (Millennium Pharms). These were combined in all 64 combinations (pairs, triplets, quads etc.) done in triplicate at the single agent IC 20 dose of each drug with the experiment repeated another day. **Results:** Using regression analyses, reproducible modest higher order relationships were observed. **Conclusion:** We have preliminary evidence that knowledge of some of the combinations is modestly predictive of others, not enough to avoid a screen but enough to make a MACS possible. Further work will entail study of additional agents, altered doses and sequences, other NSCLC cell lines and non cancerous immortalized cell lines to represent host tissue, which will be presented at the poster. Ultimately, a pilot MACS system will be constructed the parameters for which will be guided by these data.

(This study was partially supported by Department of Defense Grant DAMD 17-02-1-0706).

2968 Vol. 10, 2968–2976, May 1, 2004 Clinical Cancer Research

Phase I Study of the Farnesyltransferase Inhibitor Lonafarnib with Paclitaxel in Solid Tumors

Fadlo R. Khuri,[1] Bonnie S. Glisson,[2] Edward S. Kim,[2] Paul Statkevich,[3] Peter F. Thall,[2] Michael L. Meyers,[3] Roy S. Herbst,[2] Reginald F. Munden,[2] Craig Tendler,[3] Yali Zhu,[3] Sandra Bangert,[2] Elizabeth Thompson,[2] Charles Lu,[2] Xue-Mei Wang,[2] Dong M. Shin,[2] Merrill S. Kies,[2] Vali Papadimitrakopoulou,[2] Frank V. Fossella,[2] Paul Kirschmeier,[3] W. Robert Bishop,[3] and Waun Ki Hong[2]

[1]Winship Cancer Institute, Emory University, Atlanta, Georgia; [2]The University of Texas M. D. Anderson Cancer Center, Houston, Texas; and [3]Schering-Plough Research Institute, Kenilworth, New Jersey

ABSTRACT

Purpose: To establish the maximum tolerated dose of lonafarnib, a novel farnesyltransferase inhibitor, in combination with paclitaxel in patients with solid tumors and to characterize the safety, tolerability, dose-limiting toxicity, and pharmacokinetics of this combination regimen.

Experimental Design: In a Phase I trial, lonafarnib was administered p.o., twice daily (b.i.d.) on continuously scheduled doses of 100 mg, 125 mg, and 150 mg in combination with i.v. paclitaxel at doses of 135 mg/m^2 or 175 mg/m^2 administered over 3 h on day 8 of every 21-day cycle. Plasma paclitaxel and lonafarnib concentrations were collected at selected time points from each patient.

Results: Twenty-four patients were enrolled; 21 patients were evaluable. The principal grade 3/4 toxicity was diarrhea (5 of 21 patients), which was most likely due to lonafarnib. dose-limiting toxicities included grade 3 hyperbilirubinemia at dose level 3 (100 mg b.i.d. lonafarnib and 175 mg/m^2 paclitaxel); grade 4 diarrhea and grade 3 peripheral neuropathy at dose level 3A (125 mg b.i.d. lonafarnib and 175 mg/m^2 paclitaxel); and grade 4 neutropenia with fever and grade 4 diarrhea at level 4 (150 mg b.i.d. lonafarnib and 175 mg/m^2 paclitaxel). The maximum tolerated dose established by the continual reassessment method was lonafarnib 100 mg b.i.d. and paclitaxel 175 mg/m^2. Paclitaxel appeared to have no effect on the pharmacokinetics of lonafarnib. The median duration of therapy was eight cycles, including seven cycles with paclitaxel. Six of 15 previously treated patients had a durable partial response, including 3 patients who had previous taxane therapy. Notably, two of five patients with taxane-resistant metastatic non-small cell lung cancer had partial responses.

Conclusions: When combined with paclitaxel, the recommended dose of lonafarnib for Phase II trials is 100 mg p.o. twice daily with 175 mg/m^2 of paclitaxel i.v. every 3 weeks. Additional studies of lonafarnib in combination regimens appear warranted, particularly in patients with non-small cell lung cancer.

INTRODUCTION

Mutations of the *ras* family of oncogenes that result in unregulated cell proliferation are common in human cancers (1). The *ras* mutations have been implicated in the development of colorectal cancer and have been associated with shortened survival in several tumor types, including non-small cell lung cancer (NSCLC; Refs. 2–6). *Ras* genes encode a protein, p21, that is located on the inner surface of the plasma membrane (1, 7). The p21 protein has GTPase activity and participates in signal transduction. Activation of the ras oncoprotein requires prenylation, a process that is catalyzed by farnesyltransferase (8–12).

Farnesyltransferase inhibitors (FTIs) are a novel class of compounds that block this critical enzymatic step in the formation of active ras proteins (8–13). Lonafarnib (Sarasar; Schering-Plough Corporation, Kenilworth, NJ) is a tricyclic nonpeptidomimetic compound (Fig. 1) that is active against a variety of tumors *in vitro* and in animal models of cancer (14). The antitumor activity of lonafarnib and other FTIs is related to the inhibition of farnesylation, although controversy currently surrounds the exact farnesylated proteins that are the key targets of FTIs (15, 16). For example, Ashar *et al.* (17) and Crespo *et al.* (18) have shown that FTIs have important effects on cell cycle arrest. The data of Crespo *et al.* suggest a direct effect on spindle formation with resultant prometaphase accumulation of mitotic lung cancer cells. Ashar *et al.* also showed that CENP-E and CENP-F, two centromeric proteins preferentially expressed in mitotic cells, are direct substrates for FTIs, and that their prenylation is completely inhibited by lonafarnib (19).

Compelling data reported by Moasser *et al.* supplied the scientific underpinning for our present study (20). They showed that, in several cell lines initially resistant to paclitaxel, the addition of a FTI enhanced the sensitivity of those cell lines to paclitaxel. Subsequent preclinical studies have demonstrated synergistic effects with lonafarnib plus paclitaxel on a number of human cell lines *in vitro* (21, 22) and enhanced activity *in vivo* (22). In the NCI-H460 lung cancer xenograft model, inhi-

Received 10/15/03; revised 12/16/03; accepted 1/9/04.
Grant support: F. Khuri was supported by Schering-Plough Research Institute and DAMD 17-02-1-0706.
The costs of publication of this article were defrayed in part by the payment of page charges. This article must therefore be hereby marked *advertisement* in accordance with 18 U.S.C. Section 1734 solely to indicate this fact.
Requests for reprints: Fadlo R. Khuri, Winship Cancer Institute, Emory University, 1365 Clifton Road NE, Building C-3094, Atlanta, GA 30322. Phone: (404) 778-4250; Fax: (404) 778-5520; E-mail: fkhuri@emory.edu.

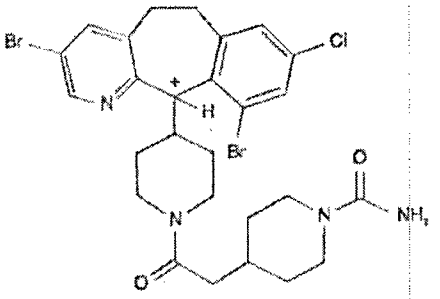


Fig. 1 Structure of lonafarnib [(11*R*)-4-[2-[4-(3,10-dibromo-8-chloro-6,11-dihydro-5*H*-benzo[5,6] cyclohepta [1,2b]pyridin-11yl)-1-piperazinyl]-2-oxoethyl]-1-piperidinecarboxamide].

bition of tumor growth was significantly greater with oral lonafarnib plus i.p. paclitaxel than with either agent alone (86% *versus* 52% and 61%, respectively; $P < 0.05$). Tumor growth inhibition on days 7 and 14 were 56 and 65% greater, respectively, with the combination than with paclitaxel alone. In line 69 wap-*ras*/F transgenic male mice, which develop paclitaxel-resistant mammary tumors at 6–9 weeks of age, oral lonafarnib significantly inhibited tumor growth ($P = 0.05$) and also sensitized the tumors to paclitaxel treatment, so that the combination of lonafarnib plus paclitaxel was more effective than lonafarnib alone ($P = 0.06$ for days 7 to 21; Refs. 22, 23). One proposed explanation for the synergistic activity is that treatment with FTI causes cells to accumulate in the G_2-M phase of the cell cycle in which paclitaxel is most effective (21, 24).

The main objectives of this trial were to establish the maximum tolerated dose (MTD) of lonafarnib, a novel FTI, in combination with paclitaxel in patients with solid tumors and to characterize the safety, tolerability, and dose-limiting toxic effects of this combination in patients with advanced solid malignancies. Furthermore, we particularly wanted to see whether durable responses could be achieved in a variety of taxane-sensitive tumors in patients previously treated with taxanes. Finally, we sought to characterize the pharmacokinetics of multiple-dose lonafarnib after its daily oral administration and of paclitaxel coadministered with daily lonafarnib.

PATIENTS AND METHODS

We sought to establish the MTD and the dose-limiting toxicity (DLT) of the lonafarnib/paclitaxel combination in adult patients with solid tumors. Previously treated patients and untreated patients were allowed to participate in the study. Eligibility criteria included a Karnofsky performance status of at least 70%, a histologically confirmed malignancy for which no curative treatment was available, measurable disease, and adequate hematological parameters [including a WBC count $\geq$ 3,000/mm^3, an absolute neutrophil count of 1,500/μl ($\geq 1.5 \times 10^9$/liter), a platelet count $\geq 100 \times 10^9$/liter, and a hemoglobin level $\geq$ 10 g/dl]. Furthermore, patients were required to have adequate renal function, with a serum creatinine level $\leq$ 1.5 times the upper limit of normal or a measured 12-h creatinine clearance time of $\geq$50 ml/min/1.73 m^2. Also mandatory were normal hepatic function (baseline transaminase levels $\leq$ 3 times the upper limit of normal, bilirubin $\leq$ 2.0 mg/dl, and albumin $\geq$ 3.0 g/dl) and no manifestations of a malabsorption syndrome. All patients had to sign a written informed consent approved by the Institutional Review Board at the University of Texas M. D. Anderson Cancer Center. Patients taking agents that might alter the metabolism of lonafarnib via the CYP3A4 hepatic enzymatic system (such as azoles, macrolides, cyclosporin, systemic corticosteroids, estrogens, antiseizure drugs, rifampin, or isoniazid), or who had metastases to the brain were excluded from the study.

Patients received lonafarnib capsules p.o. twice daily (b.i.d.) with food as 50-mg, 75-mg, and 100-mg formulations in combination with paclitaxel administered i.v. every 3 weeks at 135 mg/m^2 or 175 mg/m^2 over 3 h (Fig. 2). Premedication consisted of 20 mg i.v. dexamethasone and 8 mg of i.v. ondansetron.

Statistical Methods. The dose-finding portion of the trial was conducted in a group of patients with a variety of different head and neck and lung cancers. The principal scientific goal was to determine a MTD, defined as the dose level at which the toxicity rate was closest to 20% and less than 33% with at least 33% of patients experiencing dose-limiting toxicities (DLT) at the next higher level. DLT was defined as the following: absolute neutrophil count $< 500/\mu$l for longer than 5 days or with fever $\geq$ 38.3°C; grade 4 thrombocytopenia (platelets $< 25{,}000/\mu$l) or anemia (Hb $<$ 6.5 g/dl); grade 3–4 nausea/vomiting or grade 3 diarrhea despite optimal antiemetic or antidiarrheal treatment; or any other grade 3 treatment-related nonhematological toxicity; and treatment delay for toxicity lasting >2 weeks.

Associations between pairs of variables were assessed using the Fisher exact test, Kruskal-Wallis test, and Jonkheere-

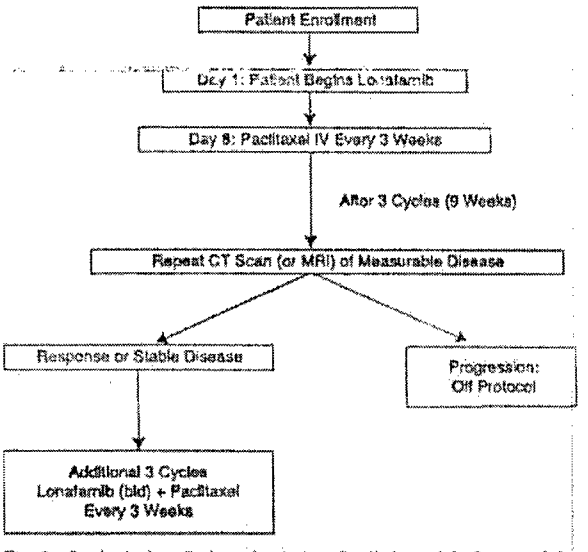


Fig. 2 Study design. Patients begin lonafarnib 1 week before receiving paclitaxel. Reevaluation occurs after every three cycles of treatment. If patients have responsive or stable disease, they proceed on study. If patients have progressive disease, they go off the study protocol. *CT*, computed tomography; *MRI*, magnetic resonance imaging.

Table 1 Number of patients and cycles by dose level of paclitaxel and lonafarnib in Phase I trial

Dose levels	Paclitaxel (mg/m²)	Lonafarnib (mg b.i.d.)	Cycles	No. of patients
1	135	50	0	0
2	135	100	1–9	3
			10–15	2
			16–32	1
3	175	100	1–3	9
			4–6	6
			7	5
			8	4
			9	2
			10–11	1
3A	175	125	1	5
			2–3	6
			4–6	5
			7–8	4
			9–10	3
			11–17	2
			18–24	1
4	175	150	1–2	4
			3–7	3
			8	2
			9–27	1

Terpstra test (25). Regression models of toxicity on the doses of paclitaxel and lonafarnib, and the indicator of prior chemotherapy, were fit using exact logistic regression (26, 27). Confidence intervals for probabilities of toxicity at particular dose and prior chemotherapy combinations were computed by repeating the exact logistic regression on 1000 bootstrap samples of the data. All of the computations were carried out using StatXact and SAS Proc Logistic.

Pharmacokinetic Methods. Plasma lonafarnib and paclitaxel concentrations were determined using validated liquid chromatography with tandem mass spectrometric detection and the high-performance liquid chromatography method, respectively. The lower limits of quantitation were 5.00 and 10.0 ng/ml plasma for lonafarnib and paclitaxel, respectively, and the linear ranges were 5.00–2500 ng/ml and 10.0–2500 ng/ml, respectively. The assay precision (% coefficient of variation) and accuracy (% Bias) were <11% and <10%, respectively, for lonafarnib, and <9% and <6%, respectively, for paclitaxel. Noninterference from the respective coadministered drug was demonstrated for both of the lonafarnib and paclitaxel methods.

Blood samples (~3 ml) for determination of plasma lonafarnib and paclitaxel concentrations were collected on day 1 of Cycle 1. Plasma was separated by centrifugation (4°C, ~3000 rpm for 15 min), then divided into two aliquots, and was stored frozen at −70°C until shipped to the analytical facility.

Individual plasma lonafarnib and paclitaxel concentrations were used for pharmacokinetic analysis using model-independent methods. The maximum plasma concentration (C_{max}) and time of maximum plasma concentration (T_{max}) were the observed values. The terminal phase rate constant (K) was calculated as the negative of the slope of the log-linear terminal portion of the plasma concentration-*versus*-time curve using linear regression. The terminal phase half-life, $t_{1/2}$, was calculated as $0.693/K$. The area under the plasma concentration-*versus*-time curve from time 0 to the time of final quantifiable sample ($AUC_{(tf)}$) and from time 0 to 12 h ($AUC_{(0-12\ h)}$) was calculated using the linear trapezoidal method. For paclitaxel, the $AUC_{(tf)}$ was extrapolated to infinity when appropriate as follows: $AUC_{(\infty)} = AUC_{(tf)} + C_{(tf)}/K$, where $C_{(tf)}$ is the estimated concentration determined from linear regression at time *tf*. Total body clearance, *CL/F* (lonafarnib) or *CL* (paclitaxel), was calculated by the following equation: CL/F = Dose/AUC. The apparent volume of distribution, *Vd/F* (lonafarnib) or *Vd* (paclitaxel), was calculated as: Vd/F = (Dose/AUC)/K.

For paclitaxel, the volume of distribution at steady state, *Vdss*, was estimated as total body clearance multiplied by mean residence time (*MRT*).

RESULTS

Twenty-four patients with a mean age of 58.3 years were enrolled on this Phase I study at the University of Texas M. D. Anderson Cancer Center, with the enrollment of new patients beginning on June 16, 1999, and continuing through March 30, 2000. Twenty-one patients actually received both paclitaxel and lonafarnib (Table 1). Patients were predominantly male (67%) and Caucasian (92%), with Karnofsky performance status of 90 to 100 (71%; Table 2). Slightly more than one-half of the patients had a primary diagnosis of NSCLC.

Toxicities. Among all of the dose levels, 92% of patients reported at least one toxicity at any grade and 54% of patients reported at least one grade 3/4 treatment-emergent nonhematological adverse event judged to be related to the study drugs. The most common treatment-related treatment-emergent nonhematological adverse events (including all grades) reported were gastrointestinal effects in 92% of patients (diarrhea 92%, nausea 79%, vomiting 50%, constipation 46%, stomatitis 38%, abdominal pain 29%); fatigue (88%), alopecia (83%), peripheral neuropathy (79%), arthralgia (71%), infections and infestations in 50% of patients (folliculitis 38%, oral candidiasis 13%, pneu-

Table 2 Patient demographics and disease characteristics

Subjects (n)	24
Age (yr)	
Median	59.5
Range	41–75
Sex	
Men	16 (67%)
Women	8 (33%)
Karnofsky performance status:	
Missing	1 (4%)
70–85	6 (25%)
90–100	17 (71%)
Histology	
NSCLC[a]	14 (58%)
Salivary	6 (25%)
HNSCC	4 (17%)
Prior chemotherapy (n = 21)	13
Prior taxane (n = 21)	9

[a] NSCLC, non-small cell lung cancer; HNSCC, head and neck squamous cell carcinoma.

Table 3 Number of patients with severe (grade 3) or life-threatening (grade 4) nonhematologic toxicities

	Dose level 2 (n = 3)		Dose level 3 (n = 9)		Dose level 3A (n = 5)		Dose level 4 (n = 4)	
Toxic effect	Grade 3	Grade 4	Grade 3	Grade 4	Grade 3	Grade 4	Grade 3	Grade 4
Bronchitis	0	0	0	0	1	0	0	0
Cardiac arrest	0	0	0	0	0	0	0	1
Chest wall pain	0	0	1	0	0	0	0	0
Diarrhea	0	0	2	0	1	1	2	0
Dysphagia	0	0	1	0	0	0	0	0
Dyspnea	0	0	0	0	1	0	0	0
Fatigue/weakness	0	0	0	0	0	0	2	0
Hyperglycemia	0	0	0	0	0	0	1	0
Neuropathy, peripheral	0	0	0	0	1	0	0	0
Fever	0	0	1	0	0	0	0	0
Infections (pneumonia)	0	0	0	0	1	0	0	0
Neoplasms, benign and malignant	0	0	1	0	0	0	0	0
Hyperbilirubinemia	0	0	1	0	0	0	0	0

Table 4 Number of patients with hematological toxicities by dose level during the treatment period

	Dose level 2			Dose level 3			Dose level 3A			Dose level 4		
Toxic effect	All	Gd[a] 3	Gd 4	All	Gd 3	Gd 4	All	Gd 3	Gd 4	All	Gd 3	Gd 4
Neutropenia	0	0	0	2	0	1	2	1	1	0	0	0
Leukopenia	1	1	0	4	1	1	3	1	0	1	1	0
Anemia	1	0	0	2	1	0	3	0	0	2	0	0

[a] Gd, grade.

monia 8%), respiratory system disorders (63%), anorexia (54%), rash (46%), weight decrease (29%); dizziness (25%); fever, blurred vision, liver and biliary system disorders, dehydration, myalgia, dry skin (21% each). All other adverse events occurred in fewer than 20% of patients. Grade 3 and grade 4 nonhematological toxicities by dose level are listed in Table 3.

Hematological toxicities occurred in 54% (13 of 24) of patients overall. Seven patients (29%) had grade 3/4 hematological toxicities. Table 4 shows that any grade and grade 3/4 anemia occurred in 34% (8 of 24) and 4% (1 of 24) of patients, respectively; any and grade 3/4 leukopenia occurred in 38% (9 of 24) and 21% (5 of 24) patients, respectively; and any and grade 3/4 neutropenia occurred in 17% (4 of 24) and 13% (3 of 24) of patients, respectively. Thrombocytopenia at any level was not observed in this study.

Both hematological and nonhematological toxic effects were generally mild and were neither more common nor more severe than those expected with paclitaxel. Patients had a median of one prior treatment with 13 of 22 evaluable patients having had prior chemotherapy including 9 who had a prior taxane (Table 2). Seven of the 9 patients previously treated with a taxane had disease progression on or within 3 months of taxane-based therapy, and 10 of 13 pretreated patients overall had progression of disease on or within 3 months of therapy.

Protocol-Defined DLTs. Overall, seven patients had DLTs as defined by protocol. No DLTs were seen at dose level 2. One patient at dose level 3 had grade 3 bilirubinemia. When the dose was escalated to level 4 (150 mg b.i.d. lonafarnib and 175 mg/m^2 paclitaxel) two of four patients had dose-limiting toxic effects in the first cycle (one grade 4 neutropenic fever, one grade 4 diarrhea). We then introduced dose level 3A (125 mg b.i.d. of lonafarnib, 175 mg/m^2 of paclitaxel) to determine whether an intermediate dose level would be tolerated. At this dose, two patients had grade 4 diarrhea in the first cycle. All of the DLTs were reversible on modification or cessation of treatment. On the basis of analysis of all available safety data, it has been determined that lonafarnib 100 mg b.i.d. and paclitaxel 175 mg/m^2 is appropriate for further evaluation in patients with NSCLC.

Table 5 Mean (percentage coefficient of variation) pharmacokinetic parameters of lonafarnib

Parameter	Dose level 2	Dose level 3	Dose level 3A	Dose level 4
C_{max}[a] (ng/ml)	760 (25)	960 (40)	1394 (35)	1267 (35)
Median T_{max} (h); range	5; 3–8	3; 0–10	8; 4–12	5; 3–6
AUC_{0-12h} (ng·h/ml)	5550 (51)	8789 (32)	12803 (36)	15443 (NA)
CL/F (ml/min)	364 (54)	207 (33)	181 (36)	165 (NA)
C_{min} (ng/ml)	286 (84)	524 (51)	883 (35)	1010 (47)

[a] C_{max}, maximum plasma concentration; T_{max}, time of maximum plasma concentration; AUC_{0-12h}, the area under the plasma concentration *versus* time curve from time 0 to 12 h; CL/F, total body clearance (lonafarnib); C_{min}, minimum plasma clearance.

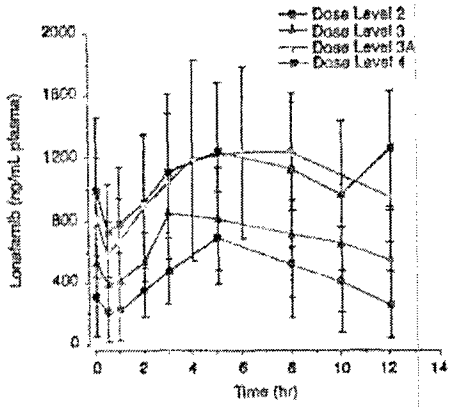


Fig. 3 Mean (±1 SD) plasma lonafarnib concentrations after multiple-dose oral administration of lonafarnib in combination with single-dose 3-h i.v. infusion of paclitaxel to patients with solid tumors.

Pharmacokinetics of Lonafarnib. Nineteen patients had samples collected for pharmacokinetic evaluations. Lonafarnib was slowly absorbed after oral administration with food. Median T_{max} ranged from 3 to 8 h (Table 5; Fig. 3). Half-life ($t_{1/2}$) could not be estimated in this study because of the lack of a definitive terminal phase in the plasma concentration-*versus*-time profiles after b.i.d. oral administration of lonafarnib with food (see Fig. 3). Mean plasma lonafarnib concentrations at 12 h after the dose were ~34–99% of the corresponding mean C_{max} values. The mean total body clearance ranged from 165 to 364 ml/min. The increases in lonafarnib *AUC* values were dose-related after oral administration of 100 mg, 125 mg, and 150 mg in combination with paclitaxel 175 mg/m^2. After administration of lonafarnib 100 mg with paclitaxel 175 mg/m^2, the mean lonafarnib C_{max} and *AUC* values were higher than those with paclitaxel 135 mg/m^2. However, given the variability of the data and sample size, the distribution of individual C_{max} and *AUC* values encompassed the same range, regardless of paclitaxel dose (Fig. 4). The C_{max} and *AUC* values obtained in this trial with lonafarnib 100 mg in combination with paclitaxel were similar to those obtained in previous Phase I trials in which lonafarnib 100 mg was administered alone (Table 6; Refs. 28–30). Thus, these observations suggest that a single dose of either 135 mg/m^2 or 175 mg/m^2 of paclitaxel did not affect the pharmacokinetics of lonafarnib.

Pharmacokinetics of Paclitaxel. Plasma paclitaxel concentrations (C_{max} and *AUC*) were similar among the dose groups for paclitaxel 175 mg/m^2 with lonafarnib 100 mg, 125 mg, and 150 mg (Table 7; Figs. 5 and 6). There appear to be no effects on paclitaxel pharmacokinetics at a dose of 175 mg/m^2 paclitaxel when the lonafarnib dose is increased from 100 mg to 150 mg. The relationships between dose and paclitaxel C_{max} or *AUC* values were disproportionate after the administration of paclitaxel 135 mg/m^2 and 175 mg/m^2 in combination with lonafarnib 100 mg; a 30% increase in paclitaxel dose resulted in an increase of ~74% in C_{max} and ~87% in *AUC*. This finding provided additional evidence for the nonlinear disposition for paclitaxel, as noted previously (31).

Plasma paclitaxel concentrations decreased rapidly immediately after cessation of the 3-h infusion, which was followed by a prolonged terminal phase (see Fig. 5). The mean terminal elimination $t_{1/2}$ of paclitaxel ranged from 12 to 19 h when blood samples were collected up to 48 h postdose for the first 17 patients. The mean $t_{1/2}$ was ~6 h when blood samples were collected up to 24 h postdose for patients 18–24 (see Table 7). The 6-h half-life was similar to that reported in the literature (31). The C_{max} and *AUC* values obtained in this study were similar to those previously reported when paclitaxel was given alone as a 3-h i.v. infusion (Table 8; Ref. 31).

Clinical Activity. The median number of treatment cycles on trial was eight, with a median of seven cycles containing paclitaxel. Activity was seen at the four dose levels studied (2, 3, 3A, and 4). Nine responses were durable, which we defined as a response detected at three or six cycles and confirmed at six or eight cycles, with median response duration of 6 months (range, 4–14 months). Most provocatively, we saw meaningful responses in three patients who had received prior taxane-based therapy, including two of five NSCLC patients who met the standard definition of taxane resistance (progression on or within 3 months

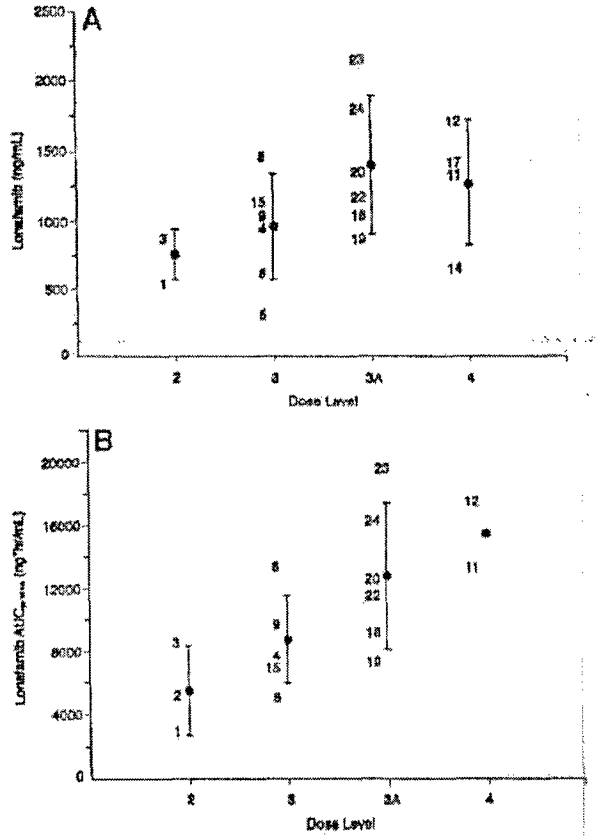


Fig. 4 Individual and mean (±1 SD) C_{max} (*A*) and $AUC_{0-12\ h}$ values (*B*) of lonafarnib after multiple-dose oral administration of lonafarnib in combination with single-dose 3-h i.v. infusion of paclitaxel to patients with solid tumors.

Table 6 Mean (coefficient of variation) pharmacokinetic parameters of lonafarnib after multiple-dose administration of lonafarnib 100 mg alone (previous Phase I studies) or in combination with paclitaxel (this study)

Study	Dose	*n*	C_{max}[a] (ng/ml)	AUC_{0-12} (ng·h/ml)
This study	100 + 135[b]	3	760 (25)	5550 (51)
This study	100 + 175[b]	8	960 (40)	8789[c] (32)
Eskens *et al.*[d]	100[e]	3	942 (58)	7299 (75)
Adjei *et al.*[f]	100	1	1680 (NA)	18295 (NA)
Hurwitz *et al.*[g]	100	2	784 (NA)	6221 (NA)

[a] C_{max}, maximum plasma concentration; AUC_{0-12}, the area under the plasma concentration - *versus* - time curve from time 0 to 12 h; NA, not appropriate (sample size < 3).
[b] Lonafarnib dose (mg) + paclitaxel dose (mg/m^2).
[c] $n = 6$.
[d] Ref. 34.
[e] Lonafarnib alone dose (mg).
[f] Ref. 32.
[g] Ref. 33.

Table 7 Mean (percentage coefficient of variation) pharmacokinetic parameters of paclitaxel

Parameter	Dose level 2	Dose level 3	Dose level 3A	Dose level 4
C_{max}[a] (ng/ml)	1937 (19)	3368 (55)	4258 (43)	3515 (38)
AUC_∞ (ng·h/ml)	9936 (7)	18563 (40)	17526 (38)	17634 (23)
$t_{1/2}$ (h)	18.6 (12)	13.3 (9)	5.62 (15)	12.1 (24)
CL (ml/min/m^2)	227 (8)	182 (43)	183 (33)	171 (19)
Vd (liter/m^2)	365 (7)	211 (47)	88.1 (35)	174 (9)
Vdss (liter/m^2)	130 (16)	90.6 (54)	40.2 (47)	66.9 (12)

[a] C_{max}, maximum plasma concentration; AUC_∞, area under the plasma concentration - *versus* - time curve from time 0 to the final quantifiable sample extrapolated to infinity; $t_{1/2}$, terminal phase half-life; *CL*, total body clearance; *Vd*, volume of distributions; *Vdss*, the volume of distribution at steady state.

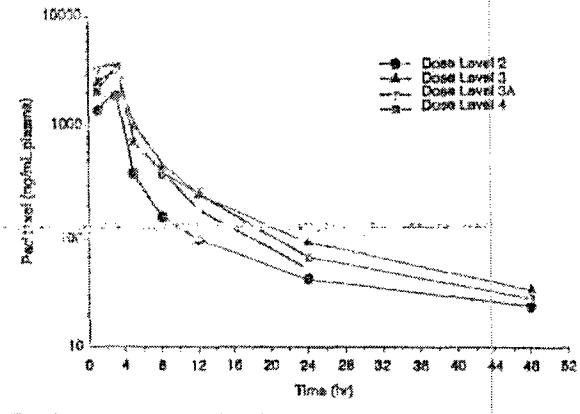


Fig. 5 Mean plasma paclitaxel concentrations after single-dose 3-h i.v. infusion of paclitaxel in combination with multiple-dose oral administration of lonafarnib to patients with solid tumors.

of taxane therapy). Only 4 of 21 patients had progressive disease by cycle 3, although all 21 patients had manifested disease progression within 3 months of study enrollment.

At the cycle-3 assessment interval, 7 patients demonstrated a partial response, 10 had minor responses or stable disease, and 4 had progressive disease (Table 9). Six of 7 responses were confirmed after six cycles. When total responses achieved on study were examined, 6 (50%) of the 12 patients with NSCLC achieved a partial response. In the setting of head and neck squamous cell carcinoma, two of the three patients had a partial response, and the one patient with a salivary gland tumor had prolonged disease stabilization and was treated for 30 cycles before disease progression. No significant associations were noted between response after three cycles or after six cycles and the dose of either lonafarnib ($P = 0.81$, $P = 0.70$, respectively) or paclitaxel ($P = 0.19$, $P = 0.32$, respectively).

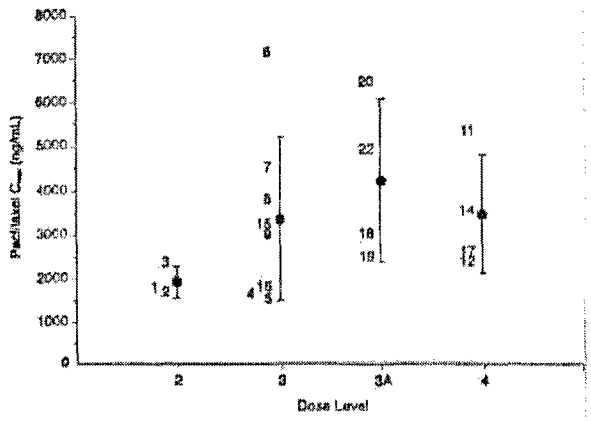


Fig. 6 Individual and mean (±1 SD) C_{max} values of paclitaxel after single-dose 3-h i.v. infusion of paclitaxel in combination with multiple-dose oral administration of lonafarnib to patients with solid tumors.

Table 8 Mean (coefficient of variation) pharmacokinetic parameters of paclitaxel after 3-h i.v. infusion of paclitaxel 135 mg/m² or 175 mg/m² in combination with multiple-dose lonafarnib 100 mg b.i.d., 125 mg b.i.d., or 150 mg b.i.d. (this study) or alone (previously reported study)

Dose	Study	*n*	C_{max} (ng/ml)	AUC_∞ (ng·h/ml)	*CL* (ml/min/m²)
135	This study	3	1937 (19)	9936 (7)	227 (8)
	Gianni *et al.*[a]	4	2818 (12)	9308 (10)	247 (9)
175	This study	16	3627 (46)	18309[c] (34)	179[c] (34)
	Gianni *et al.*[a]	3	5038 (15)	15797 (16)	190 (16)

[a] C_{max}, maximum plasma concentration; AUC_∞, area under the plasma concentration - *versus* - time curve from time 0 to the final quantifiable sample extrapolated to infinity; *CL*, total body clearance.
[b] Ref. 35.
[c] *n* = 15.

DISCUSSION

Other than the occasionally dose-limiting side effect of diarrhea, lonafarnib did not seem to contribute any significant side effects to those caused by paclitaxel. Patients with previous chemotherapy had a higher risk of toxicity. The substantial overlap of the eight 90% confidence intervals is due in large part to the small sample size ($n = 21$ evaluable patients). The only discernable trend with dose is an increase in the upper confidence limit with increasing total combined dose. Seven of the eight confidence intervals contain the targeted 30% toxicity rate. More precise estimates of the probability of toxicity would necessitate a larger sample size. The MTDs of lonafarnib and paclitaxel in this trial were lower than the doses recommended for either agent alone. The MTD of lonafarnib alone was determined to be 200 mg b.i.d. DLTs in studies of lonafarnib alone were generally similar to those seen in this trial and included reversible renal insufficiency (elevated creatinine levels), gastrointestinal symptoms (diarrhea, nausea, vomiting, anorexia), and hematological toxicities. Phase I studies of paclitaxel have demonstrated an MTD of 200 mg/m² for a single continuous infusion i.v. regimen. Myelosuppression and neurotoxicity are the primary DLTs of paclitaxel. Severe allergic reactions and skin rash associated with the vehicle (cremaphor EL) necessitate pretreatment with dexamethasone, diphenhydramine, and cimetidine or ranitidine.

No pharmacokinetic evidence was observed that either paclitaxel or lonafarnib enhanced the metabolism of the other agent. The pharmacokinetic values suggest that areas under the curve of both drugs were achieved in the active range. The target exposure for lonafarnib in clinical studies was to maintain a predose concentration in the range of 1–1.5 μM based on the concentration required to inhibit anchorage-independent growth of a series of human tumor cell lines.

We saw encouraging clinical activity in this Phase I study of combined paclitaxel and lonafarnib, confirming the preclinical activity previously reported for this combination (14, 20, 22, 32–34). Several Phase I studies of farnesyltransferase inhibitors have now been published (28–30, 35–39). Before this study, a total of two responses have been documented (one each with tipifarnib and lonafarnib) in previously treated patients with NSCLC (29, 36). The activity manifested with this protocol using fairly moderate doses of lonafarnib and paclitaxel is more

Table 9 Clinical activity of lonafarnib in combination with paclitaxel

After 3 Cycles	
Partial response	7 patients (3 previously treated with taxanes)
Minor response	3 patients
Stable disease	7 (4 previously treated with taxanes)
Progressive disease	4 (2 previously treated with taxanes)
Not assessed	3 (1 did not tolerate lonafarnib at 125 mg b.i.d.)
Median no. of total cycles on study:	8 (range, 2–30)
Median no. of paclitaxel courses on study:	7 (range, 2–30)
After 6 to 9 Cycles	
Partial response	8 patients (3 previously treated with taxanes)
Minor response	2 patients
Stable disease	6 (4 previously treated with taxanes)
Progressive disease	2 (2 previously treated with taxanes)
Not assessed	3
Median no. of total cycles on study:	8 (range, 2–30)
Median no. of paclitaxel courses on study:	7 (range, 2–30)
Any response by histology	
NSCLC[a]	12 patients (6 PR, 3 MR or StD, 3 PD)[b]
HNSCC	3 patients (2 PR, 1 StD)
Salivary	6 patients (1 PR, 4 StD, 1 PD)

[a] NSCLC, non-small cell lung cancer; PR, partial response; MR, minor response; StD, stable disease; PD, progressive disease; HNSCC, head and neck squamous cell carcinoma.
[b] Five patients (all NSCLC) were considered taxane-refractory/resistant. PRs were seen in 2 of 5 taxane-refractory/resistant NSCLC patients.

substantial. It is particularly heartening because little if any evidence exists to support the efficacy of paclitaxel as a second-line agent when administered as a 3-h infusion on a 3-week cycle (40–44).

The extent of disease stabilization that our trial revealed with this regimen was dramatic in an extensively pretreated heterogeneous patient population with progressive disease at the time of study enrollment. Recent evidence suggests that the stabilization of NSCLC may lead to clinically meaningful survival benefits.

In conclusion, this is the first reported clinical study of the combination of a taxane with a farnesyltransferase inhibitor in human solid tumors. Phase II trials of the combination as first-line and second-line therapy of stage III and IV NSCLC are ongoing to confirm or refute our data-driven hypothesis, namely, that lonafarnib may enhance taxane sensitivity and possibly overcome clinical taxane resistance in solid tumors.

ACKNOWLEDGMENTS

We thank Judie Wells for transcription and editing of the manuscript, Julie Starr for her expert editorial assistance, and Delores Curtis and Stephen Maxwell for bioanalytical support.

REFERENCES

1. Bos JL. ras oncogenes in human cancer: a review. Cancer Res 1989;49:4682–9. Erratum in: Cancer Res 1990;50:1352.

2. Slebos RJ, Kibbelaar RE, Dalesio O, et al. K-ras oncogene activation as a prognostic marker in adenocarcinoma of the lung. N Engl J Med 1990;323:561–5.

3. Rosell R, Li S, Skacel Z, et al. Prognostic impact of mutated K-ras in surgically resected non-small cell lung cancer patients. Oncogene 1993;8:2407–12.

4. Malats N, Porta M, Corominas JM, et al. Ki-ras mutations in exocrine pancreatic cancer: association with clinico-pathological characteristics and with tobacco and alcohol consumption. PANK-ras I Project Investigators. Int J Cancer 1997;70:661–7.

5. Sugio K, Molberg K, Albores-Saavedra J, et al. K-ras mutations and allelic loss at 5q and 18q in the development of human pancreatic cancers. Int J Pancreatol 1997;21:205–12.

6. Rall CJ, Yan YX, Greene-Cook F, et al. Ki-ras and p53 mutations in pancreatic ductal adenocarcinoma. Pancreas 1996;12:10–7.

7. Bollag G, McCormick F. Regulators and effectors of ras proteins. Ann Rev Cell Dev Biol 1991;7:601–32.

8. Gibbs JB. Lipid modifications of proteins in the ras superfamily. In: Birnbaumer L, Dickey B, editors. GTPases in biology. New York: Springer-Verlag; 1993. p. 335–44.

9. Hancock JF, Magee AI, Childs JE, Marshall CJ. All ras proteins are polyisoprenylated but only some are palmitoylated. Cell 1989;57:1167–77.

10. Hancock JF, Paterson H, Marshall CJ. A polybasic domain or palmitoylation is required in addition to the CAAX motif to localize p21ras to the plasma membrane. Cell 1990;63:133–9.

11. Jackson JH, Cochrane CG, Bourne JR, et al. Farnesol modification of Kirsten-ras exon 4B protein is essential for transformation. Proc Natl Acad Sci USA 1990;87:3042–6.

12. Kato K, Cox AD, Hisaka MM, et al. Isoprenoid addition of Ras protein is the critical modification for its membrane association and transforming activity. Proc Natl Acad Sci USA 1992;89:6403–7.

13. Rowinsky EK, Windle JJ, Von Hoff DD. Ras protein farnesyltransferase: a strategic target for anticancer therapeutic development. J Clin Oncol 1999;17:3631–52.

14. Liu M, Bryant MS, Chen J, et al. Antitumor activity of SCH 66336, an orally bioavailable tricyclic inhibitor of farnesyl protein transferase, in human tumor xenograft models and wap-ras transgenic mice. Cancer Res 1998;58:4947–56.

15. Cox AD, Der CJ. Farnesyltransferase inhibitors and cancer treatment: targeting simply ras? Biochim Biophys Acta 1997;1333:F51–71.

16. Du W, Prendergast GC. Activation of the PI3′K-AKT pathway masks the proapoptotic effects of farnesyltransferase inhibitors. Cancer Res 1999;59:4208–12.

17. Ashar HR, James L, Gray K, et al. The farnesyl transferase inhibitor SCH 66336 induces a G(2) → M or G(1) pause in sensitive human tumor cell lines. Exp Cell Res 2001;262:17–27.

18. Crespo NC, Ohkanda J, Yen TJ, Hamilton AD, Sebti SM. The farnesyltransferase inhibitor, FTI-2153, blocks bipolar spindle formation and chromosome alignment and causes prometaphase accumulation during mitosis of human lung cancer cells. J Biol Chem 2001;276:16161–7.

19. Ashar HR, James L, Gray K, et al. Farnesyl transferase inhibitors block the farnesylation of CENP-E and CENP-F and alter the association of CENP-E with the microtubules. J Biol Chem 2000;275:30451–7.

20. Moasser MM, Sepp-Lorenzino L, Kohl NE, et al. Farnesyl transferase inhibitors cause enhanced mitotic sensitivity to Taxol and epothilones. Proc Natl Acad Sci USA 1998;95:1369–74.

21. Nielsen LL, Shi B, Hajian G, et al. Combination therapy with the farnesyl protein transferase inhibitor SCH66336 and SCH58500 (p53 adenovirus) in preclinical cancer models. Cancer Res 1999;59:5896–901.

22. Shi B, Yaremko B, Hajian G, et al. The farnesyl protein transferase inhibitor SCH66336 synergizes with taxanes in vitro and enhances their antitumor activity in vivo. Cancer Chemother Pharmacol 2000;46:387–93.

23. Porter GM, Armstrong L, Nielsen LL. Strategy for developing transgenic assays for screening antineoplastic drugs that affect tubulin polymerization. Lab Anim Sci 1995;45:145–50.

24. Donaldson KL, Goolsby GL, Wahl AF. Cytotoxicity of the anticancer agents cisplatin and Taxol during cell proliferation and the cell cycle. Int J Cancer 1994;57:847–55.

25. Hirji, KF. Exact distributions for polytomous data. J Am Stat Assoc 1992;87:487–92.

26. Mehta CR, Patel NR, Jajoo B. Exact logistic regression: theory, methods and software. Technical report. Cambridge, MA: Cytel Software Corporation; 1993.

27. Mehta CR, Patel NR, Senchaudhuri, P. Efficient Monte Carlo methods for conditional logistic regression. J Am Stat Assoc 2000;95:99–108.

28. Adjei AA, Erlichman C, Davis JN, et al. A Phase I trial of the farnesyl transferase inhibitor SCH66336: evidence for biological and clinical activity. Cancer Res 2000;60:1871–7.

29. Hurwitz HI, Colvin OM, Petros WP, et al. Phase I and pharmacokinetic study of SCH66336, a novel FPTI, using a 2-week on, 2-week off schedule [abstract]. Proc Am Soc Clin Oncol 1999;18:599.

30. Eskens F, Awada A, Cutler D, et al. Phase I and pharmacokinetic study of the oral farnesyl transferase inhibitor SCH 66336 given twice daily to patients with advanced solid tumors. J Clin Oncol 2001;19:1167–75.

31. Gianni L, Kearns CM, Giani A, et al. Nonlinear pharmacokinetics and metabolism of paclitaxel and its pharmacokinetic/pharmacodynamic relationships in humans. J Clin Oncol 1995;13:180–90.

32. Kohl NE, Omer CA, Conner MW, et al. Inhibition of farnesyltransferase induces regression of mammary and salivary carcinomas in ras transgenic mice. Nat Med 1995;1:792–97.

33. Sun J, Qian Y, Hamilton AD, Sebti SM. Ras CAAX peptidomimetic FTI276 selectively blocks tumor growth in nude mice of a human lung carcinoma with K-Ras mutation and p53 deletion. Cancer Res 1995;55:4243–7.

34. Prendergast GC, Davide JP, deSolms SJ, et al. Farnesyltransferase inhibition causes morphological reversion of ras-transformed cells by a complex mechanism that involves regulation of the actin cytoskeleton. Mol Cell Biol 1994;14:4193–202.

35. Zujewski J, Horak ID, Bol CJ, et al. Phase I and pharmacokinetic study of farnesyl protein transferase inhibitor R115777 in advanced cancer. J Clin Oncol 2000;18:927–41.

36. Schellens JHM, de Klerk G, Swart M, et al. Phase I and pharmacologic study with the novel farnesyltransferase inhibitor (FTI) R115777 [abstract]. Proc Am Assoc Cancer Res 1999;40:4780.

37. Soignet S, Yao S-L, Britten C, et al. Pharmacokinetics and pharmacodynamics of the farnesyl protein transferase inhibitor (L-778, 123) in solid tumors [abstract]. Proc Am Assoc Cancer Res 1999;40:3413

38. Britten CD, Rowinsky E, Yao S-L, et al. The farnesyl protein transferase (FPTase) inhibitor L-78,123 in patients with solid cancers [abstract]. Proc Am Soc Clin Oncol 1999;18:597.

39. Hudes GR, Scholl J, Baab J, et al. Phase I clinical and pharmacokinetic trial of the farnesyltransferase inhibitor R115777 on a 21-day dosing schedule [abstract]. Proc Am Soc Clin Oncol 1999;18:601.

40. Huisman C, Smit EF, Giaccone G, Postmus PE. Second-line chemotherapy in relapsing or refractory non-small cell lung cancer: a review. J Clin Oncol 2000;18:3722–30.

41. Fossella FV, Lee JS, Shin DM, et al. Phase II study of docetaxel for advanced or metastatic platinum-refractory non-small cell lung cancer. J Clin Oncol 1995;13:645–51.

42. Gatzemeier U, von Pawel J, Gottfried M, et al. Phase III comparative study of high-dose cisplatin versus a combination of paclitaxel and cisplatin in patients with advanced non-small cell lung cancer. J Clin Oncol 2000;18:3390–9.

43. Socinski MA, Steagall A, Gillenwater H. Second-line chemotherapy with 96-hour infusional paclitaxel in refractory non-small cell lung cancer: report of a Phase II trial. Cancer Investig 1999;17:181–8.

44. Stewart DJ, Tomiak EM, Goss G, et al. Paclitaxel plus hydroxyurea as second-line therapy for non-small cell lung cancer. Lung Cancer 1996;15:115–23.

Vol. 10, 6119–6125, September 15, 2004

Value of $p16^{INK4a}$ and *RASSF1A* Promoter Hypermethylation in Prognosis of Patients with Resectable Non–Small Cell Lung Cancer

Jie Wang,[1,3] J. Jack Lee,[2] Luo Wang,[1] Diane D. Liu,[2] Charles Lu,[1] You-Hong Fan,[1] Waun Ki Hong,[1] and Li Mao[1]

[1]Department of Thoracic/Head and Neck Medical Oncology, and the [2]Department of Biostatistics, The University of Texas M. D. Anderson Cancer Center, Houston, Texas; and [3]Department of Oncology, Beijing University School of Oncology, Beijing Cancer Hospital, Beijing Institution of Cancer Research, Beijing, China

ABSTRACT

The $p16^{INK4a}$ and *RASSF1A* are tumor suppressor genes frequently inactivated by *de novo* promoter hypermethylation in non-small cell lung cancer. We studied 119 patients with non-small cell lung cancer (70 stage I/II and 49 stage IIIA) who had undergone surgery with curative intent. The $p16^{INK4a}$ and *RASSF1A* promoter methylation statuses were determined by methylation-specific PCR. Statistical analyses, all two-sided, were performed to determine the prognostic effect of hypermethylation on various clinical parameters. Hypermethylation of the $p16^{INK4a}$ and *RASSF1A* promoters was found in 58 (49%) and 46 (39%) tumors, respectively, and 30 tumors (25%) exhibited hypermethylation of both gene promoters. In patients with stage I/II tumors, only $p16^{INK4a}$ promoter hypermethylation was associated with a poor 5-year overall survival rate ($P = 0.002$). In patients with stage IIIA disease, however, *RASSF1A* promoter hypermethylation was a stronger predictor of a poor 5-year overall survival rate ($P < 0.0001$) than $p16^{INK4a}$ promoter hypermethylation. Among the 49 patients with stage IIIA tumors, 16 (89%) of the 18 patients whose tumors showed *RASSF1A* promoter hypermethylation died within 3 years after surgery, as compared with only 12 (39%) of the 31 patients whose tumors had no *RASSF1A* promoter hypermethylation ($P < 0.0001$). Multivariate analysis indicated that *RASSF1A* promoter hypermethylation was the stronger independent predictor for survival in patients with locally advanced non-small cell lung cancer. Our results indicate that $p16^{INK4a}$ promoter hypermethylation predicts a poor 5-year survival rates for patients with resectable non-small cell lung cancer, particularly for those with early stage tumors, whereas *RASSF1A* promoter hypermethylation is a profound prognostic predictor for patients with locally advanced non-small cell lung cancer, suggesting an important role of *RASSF1A* in non-small cell lung cancer progression.

INTRODUCTION

Non–small cell lung cancer constitutes 80% of all primary lung cancers, which are the leading cause of cancer-related death in both men and women in the United States (1). Despite advances in the treatment of the disease over the past two decades, the prognosis of patients with non-small cell lung cancer has improved only modestly, with the 5-year overall survival rate increasing from 11% in the 1970s to 15% in the late 1990s (2). Patients with early stage non-small cell lung cancer generally have a better survival than those with advanced-stage tumors. For example, patients with stage I non-small cell lung cancer are expected to have an approximate 60% 5-year overall survival rate after surgical resection of their primary tumors, whereas those with stage IIIA disease have an estimated 25% 5-year overall survival rate after surgery followed by radiation with or without chemotherapy.

Biological features of non-small cell lung cancer are determined by underlying molecular alterations of the tumors, including inactivation of the tumor suppressor genes (3–5). Besides mutations and deletions of genes, it is now clear that *de novo* promoter hypermethylation is a common mechanism to inactivate tumor suppressor genes (6–8). The $p16^{INK4a}$ tumor suppressor gene located on 9p21 encodes a cyclin-dependent kinase inhibitor important for G_1 cell cycle arrest (9, 10). Promoter hypermethylation of the gene has been observed frequently early in lung carcinogenesis, including in individuals exposed to tobacco carcinogens but without evidence of cancer (11–13). The *RASSF1A* tumor suppressor gene is located at 3p21, a region frequently deleted in non-small cell lung cancer (14). Another common mechanism to inactivate *RASSF1A* is promoter hypermethylation of the gene (15–17). RASSF1A has been shown to bind to the Ras-GTP binding protein Nore1, consistent with its role as a negative effector of Ras oncoprotein (18). In contrast to $p16^{INK4a}$, which is inactivated early in lung carcinogenesis (13, 19), hypermethylation of the *RASSF1A* promoter occurs relatively late (20), suggesting *RASSF1A* might be important in non-small cell lung cancer progression.

Because of the difference in timing between methylation of the $p16^{INK4a}$ and *RASSF1A* promoters in lung carcinogenesis, we wanted to determine the clinical impact of these abnormal-

Received 4/4/04; revised 5/28/04; accepted 6/15/04.
Grant support: Department of Defense Grant DAMD17-01-1-0689-1 and National Cancer Institute Grants PO1 CA91844, UO1 CA86390, and P30 CA 16672. J. Wang is a recipient of the Oncology Research Faculty Development Award, National Cancer Institute (USA).
The costs of publication of this article were defrayed in part by the payment of page charges. This article must therefore be hereby marked *advertisement* in accordance with 18 U.S.C. Section 1734 solely to indicate this fact.
Requests for reprints: Li Mao, Department of Thoracic/Head and Neck Medical Oncology, Unit 432, The University of Texas M. D. Anderson Cancer Center, 1515 Holcombe Boulevard, Houston, TX 77030. Phone: (713) 745-6363; Fax: (713) 796-8655; E-mail: lmao@mdanderson.org.
©2004 American Association for Cancer Research.

ities alone or in combination on patients with non-small cell lung cancer. We studied the primary tumors from 119 patients with surgically respectable, stage I-IIIA non-small cell lung cancer for their $p16^{INK4a}$ and *RASSF1A* promoter methylation status for associations between the methylation status and clinical parameters.

MATERIALS AND METHODS

Study Population. One hundred nineteen patients who were diagnosed with pathological stage I to IIIA non-small cell lung cancer and had undergone lobectomy or pneumonectomy for complete resection of their primary tumors at The University of Texas M. D. Anderson Cancer Center between 1994 and 2001 were included in the study. The selection of these patients was based on available fresh tumor tissues and corresponding normal lung tissues. The clinical information and follow-up data were based on chart review and on reports from our Tumor Registry Medical Informatics. Informed consent for the use of residual resected tissues for research was obtained from all of the patients in the study. The study was reviewed and approved by the Surveillance Committee of the institution. None of the patients with stage I or stage II disease received adjuvant chemotherapy or radiotherapy before or after surgery. Among 49 patients with stage IIIA disease, 5 received preoperative chemotherapy or chemoradiotherapy, 20 received postoperative concurrent chemoradiotherapy, 17 received postoperative radiotherapy alone, 2 received postoperative chemotherapy alone, and 5 received no additional treatment.

DNA Extraction and Methylation-Specific PCR. Frozen tissues were homogenized, and genomic DNA was extracted by digestion of the homogenized tissues in a buffer containing 50 mmol/L Tris-HCl (pH 8.0), 1% SDS, and 0.5 mg/ml proteinase K at 42°C for 36 hours. The digested products were purified with phenyl-chloroform twice. DNA was then precipitated using the EtOH precipitation method and recovered in distilled DNase-free water.

For the methylation-specific PCR, 1 μg of genomic DNA from each tissue sample was used in the initial step of chemical modification. Briefly, DNA was denatured by NaOH and treated with sodium bisulfite (Sigma Chemical Co., St. Louis, MO). After purification with Wizard DNA purification resin (Promega Corp., Madison, WI), the DNA was treated again with NaOH. After precipitation, DNA was recovered in water and prepared for PCR using specific primers for either the methylated or the unmethylated $p16^{INK4a}$ or *RASSF1A* promoter: p16-MAS (5′-ACCCGAC-CCCGAACCGCGACCGTAA-3′) and p16-MS (5′-TTATTAGAGGGTGGGGCGGATCG-CGTGC-3′) for the methylated $p16^{INK4a}$ promoter; p16-UAS (5′-CAAC-CCCAAACCACAA-CCATAA-3′) and p16-US (5′-TTATTA-GAGGGTGGGGTGGATTGT-3′) for the unmethylated $p16^{INK4a}$ promoter; RASSF1A-MAS (5′-GCTAACAAACGCGAACCG-3′) and RASSF1A-MS (5′-GGGTTTTGCGAGAGCGCG-3′) for the methylated *RASSF1A* promoter; and RASSF1A-UAS (5′-CACTAACAAACACAAACC-3′) and RASSF1A-US (5′-GGTTTTTGTGAGAGTGTGTT-TAG-3′) for the unmethylated *RASSF1A* promoter. PCR was carried out in 25 μL containing about 100 ng of modified DNA, 3% dimethyl sulfoxide, all four deoxynucleoside triphosphates (each at 200 μM), 1.5 mmol/L $MgCl_2$, 0.4 μM PCR primers, and 1.25 units of HotStar Taq DNA polymerase (Qiagen, Inc., Valencia, CA). DNA was amplified in 500-μl plastic tubes for 35 cycles at 94°C for 30 seconds, 56 to 64°C for 45 seconds, and 72°C for 60 seconds followed by a 5-minute extension at 72°C in a temperature cycler (Hybaid, Omnigene, Woodbridge, NJ). PCR products were separated on 2.5% agarose gels and visualized after staining with ethidium bromide. For each DNA sample, primer sets for methylated DNA and unmethylated DNA were used for analysis. CpGenomeTM universal methylated DNA (Chemicon International, Temecula, CA) was used as a positive control, and water replacing for DNA was used as blank controls. The hypermethylation status was determined by visualizing a 150-bp PCR product for the $p16^{INK4a}$ promoter and a 169-bp PCR product for the *RASSF1A* promoter with the respective methylation-specific primer sets. All PCRs were repeated twice, and the results were reproducible.

Statistical Analysis. The χ^2 test or Fisher's exact test were used to test the association between categorical variables. The Cochran-Armitage trend test was used to test the trend of methylation among differentiation levels. Overall survival, disease-specific survival (*i.e.*, survival rates among people who died of lung cancer-related causes specifically), and disease-free survival (*i.e.*, recurrence, metastasis, or cancer death was considered an event) were analyzed. Survival probability was estimated using the Kaplan-Meier method. The log-rank test was used to compare survival times among groups. Cox regression was used to model the risks of $p16^{INK4a}$ and/or *RASSF1A* promoter hypermethylation on survival time, with adjustment for clinical and histopathologic parameters (age, sex, tumor histology, tumor size, smoking status, and adjuvant treatment). All statistical tests were two-sided, and $P < 0.05$ was considered statistically significant.

RESULTS

Clinical characteristics of all patients enrolled in the study are summarized in Table 1. At the censor date of November 14, 2003, the median follow-up period was 51 months (range, 16 to 130 months). Of the 70 patients with stage I or stage II disease, 29 (41%) were still alive, 35 (50%) died of lung cancer, and 6 (9%) died of unrelated causes. No significant difference in 5-year overall, disease-specific, and disease-free survival rates were observed by tumor stage, gender, smoking status, differentiation status, and histologic subtype in this patient group. Among the 49 patients with stage IIIA disease, 18 (37%) were still alive, 29 (59%) died of lung cancer, and 2 (4%) died of unrelated causes. In this group of patients, smokers had significantly poorer 5-year survival rates than the nonsmokers did ($P = 0.047$, $P = 0.03$, and $P = 0.03$ for 5-year overall, disease-specific, and disease-free survival rates, respectively). Thirty-five (71%) of the 49 patients received postoperative radiotherapy with (26 patients, including 5 with preoperative chemotherapy) or without (9 patients) concomitant chemotherapy, whereas 14 patients received no adjuvant therapy after surgery.

Promoter methylation was detected in 58 (49%) and 46 (39%) of the tumor tissue for the $p16^{INK4a}$ and *RASSF1A* promoters, respectively, compared with 13 (11%, including 4

Table 1 Characteristics of patients and tumors

	$p16^{INK4a}$ promoter methylation		*RASSF1A* promoter methylation		
	Absent	Present	Absent	Present	Total
Patients	58 (49%)	61 (51%)	73 (61%)	46 (39%)	119 (100%)
Gender*					
Female	23 (49%)	24 (51%)	33 (70%)	14 (30%)	47 (39%)
Male	38 (53%)	34 (47%)	40 (56%)	32 (44%)	72 (61%)
Mean age (±SD) (y)	65.0 ± 10.9	63.5 ± 9.1	65.1 ± 10.2	63.0 ± 9.9	64.3 ± 10.1
Smoking status					
Nonsmoker	22 (58%)	16 (42%)	25 (66%)	13 (34%)	38 (32%)
Smoker	39 (48%)	42 (52%)	48 (59%)	33 (41%)	81 (68%)
Histologic type					
Adenocarcinoma	34 (57%)	26 (43%)	40 (67%)	20 (33%)	60 (50%)
Squamous cell carcinoma	23 (47%)	26 (53%)	27 (55%)	22 (45%)	49 (41%)
Large cell carcinoma	2 (29%)	5 (71%)	6 (86%)	1 (14%)	7 (6%)
Other	2 (67%)	1 (33%)	0 (0%)	3 (100%)	3 (3%)
Differentiation†					
Well	5 (45%)	6 (55%)	9 (82%)	2 (18%)	11 (9%)
Moderate	25 (50%)	25 (50%)	32 (64%)	18 (36%)	50 (42%)
Poor	31 (53%)	27 (47%)	32 (55%)	26 (45%)	58 (49%)
Stage					
I and II	37 (53%)	33 (47%)	42 (60%)	28 (40%)	70 (59%)
IIIA	24 (49%)	25 (51%)	31 (63%)	18 (37%)	49 (41%)
Stage I and II, 5-y overall survival	61.7%	28.3%	50.6%	41.1%	46.5%
Stage III, 5-y overall survival	53.5%	10.8%	45.6%	0%	30.8%

* Subset analysis indicated that male patients had a higher rate of *RASSF1A* promoter methylation than females in stage IIIa group ($P = 0.03$).

† Subset analysis indicated that poorly differentiated tumors had a higher rate of *RASSF1A* promoter methylation than well or moderately differentiated tumors in stage IIIa group ($P = 0.04$).

samples whose corresponding tumors lacked methylation of the $p16^{INK4a}$ promoter) and 4 (3%) in the corresponding normal-appearing lung tissues ($P < 0.0001$). Unmethylated promoters of $p16^{INK4a}$ and *RASSF1A* were detected in all of the normal-appearing lung tissues and in 60% of tumor tissues, most likely because of the presence of normal cells in the tumor samples. Examples of methylation-specific PCR results are shown in Fig. 1. The undetectable unmethylated promoter in some of the tumors might be because of highly enriched tumor cells in the tissues or the relatively low sensitivity of our assay to pick up small quantities of unmethylated molecules. In patients with stage I or stage II non-small cell lung cancer, tumors with methylation of the $p16^{INK4a}$ promoter had a higher frequency of *RASSF1A* promoter methylation than those without $p16^{INK4a}$ promoter methylation, 58% *versus* 24% ($P = 0.005$), suggesting that *RASSF1A* promoter methylation tends to occur in tumors with $p16^{INK4a}$ promoter methylation because *RASSF1A* promoter methylation occurs late in lung carcinogenesis (20).[4] However, this association was not significant in tumors from patients with stage IIIA disease (44% *versus* 29%, $P = 0.28$). Altogether, 30 tumors (25%; 19 stage I/II stage IIIA) showed concomitant methylation of both $p16^{INK4a}$ and *RASSF1A* promoters.

We analyzed the potential association between the methylation status of $p16^{INK4a}$ and *RASSF1A* promoters and sex, age, smoking history, histology, differentiation, and tumor stage. *RASSF1A* promoter methylation was more frequently observed in poorly differentiated tumors (50%) than in moderately differentiated (26%) or in well-differentiated tumors (0%; $P = 0.04$) from patients with stage IIIA non-small cell lung cancer, but there was no such association in tumors from patients with

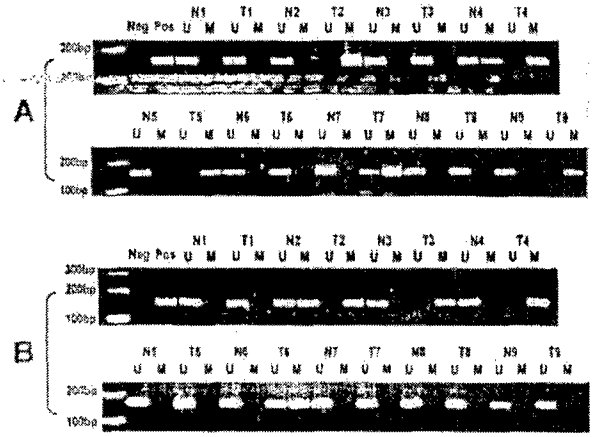


Fig. 1 Examples of promoter methylation status measured using methylation-specific PCR. *A*, PCR products of methylated or unmethylated $p16^{INK4a}$ promoter from primary non-small cell lung cancer and corresponding normal lung tissues. *B*, PCR products of methylated or unmethylated *RASSF1A* promoter from primary non–small cell lung cancer and corresponding normal lung tissues. Molecular weight markers are listed on left side. (*Neg*, negative controls using unmethylated DNA; *Pos*, positive controls using methylated DNA and methylation-specific primer sets; *T*, primary tumors; *N*, corresponding normal lung tissues; *U*, unmethylated promoter; *M*, methylated promoter.)

[4] L. Mao, unpublished data.

stage I/II disease ($P = 0.48$). Additionally, tumors from male patients with stage IIIA non-small cell lung cancer exhibited a significantly higher frequency of *RASSF1A* promoter methylation (47%) than did those from female patients (13%, $P = 0.03$).

We then analyzed the effect of $p16^{INK4a}$ and *RASSF1A* promoter methylation on the survival of the patient. Because stage IIIA patients often received adjuvant treatment after surgery, whereas stage I/II patients received only surgery, we analyzed the two groups separately. In the stage I/II group, patients whose tumors contained $p16^{INK4a}$ promoter methylation had significantly poorer 5-year overall, disease-specific, and disease-free survival rates ($P = 0.002$, $P = 0.0005$, and $P = 0.0006$, respectively) than did patients whose tumors had no $p16^{INK4a}$ promoter methylation (Fig. 2, *A–C*). However, the association between the *RASSF1A* promoter methylation status and 5-year survival rates was not statistically significant ($P = 0.09$, $P = 0.07$, and $P = 0.07$, respectively; Fig. 2, *D–F*). Multivariate analysis, including clinical parameters and promoter methylation status, indicated that $p16^{INK4a}$ promoter methylation was the only independent predictor of 5-year overall, disease-specific, and disease-free survivals. In patients with stage IIIA disease, in contrast to those with stage I/II tumors, the *RASSF1A* promoter methylation status was strongly associated with 5-year overall, disease-free, and disease-specific survivals ($P < 0.0001$, $P < 0.0001$, and $P = 0.0006$, respectively; Fig. 3, *A–C*), as was the $p16^{INK4a}$ promoter methylation status ($P = 0.003$, $P = 0.002$, and $P = 0.01$, respectively; Fig. 3, *D–F*). Although both *RASSF1A* and $p16^{INK4a}$ promoter methylation status were independent predictors of survival, *RASSF1A* was a stronger predictor for 5-year overall, disease-specific, and disease-free survival (hazard ratio = 4.76, $P < 0.0001$; hazard ratio = 6.29, $P < 0.0001$; and hazard ratio = 3.41, $P = 0.0007$ *versus* hazard ratio = 2.89, $P = 0.007$; hazard ratio = 3.16, $P = 0.005$, and hazard ratio = 2.36, $P = 0.02$, respectively).

To determine whether *RASSF1A* inactivation might have an added biological value in patients whose tumors also carried $p16^{INK4a}$ promoter methylation, we analyzed the 5-year survival rates of the group whose tumors had methylation of both gene promoters. In patients with stage I/II disease, the 5-year survival rates of patients whose tumors had methylation of both promot-

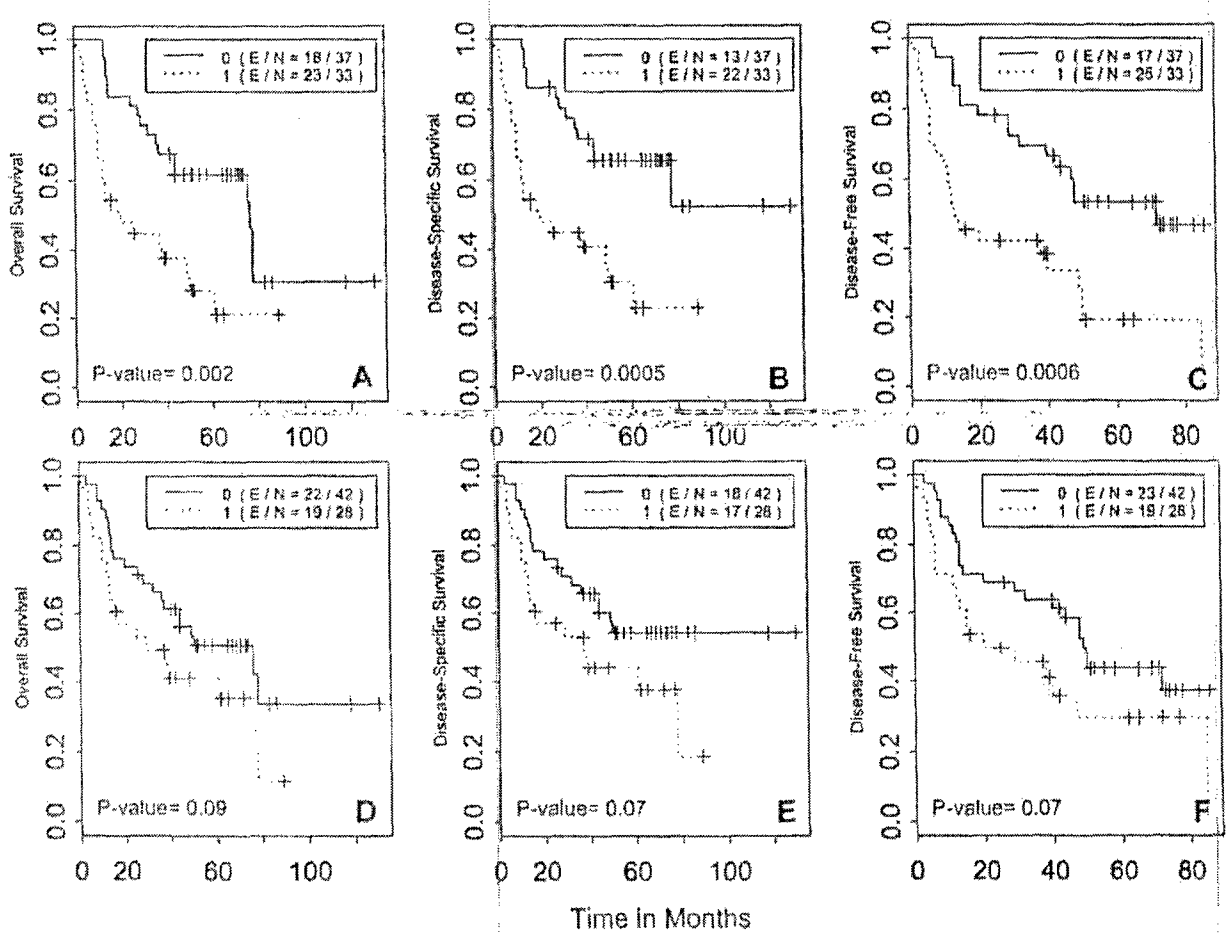


Fig. 2 Association between the $p16^{INK4a}$ promoter methylation status (*A–C*) or *RASSF1A* promoter methylation status (*D–F*) and overall, disease-specific, and disease-free survival in patients with stage I/II non–small cell lung cancer. (*0*, groups without methylation of promoter; *1*, groups with methylation of promoter; *E/N*, number of events/total number in each group.)

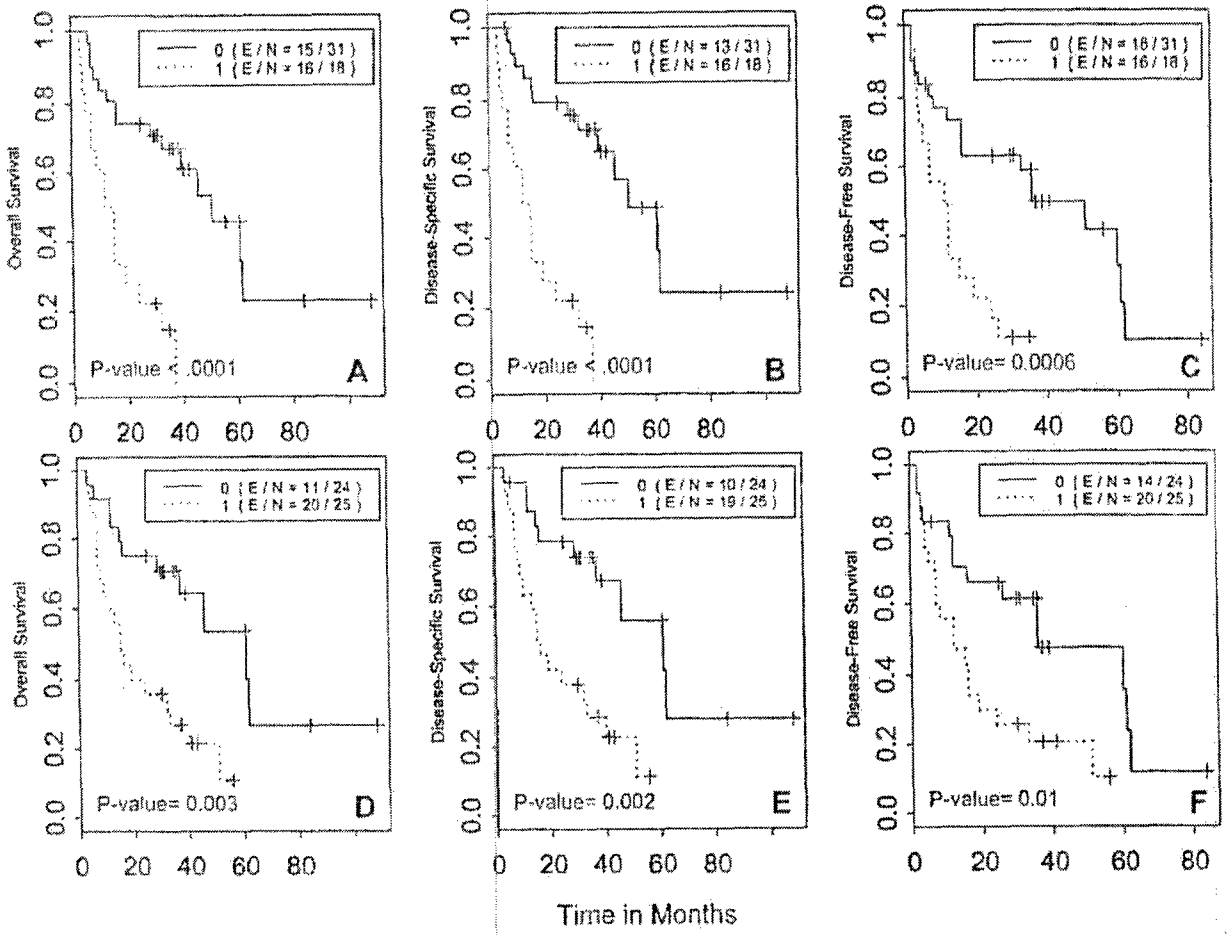


Fig. 3 Association between the *RASSF1A* promoter methylation status (*A–C*) or $p16^{INK4a}$ promoter methylation status (*D–F*) and overall, disease-specific, and disease-free survival in patients with stage IIIA non-small cell lung cancer. (*0*, groups without methylation of promoter; *1*, groups with methylation of promoter; *E/N*, number of events/total number in each group.)

ers were significantly worse than in patients whose tumors had no promoter methylation or methylation of only one promoter ($P = 0.01$, $P = 0.005$, and $P = 0.005$, respectively, for 5-year overall, disease-specific, and disease-free survival rates; Fig. 4, *A–C*). Although the number of patients was small in the stage IIIA group, the association between patients whose tumors had methylation of both promoters and poor survivals was striking (Fig. 4, *D–F*). All 11 patients (100%) in this category died of lung cancer within 3 years after surgery, whereas 13 (62%) of the 21 stage IIIA patients whose tumors had methylation of only one promoter died of lung cancer in 5 years, and only 5 (29%) of the 17 patients whose tumors had no promoter methylation died of lung cancer in 6.5 years ($P < 0.0001$ by log-rank test; Fig. 4*F*).

Because 35 (71%) of the 49 patients with stage IIIA tumors received postoperative radiotherapy and 26 (53%) of the patients received adjuvant chemotherapy, we wanted to determine whether these treatments had affected the predictive value of the methylation markers. Despite the small sample size, *RASSF1A* promoter methylation status remained a predictor of overall survival in radiotherapy and nonradiotherapy groups ($P = 0.0004$ and $P = 0.008$, respectively, for overall survival) as well as in chemotherapy and nonchemotherapy groups ($P = 0.001$ and $P = 0.01$, respectively, for overall survival).

DISCUSSION

The $p16^{INK4a}$ is frequently inactivated in non-small cell lung cancer through various mechanisms, including promoter hypermethylation (8, 11, 12, 21), but not in small cell lung cancers, which often have an inactivated retinoblastoma tumor suppressor gene. The reported frequencies of $p16^{INK4a}$ promoter hypermethylation in primary non-small cell lung cancer have been 25 to 63% (12, 22–24). The $p16^{INK4a}$ promoter hypermethylation is an early event in lung carcinogenesis even in bronchial epithelial cells chronically exposed to tobacco carcinogens (13). RASSF1A contains an RAS-associated domain, which interacts with the RAS oncoprotein to promote cellular apoptosis as well as to inhibit cyclin D1 accumulation (25, 26), and a putative ataxia telangiectasia, mutated kinase phosphoryl-

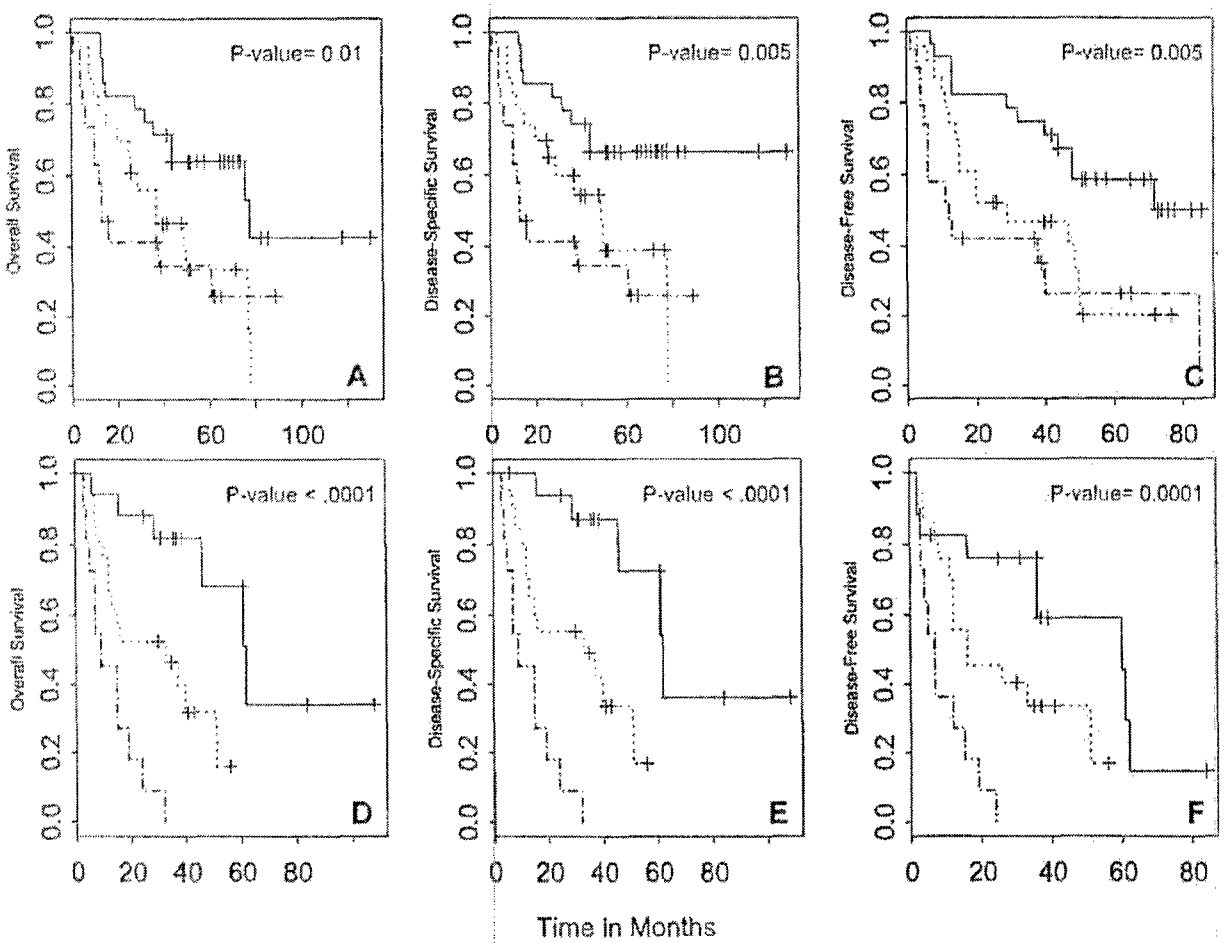


Fig. 4 Association between the $p16^{INK4a}$ promoter methylation status and/or *RASSF1A* promoter methylation status and overall survival in patients with stage I/II (*A–C*) or stage IIIA (*D–F*) non-small cell lung cancer. *Solid line* indicates groups without promoter methylation [number of events/total in group (*E/N*): 12 of 28 for *A*; 9 of 28 for *B*; 12 of 28 for *C*; 6 of 17 for *D*; 5of 17 for *E*; and 9 of 17 for *F*]; *dotted line* indicates groups with methylation of the $p16^{INK4a}$ or the *RASSF1A* promoter (*E/N*: 16 of 23 for *A*; 13 of 23 for *B*; 16 of 23 for *C*; 14 of 21 for *D*; 13 of 21 for *E*; and 14 of 21 for *F*); *dashed line* indicates groups with methylation of both promoters (*E/N*: 13 of 19 for *A*; 13 of 19 for *B*; 14 of 19 for *C*; and 11 of 11 for *D–F*).

ation consensus site, which links RASSF1A to DNA-damage response (27). RASSF1A has been found to directly bind and stabilize microtubule structures, suggesting a role of the protein in maintaining genome stability (28). It was shown in a recent study that RASSF1A regulates mitosis by inhibiting the APC-cdc20 complex (29). Although mutation of *RASSF1A* is rarely found in non-small cell lung cancer, the gene is located at 3p21, a region frequently deleted in non-small cell lung cancer, and its promoter is frequently (30 to 38%) hypermethylated in primary non-small cell lung cancer (17, 30, 31). In contrast with $p16^{INK4a}$, hypermethylation of the *RASSF1A* promoter is rarely detected in bronchial epithelial cells chronically exposed to tobacco carcinogens (18), suggesting this is a late event in carcinogenesis. In this study, the much lower frequency (3% *versus* 11%) of *RASSF1A* promoter hypermethylation compared with $p16^{INK4a}$ promoter hypermethylation detected in the adjacent normal-appearing lung tissues from patients with non-small cell lung cancer supports this notion.

In patients with early stage non-small cell lung cancer, $p16^{INK4a}$ promoter methylation was a predictor of the clinical outcome of the patient (Fig. 2, *A–C*), which is consistent with earlier reports analyzing either $p16^{INK4a}$ promoter methylation or $p16^{INK4a}$ protein expression and clinical outcome in patients with early stage non-small cell lung cancer (11, 32, 33). Two previous reports showed that patients with stage I/II non-small cell lung cancer that contained *RASSF1A* promoter methylation associated with adverse survival (31, 34). Although the association was not statistically significant in this study, patients whose stage I/II tumors carried *RASSF1A* promoter methylation had poorer 5-year survival rates (Fig. 2, *D–F*).

One of the interesting findings in our study was that patients with stage IIIA disease whose tumors carried *RASSF1A* promoter methylation had extremely poor 5-year survival rates compared with those without the abnormality. This was in contrast to the findings in patients with stage I/II disease (Figs. 2 and 3). Interestingly, in the locally advanced tumors, $p16^{INK4a}$

promoter methylation and *RASSF1A* promoter methylation were not associated ($P = 0.28$; Table 1), again in contrast with data for stage I/II tumors. These results suggest that inactivation of *RASSF1A* together with additional molecular alterations that occur between the early stage and locally advanced stage of non-small cell lung cancer renders the tumors extremely aggressive. It should be noted that *RASSF1A* methylation was not associated with survival in patients with stage III non-small cell lung cancer in a previous report (34). But that study had a smaller sample size and lower rate of methylation frequency compared with stage I/II tumors (34% *versus* 54%) in the same study (34). Additional studies are therefore needed to validate our findings.

The finding that patients with methylation of both gene promoters had a poorer 5-year overall, disease-specific, and disease-free survival rate than did those with only $p16^{INK4a}$ or *RASSF1A* promoter methylation (Fig. 4, *A–C*) suggests that the inactivation of *RASSF1A* might make the tumor cells more aggressive. This dose-dependent correlation between the methylation status and survivals among patients with no methylation in any of the two promoters, with methylation in only one promoter, and with methylation of both promoters was even more profound (Fig. 4, *D–F*). If validated, these epigenetic abnormalities may be useful biomarkers for molecular classification of patients with stage IIIA non-small cell lung cancer as well as reasonable therapeutic targets.

ACKNOWLEDGMENTS

We thank Sarah Taylor in Tumor Registry Medical Informatics for providing follow-up information and Rachel Williams in Scientific Publication for editing.

REFERENCES

1. Greenlee RT, Hill-Harmon MB, Murray T. Cancer statistics, 2001. CA - Cancer J Clin 2001;51:15–36.

2. Greenlee RT, Murray T, Bolden S, Wingo PA. Cancer statistics, 2000. CA - Cancer J Clin 2000;50:7–33.

3. Nikliński J, Niklińska W, Laudański J. Prognostic molecular markers in non-small cell lung cancer. Lung Cancer 2001;34:S53–8.

4. Fong KM, Sekido Y, Gazdar AF. Lung cancer Molecular biology of lung cancer: clinical implications. Thorax 2003;58:892–900.

5. Hirsch FR, Franklin WA, Gazdar AF, Bunn PA Jr. Early detection of lung cancer: clinical perspectives of recent advances in biology and radiology. Clin Cancer Res 2001;7:5–22.

6. Zochbauer-Muller S, Gazdar AF, Minna JD. Molecular pathogenesis of Lung cancer. Annu Rev Physiol 2002;64:681–708.

7. Forgacs E, Zochbauer-Muller S, Olah E, Minna JD. Molecular genetic abnormalities in the pathogenesis of human lung. Pathol Oncol Res 2001;7:6–13.

8. Merlo A, Herman JG, Mao L, et al. 5' CpG island methylation is associated with transcriptional silencing of the tumor suppressor p16/CDKN2/MTS1 in human cancers. Nat Med 1995;1:686–92.

9. Zhang HS, Postigo AA, Dean DC. Active transcriptional repression by the Rb-E2F complex mediates G1 arrest triggered by p16INK4a, TGFbeta, and contact inhibition. Cell 1999;97:53–61.

10. Koh J, Enders GH, Dynlacht BD, Harlow E. Tumour-derived p16 alleles encoding proteins defective in cell-cycle inhibition. Nature (Lond) 1995;375:506–10.

11. Kim DH, Nelson HH, Wiencke JK, et al. p16(INK4a) and histology-specific methylation of CpG islands by exposure to tobacco smoke in non-small cell lung cancer. Cancer Res 2001;61:3419–24.

12. Toyooka S, Toyooka KO, Maruyama R, et al. DNA methylation profiles of lung tumors. Mol Cancer Ther 2001;1:61–7.

13. Soria JC, Rodriguez M, Liu DD, et al. Aberrant promoter methylation of multiple genes in bronchial brush samples from former cigarette smokers. Cancer Res 2002;62:351–5.

14. Brauch H, Johnson B, Hovis J, et al. Molecular analysis of the short arm of chromosome 3 in small-cell and non-small-cell carcinoma of the lung. N Engl J Med 1987;317:1109–13.

15. Dammann R, Li C, Yoon JH, et al. Epigenetic inactivation of a Ras association domain family protein from the lung tumour suppressor locus 3p21.3h. Nat Genet 2000;25:315–9.

16. Pfeifer GP, Yoon JH, Liu L, et al. Methylation of the RASSF1A gene in human cancers. Biol Chem 2002;383:907–14.

17. Burbee DG, Forgacs E, Zochbauer-Muller S, et al. Epigenetic inactivation of RASSF1A in lung and breast cancers and malignant phenotype suppression. J Natl Cancer Inst (Bethesda) 2001;93:691–9.

18. Ortiz-Vega S, Khokhlatchev A, Nedwidek M, et al. The putative tumor suppressor RASSF1A homodimerizes and heterodimerizes with the Ras-GTP binding protein Nore1. Oncogene 2002;21:1381–90.

19. Belinsky SA, Nikula KJ, Palmisano WA, et al. Aberrant methylation of $p16^{INK4a}$ is an early event in lung cancer and a potential biomarker for early diagnosis. Proc Natl Acad Sci USA 1998;95:11891–6.

20. Belinsky SA, Palmisano WA, Gilliland FD, et al. Aberrant promoter methylation in bronchial epithelium and sputum from current and former smokers. Cancer Res 2002;62:2370–7.

21. Cairns P, Mao L, Merlo A, et al. Rates of p16 (MTS1) mutations in primary tumors with 9p loss. Science (Wash DC) 1994;265:415–7.

22. Esteller S, Corn PG, Baylin SB, Herman JG. A gene hypermethylation profile of human cancer. Cancer Res 2001;61:3225–9.

23. Kaye FJ. RB and cyclin dependent kinase pathways defining a distinction between RB and P16 loss in lung cancer. Oncogene 2002; 21:6908–14.

24. Zochbauer-Muller S, Fong KM, Virmani AK, et al. Aberrant promoter methylation of multiple genes in non-small cell lung cancers. Cancer Res 2001;61:249–55.

25. Khokhlatchev A, Rabizadeh S, Xavier R, et al. Identification of a novel RAS regulated proapoptotic pathway. Curr Biol 2002;12:253–65.

26. Shivakumar L, Minna J, Sakamaki T, Restell R, White MA. The RASSF1A tumor suppressor blocks cell cycle progression and inhibits cyclin D1 accumulation. Mol Cell Biol 2002;22:4309–18.

27. Kim ST, Lim DS, Canman CE, Kastan MB. Substrate specificities and identification of putative substrates of ATM kinases family members. J Biol Chem 1999;274:37538–43.

28. Liu L, Tommasi S, Lee DH, Dammann R, Pfeifer GP. Control of microtubule stability by the RASSF1A tumor suppressor. Oncogene 2003;22:8125–36.

29. Song MS, Song SJ, Ayad NG, et al. The tumour suppressor RASSF1A regulates mitosis by inhibiting the APC-Cdc20 complex. Nat Cell Biol 2004;6:129–37.

30. Agathanggelou A, Honorio S, Macartney DP, et al. Methylation associated inactivation of RASSF1A from region 3p21.3 in lung, breast and ovarian tumor. Oncogene 2001;20:1509–18.

31. Tomizawa Y, Kohno T, Kondo H, et al. Clinicopathological significance of epigenetic inactivation of RASSF1A at 3p21.3 in stage I lung adenocarcinoma. Clin Cancer Res 2002;8:2362–8.

32. Gonzalez-Quevedo R, Iniesta P, Moran A, et al. Cooperative role of telomerase activity and p16 expression in the prognosis of non-small-cell lung cancer. J Clin Oncol 2002;20:254–62.

33. Jin M, Inoue S, Umemura T, et al. Cyclin D1, p16 and retinoblastoma gene product expression as a predictor for prognosis in non-small cell lung cancer at stages I and II. Lung Cancer 2001;34:207–18.

34. Endoh H, Yatabe Y, Shimizu S, et al. RASSF1A gene inactivation in non-small cell lung cancer and its clinical implication. Int J Cancer 2003;106:45–51.

VOLUME 22 · NUMBER 22 · NOVEMBER 15 2004

JOURNAL OF CLINICAL ONCOLOGY

ORIGINAL REPORT

Prognostic Factors in Resected Stage I Non–Small-Cell Lung Cancer: A Multivariate Analysis of Six Molecular Markers

Charles Lu, Jean-Charles Soria, Ximing Tang, Xiao-Chun Xu, Luo Wang, Li Mao, Reuben Lotan, Bonnie Kemp, B. Nebiyou Bekele, Lei Feng, Waun K. Hong, and Fadlo R. Khuri

From the Departments of Thoracic/Head and Neck Medical Oncology, Clinical Cancer Prevention, Pathology, and Biostatistics, The University of Texas M.D. Anderson Cancer Center, Houston, TX; Institut Gustave Roussy, Villejuif, France; and Winship Cancer Institute, Emory University, Atlanta, GA.

Submitted January 13, 2004; accepted August 25, 2004.

Supported in part by National Cancer Institute grant No. K12 CA088084 and the Department of Defense, Biology, Education, Screening, Chemoprevention, and Treatment of Lung Cancer grant No. DAMD17-01-1-0685 and Translational Approaches for the Reversal, Genetic, Evaluation and Treatment of Lung Cancer grant No. DAMD17-02-1-0706.

Presented in part at the 93rd Annual Meeting of the American Association for Cancer Research, San Francisco, CA, April 6-10, 2002.

Authors' disclosures of potential conflicts of interest are found at the end of this article.

Address reprint requests to Charles Lu, MD, SM, The University of Texas M.D. Anderson Cancer Center, 1515 Holcombe Boulevard, Box 432, Houston, TX 77030-4009; e-mail: chu@mdanderson.org.

© 2004 by American Society of Clinical Oncology

0732-183X/04/2222-4575/$20.00

DOI: 10.1200/JCO.2004.01.091

ABSTRACT

Purpose

To analyze the prognostic significance of six molecular biomarkers (death-associated protein kinase [*DAPK*] promoter methylation, interleukin-10 [IL-10] protein expression, cyclooxygenase-2 [COX-2] mRNA expression, human telomerase reverse transcriptase catalytic subunit [hTERT] mRNA expression, retinoic acid receptor-beta [RAR-β] mRNA expression, and K-*ras* mutational status) in stage I non–small-cell lung cancer (NSCLC) patients.

Patients and Methods

Biomarker analyses were performed on tumors from 94 patients with stage I NSCLC who underwent surgical resection at our institution. A minimum follow-up period of 5 years was required. *DAPK* methylation was assessed by methylation-specific polymerase chain reaction (PCR). RAR-β, COX-2, and hTERT mRNA levels were determined by in situ hybridization with digoxigenin-labeled antisense riboprobes. K-*ras* mutation status was determined by the PCR–primer introduced restriction with enrichment for mutant alleles method. IL-10 protein expression was analyzed by immunohistochemistry using a polyclonal antihuman IL-10 antibody. Cancer-specific survival was analyzed with a Cox proportional hazards model. To identify independent prognostic factors, a stepwise selection method was used.

Results

DAPK methylation, IL-10 lack of expression, COX-2 expression, hTERT expression, RAR-β expression, and K-*ras* mutations were observed in 46.8%, 29.8%, 59.6%, 34.0%, 23.4%, and 34.0% of patients, respectively. In the final model, *DAPK* methylation and IL-10 lack of expression were significant negative prognostic factors for cancer-specific survival, whereas COX-2 expression was of borderline significance.

Conclusion

In this cohort of resected stage I NSCLC patients, molecular markers that independently predict cancer-specific survival have been identified. The prognostic roles of *DAPK* methylation, IL-10, and other biomarkers in NSCLC merit further investigation.

J Clin Oncol 22:4575-4583. © 2004 by American Society of Clinical Oncology

Lung cancer remains a worldwide public health issue of immense proportions. In the year 2003, cancers of the lung and bronchus are expected to continue to account for the most cancer deaths in the United States (157,200 deaths or 28.2%), more than the estimated total number of deaths as a result of cancers of the breast, prostate, colon, and rectum combined.[1] Approximately 80% of lung cancers will have non–small-cell carcinoma histology.[2]

Approximately 25% of patients present with early-stage disease.[3] The standard treatment is surgical resection with appropriate lymph node sampling or dissection. Although early-stage non–small-cell lung

Downloaded from www.jco.org at M D ANDERSON HOSP on March 23, 2005.
Copyright © 2004 by the American Society of Clinical Oncology. All rights reserved.

cancer (NSCLC) patients have a relatively favorable prognosis, the risk of disease recurrence and death remains substantial. Five-year survival rates for pathologic stages I and II disease are 57% to 67% and 38% to 55%, respectively.[4] Identification of reliable prognostic factors for disease recurrence and death could have significant clinical import. Patients in a high-risk group, for example, would be appropriate candidates for novel adjuvant or chemoprevention strategies.

Both our group[5-12] and others[13-16] have focused on identifying molecular prognostic factors in early-stage NSCLC. We have established a retrospective cohort of stage I NSCLC patients who underwent surgical resection at our institution. Over the past few years, investigators in our group have analyzed a number of tumor biomarkers within this valuable clinical research database.

Given the roles that retinoids play in the regulation of cell growth, differentiation, and apoptosis, Khuri et al[8] investigated the prognostic significance of retinoic acid receptor-beta (RAR-β) mRNA expression in 156 patients. Because RAR-β expression seems to be suppressed during carcinogenesis, these investigators hypothesized that lower RAR-β levels would predict a poor clinical outcome. Surprisingly, overall survival was significantly worse in patients with strongly positive RAR-β expression. Because one RAR-β isoform, RAR-β4, may promote hyperplasia and neoplasia,[17] the authors hypothesized that differential expression of RAR-β isoforms may be a possible explanation for their unexpected findings.

Khuri et al[9] subsequently evaluated cyclooxygenase-2 (COX-2) mRNA expression and correlated it with the expression of RAR-β in this cohort of stage I NSCLC patients. COX-2 overexpression had previously been demonstrated in lung, head and neck, and other tumors,[18-20] and cell line data indicated that retinoic acid could suppress COX-2.[21] These investigators found that COX-2 expression was associated with worse overall and disease-free survival and that COX-2 and RAR-β mRNA levels were correlated. These findings were in conflict with the prior cell line data, which would have predicted that RAR-β upregulation should downregulate COX-2.

Telomerase is a ribonucleoprotein that lengthens and maintains the ends of chromosomes that are shortened with successive cell divisions.[22] Telomerase is expressed in up to 85% of NSCLC tumors and plays a critical role in sustaining cellular immortality and carcinogenesis.[23,24] Wang et al[11] examined mRNA expression of the human telomerase reverse transcriptase catalytic subunit (hTERT) in 153 patients from our database. Positive hTERT expression was significantly associated with worse overall and disease-specific survival.

Tang et al[7] examined hypermethylation of the death-associated protein kinase (*DAPK*) promoter in 135 patients from this cohort. Epigenetic inactivation of tumor suppressor genes by promoter hypermethylation frequently occurs in NSCLC.[25,26] *DAPK* is a putative tumor-suppressor gene that encodes for a calmodulin-dependent kinase that possesses a death domain at its C terminus.[27] *DAPK* is required for interferon-gamma–induced apoptosis and seems to suppress the metastatic ability of lung cancer cells.[28] In the study by Tang et al,[7] *DAPK* hypermethylation was significantly associated with poorer overall and disease-specific survival.

Soria et al[12] examined the role of interleukin-10 (IL-10) protein expression among 135 patients. The immunomodulatory effects of IL-10 have demonstrated conflicting results in various tumor systems. Some reports support the role of IL-10 in helping tumors evade immunosurveillance because IL-10 can inhibit macrophage, T-cell, and antigen-presenting cell functions.[29,30] Others have demonstrated that IL-10 may function as a potent inhibitor of tumor growth and metastasis.[31,32] In this study, IL-10 lack of expression was significantly associated with poorer overall and disease-specific survival.

The aforementioned hypothesis-driven studies each focused on one or a few biomarkers. To simultaneously examine multiple potential molecular prognostic factors in this clinical research database, we identified 94 patients who had complete information for a panel of six biomarkers (RAR-β, COX-2, hTERT, *DAPK* promoter methylation, IL-10, and K-*ras*). Multivariate Cox regression analysis was used to identify independent predictors of cancer-specific survival in this population of resected stage I NSCLC patients.

PATIENTS AND METHODS

Study Population

Five hundred ninety-five consecutive patients with stage I NSCLC underwent definitive surgical resection, defined as a lobectomy or a pneumonectomy, from 1975 to 1990 at The University of Texas M.D. Anderson Cancer Center (Houston, TX). Patients did not receive preoperative or postoperative chemotherapy or radiotherapy. We retrospectively identified 185 patients for whom both tissue samples and a median follow-up period of more than 5 years were available. All available tissue blocks were reviewed by a thoracic pathologist (B.K.), and 163 cases had adequate tumor present in the surgical specimen. The patient population was identified through a search of the Tumor Registry database maintained by the Department of Medical Informatics at The University of M.D. Anderson Cancer Center. Survival status was verified and updated from Tumor Registry records as of December 1, 2000. This study was reviewed and approved by the institutional review board and conducted in accordance with its policies.

Five published studies[7-9,11,12] had previously examined different molecular prognostic factors among the 163 patients with sufficient tumor specimens and more than 5 years of follow-up data. The sample sizes ranged from 135 to 160 patients. A total of

Downloaded from www.jco.org at M D ANDERSON HOSP on March 23, 2005.
Copyright © 2004 by the American Society of Clinical Oncology. All rights reserved.

94 patients had complete information for a panel of six biomarkers, and these patients were included in our analysis.

Methylation-Specific Polymerase Chain Reaction (PCR)

These methods have been previously described.[7] Briefly, 8-μm sections from paraffin-embedded tissue blocks were obtained, and regions with tumor cells were dissected under a stereomicroscope. In the initial chemical modification step, 200 ng of DNA from each tumor was denatured by NaOH and treated with sodium bisulfite (Sigma Chemical Co, St Louis, MO). DNA was recovered in water and was ready to add to a PCR with the use of specific primers for either the methylated or the unmethylated *DAPK* promoter, as described previously.[33] DNA was amplified for 35 cycles, and PCR products were separated on 2% agarose gels and visualized. For each DNA sample, primer sets for methylated DNA and unmethylated DNA were used for analysis. The hypermethylation status was determined by visualizing a 98-base pair (bp) PCR product with the methylation-specific primer set. All PCRs were repeated twice, and the results were reproducible.

Immunohistochemical Staining for IL-10 Protein

Paraffin-embedded, 4-μm–thick tissue sections were stained for IL-10 protein using a primary goat polyclonal antihuman IL-10 antibody (AF-217-NA; R&D Systems, Minneapolis, MN) as previously described.[12] Routinely processed tissue sections of normal lymph nodes and tonsils were used as positive staining controls and were also stained with the primary antibody omitted to confirm staining specificity. Normal bronchial epithelial cells that constitutively produce IL-10 were also used as internal positive controls.[34]

The IL-10 labeling index was defined as the percentage of tumor cells displaying cytoplasmic immunoreactivity and was calculated by counting IL-10–stained tumor cells among at least 1,000 tumor cells for each section as previously described.[12] On the basis of previous reports, if 10% or more of the tumor cells were positive for IL-10, the case was considered to be IL-10 positive.[35] All slides were scored concomitantly by a pathologist (X.T.) and another investigator (J.-C.S.) in a blinded manner.

hTERT In Situ Hybridization (ISH)

These methods have been previously described.[11] The riboprobes were a 430-bp EcoRV-BamH1 fragment of the hTERT [illegible] has been used in other studies[36,37] as well as part of exon 1 from the heterogeneous nuclear ribonucleoprotein A1 as a control to verify sample quality. The single-strand–specific, digoxigenin-labeled riboprobes were generated by in vitro transcription. ISH was performed as previously described.[37] Slides displaying a diffuse but clear cytoplasmic signal were considered to be positive, as reported by Falchetti et al.[38] More specifically, our slides were rated as positive if a definite and clear signal was present in more than two large areas on the slide. Slides with faint signal, the absence of signal, or only focal positivity were considered to be negative. We did not grade the intensity of the hybridization signals.

COX-2 and RAR-β ISH

COX-2 and RAR-β mRNA were detected in 4-μm–thick sections from paraffin-embedded tissue using nonradioactive ISH with digoxigenin-labeled antisense riboprobes as previously described.[8,9,39] Retinoid X receptor-alpha (RXR-α), which is present in greater than 90% of NSCLCs,[40] was used as a control to detect RNA degradation. The rationale for using RXR-α as a control for intact RNA was the observation that all 70 cases of NSCLC and normal lung tissue expressed RXR-α mRNA in a previous study.[40] Stained sections were reviewed by three independent researchers, including two pathologists, in a blinded fashion. Only cytoplasmic staining was considered positive. Because normal bronchial epithelium expresses RAR-β, positive and aberrant RAR-β expression was defined as ≥ 10% and less than 10% intratumoral staining, respectively.[8] The RAR-β probe that was used identified all RAR-β isoforms. COX-2 expression was defined as either positive (present) or negative (absent).[9]

K-ras Mutation Analysis With PCR–Primer Introduced Restriction With Enrichment for Mutation Alleles (PCR-PIREMA)

A modified PCR-PIREMA method was used to detect K-*ras* codon 12 mutations.[41] Briefly, 8-μm sections from paraffin-embedded tissue blocks were obtained, and regions with tumor cells were dissected under a stereomicroscope. Dissected tissues were digested in 200 μL of digestion buffer containing 50 mmol/L Tris-HCl (pH 8.0), 1% sodium dodecyl sulfate, and proteinase K (0.5 mg/mL) at 42°C for 36 hours. The digested products were purified by extracting with phenol-chloroform twice. DNA was then precipitated by the ethanol precipitation method in the presence of glycogen (Roche Biochemicals, Indianapolis, IN), recovered in distilled water, and then stored at −20°C until used for PCR.

Briefly, PCR around K-*ras* codon 12 was performed using a mismatched primer (forward primer: 5′-TGAATATAAACTTGTGGTAGTTGGACCT-3′; reverse primer: 5′-CTGTATCAAAGAATGGTCC TGCACC-3′) that introduced an *MvaI* restriction site into the PCR products derived from normal alleles. *MvaI* digestion of the PCR products left only the PCR products derived from mutant alleles intact, after which further PCR selectively amplified the mutant PCR products. The first PCR reaction was performed with mixtures containing 0.5 μL of DNA recovery solution, 10 ng of each nucleotide, and the mismatched primer to introduce an *Mva* I restriction site flanking the K-*ras* exon 1, with 15 cycles at an annealing temperature of 55°C. The first PCR products were digested with *MvaI* and diluted 1:100. One microliter of the diluted product was amplified by 20 cycles of PCR with the same primers at an annealing temperature of 40°C, and the products were digested with *MvaI* a second time. The second PCR products were diluted 1:100, amplified by 35 cycles with the previous forward primer and a new reverse primer (5′-CTCTATTGTTGGATCATATTCGTCCAC-3′) at an annealing temperature of 65°C, and digested with *MvaI* a third time. The final digested products were then electrophoresed on 2.5% agarose gels and stained with ethidium bromide. A digestion-resistant 106-bp band indicated the presence of a K-*ras* codon 12 mutation. Extensive measures were taken to prevent cross-contamination of samples. A normal control sample and a known mutation sample were included in all of the experiments.

Statistical Analyses

Overall survival, disease-specific survival, and disease-free survival were analyzed in this study. Survival curves were estimated by the Kaplan-Meier method. The log-rank test was used to compare survival time between groups. Fisher's exact test was used to analyze the association between categoric variables. Using a stepwise selection method, a Cox proportional hazards model was created to identify independent predictors of survival, with adjustment for relevant clinical covariates (tumor stage, histology,

Downloaded from www.jco.org at M D ANDERSON HOSP on March 23, 2005 .
Copyright © 2004 by the American Society of Clinical Oncology. All rights reserved.

smoking status, and sex). All statistical tests were two-sided, and $P < .05$ was considered statistically significant.

All survival curves were calculated from the date of surgery. Overall survival took all deaths (cancer related or not) into account. Disease-specific survival time was calculated from the date of surgery to death from cancer-related causes. Disease-free survival time was calculated from the date of surgery to relapse or death from cancer-related causes.

RESULTS

Data for a panel of six molecular markers (RAR-β, COX-2, hTERT, *DAPK* promoter methylation, IL-10, and K-*ras*) were available for 94 patients in our retrospective cohort. These patients were the study population for our analysis. Patient characteristics are listed in Table 1. Median follow-up time for alive patients and those lost to follow-up was 10.9 years. Sixty-nine patients have died. Twenty-nine deaths were cancer related.

The frequency of each molecular marker, displayed as a negative prognostic factor, is listed in Table 2. Univariate analyses of each molecular marker and its association with disease-specific survival and overall survival were performed (Table 3). Similar univariate survival analyses of clinical variables (age, sex, and smoking status) were performed. A highly significant association was demonstrated between age (< 60 years *v* ≥ 60 years) and overall survival ($P = .003$). Sex and smoking status were not associated with overall or disease-specific survival. Age ≥ 60 years was associated with a significant increased risk of noncancer-related death ($P < .001$) and was not associated with disease-specific survival ($P = .577$). This phenomenon is likely explained by the relatively long follow-up of these subjects and by the fact that that the majority of deaths (40 of 69 deaths) were unrelated to cancer. In light of these findings, we reasoned that disease-specific survival would serve as a more clinically relevant end point for this cohort, although we continued to include overall survival in our analyses. Disease-specific survival stratified by each molecular marker is shown in Figure 1.

Table 1. Patient Characteristics

Characteristic	No. of Patients	%
Age, years		
Median	63.5	
Range	41-82	
Sex		
Male	72	77
Female	22	23
Race		
White	83	88
Other	11	12
Smoker		
Yes	82	87
No	5	5
Unknown	7	7
Histology		
Adenocarcinoma	39	41
Squamous cell carcinoma	39	41
Other	16	17
TNM stage		
T1N0M0	44	47
T2N0M0	50	53

Abbreviation: TNM, tumor-node-metastasis

Table 2. Frequency of Molecular Markers in Stage I NSCLC

Molecular Marker	Frequency (%)
COX-2 expression	60
DAPK methylation	47
K-*ras* mutation	34
hTERT expression	34
IL-10 lack of expression	30
RAR-β expression	23

Abbreviations: NSCLC, non-small-cell lung cancer; COX-2, cyclooxygenase; *DAPK*, death-associated protein kinase; hTERT, human telomerase reverse transcriptase catalytic subunit; IL-10, interleukin-10; RAR-β, retinoic acid receptor-beta

A multivariate Cox proportional hazards model was created to identify predictors of disease-specific survival (Table 4). *DAPK* promoter methylation and IL-10 lack of expression were significant negative prognostic factors for disease-specific survival, whereas COX-2 expression was of borderline significance. The same variables were selected when tumor stage, histology, smoking status, and sex were included in the model. The poorer disease-specific and overall survival of patients with both *DAPK* methylation and IL-10 lack of expression are illustrated in Figure 2. We defined these patients as a high-risk group, and the remaining patients were defined as a low-risk group. A log-rank test assessing the difference in survival between these groups was statistically significant for both disease-specific survival ($P < .0001$) and overall survival ($P < .0001$). We note that the definitions of the high- and low-risk groups are data dependent. That is, the definition of high risk was not determined a priori. A similar model for overall survival yielded three significant negative prognostic factors (age ≥ 60 years, $P = .0017$; COX-2 expression, $P = .021$; and *DAPK* methylation, $P = .044$), whereas IL-10 lack of expression was of borderline significance ($P = .069$).

Exploratory analyses of the relationships between the various molecular markers were performed. Significant associations were found between hTERT and COX-2 expression (odds ratio [OR], 6.14; 95% CI, 2.09 to 18.04; $P = .0004$) and K-*ras* mutations and *DAPK* methylation (OR, 2.64; 95% CI, 1.10 to 6.36; $P = .032$). Associations between IL-10 lack of expression and hTERT expression (OR, 2.63; 95% CI, 1.06 to 6.67; $P = .056$), IL-10 lack of

Downloaded from www.jco.org at M D ANDERSON HOSP on March 23, 2005 .
Copyright © 2004 by the American Society of Clinical Oncology. All rights reserved.

Table 3. Univariate Analysis of Molecular Markers With Disease-Specific and Overall Survival

Molecular Marker	Disease-Specific Survival			Overall Survival		
	Hazard Ratio	95% CI	*P*	Hazard Ratio	95% CI	*P*
IL-10 lack of expression	3.17	1.53 to 6.62	.002	1.98	1.21 to 3.25	.007
DAPK methylation	3.00	1.39 to 6.47	.005	1.69	1.05 to 2.72	.030
hTERT expression	2.39	1.15 to 4.97	.020	1.48	0.91 to 2.42	.116
COX-2 expression	2.44	1.08 to 5.54	.032	1.80	1.09 to 2.96	.022
RAR-β expression	1.47	0.66 to 3.25	.345	1.23	0.72 to 2.09	.446
K-*ras* mutation	1.00	0.45 to 2.20	.998	1.18	0.71 to 1.95	.517

Abbreviations: IL-10, interleukin-10; *DAPK*, death-associated protein kinase; hTERT, human telomerase reverse transcriptase catalytic subunit; COX-2, cyclooxygenase-2; RAR-β, retinoic acid receptor-beta.

expression and COX-2 expression (OR, 2.63; 95% CI, 0.99 to 7.14; $P = .066$), and COX-2 expression and RAR-β expression (OR, 2.88; 95% CI, 0.96 to 8.64; $P = .08$) were of borderline significance.

We also investigated other models by performing all two-variable, three-variable, and four-variable multivariate models. On the basis of these analyses, only *DAPK* methylation and IL-10 lack of expression were statistically significant ($P < .05$) for all models. Furthermore, the three-variable model, including *DAPK* methylation, IL-10 lack of expression, and COX-2 expression, had the lowest Akaike Information Criterion (AIC) value of 224.029 (although the two-variable model that excluded COX-2 expression had an AIC of similar value). We noted that there was some evidence of association between IL-10 lack of expression and hTERT expression (OR, 2.63; $P = .056$) and IL-10 lack of expression and COX-2 expression (OR, 2.63; $P = .066$). Moreover, hTERT and COX-2 expression were highly

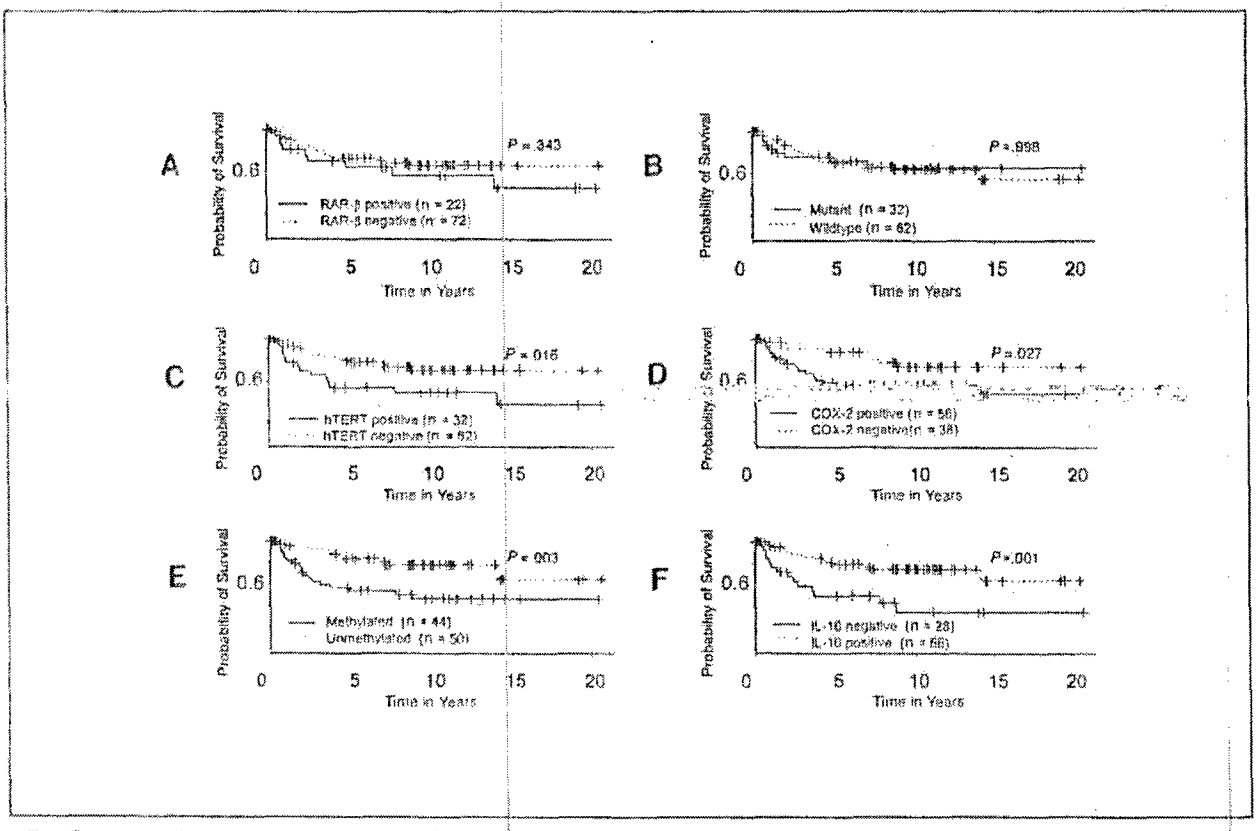


Fig 1. Disease-specific survival stratified by (A) retinoic acid receptor-beta (RAR-β) mRNA expression, (B) K-*ras* mutation status, (C) human telomerase reverse transcriptase catalytic subunit (hTERT) mRNA expression, (D) cyclooxygenase-2 (COX-2) mRNA expression, (E) death-associated protein kinase (*DAPK*) methylation, and (F) interleukin-10 (IL-10) protein expression.

Downloaded from www.jco.org at M D ANDERSON HOSP on March 23, 2005.
Copyright © 2004 by the American Society of Clinical Oncology. All rights reserved.

Table 4. Multivariate Cox Regression Model for Disease-Specific Survival

Molecular Marker	Hazard Ratio	95% CI	P
DAPK methylation	3.11	1.42 to 6.79	.004
IL-10 lack of expression	2.62	1.24 to 5.56	.012
COX-2 expression	2.13	0.92 to 4.95	.077

Abbreviations: *DAPK*, death-associated protein kinase; IL-10, interleukin-10; COX-2, cyclooxygenase-2.

associated (OR, 6.14; $P = .0004$). We ensured that the effect of these variables was not masked by colinearity by modeling them separately. Specifically, we modeled COX-2 expression with *DAPK* methylation (AIC = 228.135) and hTERT expression with *DAPK* methylation (AIC = 228.654). Neither of these models provided better fit than the model chosen.

Discussion

Our findings further characterize and extend our group's previous research efforts to identify novel molecular prognostic factors in patients with early-stage NSCLC. We identified 94 patients with complete information for a panel of six molecular markers. Each biomarker had been previously studied as a prognostic factor based on its role in carcinogenesis. When analyzed individually, five of these biomarkers (RAR-β, COX-2, hTERT, *DAPK* promoter methylation, and IL-10) were demonstrated in prior studies[7-9,11,12] by our group to be significant predictors of survival. One available marker (K-*ras*) was included in the current analysis based on published data demonstrating that it had prognostic significance in early-stage NSCLC,[14,42] even though it did not have prognostic significance in univariate analysis in our patients. Our multivariable analysis indicates that two biomarkers (*DAPK* promoter methylation and IL-10) function as independent predictors of disease-specific survival, and a third biomarker (COX-2) is of borderline significance in this cohort. These findings should be confirmed in other NSCLC patient populations.

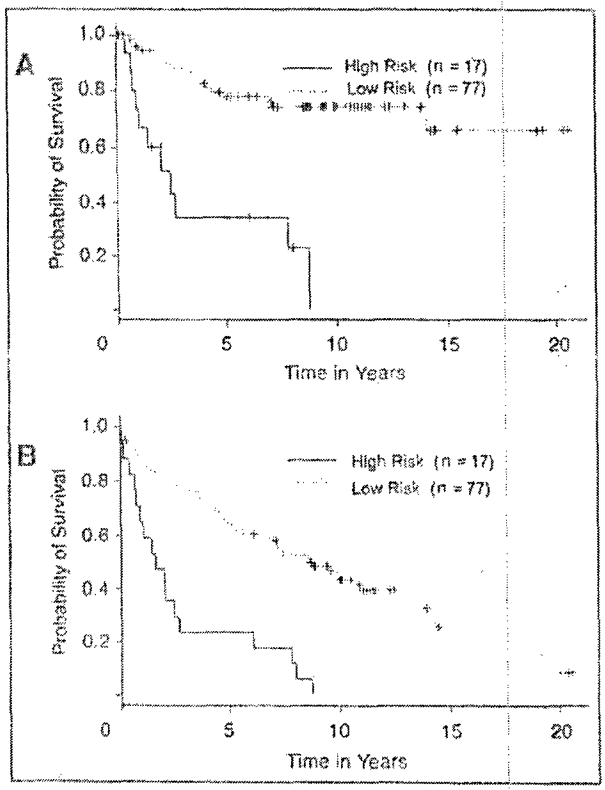


Fig 2. Disease-specific survival (A) and overall survival (B) of patients with both death-associated protein kinase methylation and interleukin-10 lack of expression (high risk) versus other patients (low risk).

Our results further support the importance of epigenetic gene regulation in lung carcinogenesis. Others have demonstrated that aberrant promoter methylation of *DAPK* and other genes frequently occurs in NSCLC tumors,[25,26] suggesting that methylation may be a common mechanism of inactivation of cancer-related genes. *DAPK* promoter methylation was the most statistically significant predictor of survival in our study. Kim et al[43] investigated the role of *DAPK* methylation in 185 NSCLC patients who underwent surgical resection, including 102 patients with stage I disease. *DAPK* methylation was significantly correlated with advanced stage, suggesting that *DAPK* may be important in the progression of NSCLC. Stage I patients with *DAPK* methylation had worse overall survival, although this association was not statistically significant. The authors noted that patient follow-up data was limited, and this factor may have contributed to their findings. Harden et al[44] examined promoter methylation of a panel of five genes in tumors and lymph nodes of 90 stage I NSCLC patients. Interestingly, patients with both *DAPK* and *adenomatous polyposis coli* gene methylation had poorer overall survival that did not reach statistical significance, although the methylation of either gene alone was not a predictor of survival. Possible explanations for these results include the relatively low frequency of *DAPK* methylation (17%) compared with our findings (47%). The smaller number of patients with *DAPK* methylation (n = 15) would result in the study having less power to detect significant associations with survival.

The role of IL-10 in carcinogenesis remains controversial. Our findings indicate that loss of IL-10 expression predicts poor disease-specific survival in early-stage NSCLC. Human bronchial epithelial cells constitutively produce IL-10, which may regulate the local immune response in normal lungs.[34] IL-10 also seems to have

Downloaded from www.jco.org at M D ANDERSON HOSP on March 23, 2005.
Copyright © 2004 by the American Society of Clinical Oncology. All rights reserved.

significant inhibitory effects on tumor growth and metastasis in multiple animal models and tumor types, including melanoma, breast cancer, prostate cancer, and Burkitt's lymphoma.[31,32,45-47] Evidence suggests that IL-10 exerts its antitumor and antimetastatic activity by inhibiting angiogenesis, and this activity is, in part, mediated by the downregulation of angiogenic molecules, such as vascular endothelial growth factor, IL-1β, tumor necrosis factor-α, IL-6, and matrix metalloproteinase-9 (MMP-9), in tumor-associated macrophages.[31] In addition, IL-10 may also directly affect the secretion of angiogenic molecules from the tumor. Stearns et al[46] demonstrated that IL-10 induces tissue inhibitor of metalloproteinase-1 production and inhibits MMP-2 and MMP-9 secretion by human prostate cancer cell lines orthotopically implanted into mice, resulting in decreased tumor microvessel formation and increased mice survival. In a murine mammary tumor model, the antitumor and antimetastatic effects of IL-10 gene transfection were associated with elevated nitric oxide levels in tumors.[48] Others have shown that IL-10 can directly inhibit the proliferation of endothelial cells stimulated with vascular endothelial growth factor or fibroblast growth factor-2 in vitro.[47] An intriguing molecular epidemiologic case-control study demonstrated that IL-10 promoter polymorphisms that resulted in lower IL-10 expression were associated with an increased risk of developing melanoma.[49] Furthermore, some authors have suggested that lung cancer cells can modulate IL-10 expression by stromal components. In the present study, only nine of 94 samples displayed tumor-infiltrating lymphocytes or tumor-associated macrophages, therefore hindering any relevant analysis of IL-10 production by infiltrating immune cells.

The data supporting the antitumor and antimetastatic activity of IL-10 are compelling, but most preclinical models using IL-10 to mediate such effects do so at concentrations that far exceed the levels demonstrated in lung cancer patients. Other authors have demonstrated that IL-10 is a potent immunosuppressive molecule that may promote lung cancer growth by suppressing T-cell and macrophage function and enabling tumors to escape immune detection.[50-52] Elevated baseline serum IL-10 levels were found to be independent predictors of poorer survival in 60 advanced-stage NSCLC patients receiving platinum-based chemotherapy.[53] Hatanaka et al[54] measured IL-10 mRNA levels by reverse transcriptase PCR in the tumors of 82 NSCLC patients who underwent surgical resection. Their assay demonstrated IL-10 expression in 83% of the surgical specimens. In contrast to our results, IL-10 expression was significantly associated with worse survival. The reasons for these discrepant findings remain unclear. These investigators included patients with stages I to IIIb disease in their study and used a different IL-10 assay (mRNA v protein) than the assay we used in our study. These factors may have contributed to these divergent results.

Our exploratory analyses demonstrate a highly significant association between hTERT expression and COX-2 expression ($P = .0004$). A precise explanation for this correlation is lacking, although various COX-2 inhibitors have been reported to inhibit both tumor growth and telomerase activity in mice.[55,56] We also observed a significant association between *K-ras* mutations and *DAPK* methylation ($P = .032$). Reports suggesting that DNA methylation may be regulated by the ras signaling pathway[57,58] are consistent with these findings. However, others have not found correlations between ras mutations and promoter hypermethylation in NSCLC tumors.[43,59] Clearly, a better understanding of the significance of these associations will require future studies. Our analyses also demonstrate a borderline significant association between IL-10 lack of expression and COX-2 expression ($P = .066$).[60,61] This finding is consistent with data suggesting that IL-10 has the capacity to potently downregulate COX-2. Therefore, in the absence of IL-10, COX-2 and its derived products would be more abundant and could further promote tumor progression.

This study is limited by its retrospective nature and the inclusion only of patients with complete information for all six biomarkers. It is difficult to speculate on potential biases affecting our results. It is possible, for example, that small tumors with limited tissue availability were underrepresented in this cohort. These results should be validated in a separate population of NSCLC patients.

In conclusion, our analysis of six molecular markers in patients with resected stage I NSCLC yielded two independent predictors of poorer disease-specific survival: *DAPK* methylation and IL-10 lack of expression. Future studies are warranted to further define their roles in tumor proliferation and metastasis. However, these and other potential molecular prognostic factors have yet to be validated, and thus, the integration of molecular marker assessments into the routine clinical management of NSCLC has remained an elusive goal. As the number of potential molecular markers increases, it has become more difficult to assess which prognostic factors are likely to be clinically relevant. A comprehensive multivariable analysis is not feasible because the majority of studies analyze only a single or a few biomarkers at a time. In this regard, the development of high-throughput technologies to determine gene-expression profiles and proteomic patterns of tissue specimens represents a significant methodologic advance. Several recent reports have demonstrated that mRNA and protein patterns of NSCLC tumors may be predictive of survival.[62,63] Hopefully, these technologies will eventually provide the clinician with a reliable, validated molecular staging system that will improve therapeutic strategies for NSCLC.

Authors' Disclosures of Potential Conflicts of Interest

The authors indicated no potential conflicts of interest.

Downloaded from www.jco.org at M D ANDERSON HOSP on March 23, 2005.
Copyright © 2004 by the American Society of Clinical Oncology. All rights reserved.

REFERENCES

1. Jemal A, Murray T, Samuels A, et al: Cancer statistics, 2003. CA Cancer J Clin 53:5-26, 2003

2. Travis W, Travis LB, Devesa SS: Lung cancer incidence and survival by histologic type. Cancer 75:191-202, 1995 (suppl 1)

3. Fry W, Phillips JL, Menck HR: Ten-year survey of lung cancer treatment and survival in hospitals in the United States. Cancer 86:1867-1876, 1999

4. Mountain CF: Revisions in the International System for Staging Lung Cancer. Chest 111:1710-1717, 1997

5. Tseng JE, Kemp BL, Khuri FR, et al: Loss of Fhit is frequent in stage I non-small cell lung cancer and in the lungs of chronic smokers. Cancer Res 59:4798-4803, 1999

6. Herbst RS, Yano S, Kuniyasu H, et al: Differential expression of E-cadherin and type IV collagenase genes predicts outcome in patients with stage I non-small cell lung carcinoma. Clin Cancer Res 6:790-797, 2000

7. Tang X, Khuri FR, Lee JJ, et al: Hypermethylation of the death-associated protein (DAP) kinase promoter and aggressiveness in stage I non-small-cell lung cancer. J Natl Cancer Inst 92:1511-1516, 2000

8. Khuri FR, Lotan R, Kemp BL, et al: Retinoic acid receptor-beta as a prognostic indicator in stage I non-small-cell lung cancer. J Clin Oncol 18:2798-2804, 2000

9. Khuri FR, Wu H, Lee JJ, et al: Cyclooxygenase-2 overexpression is a marker of poor prognosis in stage I non-small cell lung cancer. Clin Cancer Res 7:861-867, 2001

10. Zhou X, Kemp BL, Khuri FR, et al: Prognostic implication of microsatellite alteration profiles in early-stage non-small cell lung cancer. Clin Cancer Res 6:559-565, 2000

11. Wang L, Soria JC, Kemp BL, et al: HTERT expression is a prognostic factor of survival in patients with stage I non-small cell lung cancer. Clin Cancer Res 8:2883-2889, 2002

12. Soria JC, Moon C, Kemp BL, et al: Lack of interleukin-10 expression could predict poor outcome in patients with stage I non-small cell lung cancer. Clin Cancer Res 9:1785-1791, 2003

13. Pastorino U, Andreola S, Tagliabue E, et al: Immunocytochemical markers in stage I lung cancer: Relevance to prognosis. J Clin Oncol 15:2858-2865, 1997

14. Kwiatkowski DJ, Harpole DH Jr, Godleski J, et al: Molecular pathologic substaging in 244 stage I non-small-cell lung cancer patients: Clinical implications. J Clin Oncol 16:2466-2477, 1998

15. D'Amico TA, Massey M, Herndon JE II, et al: A biologic risk model for stage I lung cancer: Immunohistochemical analysis of 408 patients with the use of ten molecular markers. J Thorac Cardiovasc Surg 117:736-743, 1999

16. Ahrendt SA, Hu Y, Buta M, et al: p53 mutations and survival in stage I non-small-cell lung cancer: Results of a prospective study. J Natl Cancer Inst 95:961-970, 2003

17. Berard J, Gaboury L, Landers M, et al: Hyperplasia and tumours in lung, breast and other tissues in mice carrying a RAR beta 4-like transgene. EMBO J 13:5570-5580, 1994

18. Taketo MM: Cyclooxygenase-2 inhibitors in tumorigenesis (Part II). J Natl Cancer Inst 90:1609-1620, 1998

19. Hida T, Yatabe Y, Achiwa H, et al: Increased expression of cyclooxygenase 2 occurs frequently in human lung cancers, specifically in adenocarcinomas. Cancer Res 58:3761-3764, 1998

20. Wolff H, Saukkonen K, Anttila S, et al: Expression of cyclooxygenase-2 in human lung carcinoma. Cancer Res 58:4997-5001, 1998

21. Li M, Song S, Lippman SM, et al: Induction of retinoic acid receptor-beta suppresses cyclooxygenase-2 expression in esophageal cancer cells. Oncogene 21:411-416, 2002

22. Hahn WC: Role of telomeres and telomerase in the pathogenesis of human cancer. J Clin Oncol 21:2034-2043, 2003

23. Hiyama K, Hiyama E, Ishioka S, et al: Telomerase activity in small-cell and non-small-cell lung cancers. J Natl Cancer Inst 87:895-902, 1995

24. Kim NW, Piatyszek MA, Prowse KR, et al: Specific association of human telomerase activity with immortal cells and cancer. Science 266:2011-2015, 1994

25. Zochbauer-Muller S, Fong KM, Maitra A, et al: 5' CpG island methylation of the FHIT gene is correlated with loss of gene expression in lung and breast cancer. Cancer Res 61:3561-3565, 2001

26. Esteller M, Corn PG, Baylin SB, et al: A gene hypermethylation profile of human cancer. Cancer Res 61:3225-3229, 2001

27. Deiss LP, Feinstein E, Berissi H, et al: Identification of a novel serine/threonine kinase and a novel 15-kD protein as potential mediators of the gamma interferon-induced cell death. Genes Dev 9:15-30, 1995

28. Inbal B, Cohen O, Polak-Charcon S, et al: DAP kinase links the control of apoptosis to metastasis. Nature 390:180-184, 1997

29. Beissert S, Hosoi J, Grabbe S, et al: IL-10 inhibits tumor antigen presentation by epidermal antigen-presenting cells. J Immunol 154:1280-1286, 1995

30. Röhrer JW, Coggin JH Jr: CD8 T cell clones inhibit antitumor T cell function by secreting IL-10. J Immunol 156:5027-5027, 1996

31. Huang S, Ullrich SE, Bar-Eli M: Regulation of tumor growth and metastasis by interleukin-10: the melanoma experience. J Interferon Cytokine Res 19:697-703, 1999

32. Kundu N, Beaty TL, Jackson MJ, et al: Antimetastatic and antitumor activities of interleukin 10 in a murine model of breast cancer. J Natl Cancer Inst 88:536-541, 1996

33. Esteller M, Sanchez-Cespedes M, Rosell R, et al: Detection of aberrant promoter hypermethylation of tumor suppressor genes in serum DNA from non-small cell lung cancer patients. Cancer Res 59:67-70, 1999

34. Barnfield TL, Konstan MW, Burfeind P, et al: Normal bronchial epithelial cells constitutively produce the anti-inflammatory cytokine interleukin-10, which is downregulated in cystic fibrosis. Am J Respir Cell Mol Biol 13:257-261, 1995

35. Fujieda S, Lee K, Sunaga H, et al: Staining of interleukin-10 predicts clinical outcome in patients with nasopharyngeal carcinoma. Cancer 85:1439-1445, 1999

36. Kolquist KA, Ellisen LW, Counter CM, et al: Expression of TERT in early premalignant lesions and a subset of cells in normal tissues. Nat Genet 19:182-186, 1998

37. Soria JC, Moon C, Wang L, et al: Effects of N-(4-hydroxyphenyl)retinamide on hTERT expression in the bronchial epithelium of cigarette smokers. J Natl Cancer Inst 93:1257-1263, 2001

38. Falchetti ML, Pallini R, D'Ambrosio E, et al: In situ detection of telomerase catalytic subunit mRNA in glioblastoma multiforme. Int J Cancer 86:895-901, 2000

39. Xu XC, Ro JY, Lee JS, et al: Differential expression of nuclear retinoid receptors in normal, premalignant, and malignant head and neck tissues. Cancer Res 54:3580-3587, 1994

40. Xu XC, Sozzi G, Lee JS, et al: Suppression of retinoic acid receptor beta in non-small-cell lung cancer in vivo: Implications for lung cancer development. J Natl Cancer Inst 89:624-629, 1997

41. Jacobson DR, Mills NE: A highly sensitive assay for mutant ras genes and its application to the study of presentation and relapse genotypes in acute leukemia. Oncogene 9:553-563, 1994

42. Slebos RJ, Kibbelaar RE, Dalesio O, et al: K-ras oncogene activation as a prognostic marker in adenocarcinoma of the lung. N Engl J Med 323:561-565, 1990

43. Kim DH, Nelson HH, Wiencke JK, et al: Promoter methylation of DAP-kinase: Association with advanced stage in non-small cell lung cancer. Oncogene 20:1765-1770, 2001

44. Harden SV, Tokumaru Y, Westra WH, et al: Gene promoter hypermethylation in tumors and lymph nodes of stage I lung cancer patients. Clin Cancer Res 9:1370-1375, 2003

45. Gerard CM, Bruyns C, Delvaux A, et al: Loss of tumorigenicity and increased immunogenicity induced by interleukin-10 gene transfer in B16 melanoma cells. Hum Gene Ther 7:23-31, 1996

46. Stearns ME, Garcia FU, Fudge K, et al: Role of interleukin 10 and transforming growth factor beta1 in the angiogenesis and metastasis of human prostate primary tumor lines from orthotopic implants in severe combined immunodeficiency mice. Clin Cancer Res 5:711-720, 1999

47. Cervenak L, Morbidelli L, Donati D, et al: Abolished angiogenicity and tumorigenicity of Burkitt lymphoma by interleukin-10. Blood 96:2568-2573, 2000

48. Kundu N, Dorsey R, Jackson MJ, et al: Interleukin-10 gene transfer inhibits murine mammary tumors and elevates nitric oxide. Int J Cancer 76:713-719, 1998

49. Howell WM, Turnar SJ, Bateman AC, et al: IL-10 promoter polymorphisms influence tumour development in cutaneous malignant melanoma. Genes Immun 2:25-31, 2001

50. Sharma S, Stolina M, Lin Y, et al: T cell-derived IL-10 promotes lung cancer growth by suppressing both T cell and APC function. J Immunol 163:5020-5028, 1999

51. Spagnoli GC, Juretic A, Schultz-Thater E, et al: On the relative roles of interleukin-2 and interleukin-10 in the generation of lymphokine-

Downloaded from www.jco.org at M D ANDERSON HOSP on March 23, 2005 .
Copyright © 2004 by the American Society of Clinical Oncology. All rights reserved.

activated killer cell activity. Cell Immunol 146:391-405, 1993

52. Huang M, Sharma S, Mao JT, et al: Non-small cell lung cancer-derived soluble mediators and prostaglandin E2 enhance peripheral blood lymphocyte IL-10 transcription and protein production. J Immunol 157:5512-5520, 1996

53. De Vita F, Orditura M, Galizia G, et al: Serum interleukin-10 levels as a prognostic factor in advanced non-small cell lung cancer patients. Chest 117:365-373, 2000

54. Hatanaka H, Abe Y, Kamiya T, et al: Clinical implications of interleukin (IL)-10 induced by non-small-cell lung cancer. Ann Oncol 11:815-819, 2000

55. Nishimura G, Yanoma S, Mizuno H, et al: A selective cyclooxygenase-2 inhibitor suppresses tumor growth in nude mouse xenografted with human head and neck squamous carcinoma cells. Jpn J Cancer Res 90:1152-1162, 1999

56. Lonnroth C, Andersson M, Lundholm K: Indomethacin and telomerase activity in tumor growth retardation. Int J Oncol 18:929-937, 2001

57. Rouleau J, MacLeod AR, Szyf M: Regulation of the DNA methyltransferase by the Ras-AP-1 signaling pathway. J Biol Chem 270:1595-1601, 1995

58. Bigey P, Ramchandani S, Theberge J, et al: Transcriptional regulation of the human DNA methyltransferase (dnmt1) gene. Gene 242:407-416, 2000

59. Pulling LC, Devine KK, Klinge DM, et al: Promoter hypermethylation of the O6-methylguanine-DNA methyltransferase gene: More common in lung adenocarcinomas from never-smokers than smokers and associated with tumor progression. Cancer Res 63:4842-4848, 2003

60. Moore KW, de Waal Malefyt R, Coffman RL, et al: Interleukin-10 and the interleukin-10 receptor. Annu Rev Immunol 19:683-765, 2001

61. Molina-Holgado E, Arevalo-Martin A, Ortiz S, et al: Theiler's virus infection induces the expression of cyclooxygenase-2 in murine astrocytes: Inhibition by the anti-inflammatory cytokines interleukin-4 and interleukin-10. Neurosci Lett 324:237-241, 2002

62. Beer DG, Kardia SL, Huang CC, et al: Gene-expression profiles predict survival of patients with lung adenocarcinoma. Nat Med 8:816-824, 2002

63. Yanagisawa K, Shyr Y, Xu BJ, et al: Proteomic patterns of tumour subsets in non-small-cell lung cancer. Lancet 362:433-439, 2003

Attention Authors: You Asked For It - You Got It!

Online Manuscript System Launched November 1st

On November 1st, *JCO* formally introduced its online Manuscript Processing System that will improve all aspects of the submission and peer-review process. Authors should notice a quicker turnaround time from submission to decision through this new system.

Based on the well known Bench>Press system by HighWire Press, the *JCO* Manuscript Processing System promises to further *JCO*'s reputation of providing excellent author service, which includes an already fast turnaround time of 7 weeks from submission to decision, no submission fees, no page charges, and allowing authors to freely use their work that has appeared in the journal.

JCO's Manuscript Processing System will benefit authors by

- eliminating the time and expense of copying and sending papers through the mail
- allowing authors to complete required submission forms quickly and easily online
- receiving nearly immediate acknowledgement of receipt of manuscripts
- tracking the status of manuscripts at any time online and
- accessing all reviews and decisions online.

Authors are encouraged to register at http://submit.jco.org.

For more details on *JCO*'s new online Manuscript Processing System, go online to http://www.jco.org/misc/announcements.shtml. Also, watch upcoming issues of *JCO* for updates like this one.

Downloaded from www.jco.org at M D ANDERSON HOSP on March 23, 2005 .
Copyright © 2004 by the American Society of Clinical Oncology. All rights reserved.

VOLUME 22 · NUMBER 16 · AUGUST 15 2004

JOURNAL OF CLINICAL ONCOLOGY

ORIGINAL REPORT

Expression of Hepatoma-Derived Growth Factor Is a Strong Prognostic Predictor for Patients With Early-Stage Non–Small-Cell Lung Cancer

Hening Ren, Ximing Tang, J. Jack Lee, Lei Feng, Allen D. Everett, Waun Ki Hong, Fadlo R. Khuri, and Li Mao

From the Department of Thoracic/Head and Neck Medical Oncology, Departments of Biostatistics, Department of Pathology, The University of Texas M.D. Anderson Cancer Center, Houston, TX; Department of Pediatrics, The Johns Hopkins University, School of Medicine, Baltimore, MD.

Submitted February 10, 2004; accepted May 20, 2004.

Supported in part by Department of Defense Grant DAMD17-01-1-0689-1, and National Cancer Institute Grants PO1 CA81844, UO1 CA66330, and P30 CA 16672.

Authors' disclosures of potential conflicts of interest are found at the end of this article.

Address reprint requests to Li Mao, MD, Department of Thoracic/Head and Neck Medical Oncology, Unit 432, The University of Texas M.D. Anderson Cancer Center, 1515 Holcombe Blvd, Houston, TX 77030; e-mail: lmao@mdanderson.org.

© 2004 by American Society of Clinical Oncology.

0732-183X/04/2216-3230/$20.00

DOI: 10.1200/JCO.2004.02.083

ABSTRACT

Purpose

Hepatoma-derived growth factor (HDGF), which is unrelated to hepatocyte growth factor, can stimulate DNA synthesis and cell proliferation on entering the nucleus. We hypothesize that HDGF plays an important role in biologic behavior of early-stage non–small-cell lung cancer (NSCLC).

Patients and Methods

Ninety-eight patients with pathologic stage I NSCLC who underwent curative surgery were studied. Immunohistochemistry was used to determine the expression level of HDGF in the tumor specimens. The intensity of the protein staining and percentage of stained tumor cells were used to determine a labeling index. Statistical analyses, all two-sided, were performed to determine the prognostic effect of HDGF expression levels on clinical parameters and outcomes.

Results

The mean ± standard deviation HDGF labeling index in the 98 tumors was 185 ± 41. Patients whose tumors had higher HDGF indexes (≥ 185) had a significantly poorer probability of overall survival at 5 years after surgery than did those with lower HDGF indexes (0.26 *v* 0.82; $P < .0001$). Similarly, the 5-year disease-specific and disease-free survival probabilities were lower in those with higher HDGF indexes (0.42 *v* 0.92, and 0.34 *v* 0.71; $P < .0001$ and $P = .0008$; respectively). Multivariate analysis indicated that HDGF level was an independent predictor of overall, disease-specific, and disease-free survivals.

Conclusion

Overexpression of HDGF is common in early-stage NSCLC. The expression level in tumor cells is strongly correlated with poor overall, disease-specific, and disease-free survivals, suggesting HDGF may be a powerful prognostic marker for patients with early-stage NSCLC.

J Clin Oncol 22:3230-3237. © 2004 by American Society of Clinical Oncology

Lung cancer is the most common cause of cancer-related death in the United States, accounting for more deaths than those caused by prostate, breast, and colorectal cancers combined.[1] The prognosis for patients with lung cancer is correlated with disease stage at the time of diagnosis. Patients with stage I non–small-cell lung cancer (NSCLC), the earliest stage in current staging system, have a 5-year survival rate of approximately 60%, whereas patients with stage II to IV disease have 5-year survival rates ranging from 40% to less than 5%.[2,3] Unfortunately, even among patients with stage I NSCLC, 40% will die of the disease within 5 years after potentially curative surgery. Recent studies have shown that patients with early stage NSCLC may benefit from adjuvant chemotherapy following curative surgical attempt.[4,5] These findings may lead the adjuvant chemotherapy to become standard care for those patients. However, only 4% of the patients may actually benefit from such therapy, while most of the patients will suffer undesired and potentially fatal side effects.[5] Therefore, the identification of novel strategies to further stratify such patients

Downloaded from www.jco.org at M D ANDERSON HOSP on March 23, 2005.
Copyright © 2004 by the American Society of Clinical Oncology. All rights reserved.

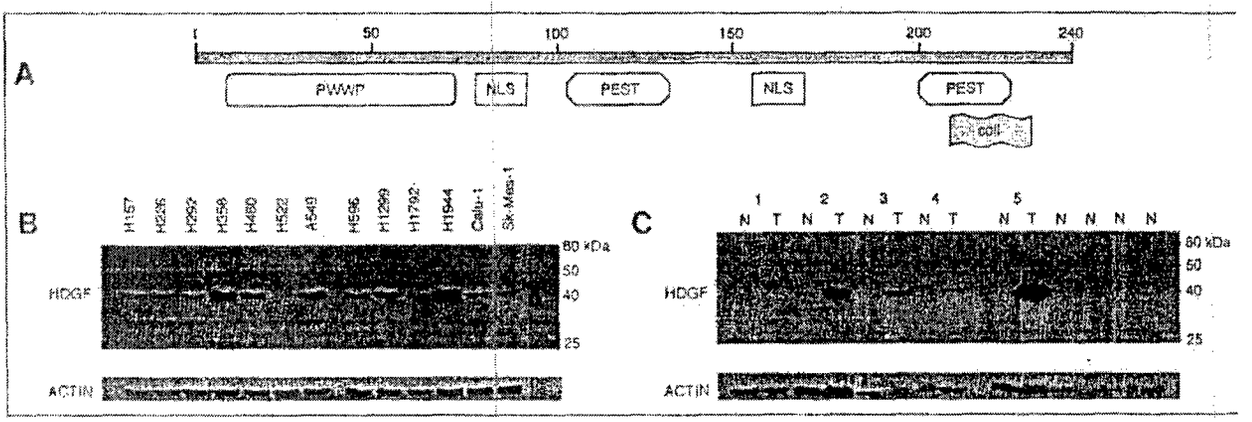


Fig 1. (A) Putative domains of hepatoma-derived growth factor (HDGF). (B) HDGF expression in non–small-cell lung cancer (NSCLC) cell lines and paired normal lung tissue specimens and primary NSCLC specimens, as well as (C) normal lung tissue specimens from patients without primary lung cancer (patients with metastatic lung tumors). Actin is used as a loading control. N, normal lung tissue specimens; T, primary NSCLC specimens.

based on their likelihood to benefit from an adjuvant therapy is an unmet need.

Hepatoma-derived growth factor (HDGF), which is unrelated to hepatocyte growth factor, is a heparin-binding growth factor originally purified from media conditioned with the human hepatoma cell line HuH-7, and can stimulate proliferation of Swiss 3T3 cells.[6] The amino acid sequence, as deduced from a cDNA clone of HDGF, contains 240 residues with a motif homologous to the consensus sequences of bipartite nuclear localization sequence and a DNA-binding PWWP motif (Fig 1A). The precise function of HDGF is unknown. Recent studies indicate that HDGF is highly expressed during early development of many tissues, including cardiovascular,[7] kidney,[8] and liver[9] tissues. Although lacking the typical secretory sequence present in most secretory proteins,[10] HDGF has been shown to act as a potent exogenous mitogen for HuH-7,[11] COS-7,[11] aortic vascular smooth muscle cells,[12] and endothelia cells.[8]

We found that HDGF is overexpressed in NSCLC cell lines and primary tumors compared to normal lung tissues. To determine the importance of HDGF in the biologic behavior of NSCLC, we further studied HDGF expression in tumor specimens from 98 patients with pathologic stage I NSCLC. The patients were treated with potentially curative surgery with a median follow-up of 10 years. Expression levels of HDGF in the primary tumors were compared to clinical parameters and outcomes.

Study Population

Patients were included in the study if they were diagnosed with pathologic stage I NSCLC; had undergone lobectomy or pneumonectomy for complete resection of their primary tumors at The University of Texas M.D. Anderson Cancer Center (Houston, TX) from 1975 through 1990; had not received adjuvant chemotherapy or radiation therapy before or after surgery; had at least 5 years of follow-up data; and had adequate paraffin-embedded tissue sections available in the institution's tumor archive. During the period between 1975 and 1990, a total of 588 patients were diagnosed as having pathologic stage I NSCLC and treated surgically at M.D. Anderson. Tissue sections were available for 105 of these 588 patients, and sections from 98 patients contained adequate tumor cells for evaluation. The follow-up information was based on chart review and from reports from the M.D. Anderson tumor registry service. The study was reviewed and approved by the institution's Surveillance Committee to allow us to study the tissues and pertinent follow-up information. Tissue sections were from each tissue block, stained with hematoxylin-eosin, and reviewed to confirm the diagnosis and the presence or absence of tumor cells. NSCLC cell lines (H157, H226, H292, H358, H460, H522, A549, H596, H1299, H1792, H1944, Calu-1, and SK-Mes-1) used in the study were obtained from American type Culture Collection (Manassas, VA) and were grown in RPMI-1640 median with 10% fetal bovine serum (Life Technologies Inc, Rockville, MD).

Immunohistochemical Analysis

Tissue sections (4 μm thick) from formalin-fixed and paraffin-embedded tissue blocks were mounted on positively charged glass slides. Slides were baked at 60°C for 1 hour and then deparaffinized through a series of xylene baths. Rehydration was performed with graded concentrations of alcohol. To retrieve antigenicity, tissue sections were treated with microwaves in 10 mmol/L citrate buffer (pH 6.0) for 10 minutes. The sections were then immersed in methanol containing 0.3% hydrogen peroxidase for 20 minutes to block the endogenous peroxidase activity, and incubated in 2.5% blocking serum for 30 minutes to reduce nonspecific binding. Sections were incubated overnight at 4°C with an affinity-purified rabbit polyclonal antibody produced against the COOH-terminal amino acids (222-237) of the mouse HDGF sequence at a dilution of 1:4000 rabbit anti-HDGF polyclonal antibody,[12] followed by incubation for 30 minutes with biotinylated antirabbit immunoglobulin G (Vector Laboratories, Burlingame, CA). The sections were then processed using standard avidin-biotin immunohistochemistry according to the manufacturer's recommendations. Diaminobenzidine was used as a chromogen, and commercial hematoxylin was used for counterstaining.

Downloaded from www.jco.org at M D ANDERSON HOSP on March 23, 2005 .
Copyright © 2004 by the American Society of Clinical Oncology. All rights reserved.

The HDGF labeling index was defined as the weighted mean of percentage of tumor cells displaying nuclear immunoreactivity (calculated by counting the number of HDGF positive tumor cells among at least 1,000 tumor cells for each tissue section manually) multiplied by the degree of the staining intensity (1, 2, or 3, defined as weak staining, moderate staining, or strong staining, respectively). The final index of each tumor was the average of indices generated by two observers (H.R. and X.T.). The differences between the two observers were less than 20% in almost all cases. The weak staining in the smooth muscle cells of blood vessels was used as an internal control and the basis for the intensity score. Almost all tumor cells showed some degree of staining.

Western Blot Analysis

Tissues or cells were either homogenized or harvested in lysis buffer 50 mmol/L HEPES, 1% Triton X-100, 10 mmol/L NaF, 30 mmol/L Na3P04, 150 mmol/L NaCl, and 1 mmol/L EDTA and freshly added 10 mmol/L glycerophosphate, 1 mmol/L Na3VO4, 20 μg/mL pepstatin A, 10 μg/mL aprotinin, 20 μg/mL leupeptin, and 40 μmol/L microcystin-LR. Twenty micrograms of total proteins from each sample was separated in sodium dodecyl sulfate-polyacrylamide gel electrophoresis using a Bio-Rad Mini-Protean II apparatus (Schleicher & Schuell BioScience, Keene, NH), and separated proteins in the gels were transfered to nitrocellulose membrane. The membranes were then blocked with 5% nonfat milk for 2 hours at room temperature followed by incubation with the rabbit anti-HDGF antibody (1:10,000 dilution) at 4° C overnight. The immune reactive band was detected using a goat-antirabbit immunoglobulin G horseradish peroxidase conjugate (1:10,000; Jackson ImmunoResearch Lab, West Grove, PA,) as the secondary antibody and SuperSignal West Pico Substrate (Pierce Biotechnology, Rockford, IL) as the detection agent. A mouse antiactin monoclonal antibody AC-15 (Sigma, St. Louis, MO) was used to normalize protein loading.

Statistical Analysis

Survival probability as a function of time was computed by the Kaplan-Meier estimator. The variance of the Kaplan-Meier estimator was computed by the Greenwood formula. The 5-year survival probabilities were estimated and compared by the asymptotic z between the high expression and low expression groups. The log-rank test was used to compare patients' survival time between groups. Overall, disease-specific (ie, those who died of lung cancer-related causes specifically), and disease-free (ie, those who developed recurrence and/or metastasis) survivals were analyzed. HDGF-labeling index was analyzed as a continuous variable as well as a categoric variable. The mean labeling index and quartiles of the labeling index were used as cutoff points for HDGF in the survival analysis. The χ^2 test was used to test equal proportion between groups in two-way contingency tables. Cox regression was used to model the risks of HDGF expression level on survival time, with adjustment for clinical and histopathologic parameters (age, sex, race, smoking status, and histologic subgroup). Martingale residual analysis was used to determine the functional form for HDGF (untransformed data on the continuous scale) to best explain its effect on survival through a Cox regression model. The Martingale residual plots using the Martingale residuals, from a Cox model that includes only baseline hazard function but no covariate, on the vertical axis and HDGF on the horizontal axis were provided. By applying a nonparametric smoother to create a line, the plots allow one to examine visually the nature of the relationship between the residuals and the HDGF scores. Appropriate transformation and/or cutoff points can be chosen accordingly. All statistical tests are two-sided and a P value of .05 or lower was considered statistically significant.

RESULTS

Of the 98 patients included in this study, 71 patients died, and 27 patients were still alive at the time of last follow-up. Among the 71 patients who died, 29 died of lung cancer, and 42 died of other causes including heart diseases, respiratory diseases, and other organ failures. The median follow-up time was 10.1 years among the patients who remained alive. Patient ages at the time of diagnosis ranged from 37 to 82 years, with a median age of 62.5 years; this is similar to the age distribution in a large database of NSCLC at M.D. Anderson (data not shown). Twenty-four (24%) of the patients were women, and 74 (76%) were men, which is comparable to the sex distribution of the disease in the 1970s and 1980s.[2] Ninety-six percent of the patients were smokers or former smokers. The histology types of squamous, adenocarcinoma, and others were found in 40%, 45%, and 15% of the patients, respectively. The 5-year overall survival rate was 55%, and the 5-year disease-specific survival rate was 71% in our patient population; these rates are similar to the rates reported in a previous study with a large number of cases from our institution.[13] The general clinical characteristics of the patients are shown in Table 1.

The high expression of HDGF in NSCLC was observed by Western blot analysis in NSCLC cell lines and primary tumors (Fig 1B and C). A single band of molecular weight about 40 kDa was detected in all 13 NSCLC cell lines using the anti-HDGF antibody (Fig 1B). Overexpression of HDGF was observed in three of five primary NSCLC tumors compared to corresponding normal lung tissues, as well as in four normal lung tissues from patients with lung metastasis of other organ origins (Fig 1C).

We analyzed the expression status of HDGF protein in the 98 primary tumor samples from patients with pathologic stage I NSCLC by immunohistochemistry using a polyclonal anti-HDGF antibody. HDGF staining was observed in all tumor sections but at various intensities (Fig 2). Strong nuclear staining with minimal cytoplasmic staining was observed in many lung adenocarcinomas (Fig 2A through C). The staining intensity was in general weaker and more variable in squamous cell type (Fig 2D and E). The mean labeling index was 185[14] in the overall tumor population with range from 100 to 291. The quartiles of the HDGF labeling index were 158, 182.5, and 211, respectively (25th, 50th, and 75th percentiles). Thirty-four percent of the adenocarcinomas exhibited an HDGF labeling index more than 211 (highest quartile) while only 15% of the squamous cell carcinomas did so; however, this difference was not statistically significant ($P = .09$). Weak cytoplasmic

Downloaded from www.jco.org at M D ANDERSON HOSP on March 23, 2005
Copyright © 2004 by the American Society of Clinical Oncology. All rights reserved.

Table 1. Demographic Characteristics of the Patient Population by HDGF Expression

Characteristic	HDGF < 185		HDGF ≥ 185		Total	
	No. of Patients	%	No. of Patients	%	No. of Patients	%
	(n = 51; 52%)		(n = 47; 48%)		(N = 98)	
Sex						
Male	39	53	35	47	74	76
Female	12	50	12	50	24	24
Age, years						
Mean	62.7		63.0		62.8	
SD	10.4		8.7		9.6	
Smoking status						
Smoker	48	53	42	47	90	96
Nonsmoker	1	25	3	75	4	4
Histology						
Squamous	24	62	15	38	39	40
Adeno	21	48	23	52	44	45
Other*	6	40	9	60	15	15
Five-year survival probability						
Overall	.82		.26		.55	
95% CI	.72 to .93		.16 to .43		.46 to .66	
Disease-specific	.92		.42		.71	
95% CI	.84 to 1.0		.28 to .62		.61 to .81	
Disease-free	.71		.34		.55	
95% CI	.60 to .85		.22 to .53		.48 to .66	

NOTE. Percentages are the row percentage of HDGF groups in each category of the variables (first two columns) and the percentage of each category for each variable (last column).

Abbreviations: HDGF, hepatoma-derived growth factor; SD, standard deviation.

*Other histology types: bronchioalveoli (seven patients), large cell (three patients), and mixed (five patients).

staining was observed in some HDGF-positive squamous carcinoma cells. In normal lung tissues, vascular smooth muscle cells might show weak staining and were used as an internal control (intensity level 1). In normal lung tissues, the HDGF expression level was low (Fig 2F). The HDGF expression level was not associated with age, sex, or race. In 40 tumors, HDGF expression and the expression of the proliferation marker Ki-67 were compared. We failed to observe an association between the two markers (Spearman's correlation coefficient = 0.1; $P = .52$).

In our analysis of potential associations between the level of HDGF in the primary tumors and survival, we found that patients whose primary tumors exhibited a high level of HDGF (when the mean labeling index of 185 was used as a cut-off point) had a significantly poorer overall survival probability ($P < .0001$, log-rank test). The probability of overall survival at 5 years after surgery was 0.82 (95% CI, 0.72 to 0.93) for patients whose tumors showed a low HDGF labeling index (< 185) compared with 0.26 (95% CI, 0.16 to 0.43) for patients whose tumors showed a high HDGF labeling index (≥ 185; Fig 3A). The probability of overall survival at 10 years after surgery was also lower for patients whose tumors had a high HDGF labeling index, but the difference was smaller compared to that at 5 years, probably as a result of an increase in non–cancer-related deaths over time in this patient population (median age of 62.5 years and 96% smokers; Fig 3A). The striking difference in disease-specific survival at 5 years remained at 10 years after surgery and beyond between the high HDGF group and the low HDGF group (Fig 3B). The probability of 5-year disease-specific survival was 0.92 (95% CI, 0.84 to 1.00) for patients with a lower HDGF labeling index compared with only 0.42 (95% CI, 0.28 to 0.62) for the group with a high HDGF labeling index. The disease-specific survival probability was highly significantly different between the two groups ($P < .0001$, log-rank test). Consistent with a role of HDGF in development of recurrence or metastasis, patients whose tumors expressed a higher level of HDGF had significantly poorer disease-free survivals ($P = .0008$, log-rank test; Fig 3C). The probability of 5-year disease-free survival was 0.71 (95% CI, 0.60 to 0.85) for patients with a high HDGF labeling index compared with 0.34 (95% CI, 0.22 to 0.53) for the group with a high HDGF labeling index.

To evaluate the robustness of the prognostic value of HDGF labeling index, we further divided the patients into four groups based on quartiles of HDGF labeling indexes and compared the survival probabilities of the groups. As the HDGF labeling index increases, overall survival (Fig 3D;

Downloaded from www.jco.org at M D ANDERSON HOSP on March 23, 2005 .
Copyright © 2004 by the American Society of Clinical Oncology. All rights reserved.

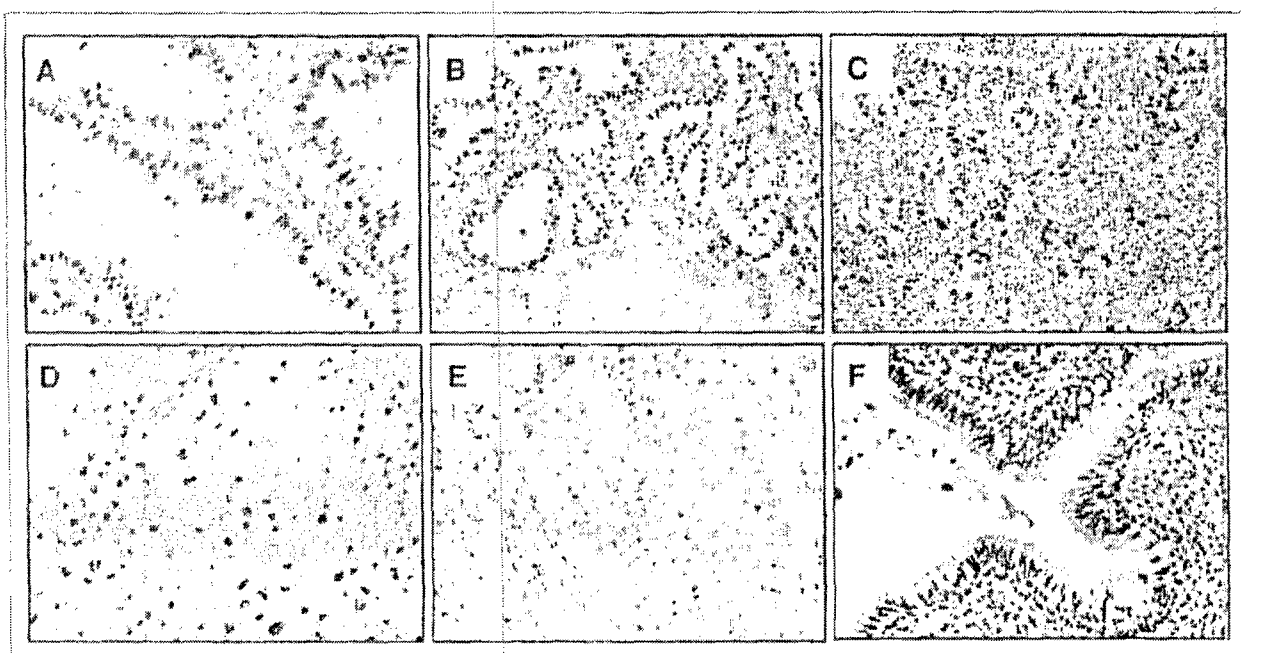


Fig 2. Hepatoma-derived growth factor expression detected by immunohistochemistry in lung adenocarcinomas (A, B, and C), lung squamous cell carcinomas (D and E) and bronchial epithelium in adjacent normal lung tissue (F).

$P < .0001$), disease-specific survival (Fig 3E; $P < .0001$), and disease-free survival (Fig 3F; $P = .0002$) decreased. When we compared patients whose tumors exhibited a labeling index less than 158 (the lowest quartile) with those whose tumors exhibited a labeling index ≥ 211 (the highest quartile), the difference in the survival probabilities was striking. At 5 years, none of the patients in the lowest quartile had died, while 84% of the patients in the highest quartile had died of any cause (95% CI, 0.07 to 0.40) and 76% died of lung cancer (95% CI, 0.11 to 0.54). Consistently, only 12% of the patients at the lowest quartile developed recurrence or metastasis at 5 years compared to 80% of the patients at the highest quartile.

To determine whether HDGF expression level is an independent factor in predicting survival probability for patients with pathologic stage I NSCLC, we performed multicovariable analysis using the Cox model. We found that HDGF expression level was the only independent predictor of disease-specific and disease-free survival probabilities ($P < .0001$) among the parameters tested, including age, sex, race, smoking status, and tumor histology. When overall survival was analyzed, HDGF expression level remained the most significant independent predictor ($P < .0001$); not surprisingly, age was also an independent predictor for overall survival ($P = .0002$). Martingale residual analysis showed that the Cox model fit the data well. It was confirmed that there was a linear relationship of higher HDGF and poorer overall, disease-specific, and disease-free survivals, suggesting that the higher the HDGF expression, the worse the clinical outcome observed in early stage NSCLC patients (Fig 4).

DISCUSSION

The capability of exogenous HDGF to stimulate the growth of fibroblasts and HuH-7 cells, aortic endothelial cells, and vascular smooth muscle cells[15] supports its role as a growth factor. Structurally, HDGF has a significant homology with the high-mobility group-1 DNA-binding protein,[11] but lacks the high-mobility box responsible for DNA binding. However, HDGF contains a PWWP domain at its *N*-terminal. The PWWP domain is a weakly conserved sequence motif found in over 50 eukaryotic proteins, including the mammalian DNA methyltransferases Dnmt3a and Dnmt3b, the transcription coactivator PC4, and the DNA mismatch repair protein MSH6,[16] all important in tumorigenesis. The precise function of the PWWP domain is not clear, but in the case of Dnmt3b, this domain has been shown to have a direct DNA-binding capability.[17] HDGF also contains two nuclear localization cassettes, two PEST (proline, glutamic/aspartic, serine, and threonine rich) domains, and a putative coiled-coil structure (Fig 1A). Recent studies have shown that nuclear localization is required for HDGF-mediated DNA synthesis and growth stimulation,[15,18] suggesting a role of HDGF as a transcription factor.

The finding that the expression level of HDGF in NSCLC strongly correlates with patients' clinical outcomes

Downloaded from www.jco.org at M D ANDERSON HOSP on March 23, 2005
Copyright © 2004 by the American Society of Clinical Oncology. All rights reserved.

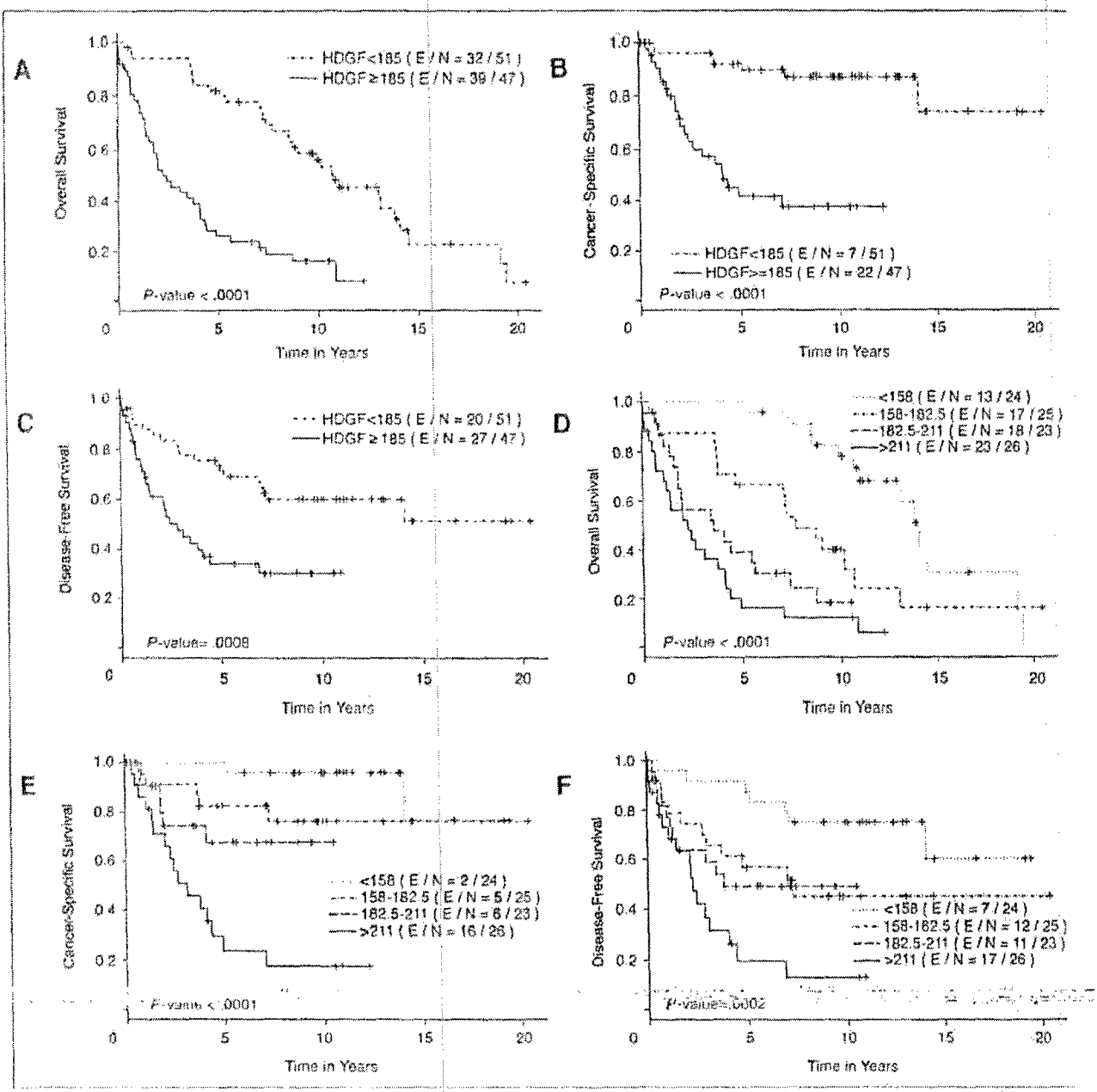


Fig 3. Probability of (A, D) overall survival; (B, E) cancer-specific survival; and (C, F) disease-free survival by levels of hepatoma-derived growth factor (HDGF) expression in primary non-small-cell lung cancer (NSCLC). The Kaplan-Meier method was used to determine the survival probability, and the log-rank test was used to compare the survival curves between groups.

suggests that HDGF plays an important role in lung tumorigenesis and in the determination of the biologic behavior of NSCLC. The analysis of HDGF labeling index by quartiles indicated a dose-dependent relationship between HDGF expression and survivals (Figs 3D through F). The striking differences between the patients in the lowest quartile and those in the highest quartile are consistent with the fact that the scoring method used for immunohistochemistry is more objective for cells expressing a very high level of proteins or a very low level of proteins while more subjective for cells expressing a medium level of proteins. A linear relationship between the HDGF expression level and patients' clinical outcome was further confirmed by using Martingale residual analysis (Fig 4). In the multivariate analysis, HDGF expression was an independent predictor of overall, disease-specific, and disease-free survivals. The consistency of

Downloaded from www.jco.org at M D ANDERSON HOSP on March 23, 2005 .
Copyright © 2004 by the American Society of Clinical Oncology. All rights reserved.

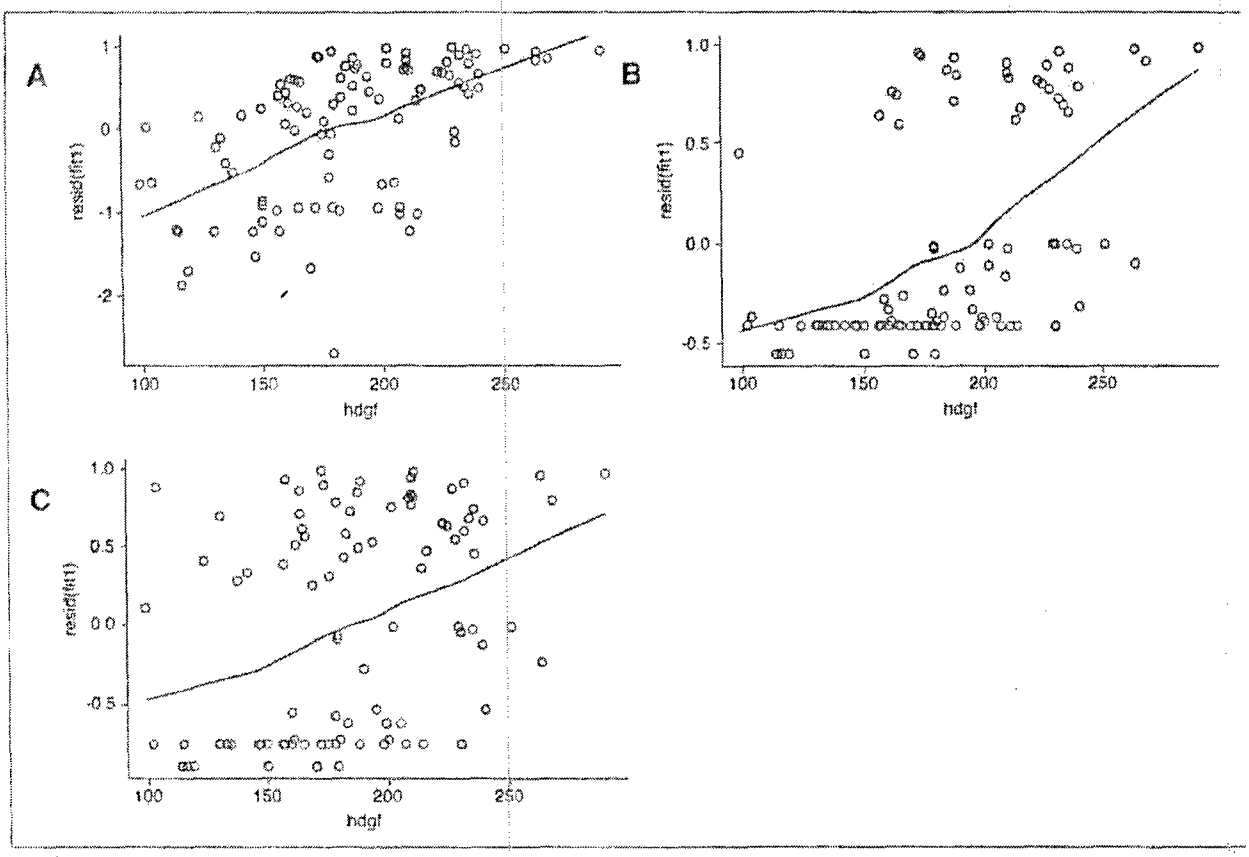


Fig 4. Martingale residual analysis shown as scatter plots of null Martingale residuals versus hepatoma-derived growth factor expressions. A linear trend was revealed in each subpanel by fitting the nonparametric lowess-smoothing regression lines through the data points. (A) overall survival; (B) cancer-specific survival; and (C) disease-free survival.

the results from different statistical analyses may allow us to conclude that HDGF has an important role in determining the behavior of NSCLC and is a promising biomarker for classifying patients with early-stage NSCLC. Given the advances in adjuvant therapy,[5] it must now be considered to offer adjuvant chemotherapy to patients whose primary tumors have been surgically resected in a curative attempt because 4% of these patients may benefit from such additional treatment. If it becomes standard care, however, most of the patients will suffer unwanted toxicity, which can be fatal to some patients, without gaining benefit in survival and quality of life. Therefore, the identification of patients with the highest risk of dying of lung cancer after potentially curative surgical treatment is a critical step in selecting patients for subsequent treatment with adjuvant therapy.

Although this study was not designed to provide direct evidence demonstrating that HDGF promotes tumorigenesis or facilitates metastasis, our findings together with data from previous reports provide a strong rationale to suggest such possibilities. In an in vitro study, Kishima et al[19] showed that downregulation of HDGF by antisense oligonucleotides can inhibit proliferation of hepatoma cell lines. Besides being mitogenic, HDGF has been shown to play a role in renal vascular development and in vascular lesion formation.[8] Mori et al[20] recently reported that HDGF can stimulate proliferation of lung epithelial cells in both in vitro and in vivo models. Therefore, HDGF may promote proliferation of tumor cells, as well as serve as a paracrine factor to facilitate neovascular formation, which is important for invasion and metastasis. Interestingly, we did not observe a correlation between HDGF and Ki-67 expression in the present study, suggesting that HDGF contributes to the aggressive biologic behavior through its paracrine activity rather than by stimulating tumor cell proliferation. We have, in fact, noticed that tumor cells at the invading front and metastases in lymph nodes exhibited stronger HDGF staining compared with the noninvading cells and the primary tumor sites (Tang and Mao, unpublished data). Interestingly, there were nine patients who developed brain metastasis after surgery in this study population. Eight of the nine patients were in the high HDGF group. The only patient whose primary tumor had a low HDGF labeling index developed brain metas-

Downloaded from www.jco.org at M D ANDERSON HOSP on March 23, 2005 .
Copyright © 2004 by the American Society of Clinical Oncology. All rights reserved.

tasis 6 months after surgery but survived for more than 6 years (data not shown).

In summary, our data demonstrated that HDGF expression is quantitatively associated with poor prognosis in all three types of clinical outcomes (disease-free survival, disease-specific survival, and overall survival) and strongly suggests that HDGF is involved in the disease aggressiveness, progression, and lethality. HDGF is a promising prognostic marker, not only to identify individuals with poor prognostic potential for more aggressive treatment, but also point to a new direction for searching effective molecular targeted therapies.

Note: The anti-HDGF antibody used in this study and/or monoclonal antibodies we are developing currently will be made available upon request.

Authors' Disclosures of Potential Conflicts of Interest

The authors indicated no potential conflicts of interest.

1. Parkin DM, Pisani P, Ferlay J: Global cancer statistics. CA Cancer J Clin 49:33-64, 1999

2. Jemal A, Thomas A, Murray T, et al: Cancer statistics, 2002. CA Cancer J Clin 52:23-47, 2002

3. Williams DE, Pariolero PC, Davis CS, et al: Survival of patients surgically treated for stage I lung cancer. J Thorac Cardiovasc Surg 82:70-76, 1981

4. Chemotherapy in non-small cell lung cancer: A meta-analysis using updated data on individual patients from 52 randomised clinical trials. Non-small Cell Lung Cancer Collaborative Group. BMJ 311:899-909, 1995

5. Le Chevalier T, for the IALT Investigators: Results of the randomized international adjuvant lung cancer trial (IALT): Cisplatin-based chemotherapy (CT) vs no CT in 1,867 patients with resected non-small-cell lung cancer. Proc Am Soc Clin Oncol 22:2, 2003 (abstr 6)

6. Nakamura H, Kambe H, Egawa T, et al: Partial purification and characterization of human hepatoma-derived growth factor. Clin Chim Acta 183:273-284, 1989

7. Everett AD: Identification, cloning, and developmental expression of hepatoma-derived growth factor in the developing rat heart. Dev Dyn 222:460-468, 2001

8. Oliver JA, Al-Awqati Q: An endothelial growth factor involved in rat renal development. J Clin Invest 102:1208-1219, 1998

9. Enomoto H, Yoshida K, Kishima Y, et al: Hepatoma-derived growth factor is highly expressed in developing liver and promotes fetal hepatocyte proliferation. Hepatology 36:1519-1527, 2002

10. von Heijne G: A new method for predicting signal sequence cleavage sites. Nucleic Acids Res 14:4683-4690, 1986

11. Nakamura H, Izumoto Y, Kambe H, et al: Molecular cloning of complementary DNA for a novel human hepatoma-derived growth factor. Its homology with high mobility group-1 protein. J Biol Chem 269:25143-25149, 1994

12. Everett AD, Lobe DR, Matsumura ME, et al: Hepatoma-derived growth factor stimulates smooth muscle cell growth and is expressed in vascular development. J Clin Invest 105:567-575, 2000

13. Mountain CF: Value of the new TNM system staging system for lung cancer. Chest 96:475-495, 1989

14. Soria JC, Jang SJ, Khuri FR, et al: Overexpression of cyclin B1 in early-stage non-small-cell lung cancer and its clinical implication. Cancer Res 60:4000-4004, 2000

15. Everett AD, Stoops T, McNamara CA: Nuclear targeting is required for hepatoma-derived growth factor-stimulated mitogenesis in vascular smooth muscle cells. J Biol Chem 276:37564-37568, 2001

16. Stec I, Nagl SB, van Ommen GJ, et al: The PWWP domain: A potential protein–protein interaction domain in nuclear proteins influencing differentiation? FEBS Lett 473:1-5, 2000

17. Qiu C, Sawada K, Zhang X, et al: The PWWP domain of mammalian DNA methyltransferase Dnmt3b defines a new family of DNA-binding folds. Nat Struct Biol 9:217-224, 2002

18. Kishima Y, Yamamoto H, Izumoto Y, et al: Hepatoma-derived growth factor stimulates cell growth after translocation to the nucleus by nuclear localization signals. J Biol Chem 277:10315-10322, 2002

19. Kishima Y, Yoshida K, Enomoto H, et al: Antisense oligonucleotides of hepatoma-derived growth factor (HDGF) suppress the proliferation of hepatoma cells. Hepatogastroenterology 49:1839-1844, 2002

20. Mori M, Morishita H, Nakamura H, et al: Hepatoma-derived growth factor is involved in lung remodeling by stimulating epithelial growth. Am J Respir Cell Mol Biol 30:459-469, 2004

Downloaded from www.jco.org at M D ANDERSON HOSP on March 23, 2005 .
Copyright © 2004 by the American Society of Clinical Oncology All rights reserved.

Hypermethylation of the Death-Associated Protein Kinase Promoter Attenuates the Sensitivity to TRAIL-Induced Apoptosis in Human Non–Small Cell Lung Cancer Cells

Ximing Tang, Weiguo Wu, Shi-yong Sun, Ignacio I. Wistuba, Waun Ki Hong, and Li Mao

Department of Thoracic/Head and Neck Medical Oncology, University of Texas M.D. Anderson Cancer Center, Houston, Texas

Abstract

Death-associated protein (DAP) kinase plays an important role in IFN-γ, tumor necrosis factor (TNF)-α, or Fas ligand–induced apoptosis. TNF-related apoptosis-inducing ligand (TRAIL) is a member of the TNF ligand family and can induce caspase-dependent apoptosis in cancer cells while sparing most of the normal cells. However, some of the cancer cell lines are insensitive to TRAIL, and such resistance cannot be explained by the dysfunction of TRAIL receptors or their known downstream targets. We reported previously that *DAP kinase* promoter is frequently methylated in non–small cell lung cancer (NSCLC), and such methylation is associated with a poor clinical outcome. To determine whether *DAP kinase* promoter methylation contributes to TRAIL resistance in NSCLC cells, we measured *DAP kinase* promoter methylation and its gene expression status in 11 NSCLC cell lines and correlated the methylation/expression status with the sensitivity of cells to TRAIL. Of the 11 cell lines, 1 had a completely methylated *DAP kinase* promoter and no detectable DAP kinase expression, 4 exhibited partial promoter methylation and substantially decreased gene expression, and the other 6 cell lines showed no methylation in the promoter and normal DAP kinase expression. Therefore, the amount of DAP kinase expression amount was negatively correlated to its promoter methylation ($r = -0.77$; $P = 0.003$). Interestingly, the cell lines without the DAP kinase promoter methylation underwent substantial apoptosis even in the low doses of TRAIL, whereas those with DAP kinase promoter methylation were resistant to the treatment. The resistance to TRAIL was reciprocally correlated to DAP kinase expression in 10 of the 11 cell lines at 10 ng/mL concentration ($r = 0.91$; $P = 0.001$). We treated cells resistant to TRAIL with 5-aza-2′-deoxycytidine, a demethylating reagent, and found that these cells expressed DAP kinase and became sensitive to TRAIL. These results suggest that DAP kinase is involved in TRAIL-mediated cell apoptosis and that a demethylating agent may have a role in enhancing TRAIL-mediated apoptosis in some NSCLC cells by reactivation of DAP kinase.

(Mol Cancer Res 2004;2(12):685–91)

Introduction

Death-associated protein (DAP) kinase is a Ca^{2+}/calmodulin-regulated, 160-kDa serine/threonine, microfilament-bound kinase shown recently to be involved in IFN-γ, tumor necrosis factor-α, or Fas ligand–induced apoptosis (1-3). Aggressiveness of malignant tumors has been associated with methylation of the promoter region of the *DAP kinase* gene (4-8) and loss of DAP kinase expression (9).

Tumor necrosis factor–related apoptosis-inducing ligand (TRAIL, also known as Apo-2L), a member of the tumor necrosis factor ligand family, is a cytokine that can induce a rapid caspase-dependent and tumor-specific apoptosis (10-16) through its specific death receptors DR4 and DR5 (17). The activation of DR4 and DR5, like that of Fas/Apo, leads to the activation of the initiator caspase, caspase-8, and its downstream targets (18). TRAIL seems to exert selective toxicity toward neoplastic cells, whereas most normal cells are resistant to TRAIL (19). Multiple factors have been proposed for such resistance, including the presence of the decoy receptors DcR1 and DcR2, the downexpression of DR4 and DR5, the silencing of caspase-8, the inactivity of Akt, and the overexpression of cFLIP and cyclooxygenase-2 (20-27).

In this study, we investigated whether DAP kinase plays a role in determining the sensitivity of cells to TRAIL using non–small cell lung cancer (NSCLC) as a model. Our data suggest that the DAP kinase may be involved in TRAIL-induced apoptosis, and restoration of DAP kinase expression may overcome TRAIL resistance in certain NSCLCs.

Results

Establishment of a Multiplex Methylation-Specific PCR

Methylation-specific PCR (MSP; ref. 28) is the most extensively used method for detecting the methylation status

Received 3/2/04; revised 10/21/04; accepted 11/22/04.
Grant support: American Cancer Society grant RPG-98-054; Tobacco Research Fund from the State of Texas; National Cancer Institute grants CA 16620, CA 68437, CA86390, and CA91844 (L. Mao); and Department of Defense grant DAMD17-01-1-01689-1.
The costs of publication of this article were defrayed in part by the payment of page charges. This article must therefore be hereby marked advertisement in accordance with 18 U.S.C. Section 1734 solely to indicate this fact.
Notes: W.K. Hong is an American Cancer Society clinical research professor.
Requests for reprints: Li Mao, Molecular Biology Laboratory, Department of Thoracic/Head and Neck Medical Oncology, University of Texas M.D. Anderson Cancer Center, Unit 432, 1515 Holcombe Boulevard, Houston, TX 77030. Phone: 713-792-6363; Fax: 713-796-8655; E-mail: lmao@mdanderson.org.
Copyright © 2004 American Association for Cancer Research.

of CpG islands in the promoter regions of genes. Combined bisulfite restriction analysis is more quantitative (29) but requires more strict experimental condition. In this study, we combined multiplex PCR and MSP to create multiplex MSP (MMSP). In this method, unmethylated and methylated DNA are amplified simultaneously with two primer sets specific for methylated and unmethylated CpG islands in the DAP kinase promoter. The intensities of PCR products between methylated and unmethylated DNA were used to determine their relative ratios. Our results indicate that MMSP is robust in quantifying methylated DAP kinase promoter (Fig. 1).

DAP Kinase Promoter Methylation in NSCLC Cell Lines

Using MMSP, we established the methylation status of the *DAP kinase* promoter in the 11 NSCLC cell lines. In 5 of the 11 (46%) cell lines, the CpG island in the promoter region was methylated (Fig. 2A). This percentage is close to the 44% that we found in early-stage NSCLC tissues in an earlier study (8). In the 5 promoter-methylated cell lines, the promoter in Calu-1 was completely methylated, whereas in H157, H460, H1792, and SK-MES-1 the promoter was partially methylated to different degrees.

To further determine the nature of mixed methylation status in some NSCLC cell lines, we isolated 98 individual clones of H460 cells and analyzed their methylation status. We found 77 clones that carried both methylated and unmethylated promoter alleles, 6 clones that contained a completely methylated promoter, and 15 clones that contained a completely unmethylated promoter. It suggests that H460 parental cell line is heterogeneous with respect to DAP kinase promoter methylation and its gene expression. It also suggests that the status of DAP kinase promoter methylation is also unstable in some of the subclones.

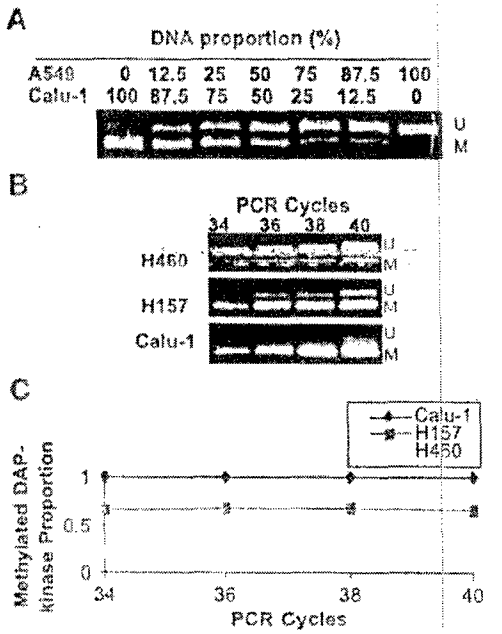


FIGURE 1. MMSP consistency for *DAP kinase* promoter methylation. A, MMSP was done using bisulfite-modified DNA from A549 cells (with unmethylated *DAP kinase* promoter) and Calu-1 cells (with methylated *DAP kinase* promoter), with ratios on *top of each lane*. B, MMSP using bisulfite-modified DNA isolated from NSCLC cell lines (H460, H157, and Calu-1). *U*, 279-bp unmethylated fragments; *M*, 218-bp methylated fragments. C, Scanning densitometry was used to measure and analyze the intensity of the fragment signal of B. Relative quantity of the methylation promoter was then calculated.

Expression of DAP Kinase in the NSCLC Cells Negatively Correlates with Its Promoter Methylation Status

Using multiplex reverse transcription-PCR, we examined DAP kinase expression in the 11 lung cancer cell lines. DAP kinase expression was completely or partially silenced in Calu-1, H1792, H157, H460, and SK-MES-1 cells (Fig. 2B), which have methylated CpG islands in their promoters, but not in A549, H226, H292, H522, H596, and H1944 cells, which have an unmethylated promoter. The extent of methylation detected in the *DAP kinase* promoter was negatively correlated with the DAP kinase mRNA level in the 11 cell lines ($r = -0.77$; $P = 0.003$ by linear correlation and regression analysis; Fig. 2C). Of the H460 subclones tested, H460-12 and H460-126, which were completely methylated, had no detectable *DAP kinase* gene and protein expression (example in Fig. 3C and D) but H460-14, H460-120, and H460-124, which were unmethylated, had detectable DAP kinase expression (example in Fig. 3C and D).

TRAIL-Induced Apoptosis of NSCLC Cells Correlates with DAP Kinase Promoter Methylation and Its Gene Expression

The 11 NSCLC cell lines with different *DAP kinase* promoter methylation status were treated with TRAIL at different doses (10, 40, and 160 ng/mL) to determine their response to TRAIL. The results (Table 1) show that cell deaths induced by TRAIL correlated with DAP kinase expression. When analyzed as a whole, the degree of cell death (% of cells dying) induced by TRAIL at low doses (10 and 40 ng/mL) were positively correlated with DAP kinase mRNA expression (10 ng/mL, $r = 0.91$, $P < 0.001$; 40 ng/mL, $r = 0.80$; $P = 0.008$ by linear correlation and regression analysis) but not at 160 ng/mL ($r = 0.46$; $P = 0.187$; Table 1). Immunochemical double staining with DAP kinase antibody and terminal deoxynucleotidyl transferase–mediated dUTP nick end labeling (TUNEL) showed that only the DAP kinase–expressing H460 cells underwent apoptosis after 12-hour incubation with TRAIL (10 ng/mL; Fig. 3A). To address the relationship of DAP kinase expression to TRAIL-induced apoptosis, we compared two H460 subclones (H460-12 and H460-124) in which the *DAP kinase* promoter was either completely methylated or unmethylated (Fig. 3B-D). 3-(4,5-Dimethylthiazol-2-yl)-2, 5-diphenyltetrazolium bromide (MTT; Fig. 3E) and DNA fragmentation (Fig. 3F) analyses showed that the H460-124 cells were sensitive, whereas the H460-12 cells were resistant to TRAIL-induced cell death.

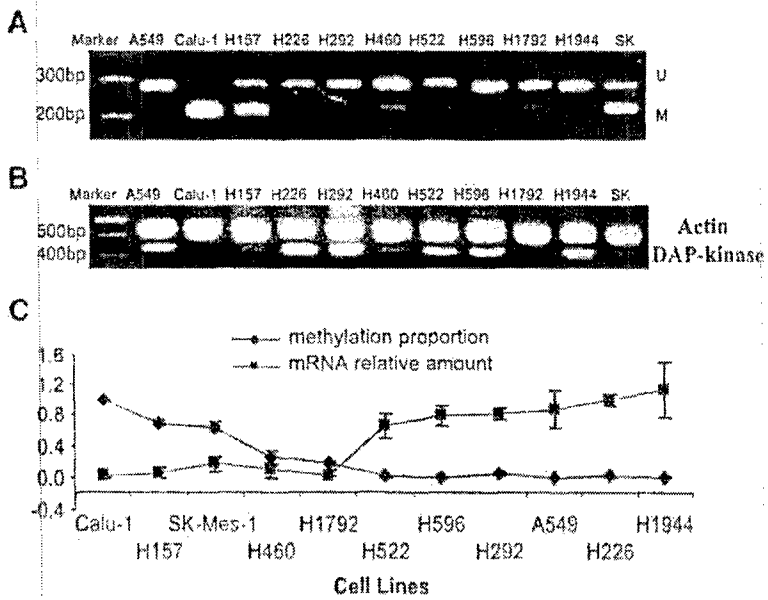


FIGURE 2. Correlation of *DAP kinase* promoter methylation status and expression of the gene in NSCLC cells. **A.** Methylation status of the *DAP kinase* promoter of the 11 NSCLC cell lines. *U*, 279-bp unmethylated PCR fragment; *M*, 218-bp methylated PCR fragment. **B.** DAP kinase mRNA expression in the 11 NSCLC cell lines. *Lane 1*, DNA size marker. **C.** Correlation of *DAP kinase* promoter methylation and expression of the gene based on data from **A** and **B**. *Points*, mean proportions of methylated *DAP kinase* promoter or relative gene expression level of three independent replicates; bars, unbiased SD.

The Restoration of DAP Kinase Expression and TRAIL Sensitivity by Promoter DNA Demethylation

To further establish that DAP kinase is involved in TRAIL-induced apoptosis in NSCLC cells, we pretreated Calu-1 and H460-12 cells, which contain a methylated *DAP kinase* promoter and lack *DAP kinase* gene expression, with 5-aza-2′-deoxycytidine (5ADC), a commonly used demethylation reagent, before TRAIL treatment. After pretreatment for 48 hours at 1 or 2 μmol/L, expression of DAP kinase was restored in both cell lines (Fig. 4A). The treatment substantially enhanced the levels of TRAIL-induced cell death/apoptosis in these cells as measured by MTT and DNA fragmentation assays (Fig. 4B and C).

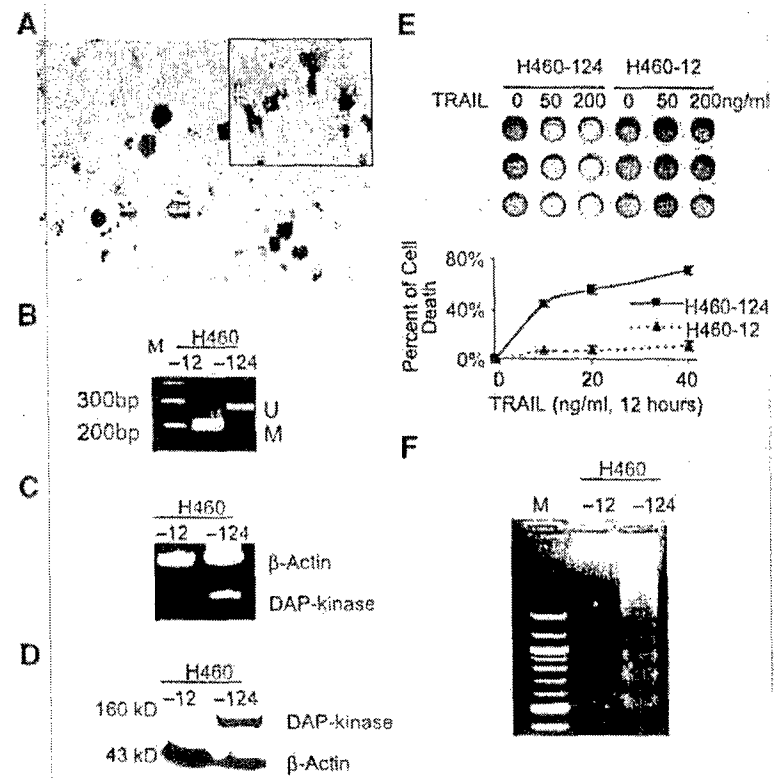


FIGURE 3. Correlation of DAP kinase expression with TRAIL-induced apoptosis in H460 cells. **A.** Double immunohistochemistry staining of H460 cells. *Black nuclear staining*, apoptosis; *red cytoplasmic staining*, expression of DAP kinase. *Top right box*, control panel without TRAIL treatment. **B.** Methylation status of two H460 subclones measured by MMSP. *U*, unmethylated fragment; *M*, methylated fragment. **C.** *DAP kinase* gene expression in H460-12 and H460-124. **D.** DAP kinase protein expression in H460-12 and H460-124. β-actin level was used as a loading control. **E.** TRAIL-induced cell death measured by MTT assay. *Top*, scanned image of the MTT results; *bottom*, measured rates of cell death. *Points*, mean cell death rates of three independent replicates; bars, SD. **F.** TRAIL-induced DNA fragmentation in the two subclones after TRAIL treatment (80 ng/mL for 12 hours). *M*, DNA size marker.

Discussion

In this study, we showed that *DAP kinase* promoter methylation and its gene expression correlate with TRAIL-induced apoptosis in NSCLC cells. We also showed that a demethylation agent activates *DAP kinase* gene expression and sensitizes the cells to TRAIL. We have shown previously that the promoter of the *DAP kinase* gene is methylated in 44% of primary NSCLC tumors (8) similar to the 46% rate we observed in NSCLC cell lines in present study. Methylation of the DAP kinase promoter in the primary tumors is associated with poor survival in patients with early-stage NSCLC (8). The methylation and lack of gene expression in hepatoma also correlated with a poor clinical outcome in patients (30). The inactivation of *DAP kinase* through its promoter methylation has been frequently detected in aggressive tumors of the brain (31), lymphoma (32), and colorectal cancer (33).

Of the 11 NSCLC cell lines studied, 5 contained a methylated *DAP kinase* promoter, including 4 that contained both methylated and unmethylated *DAP kinase* promoter, indicating that they are heterogeneous either due to differential methylation in one of the two *DAP kinase* alleles or the presence of subclones.

A highly negative correlation between *DAP kinase* methylation and gene expression was verified in the 11 NSCLC cell lines ($r = -0.77$, $P = 0.003$) and in the H460 subclones ($r = -0.97$; $P = 0.001$; data not shown). The fact that the promoter methylation status was consistent with *DAP kinase* gene expression indicates that the promoter methylation is the major mechanism to inactivate *DAP kinase*. Measurement of DAP kinase expression either by immunohistochemistry or *in situ* MSP would be helpful for predicting the functional status of the gene.

Previous studies have shown that *DAP kinase* is an important death messenger in IFN-γ, tumor necrosis factor-α, and Fas ligand–mediated apoptosis (3, 9), but *DAP kinase* involvement with TRAIL-induced cell apoptosis has not been reported. Consistent with this involvement is the observation that cells lacking DAP kinase expression were less sensitive to TRAIL-induced apoptosis than cells expressing DAP kinase. The fact that only cells expressing DAP kinase protein underwent apoptosis (Fig. 3) further supports the involvement of DAP kinase in TRAIL-induced apoptosis.

The expression of TRAIL decoy receptors DcR1 and DcR2 and death receptors DR4 and DR5 as messenger receivers directly influences TRAIL-induced apoptosis. In our previous study, we have shown DR5 was expressed, whereas decoy receptors were not expressed in H157 cells (34), yet these cells were resistant to TRAIL (Table 1), suggesting the involvement of other mechanisms for this resistance. We have not observed a strong correlation between the expression of TRAIL receptors and their sensitivity to TRAIL in the 11 cell lines we studied.[2] It has been shown that the binding of death ligands to receptors might result in recruitment of the cofactor Fas-associated death domain–containing protein with formation of a death-inducing signaling complex, which results in activation of caspase-8 (18, 35). Recent studies reported that the gene for *caspase-8* is silenced preferentially by aberrant promoter methylation in

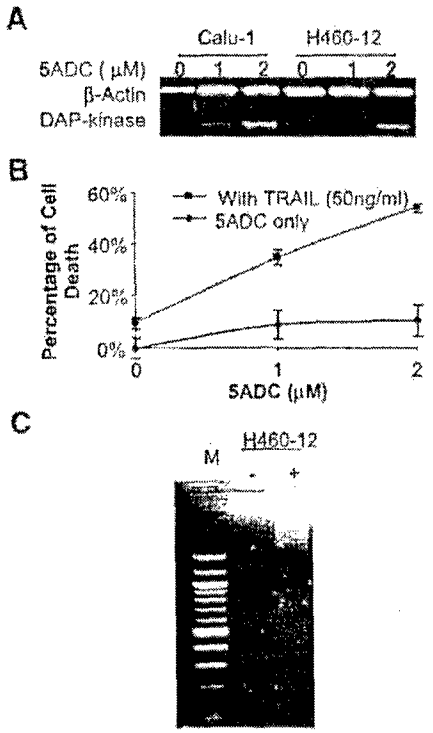


FIGURE 4. Restoration of DAP kinase expression and sensitivity to TRAIL treatment by promoter demethylation. **A.** DAP kinase expression was restored after treatment with 5ADC at the concentration of 1 or 2 μmol/L. **B.** MTT assay measuring cell death induced by TRAIL with or without 5ADC in H460-12 cells. Bars, unbiased SD of the triplicates. **C.** TRAIL-induced DNA fragmentation in H460-12 cells treated with TRAIL with (+) or without (–) 5ADC.

Table 1. Expression of DAP Kinase and TRAIL-Induced Cell Death in NSCLC Cell Lines

Cell Lines	DAP Kinase Expression*	TRAIL-Induced Cell Death (% of Control)		
		10 ng/mL†	40 ng/mL	160 ng/mL
Calu-1	0.000	0.00	6.79	7.22
H1792	0.022	0.00	10.79	24.87
H157	0.039	0.00	0.00	23.97
SK-MES-1	0.176	0.87	13.47	62.26
H522	0.644	9.48	17.95	35.81
H596	0.783	11.20	31.24	59.26
H292	0.812	12.47	13.97	43.22
A549	0.874	8.55	20.31	45.39
H226	0.900	12.61	19.13	25.22
H1944	1.120	25.85	30.05	45.70
r‡ (DAP Kinase Expression TRAIL-Induced Cell Death)		0.91	0.80	0.46
P		0.001	0.008	0.187

*mRNA relative amount to β-actin detected with multiplex reverse transcription-PCR.
†TRAIL, incubated for 12 hours, MTT analysis
‡Linear correlation and regression analysis.

[2] Unpublished data

neuroblastomas, bronchial carcinoids, and small cell lung cancer but not in NSCLC (36, 37). Nevertheless, a potential relationship between TRAIL receptors and DAP kinase warrants further investigation.

When NSCLC cells containing a methylated DAP kinase promoter were treated with 5ADC (a demethylation agent), the cells restored expression of DAP kinase and TRAIL sensitivity (Fig. 4). These results support the involvement of DAP kinase in TRAIL-induced apoptosis and provide justification for combination of demethylation agent(s) with death ligand(s) to improve the therapeutic effects.

Although different cancer cell lines carry distinct patterns of methylated promoters and 5ADC treatment sensitized TRAIL response in multiple cell lines (Fig. 4),[3] it is still possible that activation of other genes by 5ADC treatment contributes to the sensitization. Additional experiments to specifically activate *DAP kinase* or specifically inhibit *DAP kinase* may provide more direct evidence to support the role of DAP kinase in rescuing TRAIL-induced apoptosis in NSCLC.

Materials and Methods

Cell Lines, Cell Culture, and Cell Subcloning

Human NSCLC cell lines A549, Calu-1, H157, H226, H292, H460, H522, H596, H1792, H1944, and SK-MES-1 were obtained from the American Type Cell Culture (Rockville, MD) and grown in DMEM (Life Technologies, Rockville, MD) containing 10% fetal bovine serum and antibiotics. The cells were maintained at 37°C in a humidified atmosphere consisting of 5% CO_2 and 95% air in monolayers.

For each subcloning experiment, 30 to 50 H460 parental cells were seeded into a 100-mm dish and incubated for 4 hours; attached single cells were then identified by marking the back of the dish. After being cultured for 7 days, the individual clones originating from the marked single cells were transferred to 24-well plates for further culture before being transferred to 100-mm dishes for further expansion. All the subclones were harvested once on the same day to avoid biological variation in successive generations.

cDNA Preparation and Multiplex Reverse Transcription-PCR

Total RNA was extracted and purified from cultured cells using RNeasy mini kit (Qiagen, Valencia, CA) following the manufacturer's instructions. Total RNA (1 μg) was used to synthesize cDNA with SuperScript II reverse transcriptase (Life Technologies) in 20 μL, and the final product was diluted to 100 μL. The cDNA was then used for the quantitative assay of DAP kinase expression by multiplex PCR. The multiplex reverse transcription-PCR was carried out under optimal conditions after which a linear correlation between cycle numbers and product amount of PCR was obtained (data not shown). PCR reaction mixture (10 μL) contained 1 μL diluted cDNA sample, 1 unit Hotstart polymerase (Qiagen), 0.1 mmol/L deoxynucleotide triphosphates (dATP + dTTP + dCTP + dGTP), 1 μL DMSO, and 50 ng DAP kinase primers (forward 5′-GACACCGGCGAGGAACTTGGC-3′ and reverse 5′-AAAGTCAATGATCTTGATCCGA-3′). The reaction was done according to the following program: at 94°C for 15 minutes for activating the polymerase; for 34 cycles at 94°C for 30 seconds, at 60°C for 1 minute, and at 72°C for 1 minute; and at 72°C for 7 minutes. At the 6th cycle of the 2nd step, β-actin primers (forward 5′-GTTGCTATCCAGG CTGTGC-3′ and reverse 5′-GCATCCTGTCGGCAATGC-3′) were added into the reaction mixture as an internal control. The PCR products were electrophoresed on 2.5% agarose gel. Then, the gel was stained with ethidium bromide and photographed under UV light. The absorbance of the DAP kinase–specific fragments was measured by scanning densitometry using the absorbance of the internal control (β-actin) as the standard. The relative amount of the DAP kinase mRNA was calculated as absorbance of *DAP kinase/actin*.

DNA Isolation and MMSP

DNA was extracted and purified from cultured cells. The cells were collected and digested in 200 μL of digestion buffer containing 50 mmol/L Tris-HCl (pH 8.0), 1% SDS, and 0.5 mg/mL proteinase K and incubated at 42°C for 36 hours. The digested products were purified with phenol-chloroform twice. DNA was then precipitated using the ethanol precipitation method and recovered in distilled DNase-free water. Bisulfite modification of DNA was done as described by Herman et al. (28). Briefly, 1 μg of the DNA from each sample was denatured using NaOH and then treated with sodium bisulfite (Sigma, St. Louis, MO) for 16 hours. After purification using the Wizard DNA purification kit (Promega, Madison, WI), the purified DNA was treated again with NaOH, precipitated with ethanol, and recovered in distilled water. The relative quantity of methylated and unmethylated DAP kinase promoters was determined by the MMSP. The primers specific for unmethylated CpG islands were (forward) 5′-TTGTGAGTTGTTGATTTTTTTTTGT-3′ and (reverse) 5′-ATACACAATAAAACACACCAACAAA-3′, which cover a 279-bp fragment; the primers specific for methylated CpG islands were (forward) 5′-CGAGTTGTC-GAGTTTTTTTCGC-3′ and (reverse) 5′-CCGCGC-AAAACCCGCAACG-3′, which cover a 218-bp fragment. The PCR products were separated in 2.5% of agarose gel, stained with ethidium bromide, and then photographed under UV light. The absorbances of the unmethylated fragments (*U*) at 279 bp and methylated fragments (*M*) at 218 bp were determined by scanning densitometry of the photographs. The proportion of methylation alleles was calculated as $M / U + M$.

Protein Extraction and Western Blot Analysis

Cellular proteins were collected in lysis buffer containing 150 mmol/L NaCl, 1% Triton X-100, 1% sodium deoxycholate, 0.1% SDS, 10 μg/mL phenylmethylsulfonyl fluoride, 30 μg/mL aprotinin, and 50 mmol/L Tris-HCl (pH 8.0). The samples were then placed on ice for 60 minutes and then centrifuged at 14,000 × *g* at 4°C for 30 minutes. The protein concentration was measured using a protein assay kit (Bio-Rad, Hercules, CA). Each protein sample (30 μg) was subjected to SDS-PAGE

[3] Unpublished data

using 8% denaturing polyacrylamide gel. The proteins were then transferred to Hybond-C nitrocellulose membranes (Amersham Pharmacia Biotech, Inc., Piscataway, NJ). The nitrocellulose membranes were incubated in a blocking solution containing 5% bovine skim milk in 10 mmol/L PBS containing 0.1% Tween 20 for 1 hour followed by incubation for 3 hours with monoclonal anti-DAP kinase antiserum (DAPK-55, Sigma) at a concentration of 1:1,000 or monoclonal anti-β-actin (AC15, Sigma) antibody at a concentration of 1:5,000. The membranes were washed with PBS and then incubated with the secondary anti-mouse antibody supplied in the enhanced chemiluminescence kit (Amersham Pharmacia Biotech) for 1 hour. After this incubation, the membranes were washed thrice in PBS, developed in enhanced chemiluminescence solution for 1 to 2 minutes, and exposed to X-ray film for chemiluminescence detection of the positive protein bands.

TUNEL and DAP Kinase Protein Detection by Immunohistochemistry Double Staining

H460 cells were seeded on two glass slides, incubated for 24 hours, and then treated with or without TRAIL (10 ng/mL, Calbiochem, San Diego, CA) for 12 hours. The slides were then fixed in 10% paraformalin [prepared with PBS (pH 7.4)] for 20 minutes and washed in PBS for 5 minutes. The TUNEL assay was done with TUNEL kit (Intergen, Burlington, MA) according to instructions provided by the manufacturer. 3,3'-Diaminobenzidine-conjugated nickel was used as a chromogen to stain the apoptotic cells. The slides were then subjected to double staining with immunohistochemistry to detect the expression of DAP kinase protein by the following procedures: the slides were treated thrice for 5 minutes in a microwave oven with 10 mmol/L citrate buffer (pH 6.0) to retrieve the antigenicity, immersed in methanol containing 0.3% hydrogen peroxidase for 20 minutes to block the endogenous peroxidase, and incubated in 2.5% blocking serum to reduce nonspecific binding. The slides were incubated overnight at 4°C with primary anti-DAP kinase monoclonal antiserum (DAPK-55, Sigma) as a dilution 1:160 and then processed using standard avidin-biotin immunohistochemistry according to the manufacturer's recommendations (Vector Laboratories, Burlingame, CA). Vector NovaRed (Vector Laboratories) was used as a chromogen to detect DAP kinase expression as red in the cytoplasm. Methyl green was used for nuclear counterstaining.

DNA Fragmentation Assay

After treatment with TRAIL, both floating and attached cells were collected, pelleted, and resuspended in Tris-EDTA buffer (pH 8.0). The plasma membrane of the cell was lysed on ice in a mixture of 10 mmol/L Tris-HCl (pH 8.0), 10 mmol/L EDTA, and 0.5% Triton X-100 for 15 minutes. The lysate was centrifuged at 12,000 × *g* for 15 minutes to separate the soluble (fragmented) from pellet (intact genomic) DNA. The soluble DNA was treated with RNase A (50 μg/mL) at 37°C for 1 hour and proteinase K (100 μg/mL) in 0.5% SDS at 50°C for 2 hours, extracted with phenol-chloroform, precipitated in ethanol, electrophoresed on a 1.8% agarose gel, and stained with ethidium bromide. The gels were then photographed under UV illumination.

Demethylation

Cells were treated with 5ADC (Sigma) at 1 or 2 μmol/L concentrations for 48 hours before further treatment with TRAIL.

MTT Assay

About 30,000 cells of each line were seeded in 96-well plates in 0.1 mL DMEM in triplicate and incubated for 24 hours. The medium was then replaced with medium containing a designated concentration of TRAIL and incubated for another 12 hours. At the end of treatment, 10 μL (5 mg/mL) MTT (Sigma) were added and incubated for 3 hours. The medium containing MTT was absorbed off and washed with PBS carefully, and 0.1 mL DMSO was added to each well. Absorbances of controls (A_c) and experimental samples (A_t) at a wavelength of 540 nm with background subtraction at 620 nm were measured using the E_{max} precision microplate reader (Molecular Devices, Sunnyvale CA). Cell death (%) is calculated as $100 \times (1 - A_t / A_c)$.

References

1. Deiss LP, Feinstein E, Berissi H, Cohen O, Kimchi A. Identification of a novel serine/threonine kinase and a novel 15-kD protein as potential mediators of the γ interferon-induced cell death. Genes Dev 1995;9:15–30.

2. Cohen O, Feinstein E, Kimchi A. DAP-kinase is a Ca^{2+}/calmodulin-dependent, cytoskeletal-associated protein kinase, with cell death-inducing functions that depend on its catalytic activity. EMBO J 1997;16:998–1008.

3. Cohen O, Inbal B, Kissil JL, et al. DAP-kinase participates in TNF-α- and Fas-induced apoptosis and its function requires the death domain. J Cell Biol 1999;146:141–8.

4. Shiramizu B, Mick P. Epigenetic changes in the DAP-kinase CpG island in pediatric lymphoma. Med Pediatr Oncol 2003;41:527–31.

5. Ueki T, Toyota M, Sohn T, et al. Hypermethylation of multiple genes in pancreatic adenocarcinoma. Cancer Res 2000;60:1835–9.

6. Katzenellenbogen RA, Baylin SB, Herman JG. Hypermethylation of the DAP-kinase CpG island is a common alteration in B-cell malignancies. Blood 1999;93:4347–53.

7. Sanchez-Cespedes M, Esteller M, Wu L. Gene promoter hypermethylation in tumors and serum of head and neck cancer patients. Cancer Res 2000;60:892–5.

8. Tang X, Khuri FR, Lee JJ, et al. Hypermethylation of the death-associated protein (DAP) kinase promoter and aggressiveness in stage I non-small-cell lung cancer. J Natl Cancer Inst 2000;92:1511–6.

9. Inbal B, Cohen O, Polak-Charcon S, et al. DAP kinase links the control of apoptosis to metastasis. Nature 1997;390:180–4.

10. Pan G, O'Rourke K, Chinnaiyan AM, et al. The receptor for the cytotoxic ligand TRAIL. Science 1998;276:111.

11. Sedger LM, Shows DM, Blanton RA, et al. IFN-γ mediates a novel antiviral activity through dynamic modulation of TRAIL and TRAIL receptor expression. J Immunol 1999;163:920.

12. Yu R, Mandlekar S, Ruben S, Ni J, Kong AN. Tumor necrosis factor-related apoptosis-inducing ligand-mediated apoptosis in androgen-independent prostate cancer cells. Cancer Res 2000;60:2384–9.

13. Thomas WD, Hersy P. TNF-related apoptosis-inducing ligand (TRAIL) induces apoptosis in Fas ligand-resistant melanoma cells and mediates in CD4 T cell killing of target cells. J Immunol 1998;161:2195–200.

14. Walczak H, Miller RE, Ariail K, et al. Tumoricidal activity of tumor necrosis factor-related apoptosis-inducing ligand *in vivo*. Nat Med 1999;5:157–63.

15. Mitsiades N, Poulaki V, Tseleni-Balafoula S, Koutras DA, Stamenkovic I. Thyroid carcinoma cells are resistant to FAS-mediated apoptosis but sensitive to tumor necrosis factor-related apoptosis-inducing ligand. Cancer Res 2000;60:4122–9.

16. Wu M, Das A, Tan Y, Zhu C, Cui T, Wong MC. Induction of apoptosis in glioma cell lines by TRAIL/Apo-2L. J Neurosci Res 2000;61:464–70.

17. Ashkenazi A. Targeting death and decoy receptors of the tumour-necrosis factor superfamily. Nat Rev Cancer 2002;2:420–30.

18. Kischkel FC, Lawrence DA, Chuntharapai A, Schow P, Kim KJ, Ashkenazi A. Apo2L/TRAIL-dependent recruitment of endogenous FADD and caspase-8 to death receptors 4 and 5. Immunity 2000;12:611–20.

19. Pan G, Ni J, Wei YF, Yu G, Gentz R, Dixit VM. An antagonist decoy receptor and a death domain-containing receptor for TRAIL. Science 1997;277:815–8.

20. Kim K, Fisher MJ, Xu S-Q, El-Deiry WS. Molecular determinants of response to TRAIL in killing of normal and cancer cells. Clin Cancer Res 2000;6:335–46.

21. Pitti RM, Marsters SA, Ruppert S, Donahue CJ, Moore A, Ashkenazi A. Induction of apoptosis by Apo-2 ligand, a new member of the tumor necrosis factor cytokine family. J Biol Chem 1996;271:12687–90.

22. Fanger NA, Maliszewski CR, Schooley K, Griffith TS. Human dendritic cells mediate cellular apoptosis via tumor necrosis factor-related apoptosis-inducing ligand (TRAIL). J Exp Med 1999;190:1155–64.

23. Zhang XD, Nguyen T, Thomas WD, Sanders JE, Hersey P. Mechanisms of resistance of normal cells to TRAIL induced apoptosis vary between different cell types. FEBS Lett 2000;482:193–9.

24. Hopkins-Donaldson S, Ziegler A, Kurtz S, et al. Silencing of death receptor and caspase-8 expression in small cell lung carcinoma cell lines and tumors by DNA methylation. Cell Death Differ 2003;10:356–64.

25. Chen X, Thakkar H, Tyan F, et al. Constitutively active Akt is an important regulator of TRAIL sensitivity in prostate cancer. Oncogene 2001;20:6073–83.

26. Jonsson G, Paulie S, Grandien A. High level of cFLIP correlates with resistance to death receptor-induced apoptosis in bladder carcinoma cells. Anticancer Res 2003;23:1213–8.

27. Tang X, Sun YJ, Half E, Kuo MT, Sinicrope F. Cyclooxygenase-2 overexpression inhibits death receptor 5 expression and confers resistance to tumor necrosis factor-related apoptosis-inducing ligand-induced apoptosis in human colon cancer cells. Cancer Res 2002;62:4903–8.

28. Herman JG, Graff JR, Myohanen S, Nelkin BD, Baylin SB. Methylation-specific PCR: a novel PCR assay for methylation status of CpG islands. Proc Natl Acad Sci U S A 1996;93:9821–6.

29. Xiong Z, Laird PW. COBRA: a sensitive and quantitative DNA methylation assay. Nucleic Acids Res 1997;25:2532–4.

30. Matsumoto H, Nagao M, Ogawa S, et al. Prognostic significance of death-associated protein-kinase expression in hepatocellular carcinomas. Anticancer Res 2003;23:1333–41.

31. Gonzalez-Gomez P, Bello MJ, Alonso ME, et al. Frequent death-associated protein-kinase promoter hypermethylation in brain metastases of solid tumors. Oncol Rep 2003;10:1031–3.

32. Nakatsuka S, Takakuwa T, Tomita Y, et al. Hypermethylation of death-associated protein (DAP) kinase CpG island is frequent not only in B-cell but also in T- and natural killer (NK)/T-cell malignancies. Cancer Sci 2003;94:87–91.

33. Yamaguchi S, Asao T, Nakamura J, Ide M, Kuwano H. High frequency of DAP-kinase gene promoter methylation in colorectal cancer specimens and its identification in serum. Cancer Lett 2003;194:99–105.

34. Wu W, Soria J, Wang L, Kemp BL, Mao L. TRAIL-R2 is not correlated with p53 status and is rarely mutated in non-small cell lung cancer. Anticancer Res 2000;20:4525–30.

35. Bodmer JL, Holler N, Reynard S, et al. TRAIL receptor-2 signals apoptosis through FADD and caspase-8. Nat Cell Biol 2000;2:241–3.

36. Shivapurkar N, Toyooka S, Eby MT, et al. Differential inactivation of caspase-8 in lung cancers. Cancer Biol Ther 2002;1:65–9.

37. Teitz T, Wei T, Valentine MB, et al. Caspase-8 is deleted or silenced preferentially in childhood neuroblastomas with amplification of MYCN. Nat Med 2000;6:529–35.

[Cancer Biology & Therapy 3:9, 847-852, September 2004]; ©2004 Landes Bioscience

Research Paper

Eicosanoid Metabolism in Squamous Cell Carcinoma Cell Lines Derived from Primary and Metastatic Head and Neck Cancer and its Modulation by Celecoxib

Claudia P. Schroeder[1]
Peiying Yang[2]
Robert A. Newman[2]
Reuben Lotan[1,*]

[1]Department of Thoracic Head and Neck Medical Oncology; [2]Department of Experimental Therapeutics; The University of Texas M. D. Anderson Cancer Center; Houston, Texas, USA

*Correspondence to: Reuben Lotan, The University of Texas M. D. Anderson Cancer Center; 1515 Holcombe Blvd.; Houston, Texas 77030 USA; Tel.: 713.792.3467; Fax: 713.745.5656; Email: rlotan@mdanderson.org

Received 05/19/04; Accepted 06/18/04

Previously published online as a *Cancer Biology & Therapy* E-publication: http://www.landesbioscience.com/journals/cbt/abstract.php?id=1097

KEY WORDS

celecoxib, COX-2 inhibitors, cyclooxygenases, eicosanoid metabolism, HNSCC cell lines, leukotrienes, lipoxygenases, prostaglandins

ABBREVIATIONS

BHT	butylated hydroxytoluene
COX	cyclooxygenase
DMEM	Dulbecco's Modified Eagle's Minimal Essential Medium
DMSO	dimethyl sulfoxide
FBS	fetal bovine serum
HETE	hydroxyeicosatetraenoic acid
HNSCC	head and neck squamous cell carcinoma
HODE	hydroxyoctadecadienoic acid
[illegible]/MS/MS	electrospray ionization liquid chromatography tandem mass spectrometry
LOX	lipoxygenase
MTT	[3-(4,5-dimethylthiazol-2-yl)2,5-diphenyl-2H-terrazolium bromide]
NSAIDs	nonsteroidal anti-inflammatory drugs
PBS	phosphate-buffered saline
PG	prostaglandin

ACKNOWLEDGEMENTS

This work was supported by a fellowship from the Deutsche Forschungsgemeinschaft (DFG, Germany); PO1 CA98144 from the National Cancer Institute, and BESCT Lung Cancer Program from the Department of Defense (grant DAMD17-01-1-0689-2).

ABSTRACT

Eicosanoid metabolism through cyclooxygenases (COXs) and lipoxygenases (LOXs) generates various lipids that play a role in squamous cell carcinogenesis. We used pairs of head and neck squamous cell carcinoma (HNSCC) cell lines derived from primary and metastatic tumors of the same patient to analyze eicosanoid metabolites by ESI-LC/MS/MS and COX/LOX expression by western immunoblotting. The effects of celecoxib on eicosanoid synthesis and HNSCC cell growth were examined. Prostaglandin E_2 (PGE_2) was the major metabolite in three of six cell lines. COX-2 was detected in three cell lines, which produced PGE_2 (two from metastases). We found low expression of COX-1 at similar intensities for each pair of cell lines. 5-LOX was detected in all cells. Some expressed 12-LOX, 15-LOX-1, and 15-LOX-2, but there was no correlation between enzyme expression and endogenous product content in cells. Exogenous arachidonic acid did not change the profile of eicosanoid biosynthesis. Low doses of celecoxib inhibited formation of PGE_2 in UMSCC-14A cells by 84% as early as 6 hours. In contrast, 5-HETE, 12-HETE, and 15-HETE levels were increased by approximately 40-, 5- and 3-fold, respectively, with a decline to baseline levels within 24 hours. High dose celecoxib increased the 12-HETE level 2.3-fold after 3 days of incubation. Celecoxib inhibited growth of all HNSCC cell lines in a concentration-dependent manner regardless of their COX expression (IC_{50} values after 3 days; 33 to 62 μM). Our findings provide new informations about individual eicosanoids produced by HNSCC cells and their differential regulation by the selective COX-2 inhibitor celecoxib.

INTRODUCTION

Squamous cell carcinomas (SCC) of the head and neck (HN) are potentially aggressive tumors characterized by considerable morbidity and mortality due to a high incidence of local recurrence and lymph node metastasis.[1] The long-term survival of patients could be improved by prevention of carcinogenesis and secondary lesions that are associated with invasive behavior of the primary tumor. Therefore, understanding mechanisms that affect growth, survival, and invasiveness of rumor cells may benefit future rational design for treatment and prevention of cancer. A body of evidence suggests that the metabolism of polyunsaturated fatty acids (e.g., arachidonic acid) is critically involved in the development of HNSCC.[2-4] In particular, altered expression and activity of cyclooxygenases (COXs) and lipoxygenases (LOXs) including their metabolites referred to as eicosanoids have been implicated in squamous cell carcinogenesis.[5-8]

Arachidonic acid, derived from membrane phospholipids through the action of phospholipase, is metabolized by COXs to prostaglandins (PGs) and thromboxanes, and by LOXs to leukotrienes, lipoxins and a variety of mono-hydroxylated fatty acids such as HETEs.[9] The oxidative pathway of linoleic acid leads to hydroxyoctadecadienoic acids (HODEs) predominantly formed by 15-LOX-1.[10] Although, multiple enzymes related to eicosanoid metabolism are similar in terms of structure, substrate preference and mechanisms of action, a variety of biological effects have been demonstrated for their products in various experimental models.[11-14] In fact, elevated PG levels have been detected in HNSCC cell lines and neoplastic tissues resected from patients.[15-17] Furthermore, there is evidence for a strong correlation between PGE_2 synthesis and prognostic significance as well as metastatic ability of tumor cells in vivo.[18,19] Accordingly, COX-2 isoenzyme is frequently upregulated in HN cancers that have been reported to be associated with tumor growth, resistance to apoptosis, metastasis, and angiogenesis.[7,20-22] The function and molecular mechanisms of LOX products in cancer, however, remain less clear although recent studies have suggested that LOX activation may be involved in both pro- and

anti-tumorigenic effects.[11,13,14] Analysis of human saliva and primary tumor tissue samples from patients with SCC showed significantly elevated levels of 12-HETE, 5-HETE, and 15-HETE.[5,23] In addition, data on SCC cell lines have postulated a close relationship between growth control and LOX pathways.[11] Recent studies have shown that nonsteroidal anti-inflammatory drugs (NSAIDs) can increase the expression of 15-LOX-1 and 15-LOX-2 isoenzymes, which were downregulated in HN cancer cells. These effects were accompanied by inhibition of cell proliferation and induction of apoptosis.[13,14] Nonetheless, modulation of the eicosanoid metabolism by COX-inhibitors such as aspirin and other NSAIDs exerts chemopreventive activity on the development of SCC.[24-26] Celecoxib, a selective COX-2 inhibitor, was found to suppress oral cancer growth and angiogenesis in a nude mouse model.[27] Although the most likely antitumoral effects of NSAIDs are based on the blockade of PG synthesis, accumulating evidence suggests that mechanisms of action may not be exclusively mediated by inhibition of COX activity.[11,13,28-31]

In this study we analyzed eicosanoid metabolites and related enzymes in pairs of HNSCC cell lines derived from primary and recurrent or metastatic tumor samples of the same patient. We found a correlation between PGE_2 production and COX-2 expression, which appeared to be higher in HNSCC cell lines derived from metastasis. We therefore investigated the effects of the selective COX-2 inhibitor, celecoxib, on eicosanoid production and HNSCC cell growth.

MATERIALS AND METHODS

Reagents. Dulbecco's Modified Eagle's Minimal Essential Medium (DMEM)/Ham's F12, penicillin, streptomycin, phosphate-buffered saline (PBS) and trypsin were purchased from Gibco™ Invitrogen Corporation (Carlsbad, CA). Fetal bovine serum (FBS) was from HyClone Laboratories, Inc. (Logan, UT) and celecoxib (Celebrex®) was obtained from GD Searle & Co (Chicago, IL). Arachidonic acid, bovine serum albumin, butylated hydroxytoluene (BHT), citric acid, dimethyl sulfoxide (DMSO), ethylene diamine terra-acetic acid (EDTA), [3-(4,5-dimethylthiazol-2-yl)2,5-diphenyl-2H-tetrazolium bromide] (MTT) and sodium dodecyl sulfate (SDS) were from Sigma Chemical Co. (St. Louis, MO). Mouse monoclonal antibody against human prostaglandin H synthase-1 peptide (PGHS-1, COX-1), and rabbit polyclonal antibodies against PGHS-2 (COX-2), 12-LOX and 15-LOX-2 were from Oxford Biomedical Research Inc. (Oxford, MI). Anti-actin was obtained from Santa Cruz Biotechnology Inc. (Santa Cruz, CA) and anti-human 5-LOX antiserum was from BD Bioscience Pharmingen (San Diego, CA). Rabbit polyclonal antiserum to human 15-LOX-1 was kindly provided by Dr. I. Shureiqi (Shureiqi et al., 2001). Secondary antibody to IgG conjugated to horseradish peroxidase was from Amersham Biosciences Corp. (Piscataway, NJ). The deuterium-labeled eicosanoids PGE_2, 5-HETE, 12-HETE, 15-HETE, and 13-HODE used as internal standard for ESI-LC/MS/MS analyses were purchased from Cayman Chemical Co. (Ann Arbor, MI).

Human Squamous Carcinoma Cell Lines of the Head and Neck. The continuous human squamous carcinoma cell lines UMSCC-11A/-11B, UMSCC-14A/-14B, UMSCC-17A/-17B, and UMSCC-22A/-22B were kindly provided by Dr. T. Carey (University of Michigan, Ann Arbor, MI) and have been characterized elsewhere.[32] The cell lines derived from the primary tumor *suffix A* and the corresponding recurrent or metastatic lesion *suffix B* of the same patient are shown in Table 1. Cells were routinely maintained in DMEM/Ham's F12 (1:1, v/v) supplemented with 5% FBS, penicillin (100 units/ml) and streptomycin (100 µg/ml) defined as standard medium at 37°C in a humidified atmosphere of 95% air and 5% CO_2. Cultures were passaged twice a week using 0.25% trypsin containing 0.02% EDTA. The desired concentrations of celecoxib were made by diluting the stock solution (0.05 M/DMSO) directly into the culture medium keeping the final concentration of DMSO less than 0.1%. All experiments were carried out in the presence of 5% FBS.

Table 1 **Source of HNSCC Cell Lines** [a]

Cell line	Location of tumor
UMSCC-11A	Hypopharynx
UMSCC-11B	Recurrence from 11A tumor specimen
UMSCC-14A	Floor of the mouth
UMSCC-14B	Recurrence from 14A tumor specimen
UMSCC-17A	Larynx (supraglottis)
UMSCC-17B	Neck soft tissue metastasis from 17A tumor
UMSCC-22A	Hypopharynx
UMSCC-22B	Lymph node metastasis from 22A tumor

[a]Carey TE. Head and neck tumor cell lines. In: Hay RJ, Park JG, Gazdar A (eds.) Atlas of human tumor cell lines 1994. New York Academic Press:p79.

Cell Growth Studies. The effect of celecoxib on growth of various HNSCC cell lines was determined by MTT colorimetric assay.[33] Briefly, the cells were harvested, centrifuged, and resuspended in standard medium before seeding 2×10^4 cells/well in 96-well culture plates (BD Bioscience Labware, Bedford, MA) and incubated overnight at 37°C. Cells were then treated with celecoxib at different concentrations or equal amounts of medium containing DMSO for control cultures. After 72 hours of incubation, MTT (2 mg/ml) was added and the generated formazan crystals were solubilized in 25% SDS/0.075 N NaOH before reading the absorbance at 550/690 nm in a microtiter plate reader MR5000 (Dynatech Laboratories Inc., Chantilly, VA). The percentage of growth inhibition was calculated from the equation, % of control = $(OD_t/OD_c) \times 100\%$ whereas OD_t and OD_c are optical densities of treated and control cultures, respectively. Concentration-response curves were plotted and levels of celecoxib resulting in 50% inhibition of cell growth (IC_{50} values) were calculated. The data represent mean ± standard deviations (SD) of three independent experiments performed in quadruplicate.

Western Blot Analysis. Immunoblot analyses were performed on cell lysates using 8% SDS-polyacrylamide gel electrophoresis. Cell layers at approximately 80% confluence were washed twice with ice-cold PBS and collected in lysis buffer containing 150 mM NaCl, 0.02% NaN_3, 2% Igepal CA-630, 0.5% sodium deoxycholate, 0.2% SDS, and 50 mM Tris HCl, pH 8.0) supplemented with protease inhibitors leupeptin (1 µg/ml), aprotinin (1 µg/ml), pepstatin (0.5 µg/ml), and phenylmethylsulfonyl fluoride (100 µg/ml). Protein concentrations were measured using Bio-Rad Protein Assay (Bio-Rad Laboratories, Hercules, CA) with bovine serum albumin used as standard protein. A total of 50 µg of protein was mixed with sample buffer (0.5 M Tris, pH 6.8; 0.3% glycerol; 0.03% β-mercaptoethanol; 10% SDS; 0.001% bromphenolblue), and electrophoretically separated and transferred onto Trans-Blot®nitrocellulose membranes (Bio-Rad Laboratories, Hercules, CA) prior blocking overnight at 4°C in 5% nonfat dry milk solution in 0.1% (w/v) Tween 20 in PBS. The membranes were probed with anti-human antibodies against COX-1 (1:1000), COX-2 (1:1000), 5-LOX (1:500), 12-LOX (1:100), 15-LOX-1 (1:2000) and 15-LOX-2 (1:3000) and incubated with peroxidase conjugated secondary antibody (1:5000). Bands were visualized by either ECL™ Western Blotting Detection Kit from Amersham Biosciences Corp. (Piscataway, NJ) or SuperSignal® West Femto Maximum Kit from Pierce (Rockford, IL) before exposure to Kodak X-Omat film (Eastman Kodak Co., Rochester, NY). Loading and transferring control was confirmed by probing the membranes with anti-β-actin antibody (1:1000).

Determination of Eicosanoid Levels by ESI-LC/MS/MS. Electrospray ionization liquid chromatography tandem mass spectrometry (ESI-LC/MS/MS) was performed to quantify eicosanoids as described previously.[34] For determination of intracellular eicosanoid levels, cells were harvested by

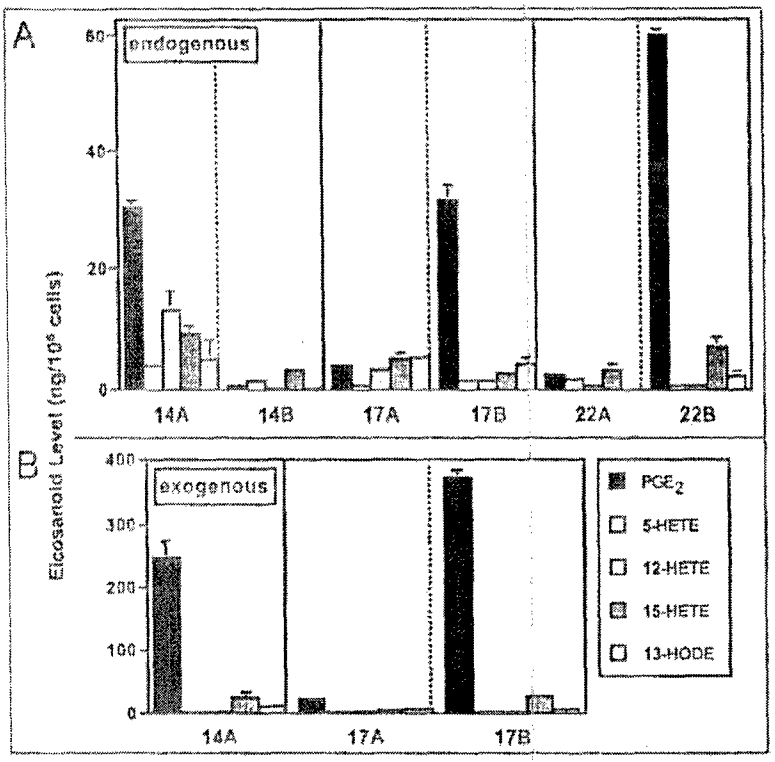


Figure 1 (Left). (A) Endogenous and (B) exogenous production of PGE_2, 5-HETE, 12-HETE, 15-HETE, and 13-HODE in pairs of UMSCC cell lines derived from primary (*suffix A*) and recurrent or metastatic (*suffix B*) tumors of the same patient. Cells were seeded and grown in 5% FBS-containing DMEM/Ham's F12 for 3 days prior to extraction with hexane: ethyl acetate (1:1) and analysis by ESI-LC/MS/MS. For exogenous eicosanoid levels, culture medium of three representative cell lines (UMSCC-14A, UMSCC-17A/-17B) were incubated with arachidonic acid (10 μM, 30 min) prior to collection, extraction, and analysis by ESI-LC/MS/MS as described under Materials and Methods.

trypsinization and resuspended in 500 μl PBS followed by addition of 20 μl of 1 N citric acid and 2.5 μl of 10% BHT to prevent free radical peroxidation. Samples were spiked with a mixture of deuterium-labeled eicosanoids of interest that served as internal standards (PGE_2-d_4, 5-HETE-d_8, 12-HETE-d_8, 15-HETE-d_8, and 13-HODE-d_4). Eicosanoids were extracted with 2 ml of hexane:ethyl acetate (v/v, 1:1) and vortex mixed prior to centrifugation at 1800 x *g* for 10 min. All extraction steps were performed under conditions of minimal light and 4°C. Samples were reconstituted in 200 μl methanol:10 mM ammonium acetate buffer (v/v, 70:30, pH 8.5) prior to analysis by ESI-LC/MS/MS. Eicosanoids secreted into cell culture medium were extracted using a solid phase method. Specifically, an aliquot of 10 μl of 10% BHT and 10 μl of a mixture of internal standards (PGE_2-d_4, 5-HETE-d_8, 12-HETE-d_8, 15-HETE-d_8, and 13-HODE-d_4) was added to 1 ml of culture medium. The solution was applied to a Sep-Pak C18 cartridge (Waters Corp., Milford, MA) that had been preconditioned with methanol and water. Eicosanoids were eluted with 1 ml of methanol and evaporated under a stream of nitrogen. Samples were then reconstituted in 100 μl methanol:10 mM ammonium acetate buffer (v/v, 70:30, pH 8.5) prior to analysis. For determination of exogenous eicosanoid levels, 10 μM arachidonic acid was added prior to collection of media and cells for 30 min.

ESI-LC/MS/MS was performed using a Quattro Ultima tandem mass spectrometer (Micromass, Beverly, MA) equipped with an Agilent HP1100 binary pump HPLC inlet. Metabolites were separated using a Luna 3 μm phenyl hexyl 2 x 150 mm analytical column (Phenomenex, Torrance, CA). The mobile phase consisted of 10 mM ammonium acetate (pH 8.5) and methanol. The flow rate was 250 μl/min with a column temperature maintained at 50°C and an injection volume of 25 μl. Fragmentation for all compounds was performed using argon as the collision gas at a collision cell pressure of 2.10×10^{-3} Torr. The results were expressed as nanograms of each eicosanoid per 10^6 cells. To normalize data, the cell number was measured with an electronic particle counter (Coulter, Hialeah, FL). Results shown represent mean values of at least two independent experiments.

RESULTS

Endogenous and Exogenous Level of Eicosanoids in HNSCC Cell Lines Derived from Primary and Recurrent or Metastatic Tumors. To determine whether progression of HNSCC from primary to metastatic lesion was associated with alterations in their eicosanoid metabolism, we analyzed a series of HNSCC cell lines (Table 1) for their endogenous level of various arachidonic acid and linoleic acid metabolites using ESI-LC/MS/MS. As shown in Figure 1A, three of the six cell lines produced relatively high levels of PGE_2 while 12-HETE was the second most abundant metabolite in UMSCC-14A cells. In two of three pairs, the cell lines which were derived from metastasis maintained considerably higher levels of PGE_2 than cells established from the corresponding primary tumor. The production of eicosanoids other than PGE_2 was found to be low in all HNSCC cell lines. Next, we provided the culture medium of three representative cell lines with exogenous arachidonic acid (10 μM, 30 min) in order to estimate the activity of COXs and LOXs under conditions of substrate abundance. Figure 1B demonstrates that PGE_2 was the major metabolite in UMSCC-14A and UMSCC-17B cells reaching levels of 246 and 372 ng/10^6 cells, respectively. That indicates an approximately 8- and 12-fold increase

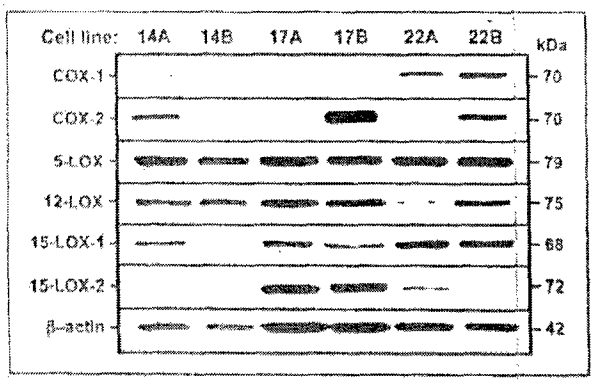


Figure 2. Expression of arachidonic acid and linoleic acid metabolizing enzymes in HNSCC cell lines established from primary (*suffix A*) and recurrent or metastatic (*suffix B*) tumors of the same patient. A total of 50 μg of protein per sample was separated using 8% SDS-polyacrylamid gel electrophoresis and transferred onto nitrocellulose membranes. The immunoblot was probed with antibodies specific for COX-1, COX-2, 5-LOX, 12-LOX, 15-LOX-1, and 15-LOX-2. β-actin was used as loading control. COX-2 protein was overexpressed in two of three HNSCC cell lines derived from metastatic than from primary tumor tissue, whereas COX-1 revealed low levels with similar intensities for each pair of cell lines. 5-LOX was universally detected in all UMSCC cell lines. Likewise for 12-LOX but one of the cell lines, UMSCC-22A, exhibited less protein. For 15-LOX-1 staining, HNSCC cell lines established from primary lesions expressed the protein more profoundly (UMSCC-14A, UMSCC-17A) or similarly (UMSCC-22A/22B) than those derived from metastatic or recurrent tumor. 15-LOX-2 expression was high in UMSCC-17A/-17B cells, low in UMSCC-22A, and absent in UMSCC-14A/- 14B cells.

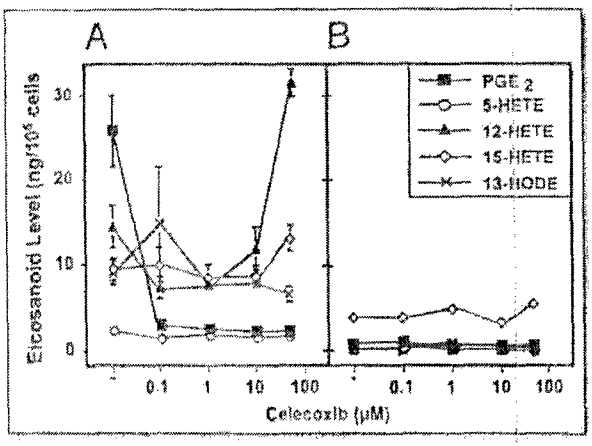


Figure 3. Concentration-dependent effect of celecoxib on endogenous production of PGE_2, 5-HETE, 12-HETE, 15-HETE, and 13-HODE in UMSCC-14A (A) and UMSCC-14B cells (B). Cell cultures were treated with different concentrations of celecoxib for 72 hours before extraction of eicosanoids with hexane:ethyl acetate (1:1) and analysis by ESI-LC/MS/MS. Data presented are the mean ± SD of two separate experiments

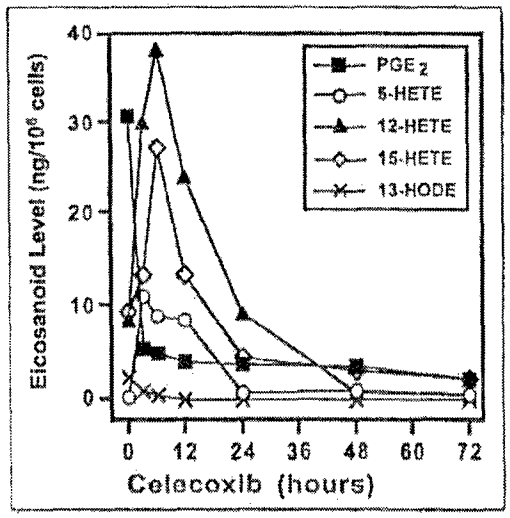


Figure 4. Time-dependent effect of celecoxib (1 μM) on endogenous eicosanoid level in UMSCC-14A cells. Cells were seeded and grown in 5% FBS-containing DMEM/Ham's F12 medium prior to extraction with hexane: ethyl acetate (1:1) and analysis by ESI-LC/MS/MS described under Materials and Methods.

compared with their endogenous production of 30 and 32 ng/10^6 cells, respectively. However, the biosynthesis of other metabolites remained at low levels in spite of exogenous availability of arachidonic acid. UMSCC-17A cells failed to generate detectable levels of any eicosanoids examined.

Expression of Arachidonic Acid- and Linoleic Acid-Metabolizing Enzymes in HNSCC Cell Lines. Next we asked, whether the predominance of PGE_2 among other metabolites resulted in the preferential expression of COXs in HNSCC cells. To address this question, we investigated the constitutive levels of COX-1 and COX-2 including other eicosanoid-generating enzymes such as 5-LOX, 12-LOX, 15-LOX-1, and 15-LOX-2 by western immunoblotting. As shown in Figure 2, COX-1 was weakly expressed in UMSCC-14A/-14B and UMSCC-17A/-17B cells but had a higher level of expression in UMSCC-22A/-22B cells. Immunoreactive bands for COX-1 revealed similar intensities for each pair of cell line. In contrast, COX-2 was differentially regulated in HNSCC cell lines derived from primary or metastatic tumor with a higher expression in two of three pairs in the latter. We found that 5-LOX protein was expressed in all cell lines as well as 12-LOX except for UMSCC-22A cells, which exhibited less protein. Incubation of the same membrane with anti-15-LOX-1 demonstrated that HNSCC cell lines established from primary lesions expressed bands with higher and in case of UMSCC-22A/22B cells, similar intensities than those derived from metastases. 15-LOX-2 expression was high in UMSCC-17A/-17B, low in UMSCC-22A, and absent in UMSCC-14A/14B or UMSCC-22B cells.

Effect of Celecoxib on Eicosanoid Levels in UMSCC-14A and -14B Cells. Because PGE_2 levels correlated with COX-2 protein expression in HNSCC cells, we examined the effect of the selective COX-2 inhibitor, celecoxib, on endogenous production of eicosanoids in UMSCC-14A/ and -14B cells by ESI-LC/MS/MS. Data in Figure 3A indicate that the production of PGE_2, the major metabolite generated by COX-2, was markedly inhibited by 89% (from 25.9 to 2.9 ng/10^6 cells) with as little as 0.1 μM celecoxib after a 3-day treatment of UMSCC-14A cells. No further reduction was observed after treatment with higher doses of celecoxib. The results further demonstrate that celecoxib at concentrations up to 50 μM exerted only minor effects on the production of 5-HETE, 15-HETE, and 13-HODE in UMSCC-14A cells. However, the synthesis of 12-HETE increased from 14.3 to 31.6 ng/10^6 cells after treatment with 50 μM celecoxib. No effects on PGE_2 production and other eicosanoid metabolites were detected in celecoxib treated UMSCC-14B cells (Fig. 3B). These cells produced relatively little PGE_2 (0.9 ng/10^6 cells) and lacked COX-2 expression. However, the cells displayed a considerable amount of 5-LOX and 12-LOX enzymes estimated by immunoblotting (Fig. 2).

The suppression of PGE_2 in UMSCC-14A cells was observed as early as 3 hours after exposure to 1 μM celecoxib (Fig. 4). In contrast, the production of LOX-derived metabolites 5-HETE, 12-HETE, and 15-HETE increased from 0.23, 8.5, and 9.3 to 8.9, 38.2, and 27.3 ng/10^6 cells, respectively. These effects occurred within 6 hours followed by a subsequent decline to baseline levels after 24 hours of celecoxib treatment. The low synthesis of 13-HODE (2.22 ng/10^6 cells) in UMSCC-14A cells did not change. Rather, it decreased to undetectable levels after 12 hours of incubation with celecoxib.

Effect of Celecoxib on Growth of Various HNSCC Cell Lines. The ability of celecoxib to suppress PGE_2 raised the question whether these effects were associated with growth inhibition in HNSCC cell lines. We examined celecoxib concentrations causing 50% growth inhibition (IC_{50} values) obtained from concentration-response curves after 72 hours of incubation and compared those with constitutive COX expression. Celecoxib inhibited growth of HNSCC cell lines in a concentration-dependent manner between 25 and 75 μM (Fig. 5A). The IC_{50} values ranged from 33 to 62 μM celecoxib (Fig. 5B). The level of COX-2 expression revealed no correlation with the relative sensitivity of HNSCC cell lines to celecoxib (Fig. 5C). In fact, cell lines that expressed COX-2 (UMSCC-11A/11B, UMSCC-14A, UMSCC-17B, UMSCC-22B) were as sensitive as cell lines with low or undetectable COX-2 protein levels (UMSCC-14B, UMSCC-17A, UMSCC-22A). Likewise, no direct correlation between COX-1 and the growth-inhibitory effects of celecoxib in HNSCC cell lines was observed (Fig. 5C).

DISCUSSION

Eicosanoid metabolism leads to generation of bioactive lipids known to promote cancer.[2,9] Metabolites of both, COX and LOX pathways, have been found to be elevated in tumor tissues, plasma and saliva obtained from patients with HN cancer.[5,15,19,23] In addition, altered expression of various enzymes and genes related to arachidonic acid metabolism are known to contribute to squamous cell carcinogenesis.[4,7,8]

In this study, we used an in vitro model consisting of paired SCC cell lines derived from primary and recurrent or metastatic HN tumors to investigate the production of various metabolites of arachidonic acid and linoleic acid pathways by ESI-LC/MS/MS. We found that PGE_2 was the most abundant metabolite in three of six

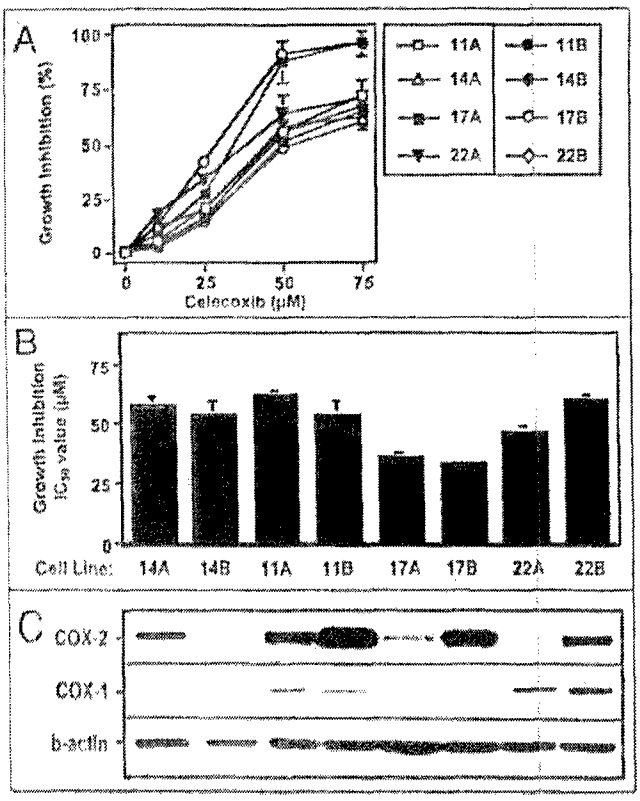


Figure 5. Effect of the selective COX-2 inhibitor celecoxib on growth inhibition of HNSCC cell lines derived from primary (*suffix A*) and recurrent or metastatic (*suffix B*) tumors of the same patient. Cells were seeded into 96-well culture plates and allowed to adhere overnight before treated with celecoxib at different concentrations. Changes in cell survival as a function of the dose of celecoxib was determined by MTT assay after 72 hours of incubation (A). Concentrations required for the determination of IC_{50} values of celecoxib were obtained by interpolation of dose-response curves (B). Results represent mean ± SD of quadruplicate measurements of three independent experiments. Inhibitory effects of celecoxib on cell growth were independent of neither constitutive COX-2 nor COX-1 expression in different HNSCC cell lines analyzed by western blotting. β-actin served as loading control (C).

HNSCC cell lines. Interestingly, two of the three were established from metastases. Other eicosanoid metabolites (e.g. 15(*S*)-HETE i.e. 15-HETE) were identified in UMSCC-14A cells but were produced at very low levels in all HNSCC cell lines examined. Subsequent western blot analysis of a battery of arachidonic acid- and linoleic acid-metabolizing enzymes has indicated that multiple proteins in addition to COX-1 and COX-2 were expressed. However, with the exception of PGE_2, that correlated with COX-2 levels, other metabolites produced by HNSCC cells showed no correlation with the expression of their corresponding enzymes. The obtained lack of correlation was not due to a limited amount of endogenous arachidonic acid as indicated by the findings that addition of arachidonic acid to the culture medium resulted in an approximately 10-fold increase of PGE_2 only in COX-2 positive HNSCC cell lines but failed to enhance the production of other eicosanoids despite the presence of their metabolizing enzymes. Thus, the activities of eicosanoid-generating enzymes, with the exception of COXs, were impaired in HNSCC cell lines examined for unknown reason(s). Plausible explanations are that particular enzymes might be mutated or localized in intracellular sites that are distinct from the site of their specific substrates. For example, the activities of 15-LOX-1 and 5-LOX have been found to be dependent on the localization of these enzymes in the cytoplasm, nucleoplasm, and intracellular biomembranes, respectively.[35,36] Moreover, COX-2 enzyme was detected in HT-29 colorectal cancer cells by western blotting yet these cells were unable to convert arachidonic acid to prostaglandins.[37] Interestingly, the COX-2 cloned from HT-29 cells was catalytically active when transfected into HCT-116 cancer cells. The authors suggested that a putative endogenous inhibitor of COX-2 may be present or conversely, a cofactor is missing that is necessary for COX-2 activity in HT-29 cells. However, our data on paired HNSCC cell lines revealed a good correlation between COX-2 expression and COX-2 activity measured as PGE_2 production. Here, we show a discrepancy between protein levels and enzymatic activities of a large number of eicosanoid-generating enzymes other than COXs.

The fact that PGE_2 synthesis correlated with the expression levels of COX-2 has led us to investigate the effects of the selective COX-2 inhibitor, celecoxib, on eicosanoid metabolism and growth of HNSCC cells. Here, we demonstrate for the first time, that inhibition of the COX pathway by celecoxib resulted in a time-dependent activation of the LOX pathway. Specifically, the production of multiple LOX-metabolites, e.g., 5-HETE, 12-HETE, and 15-HETE, increased as the PGE_2 level declined in UMSCC-14A cells treated with celecoxib at 1 μM, a concentration that is easily achieved in patients. The increase of various LOX metabolites may be considered as a cellular response to the profound decline of PGE_2 levels. Our results further indicate that inhibition of HNSCC cell growth by celecoxib was not closely related to the expression of COX-2. Comparable IC_{50} values were observed in all HNSCC cell lines regardless of their COX-2 status. Furthermore, celecoxib was effective in decreasing PGE_2 levels at concentrations that showed no effect on cell growth. This suggests that the growth inhibitory activity of celecoxib was at least partially independent of the suppression of PGE_2 synthesis. PGs are important regulators of cellular proliferation known to promote tumorigenesis and suppress immune response in vivo.[9] The prognostic significance of elevated PGE_2 levels in SCC is not entirely known. While increased levels have been detected in carcinomas, the cellular origin of PGE_2 in fresh tumor biopsies is difficult to determine due to the fact that the majority of PGE_2 derives from inflammatory cells participating in tumor-directed immune response.[15,16] The functional relevance of COX-2 derived PGE_2 on HNSCC cell growth has been supported by observations that exogenous PGE_2 was able to abrogate the antiproliferative effects of selective COX-2 inhibitors.[17,30,38] In addition, PGE_2 levels were significantly higher in COX-2 expressing compared to nonexpressing oral cancer cell lines associated with inhibition of proliferation and induction of apoptosis after treatment with selective COX-2 inhibitors.[21] However, a controversy has been raised by reports that COX-2 inhibitors may act independently of inhibition of PG synthesis.[11,13,14,30,31] Our data show that much higher concentrations of celecoxib are needed to suppress cell growth in vitro than those achievable in humans. On the other hand, concentrations required for the inhibition of PGE_2 synthesis in vitro are clinically attainable. The precise mechanisms by which celecoxib suppresses tumor growth has not been fully defined. It is more likely to be related to suppression of PGE_2 synthesis than to direct inhibition of tumor cell growth. For example, suppression of COX-2 derived PGE_2 decreased microvessel density and inhibited mammary tumor progression.[39] Besides, a study using a mouse model of oral cancer has shown that celecoxib significantly delayed cell growth, reduced tumor volume and exerted antiangiogenic activity.[27] Nonetheless, accumulating evidence suggest that COX-2 independent molecular targets may

contribute to the antitumoral effects of NSAIDs including 15-LOX-1,[13] 15-LOX-2,[14] arachidonic acid,[40] NF-κB,[28] and PPARγ.[29] The expression of COX-2, classified as immediate-early response gene, is well known to be upregulated in response to pathological processes such as inflammation and cancer.[2,9] In contrast, COX-1 has been found in both normal and malignant cells. Recently, it has been reported that COX-1 can also be induced in human esophageal SCC by a variety of proinflammatory stimuli and its expression under neoplastic conditions seems related to cellular differentiation.[8] We included the expression levels of COX-1 in our study due to the fact that PGE_2 is synthesized from arachidonic acid by both isoenzymes. Similarly, we found no correlation between COX-1 status and the antiproliferative activity of celecoxib. The levels of LOX products, namely 5-HETE, 12-HETE, and 15-HETE have been reported to be elevated in HN cancer patients.[5,23] Moreover, inhibition of arachidonic acid metabolism, particularly the LOX pathway, exerted antitumor effects postulating a role for LOX metabolites in HN tumorigenesis.[11] Our data indicate an increase of 12-HETE after 3 days of incubation with celecoxib at a concentration above the estimated IC_{50} value. 12-HETE is the only metabolite of the arachidonic acid-metabolizing enzyme 12-LOX suggested to act as regulator of tumor growth and motility.[2] However, the role of 12-HETE in SCC of the HN has not been adequately investigated.

In conclusion, our study demonstrates that western blot analysis of enzymes related to the arachidonic acid and linoleic acid cascade is insufficient for assessment of the eicosanoid metabolism. Therefore, ESI-LC/MS/MS analysis or comparable analytical methods are warranted for a more reliable evaluation. In addition, we have shown that suppressing PGE_2 levels by celecoxib leads to an enhanced activity of 5-LOX, 12-LOX and 15-LOX-2 as indicated by the increases of their products 5-HETE, 12-HETE and 15-HETE. Whereas suppression of PGE_2 was persistent, the increase in LOX metabolites appeared to be transient. Nevertheless, the dynamic transition between COX and LOX pathways may play a role in the cellular response to celecoxib in vivo and raises the need to consider targeting both enzymatic pathways by using COX in combination with LOX inhibitors.

References

1. Greenlee RT, Hill-Harmon MB, Murray T, Thun M. Cancer statistics, 2001. CA Cancer J Clin 2001; 51:15-36.
2. Maruyama IJ, Hano KV. Overview of articles on eicosanoids and cancer. Cancer Metastasis Rev 1994; 13:237-9.
3. Long JD, Orlando RC. Eicosanoids and the esophagus. Prostaglandins Other Lipid Mediat 2000; 61:91-104.
4. Zhi H, Zhang L, Hu G, Lu J, Wang X, Zhou C, et al. The deregulation of arachidonic acid metabolism-related genes in human esophageal squamous cell carcinoma. Int J Cancer 2003; 106:327-33.
5. Metzger K, Angres G, Maier H, Lehmann WD. Lipoxygenase products in human saliva: Patients with oral cancer compared to controls. Free Radical Biol Med 1995; 18:185-94.
6. Morgan G. Deleterious effects of prostaglandin E2 in oesophageal carcinogenesis. Med Hypotheses 1997; 48:177-81.
7. Mauer K, Dubbler P, Barthel B, Heine B, von Lampe B, Stein H, et al. Oesophageal squamous cell neoplasia in head and neck cancer patients: Upregulation of COX-2 during carcinogenesis. Brit J Cancer 2003; 88:1217-22.
8. Kase S, Osaki M, Honjo S, Hashimoto K, Adachi H, Tsujitani S, et al. Expression of cyclooxygenase-1 and cyclooxygenase-2 in human esophageal mucosa dysplasia and carcinoma. Pathobiology 2004; 71:84-92.
9. Funk CD. Prostaglandins and leukotrienes: Advances in eicosanoid biology. Science 2001; 294:1871-5.
10. Brash AR, Boeglin WE, Chang MS. Discovery of a second 15S-lipoxygenase in humans. Proc Natl Acad Sci USA 1997; 94:6148-52.
11. Ondrey FG, John SK, Adams GL. Inhibition of head and neck tumor cell growth with arachidonic acid metabolism inhibition. Laryngoscope 1996; 106:129-34.
12. Sciuscio KA, Snyderman CH, D'Amico F, Correa S, Rueger R, Light B. Effects of arachidonic acid metabolites in a murine model of squamous cell carcinoma. Head Neck 2000; 22:149-55.
13. Shureiqi I, Xu X, Chen D, Lotan R, Morris JS, Fischer SM, et al. Nonsteroidal anti-inflammatory drugs induce apoptosis in esophageal cancer cells by restoring 15-lipoxygenase-1 expression. Cancer Res 2001; 61:4879-84.
14. Xu XC, Shappell SB, Liang Z, Song S, Menter D, Subbaraya V, et al. Reduced 15S-lipoxygenase-2 expression in esophageal cancer specimens and cells and upregulation in vitro by the cyclooxygenase-2 inhibitor, NS398. Neoplasia 2003; 5:121-7.
15. Jung TTK, Berlinger NT, John SK. Prostaglandins in squamous cell carcinoma of the head and neck: A preliminary study. Laryngoscope 1985; 95:307-12.
16. Snyderman CH, Milanovich M, Wagner RL, Johnson JT. Prognostic significance of prostaglandin E_2 production in fresh tissues of head and neck cancer patients. Head Neck 1995; 17:108-13.
17. Sumitani K, Kamijo R, Toyoshima T, Nakanishi Y, Takizawa K, Harnoi M, et al. Specific inhibition of cyclooxygenase-2 results in inhibition of proliferation of oral cancer cell lines via suppression of prostaglandin E2 production. J Oral Pathol Med 2001; 30:41-7.
18. Botha JH, Robinson KM, Ramchurren N, Reddi K, Norman RJ. Human esophageal carcinoma cell lines: Prostaglandin production, biological properties, and behavior in nude mice. J Nat Cancer Inst 1986; 76:1053-6.
19. Klapan I, Katic V, Cule P, Cuk V. Prognostic significance of plasma prostaglandin E concentration in patients with head and neck cancer. J Cancer Res Clin Oncol 1992; 118:308-13.
20. Mestre JR, Chan G, Zhang F, Yang EK, Sacks PG, Boyle JO, et al. Inhibition of cyclooxygenase-2 expression. An approach to preventing head and neck cancer. Ann NY Acad Sci 1999; 889:62-71.
21. Zimmermann KC, Sarbia M, Weber AA, Borchard F, Gabbert HE, Schrör K. Cyclooxygenase-2 expression in human esophageal carcinoma. Cancer Res 1999; 59:198-204.
22. Gallo O, Franchi A, Magnelli L, Sardi I, Vannacci A, Boddi V, et al. Cyclooxygenase-2 pathway correlates with VEGF expression in head and neck cancer. Implications for tumor angiogenesis and metastasis. Neoplasia 2001; 3:53-61.
23. El Attar TMA, Lin HS, Vanderhoeck JY. Biosynthesis of prostaglandins and hydroxy fatty acids in primary squamous carcinomas of head and neck in humans. Cancer Lett 1985; 27:255-9.
24. Funkhouser EM, Sharp GB. Aspirin and reduced risk of esophageal carcinoma. Cancer 1995; 76:1116-9.
25. Farrow DC, Vaughan TL, Hansten PD, Stanford JL, Risch HA, Gammon MD, et al. Use of aspirin and other nonsteroidal anti-inflammatory drugs and risk of esophageal and gastric cancer. Cancer Epidemiol Biomarkers Prev 1998; 7:97-102.
26. Langman MJS, Cheng KK, Gilman EA, Lancashire RJ. Effect of anti-inflammatory drugs on overall risk of common cancer: Case-control study in general practice research database. Brit Med J 2000; 320:1642-46.
27. Wang Z, Fuentes CF, Shapshay SM. Antiangiogenic and chemopreventive activities of celecoxib in oral carcinoma cell. The Laryngoscope 2002; 112:839-43.
28. Niederberger E, Tegeder I, Vetter G, Schmidtko A, Schmidt H, Euchenhofer C, et al. Celecoxib loses its anti-inflammatory efficacy at high doses through activation of NF-κB. FASEB J 2001; 15:1622-4.
29. Nikitakis NG, Hebert C, Lopes MA, Reynolds MA, Sauk JJ. PPARgamma-mediated antineoplastic effect of NSAID sulindac on human oral squamous carcinoma cells. Int J Cancer 2002; 98:817-23.
30. Minter HA, Eveson JW, Huntley S, Elder DJE, Hague A. The cyclooxygenase 2-selective inhibitor NS398 inhibits proliferation of oral carcinoma cell lines by mechanisms dependent and independent of reduced prostaglandin E_2 synthesis. Clin Cancer Res 2003; 9:4366-73.
31. Fife RS, Sitzer B, Carr RE. Effects of a selective cyclooxygenase-2 inhibitor on cancer cells in vitro. Cancer Biol Ther 2004; 3:228-32.
32. Carey TE. Head and neck tumor cell lines. In: Hay RJ, Park JG, Gazdar A, eds. Atlas of human tumor cell lines. New York Academic Press; 1994:79.
33. Mosmann T. Rapid colorimetric assay for cellular growth and survival: Application to proliferation and cytotoxicity assays. J Immunol Methods 1983; 65:55-63.
34. Kempen EC, Yang P, Felix E, Madden T, Newman RA. Simultaneous quantification of arachidonic acid metabolites in cultured tumor cells using high performance liquid chromatography/electrospray ionization tandem mass spectrometry. Anal Biochem 2001; 297:183-90.
35. Walther M, Wiesner R, Kuhn H. Investigations into calcium-dependent membrane associations of 15-lipoxygenase-1. Mechanistic roles of surface-exposed hydrophobic amino acids and calcium. J Biol Chem 2004; 279:3717-25.
36. Luo M, Jones SM, Peters-Golden M, Brock TG. Nuclear localization of 5-lipoxygenase as a determinant of leukotriene B4 synthetic capacity. Proc Natl Acad Sci USA 2003; 100:12165-70.
37. Hsi LC, Baek SJ, Eling TE. Lack of cyclooxygenase-2 activity in HT-29 human colorectal carcinoma cells. Exp Cell Res 2000; 256:563-70.
38. Zweifel BS, Davis TW, Ornberg RL, Masferrer JL. Direct evidence for a role of cyclooxygenase 2-derived prostaglandin E_2 in human head and neck xenograft tumors. Cancer Res 2002; 62:6706-11.
39. Chang SH, Liu CH, Conway R, Han DK, Nithipatikom K, Trifan OC, et al. Role of prostaglandin E2-dependent angiogenic switch in cyclooxygenase 2-induced breast cancer progression. Proc Natl Acad Sci USA 2004; 101:591-6.
40. Levine L. Does the release of arachidonic acid from cells play a role in cancer chemoprevention? FASEB J 2003; 17:800-2.

Phenotypic Diversity of the Lung Vasculature in Experimental Models of Metastases

Yun Oh[1], Imran Mohiuddin[2], Connie Sun[3], Joseph B. Putnam, Jr.[2], Waun Ki Hong[1], Wadih Arap[3,4] and Renata Pasqualini[3,4]

[1]Department of Thoracic/Head & Neck Medical Oncology, [2]Department of Thoracic Surgery, [3]Department of Genitourinary Medical Oncology, and [4]Department of Cancer Biology, The University of Texas M. D. Anderson Cancer Center, 1515 Holcombe Boulevard, Houston, Texas 77030

This work was funded in part by an award from the Gilson-Longenbaugh Foundation (Drs. Arap and Pasqualini) and the BESCT (Biology, Education, Screening, Chemoprevention and Treatment) Lung Cancer Program, DAMD17-01-1-0689 (Dr. Oh).

Correspondence to: Wadih Arap, MD, PhD or Renata Pasqualini, PhD. M.D. Anderson Cancer Center; 1515 Holcombe Boulevard, Houston, TX 77030. E-mail: *warap@mdanderson.org* or *rpasqual@mdanderson.org*.

Key words: lung endothelium, membrane dipeptidase, metastasis, phage display, random peptide library, vascular targeting

Abstract

In vivo phage display is a screening method in which peptides homing to specific vascular beds are selected after intravenous administration of a random peptide library (1). This strategy has revealed a vascular address system that allows tissue-specific targeting of normal blood vessels (2,3) and angiogenesis-related targeting of tumor blood vessels (4-10) by selected peptides. Many vascular receptors or "addresses" targeted by homing peptides have been identified (1-3). One such vascular receptor of normal lung endothelium is membrane dipeptidase (MDP), which was found by *in vivo* phage display to bind the tripeptide motif Gly-Phe-Glu (GFE) (11). Our studies with GFE peptide and lung vasculature suggest that MDP mediates cancer cell adhesion to lung vasculature and development of lung metastases but that MDP is not present in vasculature of lung metastases. MDP appears to occupy a vascular distribution similar to the pulmonary artery circulation. These results demonstrate the promise of defining critical functional and anatomic characteristics of endothelial cells in lung and other organs by *in vivo* phage display.

IN VIVO PHAGE DISPLAY

Efforts to target therapeutics and imaging agents to blood vessels in an organ- specific or disease-specific manner has led to the development of a technique by which small peptides that target receptors on endothelial cells can be identified (1-3). This approach, using large random peptide libraries displayed on the surface of bacteriophage, has been termed 'in vivo phage display'. A random peptide phage library is injected intravenously, and peptides that home selectively to specific organs or tumors are then recovered. Putative human homologs have been identified from ligands and receptors isolated by this approach in mouse models suggesting that at least some ligand peptide motifs and their corresponding receptors may be evolutionarily conserved and pertinent in humans (12). In vivo phage display is uncovering a vascular address system that can be used for organ-specific targeting of normal blood vessels and angiogenesis-related targeting of blood vessels in tumors (4-10). Methods are also being developed for determining the in vivo distribution of probes targeted to the vasculature (2,3), and their organ-specificity, vessel-specificity and cellular targets. As the complexity of vascular diversity is further revealed, *in vivo* phage display will target particular regions of organs, such as pancreatic islets or the glomeruli of the kidney (13), and eventually identify receptor ligand pairs for functionally distinct vessels within these regions.

MDP AND ITS LIGAND *GFE* IN LUNG VASCULATURE

MDP was biochemically identified as a vascular receptor for lung-homing peptides containing the tripeptide motif Gly-Phe-Glu (GFE) selected by *in vivo* phage display (2,11) and appears to be a vascular receptor that binds to and mediates GFE homing to normal lung endothelium . MDP is a member of the zinc-metalloprotease family and a GP-anchored cell surface protein expressed primarily in lung and kidney (14). In rat and mouse, levels of MDP activity are highest in lung (14, 15). MDP is involved in the metabolism of glutathione and cysteinyl leukotrienes (14, 16) and it is the only known mammalian enzyme capable of degrading β-lactam antibiotics (14). The work presented

here describes the expression and functional role of MDP in the dual circulation of the lung and in the context of vasculature of pulmonary metastases.

ROLE OF MDP IN EXPERIMENTAL MELANOMA LUNG METASTASES

To determine whether the lung vascular receptor MDP mediates the homing of tumor cells and subsequent development of experimental pulmonary metastases in mice, we used the C8161 human melanoma cell model of experimental lung metastases (17, 18). C8161 cells were co-administered intravenously with either the GFE-containing peptide (a ligand targeting MDP; refs. 2,11) or a negative control peptide (Fig. 1). The median weight of lungs from mice that received GFE peptide was only 12% greater than that of normal lungs whereas the median weight of lungs from mice that received control peptide or no peptide (vehicle alone) was 88% greater than that of normal lungs (t-test, $p<0.01$). Consistent with these findings, histological examination showed many fewer and smaller metastatic foci in mice treated with GFE. Moreover, GFE did not affect cell viability, as demonstrated by Trypan Blue exclusion and MTT assays on aliquots of melanoma cells prepared for injection into mice; cell viability was higher than 95% (results not shown). These results suggest that the tripeptide GFE binds to MDP and blocks the vascular homing of metastatic melanoma cells via this receptor.

BRONCHIAL VS. PULMONARY ARTERY PERFUSION OF METASTASES

Photomicroscopy of lung metastases in the C8161 model demonstrated that the earliest visible lung metastases grew preferentially in close proximity to bronchioles (Fig. 2). These observations led to the hypothesis that these metastatic tumors were preferentially recruiting angiogenic blood vessels from the bronchial versus pulmonary artery circulations. To test this hypothesis, we used a rat fibrosarcoma (RFS) lung metastasis model (19) and isolated rat lung perfusion model (20). After surgically isolating the left pulmonary artery circulation of rats under general anesthesia, Evans blue (with red fluorescence) was perfused; the remaining systemic circulation was perfused with FITC-dextran via left ventricular injection. Rats were sacrificed after a 2 minute circulation time, and lung tissue was processed according to the method of Li, et al (21). Indeed, we found that microscopic lung metastases of rat fibrosarcoma cells recruited tumor blood vessels preferentially from the bronchial vasculature, at least in early stages of growth (Fig. 3). This was a surprising result since intravenously inoculated cancer cells pass through the pulmonary artery circulation first and would have a greater chance to deposit in the lung near pulmonary arteriolar capillaries than around the bronchial circulation.

DISTRIBUTION OF MDP IN C8161 METASTASES TO THE LUNG

Finally, we analyzed the distribution of GFE binding to lung vasculature to evaluate whether MDP is expressed in the angiogenic vasculature of lung metastases because the expression of MDP in the lung endothelium closely recapitulates the distribution of GFE-displaying phage (2, 11). Either GFE-displaying phage or control insertless phage were injected intravenously into mice bearing C8161 lung metastases and examined for their ability to home to tumor vasculature. Strong phage immunoreactivity was observed in normal lung tissue, but the lung metastases were clearly negative (Fig. 4). Failure of

GFE-displaying phage to accumulate in tumor blood vessels indicates that its homing receptor, MDP, is not expressed in these blood vessels.

CONCLUSIONS

The molecular differences based on heterogeneous expression of MDP in lung and lung tumors could be explained by tumors differentially recruiting the dual blood circulations of the lung. Based on our perfusion experiments, we conclude that early lung metastases derive their blood supply primarily from the bronchial artery circulation. In contrast, based on the pattern of GFE-displaying phage binding in alveolar capillaries and pulmonary arterioles, it appears that MDP is selectively expressed in pulmonary artery vasculature.

The patterns and function of MDP based on the results presented here imply that normal organ vascular receptors are still not necessarily valid targets for imaging or treating tumors in those organs. Previous studies have identified vascular receptors that can be used to deliver therapeutic agents to cancers originating in host organs (4 -10) or to normal organs (22- 24). MDP likely cannot be utilized in this manner since it appears to be absent in the vasculature of lung metastases. Even if MDP were present in lung tumor vasculature, it would not be an optimal target for delivering drugs to lung tumors: unlike prostate and breast, lung is an essential organ for survival and the risk of collateral damage to normal lung vasculature may be unacceptable. On the other hand, the delivery of radioprotective agents to the lungs would remain an open possibility.

Taken together, these data illustrate the diversity and functional relevance of a vascular receptor in the lung vasculature. Novel anti-metastatic strategies may emerge from interfering with tumor cell attachment to MDP and/or mechanisms underlying angiogenesis in lung cancer.

ACKNOWLEDGEMENTS

We thank Dr. Wolfgang Kuschinsky for references and advice on vascular imaging technique.

REFERENCES

1. Kolonin MG, Arap, W., Pasqualini, R. Molecular addresses in blood vessels as targets for therapy. Curr. Opinion. Chem. Biol. 2001; 5:308-313

2. Rajotte, D., Arap, W., Hagedorn, M., Koivunen, E., Pasqualini, R., and Ruoslahti, E. Molecular heterogeneity of the vascular endothelium revealed by in vivo phage display. J. Clin. Invest., 102: 430-437, 1998.

3. Pasqualini, R. and Ruoslahti, E. Organ-targeting in vivo using phage display peptide libraries. Nature, 380: 364- 366, 1996.

4. Ellerby, H.M. et al. Anti-cancer activity of targeted pro-apoptotic peptides. Nature Med. **5**, 1032-1038, 1999.

5. Koivunen, E. et al. Tumor targeting with a selective gelatinase inhibitor. Nature Biotechnol. **17**, 768-774, 1999.

6. Burg, M.A., Pasqualini, R., Arap, W., Ruoslahti, E. & Stallcup, W.B. NG2 proteoglycan-binding peptides target tumor neovasculature. Cancer Res. **59**, 2869-2874, 1999.

7. Arap, W., Pasqualini, R. & Ruoslahti, E. Cancer treatment by targeted drug delivery to tumor vasculature in a mouse model. Science **279**, 377-380, 1998.

8. Pasqualini, R., Koivunen, E. & Ruoslahti, E. α_v integrins as receptors for tumor targeting by circulating ligands. Nature Biotechnol. **15**, 542-546 1997.

9. Zurita AJ, Troncoso P, Cardo-Vila M, et al. Combinatorial screenings in patients: the interleukin-11 receptor alpha as a candidate target in the progression of human prostate cancer. Cancer Research 2004; 64:435-439.

10. Marchio S, Lahdenranta J, Schlingemann RO, et al. Aminopeptidase A is a functional target in angiogenic blood vessels. Cancer Cell 2004; 5:151-162.

11. Rajotte, D. and Ruoslahti, E. Membrane dipeptidase is the receptor for a lung-targeting peptide identified by in vivo phage display. J. Biol. Chem., 274: 11593- 11598, 1999.

12. Arap W. Kolonin MG. Trepel M. Lahdenranta J. Cardo-Vila M. Giordano RJ. Mintz PJ. Ardelt PU. Yao VJ. Vidal CI. Chen L. Flamm A. Valtanen H. Weavind LM. Hicks ME. Pollock RE. Botz GH. Bucana CD. Koivunen E. Cahill D. Troncoso P. Baggerly KA. Pentz RD. Do KA. Logothetis CJ., Pasqualini, R. Steps toward mapping the human vasculature by phage display. Nature Medicine, 8(2):121-127, Feb, 2002.

13. Yao VJ OM, Trepel M, Arap W, McDonald DM, and Pasqualini R. Targeting Pancreatic Islets with Phage display Assisted by Laser Pressure Catapult Microdissection. Am J Path 2004 in press

14. Keynan S, Hooper NM, Turner A. Zinc metalloproteases in health and disease. London: Taylor & Francis Ltd, 1995; 285-309.

15. Hirota T., Nishikawa Y., Tanaka M., Igarashi T., and Kitagawa H. Characterization of dehydropeptidase I in the rat lung. Eu. J. Biochem. 160: 521-525, 1986.

16. Habib G.M., Shi Z.Z., Cuevas A.A., Guo Q., Matzuk M.M., and Lieberman M.W. Leukotriene D4 and cystinyl-bis-glycine metabolism in membrane-bound dipeptidase-deficient mice. Proc. Natl. Acad. Sci. USA 95: 4859-4863, 1998.

17. Welch DR, et al. Characterization of a highly invasive and spontaneously metastatic human malignant melanoma cell line. Int. J. Cancer 1991; 47:227-237.

18. Pasqualini, R., Bourdoulous, S., Koivunen, E., Woods, V.L. ,Jr., Ruoslahti E. A polymeric form of fibronectin has antimetastatic effects against multiple tumor types. Nature Medicine, 2(11):1197-203, 1996.

19. Tsunenari I, Yamate J, Iwaki M, et al. Angioarchitecture of tumors induced by two different cloned cell lines established from a transplantable rat malignant fibrous histiocytoma. Microscopy & Microanalysis 2003; 9:532-541.

20. Wang HY. Port JL. Hochwald SN. Burt ME. Revised technique of isolated lung perfusion in the rat. Annals of Thoracic Surgery. 60(1): 211-2, 1995.

21. Li, P-A., Vogel, J., He, Q.-P., Smith, M-L., Kuschinsky, W. and Siesjo¨, B.K., Preischemic hyperglycemia leads to rapidly developing brain damage with no change in capillary patency, Brain Res., 782 (1998) 175–183.

22. Kolonin MG, Saha PK, Chan L, et al. Reversal of obesity by targeted ablation of adipose tissue.[see comment]. Nature Medicine 2004; 10:625-632.

23. Trepel, M., Arap W, and Pasqualini R. (2002) *In vivo* phage display and vascular heterogeneity: implications for targeted medicine. *Curr. Opin. Chem. Biol.* 6, 399–404.

24. Pasqualini R, Arap W. Translation of vascular proteomics into individualized therapeutics. In: Licinio J, Wong ML, ed. Pharmacogenomics: The Search for Individualized Therapies. Wiley-VCH Verlag GmbH, 2002; 525-530.

FIGURE LEGENDS

Fig. 1. The GFE lung homing peptide inhibits experimental metastasis of intravenously administered C8161 melanoma. Tumor cells were pre-incubated for 10 minutes with GFE or a control peptide, as indicated, and then injected in the tail vein (10^6 cells/mouse, 10 mice per group). Lung weights are shown for three experimental groups. Average normal lung weight (0.175 g) is marked with a line. Relative to the vehicle (DMEM) and control peptide groups, p values were less than 0.01. Shown is one of 5 experiments, in which similar results were obtained.

Fig. 2. Lung tumor foci develop preferentially around the bronchia. Trichrome stained sections of mouse lungs with C8161 metastases demonstrate that early tumors are found centered around bronchioles (arrows indicate lumens with blue-green borders, indicating collagen within the bronchial walls). Tumors secondarily also envelop pulmonary arteries that accompany the bronchioles. Normal lung is shown in B, for comparison.

Fig. 3. Tumor vasculature is preferentially recruited from the bronchial circulation. A. FITC-dextran was perfused into the left ventricle and Evans blue into the isolated left pulmonary artery of anesthetized rats. B. A photograph of the operative field demonstrates left lung (LL), right lung (RL), pulmonary artery catheter (PA), clamps placed on both pulmonary veins (PV), the left ventricle of the heart (H), and the ascending aorta (AA). C. High-power views of the earliest detectable microscopic tumor nodules, the largest of which at far right, appears to have central necrosis with only punctate peripheral perfusion.

Fig. 4. GFE does not bind to the vasculature within lung tumors. Lungs were harvested from mice bearing C8161 metastases after the animals had been injected with phage displaying the GFE peptide. Tissue sections were immunostained with an anti-M13 antibody to detect phage particles. In A, brown peroxidase staining indicates phage are distributed throughout the lung vasculature (arrows). Phage staining, however, is absent in tumor (T) vasculature. As a negative control for the staining, a serial tissue section obtained from the GFE-injected mouse lung was processed with the secondary antibody alone, B; and control tissues are shown in C (skin) and D (brain).

Implication of hypoxia-inducible factor-1α in antiangiogenic activity of farnesyl transferase inhibitor SCH66336 in human aerodigestive tract cancer

Ji-Youn Han, Seung-Hyun Oh, Edward Kim, Waun Ki Hong, Ho-Young Lee

Affiliations of authors: J.-Y. Han, S.-H. Oh, E. Kim, K. W. K. Hong, and H.-Y. Lee, Department of Thoracic/Head and Neck Medical Oncology, The University of Texas M. D. Anderson Cancer Center, Houston, TX

Running Title: Inhibition of angiogenesis and HIFα expression by SCH66336

Correspondence to: Ho-Young Lee, Ph.D., Unit 432, Department of Thoracic/Head and Neck Medical Oncology, The University of Texas M. D. Anderson Cancer Center, 1515 Holcombe Boulevard, Houston, TX 77030. Phone: (713) 792-6363; Fax: (713) 796-8655; e-mail: hlee@mdanderson.org

ACKNOWLEDGMENTS

This work was supported by National Institutes of Health grants RO1 CA100816-01 and R01 CA109520-01 (to H-Y. Lee), American Cancer Society grant RSG-04-082-01-TBE 01 (to H-Y. Lee), and partly by U.S. Department of Defense grant DAMD17-01-1-0689 (to W. K. Hong) and NFCR grant LF01-065-1; W. K. H. is an American Cancer Society clinical research professor.

Abstract

Background: This study was designed to investigate the potential of SCH66336 as an antiangiogenic agent and to examine the mechanisms of action of FTIs in aerodigestive tract cancer cells, including non-small cell lung cancer (NSCLC) and head and neck squamous cell carcinoma (HNSCC) cells. ***Methods***: The antiangiogenic activities of SCH66336 were examined by *in vitro* 3-(4,5-dimethylthiazol-2-yl)-2,5-diphenyltetrazolium bromide (MTT), tube formation, *ex vivo* chick aorta, and *in vivo* Matrigel plug assays, and reverse-transcriptase PCR and western blot analyses. The specific roles of the ubiquitin-mediated proteasome machinery, MAPK and Akt pathways, and Hsp90 in SCH66336-mediated HIF-1α regulation were assessed by the use of ubiquitin inhibitors, and adenoviral vectors that express constitutively active MEK1, constitutively active Akt, or Hsp90. ***Results***: FTI SCH66336 yielded antiangiogenic activities and decreased VEGF and HIF-1α expression in hypoxic, normoxic insulin growth factor 1(IGF)-stimulated, as well as unsimulated aerodigestive tract cancer and endothelial cells. SCH66336 reduced the half-life of the HIF-1α protein, and ubiquitin inhibitors protected the hypoxia- or IGF–stimulated HIF-1α protein from SCH66336-mediated degradation. The SCH66336 inhibited the interaction between HIF-1α and Hsp90, and overexpression of Hsp90, but not constitutive Akt or constitutive MEK, restored HIF-1α expression in IGF–stimulated or hypoxic cells, but not in unstimulated cells, that were pretreated with SCH66336. ***Conclusions***: FTI SCH66336 inhibits angiogenic activities of NSCLC and HNSCC cells partly by inhibiting hypoxia- or IGF-stimulated HIF-1α and thus VEGF production *via* blocking the interaction HIF-1α and Hsp90 and inducing proteasomal degradation of HIF-1α. These findings provide the rationale for clinical application of FTIs for antiangiogenic treatment targeting HIF-1α in aerodigestive tract cancers.

Introduction

Despite recent advances in therapeutic approaches, the survival rate of patients with aerodigestive tract cancer has not improved substantially (1). Conventional treatments have targeted tumor cells alone, but a majority of patients with aerodigestive tract cancer die of metastatic disease, even after complete resection of the primary tumor (2). Generation of blood vessels (*i.e.*, angiogenesis) has a critical role in malignant solid tumor growth and subsequent metastasis to other organs throughout the body (3), suggesting that a promising therapeutic approach for aerodigestive tract cancer could be targeting the mechanisms stimulating tumor angiogenesis.

Among a variety of proteins that have been identified as potential targets of antiangiogenesis therapy, one of the key mediators is vascular endothelial cell growth factor (VEGF). VEGF is expressed by activated endothelial cells and promotes the proliferation, survival, and migration of endothelial cells, and thus is essential for blood vessel formation (4). More importantly for tumor angiogenesis, VEGF expression and secretion are stimulated in tumor cells by activation of Ras (5) and the phosphatidylinositol 3-kinase (PI3K)/Akt pathway (6,7). The major physiological stimulus for VEGF expression is hypoxia, resulting in transcriptional induction of the *VEGF* gene by hypoxia-inducible factor 1 (HIF-1), a heterodimeric transcription factor composed of HIF-1α and HIF-1β subunits (1,8). A nuclear localization signal at the *C*-terminal end of HIF-1α allows its transport from the cytoplasm to the nucleus, where it forms an active HIF-1 complex by binding to HIF-1β. HIF-1β is constitutively expressed, whereas the expression and activity of HIF-1α protein are regulated by O_2–dependent and –independent mechanisms (reviewed in 9). In normoxic conditions, HIF-1α is

subject to O_2–dependent prolyl hydroxylation, which triggers binding of von-Hippel-Lindau tumor suppressor protein (VHL) and ubiquitin-mediated protein degradation by proteasome (10,11). Under hypoxic conditions, O_2 becomes limiting for prolyl hydroxylase activity, and ubiquitination of HIF-1α is inhibited; as a result, active HIF-1 complex can be formed. Recently, however, the level of HIF-1α has been shown to increase via an O_2–independent mechanism (6,7). Growth factors, such as epidermal growth factor (EGF), heregulin, insulin-like growth factors (IGF)-1 and -2, and insulin, induce expression of HIF-1α protein in nonhypoxic conditions (7,12,13). They bind to cognate receptor tyrosine kinases and activate the PI3K or mitogen-activated protein kinase (MAPK) pathways, which in turn increases the rates of translation and HIF-1α protein synthesis. PI3K/Akt and MAPK are also implicated in the stabilization of HIF-1α induced by oncogenes, hypoxia, and growth factors (reviewed in 14). It has been demonstrated that HIF-1 associates with the molecular chaperone heat shock protein 90 (Hsp90) and that pharmacological disruption of this association promotes the ubiquitination and proteasome-mediated degradation of HIF-1 in a manner that is independent of both oxygen and VHL (15), suggesting that inhibitors of HIF-1α/Hsp90 interaction could be used to regulate hypoxia- or IGF-1-induced HIF-1α protein expression.

We previously found that SCH66336, a nonpeptide tricyclic farnesyl transferase inhibitor (FTI), inhibits the growth of non-small cell lung cancer (NSCLC) cells in combination with other inhibitors of the receptor tyrosine kinase signaling pathway (16). Recently, we have observed tumor regression in mice bearing orthotopic tongue tumors with human head and neck squamous cell carcinoma (HNSCC) or xenograft tumor with human NSCLC (16) by SCH66336 in single or in combination with other signaling inhibitror. Because angiogenesis is an essential step in the transition of a tumor from a small cluster of mutated cells to a large, malignant growth (17), we performed a series of experiments to determine the effects of SCH66336 on VEGF and HIF-1α expression and to investigate the mechanisms of action of SCH66336 in aerodigestive tract cancers. Here, we demonstrate that SCH66336 effectively inhibits expression of VEGF, partly by inhibiting HIF-1α/Hsp90 association, and thus promotes ubiquitination and proteasome-mediated degradation of HIF-1α in a manner that is independent of both oxygen and VHL.

Materials and Methods

Cells, Animals, and Materials.

Human HNSCC cell lines UMSCC38 was obtained from Dr. T. Carey (University of Michigan, Ann Arbor, MI). Human NSCLC cell lines H1299 was purchased from American Type Culture Collection (Manassas, VA). These cells were cultured in RPMI1640 supplemented with 10% fetal bovine serum (FBS) and antibiotics. HUVEC (Cambrex Bio Science, Walkersville, MD) were maintained in a gelatin-coated dish in endothelial cell basal medium (EBM) (Cambrex BioScience) containing endothelial cell growth supplement (ECGS) at 37°C in a humidified environment with 5% CO_2. HUVEC used in this study were from passages 2 to 7. Tissue culture reagents and plasticware were from Nunc (Roskilde, Denmark). Transwell chamber was from Corning-Costar, Inc. (Corning, NY). Amicon Ultra-4 was obtained from Millipore Co. (Bedford, MA). Cell

culture inserts incorporating PET membranes (6.4-mm diameter, 8-μm pore size) and 24-well plates were from Costar (Cambridge, MA). We used the following adenoviral vectors for these experiments: vector expressing constitutively active MEK1 (Ser217/221 to Glu), referred to here as Ad-MEK1 (kindly provided by Dr. J.D. Molkentin, Cincinnati, OH) (18); vector expressing constitutively active Akt (MyrAkt), referred to here as Ad-MyrAkt (19); vector expressing hemagglutinin (HA)-tagged Hsp90, referred to here as Hsp90 (kindly provided by Dr. William C. Sessa, Yale University, New Haven, CT) (20); and an empty vector, referred to here as EV. These vectors were amplified as described previously (16). Female nude mice, 6 weeks of age, were purchased from Harlan-Sprague Dawley (Indianapolis, IN). Bovine serum albumin (BSA), gelatin, and MTT were obtained from Sigma-Aldrich (St. Louis, MO). SCH66336 ([+]4-{2-[4-(8-chloro-3,0-dibromo-6,11-dihydro-5-benzocyclohepa{1,2-β}pyridin-11-yl)-1-piperidinyl]-2-oxoethyl}-1-piperidinecarboxamide) was obtained from Schering-Plough (Kenilworth, NJ). We confirmed the activity of SCH66336 in inhibiting farnesylation (Gibbs, J.B. et al. Farnesyltransferase inhibitors versus Ras inhibitors. *Curr Opin Chem Biol* 1, 197-203 (1997).) measured as an enhancement in the level of unfarnesylated H-Ras in NSCLC cell lines (data not shown). FTI-277 was purchased from Calbiochem (San Diego, CA). SCH66336 and FTI-277 were dissolved in dimethyl sulfoxide (DMSO) at various concentrations to establish dose responses. Bovine serum albumin (BSA), gelatin, MG132, ALLN, cycloheximide (CHX), cobalt chloride ($CoCl_2$), and 3-(4,5-dimethylthiazol-2-yl)-2,5-diphenyltetrazolium bromide (MTT) were obtained from Sigma-Aldrich (St. Louis, MO). Inhibitors were prepared as 20 m*M* stock solutions in dimethyl sulfoxide (DMSO) and stored at -20°C. Synthetic siRNAs targeting H-Ras, VHL, or HIF-1α were purchased from Ambion (Austin, TX).

Cell Treatment

In experiments assessing effects of the FTIs on protein and mRNA expression by western blot and RT-PCR analyses, 1 X 10^6 cells of H1299 NSCLC, UMSCC38 HNSCC cell lines, or HUVECs were transferred to 100mm^3 dish. For siRNA transfection, H1299 cells were plated at concentrations of 1 X 10^5 cells/well in 6-well plates. The next day, cells were transfected with nmol of siRNA using Oligofectamine (Invitrogen, Carlsbad, CA) for 6 h. These cells were treated with SCH66336 (0.5, 1, or 5 μM) for different time periods in complete medium. For hypoxia or IGF-1 stimulation, cells were serum-starved for 24 h and then stimulated by hypoxia (1% O_2) or 100 ng/ml IGF-1 in normoxia (20% O_2) for 4 h before harvest. Total protein extracts were collected for western blot analysis. In experiments assessing the contribution of the MAPK and Akt signaling pathways and expression of Hsp90, H1299 cells were infected with Ad-HA-Myr-Akt (25 pfu/cell), Ad-MEK (25 pfu/cell), Ad-HA-Hsp90 (50 pfu/cell), or with Ad-EV (parental virus, 25-50 pfu/cell) as a viral control. Infection was allowed to occur for 2 h in the absence of serum, and then cells were incubated in the medium containing various concentration of SCH66336 (0.5-5 μM) for 3d in complete media (unstimulated condition). For hypoxia or IGF-1 stimulation, cells were serum-free starved for 1d and then stimulated by IGF-I or hypoxia for 4h as described above. When cells were treated with CHX, CHX (100ng/mL) was added to the medium of H1299 cells that were treated with SCH66336 and stimulated with IGF-I of hypoxia for 4 h, and whole cell extracts were prepared at

different time points. In indicated experiments, MG132 (1μM) and ALLN (1μM) were added to growth medium when cells were stimulated with IGF-I or hypoxia.

Hypoxic Treatment

Tissue culture dishes were transferred to a modular incubator chamber (Billups-Rothenberg, Del Mar, CA), sealed, and placed at 37 °C. For hypoxic exposures, Cells were placed in airtight chamber (Biospherix, Redfield, NY), which was flushed with 1% O_2, 5% CO_2, 94% N_2 to maintainn O_2 concentration at 1% using Pro-Ox Model 110 O_2 regulators (BioSpherix), and incubated at 37°C.

Conditioned Media

To determine the effects of SCH66336 on angiogenic activities of H1299 NSCLC cell line, conditioned media (CM) was collected from H1299 NSCLC cell lines. H1299 cells were seeded in 10-cm plates (1×10^6 cells/plate) and, 24 h later, cells were changed to growth medium with or without different concentrations (0.5, 1, or 5 μM) of SCH66336 or FTI277. The plates were then placed under normoxic or hypoxic conditions. Following the 3 days of incubation, cells were washed with phosphate-buffered saline and re-supplied with serum free medium containing same concentrions of SCH66336. After 2 days of incubation, conditioned medium was removed and centrifuged twice in succession through Centricon filters (YM3, Millipore) to remove any traces of SCH66336. The molecular mass cutoff of the filters was 3 kDa; the molecular mass of SCH66336 is 0.56 kDa, so the flow-through containing excess SCH66336 was discarded and the retentate was collected. Because SCH66336 itself may have an inhibitory effect on this assay, we confirmed that this approach efficiently removed SCH66336 from conditioned medium by treating UMSCC38 HNCC cells with the CM and measuring farnesylated H-Ras level in the cells by Western blot analysis. We found that inhibition of H-Ras farnesylation requires more than 0.5μM of SCH66336, which was insufficient to induce antiangiogenic effects on H1299 cells. Comparing with the control cells treated with known concentrations of SCH66336, it was determined that the amount of SCH66336 remaining after two successive filtration spins was not able to inhibit H-Ras farnesyltaion when the starting concentration did not exceed 10 μM. The final filter retentate was concentrated 40-fold for use in the angiogenesis assay. CM were used for several analyses, including Matrigel plug, chick aortic arch, and HUVEC cell proliferation and tube formation assays. To test the effects of CM on proliferation of vascular endothelial cells, ten micrograms of CM from each cell group was directly applied onto HUVEC cells that were plated at 3×10^3 cells/well in 96-well culture plates. After 72 hours of incubation, cell proliferation was assessed by the MTT assay. Six replicate wells were used for each analysis and at least three independent experiments were performed.

Matrigel Plug Assay

In vivo mouse Matrigel plug assay was performed as described elsewhere (22). Briefly, 10μl of CM from SCH66336-treated or untreated H1299 cells or EBM were mixed with heparin (conc.) and growth factor–reduced Matrigel (10μl) and then injected subcutaneously into nude mice. After 7 days, Matrigel plugs were excised and vessel

formation was observed. Each treatment group included three mice, and one representative result from two independent experiments was shown.

Chick Aortic Arch Assay

Chick aortic arch assay was performed as described elsewhere (21). Thoracic aortas were obtained from chick eggs (13–15 days). Excess perivascular tissue was removed, transverse sections (1–2 mm) cut, and the resulting aortic rings washed in medium 199 (Life Technologies, Inc.). The rings were embedded in 10μl of Matrigel in 48-well plates (Costar, Corning, NY) with the lumen perpendicular to the base of the well. The ring was covered with 10μl of Matrigel, which was allowed to gel. 10μl CM was added to the aortic rings. The plates were incubated for 24 hours or 48 hours at 37°C to allow microvessel sprouting from the adventitial layer. Average sprouting was measured with the imageJ program (NIH) after the plates were photographed under the stereomicroscope (Zeiss, Göttingen, Germany). Each condition was tested in six wells. The experiment was repeated three times with similar results.

***In vitro* Tube Formation Assay**

Tube formation assay was done as described elsewhere (22). HUVEC (5×10^4) were seeded on the 10μl of Matrigel surfaces depleted of growth factors (Matrigel, Becton Dickinson, Bedford, MA) and incubated in EBM containing 10μl of CM, which were collected from H1299 cells cultured in hypoxic or normoxic condition. To test direct effects of SCH66336 on HUVECs, cells were incubated in complete medium containing SCH66336 (1,5 μM) in normoxic or hypoxic conditions. After incubation at 37°C for 4-6 hours, tube network formation was quantified as described elsewhere (22). Morphologic changes of the cells were observed under a microscope and photographed at a ×40 magnification using ImagePro Plus software (Media Cybernetics, Inc., Silver Springs, MD). Tube formation was scored in one 4x microscopic field; a three branch-point event was scored as one tube (Reimer, C.L., Agata, N., Tammam, J.G., Bamberg, M., Dickerson, W.M., Kamphaus, G.D., Rook, S.L., Milhollen, M., Fram, R., Kalluri, R., Kufe, D., and Kharbanda, S. (2002). Antineoplastic effects of chemotherapeutic agents are potentiated by NM-3, an inhibitor of angiogenesis. Cancer Res *62*, 789-795?). The experiment was performed in triplicate with similar results. The experiment was repeated three times with similar results.

Immunoblot Assays

Whole-cell lysates from 1×10^6 cells were prepared in lysis buffer as described elsewhere (16). Equivalent amounts of protein were resolved by sodium dodecyl sulfate (SDS)–polyacrylamide gels (7.5%–12%) and transferred to a nitrocellulose membrane. After the membrane was blocked in Tris-buffered saline (TBS) containing 0.05% Tween 20 (TBST) and 5% (w/v) nonfat powdered milk, the membrane was incubated with primary antibody at the appropriate dilution in TBS–5% nonfat milk at 4°C for 16 hours. The membrane was then washed multiple times with TBST and incubated with the appropriate horseradish peroxidase–conjugated secondary antibody for 1 hour at room temperature. The protein-antibody complexes were detected by using the enhanced chemiluminescence (ECL) kit (Amersham, Arlington Heights, IL), according to the manufacturer's recommended protocol. For HIF-1α, 80-μg aliquots of protein were

analyzed by using a monoclonal antibody against HIF-1α (Novus Biologicals, Littleton, CO) at 1:500 dilution as described previously (21). 30-μg aliquots were used for other western blot analyses using mouse monoclonal antibodies against phosphorylated MAPK (ppP44/42 MAPK) (Thr202/Tyr204) (1:500) or HIF-1β (H1β234; Novus Biologicals) (1:1000), rabbit polyclonal antibodies against phosphorylated Akt (pAkt) (Ser473) (1:1000), phosphorylated glycogen synthase kinase 3β (pGSK-3β) (1 : 1000), GSK-3β antibody (1 : 1000) (Cell Signaling Technology, Beverly, MA); goat polyclonal antibodies against extracellular elated kinase 1/2 (p44/42 MAPK)(1:1000), rabbit polyclonal anti-Akt, -HA, MEK1/2, and anti-β-actin (1:4000) antibodies (1:1000) (Santa Cruz Biotechnology, Inc., Santa Cruz, CA); rabbit anti-mouse immunoglobulin G (IgG)–horseradish peroxidase conjugate (1:2000) (DAKO, Carpinteria, CA); and donkey anti-rabbit IgG–horseradish peroxidase conjugate (1:2000) and rabbit anti-goat IgG–horseradish peroxidase conjugate (1:2000) (Amersham Pharmacia Biotech, Arlington Heights, IL). VHL, Hsp90,

RT-PCR Assay

Total RNA was isolated from cells with the use of Trizol reagent (Invitrogen). cDNA was synthesized from 1μg of total RNA as templates in a 50 μl reaction by using TaqMan RT reagents according to the manufacturer's protocol (Applied Biosystems, Foster City, CA). The reaction was incubated at 25°C for 10 minutes at 48°C for 30 minutes, and inactived at 95°C for 5 min. After inactivation, the cDNA was stored at -20°C until use. RT-PCR was performed by coamplification of the genes together with a reference gene (18s RNA) using the cDNA template and corresponding gene-specific primer sets. The primer sequences are as follows: (sense) 5'-GGGAGAAAATCAAGTCGTGC-3' and (antisense) 5'-AGCAAGGAGGGCCTCTGATG-3' for HIF-1α; (sense)5'-CCATGAACTTTCTGCTGTCTT-3' and (antisense) and ATCGCATCAGGGGCACACAG -3' for VEGF; 5'-GGT GAA GGT CGG TGT GAA CGG ATT T-3' (sense) and 5'-AAT GCC AAA GTT GTC ATG GAT GAC C-3' (antisense) for GAPDH. To avoid amplification of genomic DNA, the primers were chosen from different exons. PCR was carried out in a total volume of 25 μl containing 1 μl of cDNA solution and 0.2 μM of sense and antisense primers. The RT-PCR exponential phase was determined on 28-33 cycles to allow quantitative comparisons among the cDNAs developed from identical reactions. The thermocycler conditions used for amplification were 94°C for 6 minutes hot start; 94°C for 45 seconds; 56-60°C for 45 seconds; and 72°C for 1 minute. The control PCR was performed for 26-27 cycles with 0.5 μl of cDNA solution to allow quantitative comparisons among the cDNAs developed from identical reactions with primers for GAPDH. Amplification products (8 μL) were resolved on 2% agarose gels, stained with ethidium bromide, and visualized in a transilluminator and photographed.

***In Vivo* Tumor Model and Imunohistochemical Staining**

Sublingual injections for implantation of orthotopic tumors were performed as described elsewhere (23). We purchased 5-week-old female nude mice from Harlan-Sprague Dawley. All animal procedures were performed in accordance with a protocol approved by our institutional Animal Care and Usage Committee. UMSCC38 cells (2 X 10^6) were

injected into the lateral tongue of anesthetized mice (n=5). One week later, when tumors started to develop, 40 mg/kg of oral SCH66336 or 20% hydroxyl-propyl-betacyclodexatrin (HPCD) control vehicle was given twice a day for 3 weeks. At the second week after tumor cell injection, tumor size and body weight were measured, and thereafter the mouse food was replaced by commercially available soft food (transgenic mice dough; Bio-serv, Frenchtown, NJ), which could be swallowed by the mice even when the oral cavity was blocked by tumor. Four weeks after the tumor cell injection, the mice were humanely killed by CO_2 after checking their body weight and tumor size was measured. If mice had lost >20% of their preinjection body weight (average 18.92g), they were humanely killed by CO_2. Tumor growth was quantified by measuring the tumors in two dimensions and calculating as described elsewhere (Lee, H.Y., Chun, K.H., Liu, B., Wiehle, S.A., Cristiano, R.J., Hong, W.K., Cohen, P., and Kurie, J.M. (2002). Insulin-like growth factor binding protein-3 inhibits the growth of non-small cell lung cancer. Cancer Res *62*, 3530-3537.). The tongues were removed and separated into two parts. One part was fixed, embedded in paraffin, and sectioned for VEGF, and HIF-1α staining. The 5-μm-thick tumor tissue sections were deparaffinized through a series of xylene baths and rehydrated through a series of graded ethanol baths. The sections were then immersed in methanol containing 0.3% hydrogen peroxidase for 20 min to block endogenous peroxidase activity and incubated in 2.5% blocking serum to reduce nonspecific binding. Sections were incubated overnight at 4C with primary antibody against VEGF (SantaCruz, 1:100 dilution) or HIF-1α (SantaCruz,1:40 dilution). The sections were then processed using standard avidin-biotin immunohistochemical techniques according to the manufacturer's recommendations (Vector Laboratories, Burlingame, CA). Diaminobenzidine was used as a chromogen, and commercial hematoxylin was used for counterstaining. For CD31 staining, frozen sections of tumor tissues were stained with anti-CD31 antibody (BD-Pharmingen 1:100 dilution) and then detected by Cy3-conjugated secondary antibody as previously described (ref).

Immunoprecipitation

Cells treated with SCH66336 5 μM for 3 days were untreated or stimulated with IGF-1 (100 ng/ml) in normoxia or hypoxia for 4h, as described above. Whole-cell lysates were prepared in lysis buffer (50 mM Tris, 150 mM NaCl, 5 mM EDTA, 0.5% Nonidet P-40, 5% glycerol, 1 mM phenylmethylsulfonyl fluoride, protease inhibitor mixture, pH 7.5), followed by immediate vortexing (3 x 15 s). Following centrifugation (15,000 x g for 30 min) supernatants were transferred to fresh tubes. Supernatants, 1 mg of protein each, were supplied with 1 μg of anti-HIF-1 α antibody (purchased from Santa Cruz Biotechnology) and incubated at 4 °C for overnight. Thereafter, 50-μl protein A Sepharose beads (Amersham Pharmacia Biotech AB. Uppsala, Sweden) were added and incubations at 4 °C for 4 h. Beads were washed three times with the lysis buffer and two times with 1XPBS, boiled in Laemmli loading buffer, and separated by SDS–PAGE (8%). HIF-1α (H1α67, BD-Transduction Laboratories, Lexington, KY), HSP90 (BD-Transduction Laboratories) and ubiquitin (Santa Cruz) were detected by immunoblot analysis as described above.

Statistical analysis

All data are expressed as means ± SD, and 95% confidence intervals from triplicate samples were calculated using Microsoft Excel software (version 5.0; Microsoft Corporation, Seattle, WA). The Student's *t*-test was used to establish which groups differed from the control group. A *P* value of less than 0.05 was considered statistically significant.

Results

Effects of SCH66336 on angiogenic activities of aerodigestive tract cancer cells

The effects of SCH66336 on angiogenic activities of aerodigestive tract cancer cells, including NSCLC and HNSCC cells, were tested using CM derived from SCH66336-treated H1299 NSCLC or UMSCC38 HNSCC cells. The Matrigel plug assay, an established *in vivo* angiogenesis model, revealed that control plugs in which Matrigel was injected with heparin alone showed few vessels, whereas plugs treated with CM (100 ng/ml) from untreated H1299 cells, but not with CM from SCH66336-treated cells, had abundant vessel development (Fig. 1A). Since tumor angiogenesis is stimulated hypoxia, we next performed the *ex vivo* chick aortic ring arch assay using CM from H1299 cells incubated in hypoxic- (1% O_2) or normoxic (20% O_2) conditions. [redacted] We found that CM from hypoxic- or unstimulated normoxic H1299 [redacted] cells significantly stimulated endothelial cell sprouts compared with EBM-treated chick aortas; in contrast, CM from SCH66336-treated cells showed significantly less endothelial cell sprouts than cells treated with CM from control cells($P<0.01$) (Fig. 1B). We next performed the *in vitro* capillary tube formation assay to analyze the effects of SCH66336 on morphogenesis of endothelial cell. CM from untreated hypoxic- or unstimulated normoxic H1299 cells significantly stimulated tube formation of HUVECs on Matrigel-coated culture plates (Fig. 1C). However, pretreatment with 5 μM of SCH66336 blocked the morphological differentiation-stimulating activities of H1299 cells. These findings indicated the SCH66336 inhibited angiogenic activities of H1299 cells.

We explored mechanisms of antiangiogenic action of SCH66336. Since tumor angiogenesis is induced by angiogenic growth factors that are secreted from hypoxia- or growth factor-stimulated cancer cells and interact with their receptors expressed on endothelial cells to stimulate their proliferation (Shepherd, F.A. (2001). Angiogenesis inhibitors in the treatment of lung cancer. Lung Cancer *34 Suppl 3*, S81-89. Kerbel, R.S. (2000). Tumor angiogenesis: past, present and the near future. Carcinogenesis *21*, 505-515.), we tested whether CM from SCH66336-treated H1299 cells could affect the HUVECs proliferation. CM from hypoxic-, normoxic IGF-stimulated, or unstimulated normoxic H1299 cells significantly increased proliferation of HUVECs. However, CM from SCH66336-treated cells showed significantly less proliferation compared with HUVECs incubated with CM from untreated H1299 cells ($P<0.01$) (Fig. 1D). HUVECs incubated CM from hypoxic-, normoxic IGF-stimulated, or unstimulated normoxic UMSCC38 cells showed similar patterns of decreased proliferation (data not shown). These findings suggest that SCH66336 inhibits hypoxia- or growth factor-stimulated as well as constitutive secretion of angiogenic growth factors from aerodigestive tract cancer cells.

Role of HIF-1α in VEGF expression and effects of SCH66336 on HIF-1α and VEGF production in NSCLC, HNSCC, and HUVEC cells

We investigated the mechanisms that inhibit secretion of angiogenic growth factors from SCH66336-treated aerodigestive tract cancer cells. Since VEGF plays an important role in angiogenesis, and its expression is largely regulated by the transcription factor HIF-1α, we focused on the effects of SCH66336 on HIF-1α and VEGF expression

in aerodigestive tract cancer cells. To this end, we first determined whether HIF-1α has an important role in the production of VEGF in H1299 cells by measuring VEGF levels in CM from the cells transfected with siRNA targeting HIF-1α. As shown in Fig 2A (left), the basal level of HIF-1α protein expression was very weak and markedly increased when H1299 cells were incubated in hypoxia for 4 h. Expressions HIF-1α and VEGF protein in the H1299 cells transfected with HIF-1α siRNA was decreased both in normoxia and hypoxia compared with those in the scrambled (Scr) siRNA-transfected cells. HIF-1β protein expression remained unchanged in these cells. These findings indicated an important role of HIF-1α in VEGF expression.

Since growth factors and oncogenes can increase HIF-1α expression (Semenza, Reivew) (Rak, J., Mitsuhashi, Y., Sheehan, C., Tamir, A., Viloria-Petit, A., Filmus, J., Mansour, S.J., Ahn, N.G. and Kerbel, R.S., 2000. Oncogenes and tumor angiogenesis: differential modes of vascular endothelial growth factor up-regulation in ras-transformed epithelial cells and fibroblasts. *Cancer Res.* **60**, pp. 490–498.)(Lim JH, Lee ES, You HJ, Lee JW, Park JW, Chun YS. Ras-dependent induction of HIF-1alpha785 via the Raf/MEK/ERK pathway: a novel mechanism of Ras-mediated tumor promotion. Oncogene. 2004 Dec 16;23(58):9427-31.), we next tested whether HIF-1α protein levels in H1299 cells are regulated by *ras* or IGF-I. The role of *ras* on HIF-1α expression was tested in H1299 cells transfected with siRNA targeting H-*ras*. H1299 cells transfected with H-*ras* siRNA decreased H-*ras* mRNA and protein expression in normoxia (Fig. 2B, top panels) and in hypoxia (data not shown) compared with control scrambled siRNA (Scr)-transfected cells. Expression of *GAPDH* mRNA and β-Actin protein expression levels remained unchanged in these cells (data not shown). As shown in Fig.2B (bottom panels), HIF-1α protein levels were not affected by *H-ras* siRNA both in hypoxia and normoxia. We next tested if HIF-1α expression was affected by IGF-I. Consistent with previous findings (Semenza), treatement of serum-starved H1299 cells with IGF-I (50ng/ml) induced HIF-1α protein expression at 4h (Fig. 2B). These findings indicated that HIF-1α protein levels are mainly regulated by hypoxia and growth factors in H1299 cells.

We then examined the effects of SCH66336 on HIF-1α protein levels in hypoxic-, normoxic IGF-stimulated, or unstimulated normoxic H1299 cells. The hypoxia- or IGF-induced increase in HIF-α protein expression in H1299 cells was abolished by SCH66336 in time- and dose-dependent manner (**Fig. 2D**). HIF-1α protein expression in unstimulated H1299 cells was also reduced by the SCH66336 treatment. HIF-1β protein level was not affected by SCH66336 in any conditions applied. Another FTI, FTI-277, also decreased HIF-1α protein levels in hypoxic-, normoxic-IGF-stimulated, and normoxic-unstimulated H1299 cells (**Fig. 2E**). Similar patterns of decrease in HIF-1α protein levels were observed in hypoxic-, normoxic-IGF-stimulated, and normoxic-unstimulated UMSCC38 HNSCC cells treated with SCH66336 or FTI-277 (**Fig 2F**). These findings indicated that inhibition of HIF-1α protein in aerodigestive tract cancer cells is a generic response to FTIs. We next tested the SCH66336-mediated decrease in HIF-1α protein expression is well correlated with VEGF mRNA expression in hypoxic-, normoxic-IGF-stimulated, and normoxic-non-stimulated H1299 cells. VEGF mRNA expression was decreased by SCH66336 under all conditions, whereas GAPDH mRNA was not affected (**Fig.2G**), suggesting that suppression of HIF-1α expression by

SCH66336 contribute to the inhibition of the hypoxia- or IGF-stimulated as well as constitutive production of VEGF.

Since the importance of HIF1α on survival of endothelial cells have recently demonstrated (Cancer Cell 6:485 (2004)), we evaluated direct effects of SCH66336 on endothelial cells (EC). Firstly, we tested the effects of SCH66336 on HIF-1α expression in HUVECs. Similar inhibitory effects of SCH66336 on HIF-1α protein and VEGF mRNA expression were observed in hypoxic-, normoxic-IGF-stimulated, and normoxic-unstimulated HUVECs that were pretreated with 5μM of SCH66336 (**Fig. 3A**). We further examined the effect of SCH66336 on HUVEC tube formation and proliferation. For the assay, HUVECs were untreated or treated with 5 μM of SCH66336 for 24h in hypoxic or normoxic condition, and then equal number of untreated or treated cells were seeded on a Transwell chamber coated with a thin layer of Matrigel. Capillary tube structure formation was obvious at 6 h of incubation and was almost completed at 24 h in the control medium (**Fig. 3B**). However, SCH66336-treated HUVECs showed significantly decreased ability to extend and differentiate into tube-like structures following 3-d incubation with 5 μM SCH66336. We next tested the effect of SCH66336 on proliferation of HUVECs. HUVECs treated with 5 μM SCH66336 for 3d in hypoxic or normoxic conditions showed a significantly decreased proliferation (**Fig. 3C**). These data suggested that SCH66336 can act directly on endothelial cells to inhibit their angiogenic processes including tube formation and proliferation.

Effects of SCH66336 on angiogenic activities in HNSCC

The data presented above suggest that SCH66336 inhibits expression of HIF-1α protein and VEGF and suprresses tumor angiogenesis, and if growth of aerodigestive tract cancer is dependent on tumor vascularization, then inhibition of HIF-1α and VEGF protein expression by SCH66336 should also induce tumor growth inhibition. To determine whether SCH66336 inhibits HIF-1α protein and VEGF expression *in vivo*, and inhibition of these proteins affected tumor angiogenesis and tumor growth *in vivo*, we established HNSCC orthotopic tongue tumors in nude mice and treated the mice with SCH66336 and treated mice with established tumors with SCH66336. Representative tongue tissues from a healthy mouse (Normal), and tongue tumors from SCH66336-untreated (Con) and -treated mice (SCH66336) are depicted in Fig. 4A. Three weeks of oral treatment with SCH66336 (40 mg/kg) significantly suppressed tongue tumor growth ($P<0.005$); on day 28, the last day of measurement, the average tumor volume for untreated control mice had increased to 319.7 + 60.7% (mean ± s.d.) of the pretreatment volume, while that for SCH66336-treated mice was 123.8 ± 13.4% of the pretreatment volume (**Fig. 4B-left**). The average body weight of SCH66336-treated mice was not reduced during the treatment (**Fig. 4B-middle**), indicating that side effects of SCH66336 are minimal. We next evaluated effects of SCH66336 on angiogenesis and HIF-1α and VEGF expression in HNSCC. As shown in **Fig. 4B** (right), SCH66336 significantly decreased tumor vascularization ($P < 0.01$) as determined by microvessel density in anti-CD31-stained tongue tumor tissues from control and SCH6636-treated nude mice. Representative control and SCH66336-treated tongue tissues stained with CD31 are depicted in **Fig. 4C**. In addition, SCH66336-treated tongue tumor tissues also showed obvious decreases in HIF-1α and VEGF levels, while tongue tumor tissues from

untreated control mice didn't show such changes (**Fig. 3C**). These data indicate that SCH66336 is an efficient antiangiogenic therapeutic agent targeting HIF-1α and VEGF expression in aerodigestive tract cancer.

SCH66336 inhibits IGF-1–induced HIF-1α protein synthesis

We investigated the mechanism that mediates down-regulation of HIF-1α by SCH663636. Since HIF-1α protein expression is very weak in normoxic unstimulated cells, we focused on the effects of SCH66336 on hypoxic- and normoxic-IGF-stimulated HIF-1α protein levels. We first performed RT-PCR in H1299 cells treated with SCH66336. SCH66336 treatment did not measurably alter *HIF-1α* mRNA levels in the hypoxic- and normoxic-IGF-stimulated (Fig 5A), indicating that HIF-1α regulation by SCH66336 occurs at the posttranscriptional level. The increase in HIF-1α protein level could be due to a decreased rate of degradation and/or increased rate of synthesis (14). To determine which of these mechanisms is involved in SCH66336-mediated inhibition of HIF-1α protein level, H1299 cells incubated with 5 μM SCH66336 for 3 days were exposed to hypoxic conditions or IGF-1 for 4 hours to induce HIF-1α expression; CHX was then added to block protein synthesis. HIF-1α protein levels were measured before (time 0) and at various time intervals during CHX treatment. In the SCH66336-treated cells, the half-lives of both hypoxia- and IGF-1–induced HIF-1α proteins were significantly deceased. The half-life of hypoxia-induced HIF-1α protein was 180 minutes in untreated H1299 cells but 115 minutes in SCH66336-treated cells (Fig. 5B). Similarly, the half-life of IGF-1–induced HIF-1α protein was decreased from >30 minutes in untreated cells to 17 minutes in SCH66336-treated cells (Fig. 5B). These findings indicate that SCH66336 influences HIF-1α protein stability in H1299 cells.

Since HIF-1α protein is degraded mainly through the ubiquitin-proteasome pathway, we questioned whether the effect of SCH66336 on HIF-1α protein accumulation is dependent on proteasomal degradation. To answer this question, we tested whether proteasome inhibitors affect the HIF-1α protein level in SCH66336-treated cells. Pretreatment for 8 hours with different proteasome inhibitors, including MG132 (10 μM) and ALLN (50 μM), prevented the SCH66336-mediated decrease in HIF-1α protein level stimulated by hypoxia or IGF-1 (Fig. 5C). The majority of proteins degraded in the proteasome are first modified by a polyubiquitin chain, which serves as a recognition signal for targeting the proteasome (24). Indeed, treatment of cells with a proteasome inhibitor alone or in combination with SCH66336 resulted in formation of polyubiquitinated, higher molecular weight forms of HIF-1α (Fig. 5D). These findings indicate that SCH66336 inhibits HIF-1α protein accumulation through a proteasome-dependent degradation pathway in hypoxic- and normoxic-IGF-stimulated conditions.

Role of VHL in SCH66336-mediated degradation of HIF-1α

We next investigated the mechanism by which SCH66336 decreased HIF-1α level in H1299 cells. HIF-1α is constitutively stabilized in normoxic tumors and in cell lines that are VHL-null or express a nonfunctional mutant form of VHL (25), and VHL-inactivated tumors are highly vascular and overproduce VEGF (26). We therefore investigated whether VHL protein is implied in the action mechanisms of SCH66336. To address this

question, we tested the levels of VHL in hypoxic- and normoxic-IGF-stimulated as well as normoxic unstimulated H1299 cells that were pretreated with SCH66336. As shown in Fig. 5A, VHL protein expression was not changed by 5uM of SCH66336 treatment in these cells. We further tested whether inhibition of VHL expression abrogates the effects of SCH66336 on HIF-1α expression in H1299 cells. To this end, H1299 cells were untransfected or transfected with VHL or control scrambled (Scr) siRNA. After confirmation of decrease in VHL expression in VHL siRNA-transfected cells (data not shown), we determined HIF-1α protein levels in these H1299 cells, As shown in Fig 5B, HIF-1α protein expression was decreased in hypoxic- and normoxic-IGF-stimulated as well as normoxic unstimulated H1299 cells that had been transfected with VHL siRNA, compared with control scrambled siRNA (Scr)-transfected cells cultured in same conditions. These results indicated that HIF-1α regulation by SCH66336 is through VHL-indendent pathways.

Role of of MAPK and PI3K/Akt pathways in SCH66336-mediated degradation of HIF-1α

Because PI3K/Akt and p44/42 MAPK pathways have been implicated in synthesis and stabilization of HIF-1α protein (reviewed in 14), SCH66336 has a potential to inhibit these pathways, we next tested whether PI3K/Akt and p44/42 MAPK pathways are involved in SCH66336-mediated decreases in HIF-1α in H1299 cells. SCH66336 decreased the levels of phosphorylated Akt (Ser473) and phosphorylated P44/42 MAPK (pP44/42 MAPK) in hypoxic- and normoxic-IGF-stimulated cells. Whereas, in normoxic unstimulated H1299 cells, pAkt was mildly decreased and p44/42 MAPK was not affected by SCH66336 treatment (Fig. 6A). Akt and p44/42 MAPK were remained unchanged in the cells in every condition. Expression of Akt and p44/42 MAPK was not affected by SCH66336 in any case.

To further test whether PI3K/Akt and p44/42 MAPK signaling pathways is involved in the SCH66336-mediated decrease in HIF-1α protein levels, H1299 cells were infected with control adenoviral vector (EV) or adenovirus expressing HA-MyrAkt (Ad-HA-MyrAkt)(to generate constitutively active Akt) or MEK1 (Ad-MEK1) (to generate constitutively active MEK1). The induced expression of HA-MyrAkt and MEK1 and constitutive activity of these proteins were confirmed by western blot analysis on HA, MEK1, phosphorylated GSK-3β, and p44/42MAPK, as previously described (18) (Fig. 6D,E). We next determined whether infection by Ad-HA-MyrAkt or Ad-MEK1 could protect HIF-1α expression by from SCH66336-mediated decrease. Basal levels of HIF-1α protein levels were increased by Ad-HA-MyrAkt or Ad-MEK1 in hypoxic- **(Fig 6D)**, normoxic-IGF-stimulated **(Fig 6E)**, and normoxic-non-stimulated **(Fig 6F)** H1299 cells. However, SCH66336-mediated decrease in HIF-1α protein levels in these cells was not completely recovered by the overexpression of HA-MyrAkt or MEK1, suggesting that neither PI3K/Akt nor MAPK pathway played a major role in maintaining HIF-1α protein stability against SCH66336 in H1299 cells.

Effects of Hsp90 on destabilization of HIF-1α induced by SCH66336 in normoxic and hypoxic conditions

The protein chaperone Hsp90 plays a pivotal role in mediating the proper folding and subsequent activation of its numerous client proteins including HIF-1α (27). Thus, we studied the role of Hsp90 in HIF-1α protein expression in hypoxic-, normoxic-IGF-stimulated, and normoxic-non-stimulated H1299 cells. We first tested whether overexpression of Hsp90 would protect the cells from SCH66336-induced decrease in HIF-1α protein levels in H1299 cells. To this end, we infected H1299 cells with an adenoviral vector containing HA-tagged Hsp90 under the control of the cytomegalovirus promoter (Ad-HA-Hsp90). Induction of Hsp90 protein expression in the cells infected with Ad-HA-Hsp90 was determined by the appearance of the HA band in western blotting using an anti-HA antibody (Fig. 7A). In hypoxic- and normoxic-IGF-stimulated conditions, cells infected with Ad-HA-Hsp90 were completely rescued from the HIF-1α–inhibiting effect of SCH66336, unlike cells infected with EV (Fig. 7A). However, SCH66336-mediated decrease in HIF-1α protein level was not restored by overexpression of Hsp90 in normoxic unstimulated cells. These findings indicated that Hsp90 activity is required for accumulation of HIF-1α protein induced by hypoxia or IGF-1. However, constitutive expression of HIF-1α protein is regulated by SCH66336 through Hsp90-independent pathway in normoxic unstimulated condition.

Because hypoxia or IGF-induced decreases in HIF-1α protein is recovered by the overexpression of Hsp90, we next tested whether SCH66336 regulates Hsp90 expression in hypoxic- and normoxic-IGF-stimulated H1299 cells. SCH66336 showed no change in total Hsp90 protein expression in these cells (Fig. 6B). HIF-1α is known to interact with Hsp90 (28), and pharmacological disruption of the HIF-1α/Hsp90 association promotes ubiquitination and proteasome-mediated degradation of HIF-1α (15). Therefore, we explored whether SCH66336 affected the HIF-1α/Hsp90 interaction in H1299 cells. Co-immunoprecipitation assays were carried out in protein extracts of H1299 cells treated with 5 μM SCH66336 for various time intervals then exposed to 1% O_2 or 100 ng/ml IGF-1 for 6 hours. HIF-1α protein was immunoprecipitated with anti- HIF-1α antibody and the co-immunoprecipitated proteins were resolved on a polyacrylamide gel, and the Hsp90 protein was detected by western blotting using anti-Hsp90 antibody. As shown in Figure 7C, obvious interaction between Hsp90 and HIF-1α was detected in cells treated with 1% O_2 or IGF-1. The interaction was disturbed, however, by SCH66336 treatment, which preceded the decreases in HIF-1α protein and Hsp90 levels in hypoxic- and normoxic-IGF-stimulated H1299 cells. These findings suggested that SCH66336 inhibited expression of Hsp90α as well as interaction between Hsp90 and HIF-1α and thus interrupted the function of Hsp90 as a chaperone protein.

Discussion

Angiogenesis has a critical role in primary tumor growth and metastasis (29,30). A principal mediator of tumor angiogenesis is *VEGF*, and a major transcriptional activator of that gene is HIF-1α (9). An increasing body of evidence indicates that oncogenes, growth factors, and hypoxia regulate *VEGF* expression by elevating HIF-1α translational rate and its stabilization via activating MAPK or PI3K/Akt pathways (31,32). Moreover, Hsp90 associates with HIF-1α and increases its stability and function (14,15). Therefore, agents that block PI3K/Akt and MAPK signaling pathways and/or

Hsp90 function are likely candidates to inhibit tumor angiogenesis via decreasing HIF-1α and VEGF expression.

The studies reported herein demonstrate that FTI SCH66336 has antiangiogenic activity in aerodigestive tract cancers, including NSCLC and HNSCC. The FTIs, either alone or in combination with other apoptotic agents, have shown a very encouraging capacity to cause tumor regression in mice bearing human NSCLC (16) or HNSCC (unpublished data). However, the mechanism of action of SCH66336 is not completely understood. Here in this report, we demonstrate that SCH66336 has inhibitory effects on the angiogenesis-stimulating activities of aerodigestive tract cancer cells, including NSCLC and HNSCC cells.

When CM from the SCH66336-treated HNSCC cells were used, *in vivo* angiogenesis were significantly inhibited, as shown by the mouse Matrigel plug assays. Furthermore, compared with CM from NSCLC and HNSCC cells, CM from the cells treated with SCH66336 in either hypoxic or normoxic conditions showed a reduced ability to stimulate endothelial cell sprouting from chick aortas and proliferation and morphogenesis of HUVECs. These antiangiogenic actions of SCH66336 in aerodigestive tract cancers could be due to blocking farnesylation of Ras or inducing geranylgeranylation of RhoB (33). However, none of the cells used in our study has *ras* mutations (16,34). Moreover, the antiangiogenic activities of SCH66336 were unchanged when H-Ras or RhoB expression was knockdown by transfection with H-Ras or RhoB small interference RNA (unpublished data), indicating the presence of other targeted proteins which are yet to be identified.

In our ongoing efforts to identify the mechanisms of antiangiogenic action of SCH66336, we observed that FTIs inhibit HIF-1α protein in NSCLC and HNSCC lines and HUVECs. Since the importance of HIF1α and VEGF on survival of endothelial cells have recently demonstrated (Cancer Cell 6:485 (2004,), Cohen), we hypothesized that loss of HIF-1α by SCH66336 in these cells disrupts HIF-1α-driven VEGF-induced autocrine and paracrine loops, inhibiting endothelial cell proliferation and suppressing tumor angiogenesis. In support of our hypothesis, SCH66336 inhibited VEGF expression, which is well-correlated with HIF-1α protein level, in hypoxic, normoxic IGF-stimulated, of normoxi unstimulated NSCLC, HNSCC, and HUVECs. Moreover, SCH66336 directly inhibited proliferation of HUVECs.

under normoxic and hypoxic conditions *via* its effects on the PI3K/Akt pathway.

further performed series of experiments to investigate the effects of SCH66336 on HIF-1α levels in these aerodigestive tract cancer cells.

SCH66336 induced a decrease in HIF-1α levels in aerodigestive tract cancer cells under normoxia and hypoxia. It also reduced the half-life of the HIF-1α protein, and ubiquitin inhibitors protected the HIF-1α protein from SCH66336-mediated degradation in normoxic insulin growth factor 1(IGF)–stimulated or hypoxic cells.

Since serum in growth medium for cancer cells contains many growth factors, we next tested the effects of CM from H1299 cells treated with SCH66336 in serum-free medium containing IGF and observed similar patterns of decrease in HUVECs proliferation by the CM.

Since the half-life of the HIF-1α protein was decreased by SCH66336 in CHX-treated cells and the SCH66336-mediated decrease in HIF-1α protein level was blocked by MG132, a proteasome inhibitor, we have focused on the mechanisms that mediate posttranslational degradation of HIF-1α by SCH66336.

We first reasoned that SCH66336-mediated HIF-1α regulation could be at least in part due to decreased MAPK and PI3K/Akt activities, considering that 1) MAPK and PI3K/Akt pathways have critical roles in HIF-1α expression; 2) SCH66336 inhibited activation of MAPK and Akt in hypoxic- and normoxic-IGF-stimulated H1299 cells; and 3) expression of HIF-1α was remarkably increased in H1299 cells by constitutive activation of MAPK and Akt in both hypoxic and normoxic conditions. However, overexpression of constitutively active Akt or constitutively active MEK1 failed to overcome the SCH66336-mediated decrease in HIF-1α protein level, indicating that effects of SCH66336 on HIF-1α protein levels may be independent of its inhibitory effects on PI3K/Akt and MAPK pathways. We also studied whether VHL is implicated in the SCH66336-mediated decrease in HIF-1α protein level, since VHL has an important role in ubiquitin-mediated degradation of HIF-1α in normoxia; HIF-1α is constitutively stabilized in normoxic tumors and in cell lines that are VHL-null or express a nonfunctional mutant form of VHL (25). However, VHL protein expression and its binding to HIF-1α were not influenced by SCH66336 treatment, and down-regulation of HIF-1α expression was still inhibited by SCH66336 in H1299 cells treated with SCH66336. Therefore, it seems reasonable to postulate that mechanisms other than inactivation of MAPK, PI3K/Akt, or VHL exist for the regulation of HIF-1α in response to SCH66336 treatment.

Since Hsp90 has also been shown to have an important role in HIF-1α stability, Hsp90 was another candidate as targets of FTI function. Hsp90 binds to HIF-1α and prevents its ubiquitination and proteasome-mediated degradation independently of both oxygen and VHL (15). Geladanomycin, which specifically binds in the NH_2-terminal ATP binding site of Hsp90 and inhibits Hsp90-dependent ATPase activity, induces destabilization and degradation of HIF-1α (Nicola J. Mabjeesh, Dawn E. Post, Margaret T. Willard, Balveen Kaur, Erwin G. Van Meir, Jonathan W. Simons[2] and Hua Zhong. Geldanamycin Induces Degradation of Hypoxia-inducible Factor 1□ Protein via the Proteosome Pathway in Prostate Cancer Cells[1] *Cancer Research* 62, 2478-2482, May 1, 2002).(Jennifer S. Isaacs, Yun-Jin Jung, Edward G. Mimnaugh, Alfredo Martinez, Frank Cuttitta, and Leonard M. Neckers. Hsp90 Regulates a von Hippel Lindau-independent Hypoxia-inducible Factor-1□-degradative Pathway. J. Biol. Chem., Vol. 277, Issue 33, 29936-29944, 2002). Data from our study revealed that overexpression of Hsp90 via infection by an adenoviral vector completely blocked SCH66336-mediated decrease in HIF-1α in hypoxic- and normoxic-IGF-stimulated H1299 cells. Moreover, SCH66336 induced dissociation of HIF-1α from Hsp90 before HIF-1α protein levels decreased in these cells. Therefore, it is likely that, in normoxic conditions, most of growth factor-induced HIF-1α is changed to a hydroxylated form, binds to VHL, degraded by the ubiquitin-mediated proteasome (Fig.8). HIF-1α that remained bound to Hsp90 and thus protected could function as a transcription factor for VEGF. We also observed that overexpression of Hsp90 could restore HIF-1α protein levels in H1299 cells treated with SCH66336 under hypoxia. These data demonstrates that Hsp90 is required to chaperone

growth factor- and hypoxia-induced HIF-1α protein in normoxia as well as in hypoxia. These data also point to novel oxygen-independent E3 ubiquitin ligases working in hypoxic conditions. We are currently screening several candidate E3 enzymes, such as mdm2 and Hsp90/Hsp70-binding ubiquitin ligase CHIP (carboxyl terminus of Hsc70-interacting protein) (38,39) in an effort to identify the oxygen-independent ubiquitin ligase responsible for SCH66336-induced ubiquitination of HIF-1α. Importantly, although HIF-1α protein expression was decreased by the SCH66336 treatment, overexpression of Hsp90 did not protect unstimulated H1299 cells from SCH66336-induced HIF-1α protein degradation under normoxia. This demonstrates conclusively that constitutively expressed HIF-1α protein in unstimulated H1299 cells was regulated by SCH66336 in Hsp90-independent mechanisms.

In conclusion, we provide evidence here for the first time that SCH66336, a FTI, has potent antiangiogenic activity in aerodigestive tract cancers, including NSCLC and HNSCC. We show that (1) SCH66336 reduces HIF-1α protein expression and consequently inhibits *VEGF* expression in hypoxic, normoxic IGF-induced, and normoxic unstimulated H1299 cells. (2) SCH66336 inhibits normoxic IGF-induced or hypoxia-accumulated HIF-1α protein expression *via* ubiquitination and proteasome-mediated degradation pathway; (3) degradation of HIF-1α protein by SCH66336 is independent of VHL and PI3K/Akt and MAPK pathways both in normoxic and hypoxic conditions.; (4) Hsp90 associates with normoxic IGF-induced or hypoxia-accumulated HIF-1α protein, and SCH66336 inhibits this interaction. Important role of Hsp90 in maintaining HIF-1α stability has been previously documented, insofar as Hsp90 inhibitors cause ubiquitination of HIF-1α, targeting to the proteasome, and degradation (15,36,37,40,41). Therefore, SCH66336-mediated blockade of the interaction between Hsp90 and HIF-1α may be quite significant in decreasing HIF-1α expression and thus *VEGF* gene transcription in normoxic IGF-induced and hypoxic cells. Interestingly, SCH66336-induced decrease in HIF-1α protein expression and HIF-1α/Hsp90 interaction in normoxia was not restored by overexpression of Hsp90, which may indicate that the SCH66336 effect on HIF-1α expression could be through Hsp90-independent pathways rather than mechanism involving the direct interaction between HIF-1α and Hsp90. The data presented here, however, support a significant role for Hsp90 in the regulation of HIF-1α and VEGF expression by SCH66336.

Overexpression of HIF-1α protein has been demonstrated in a variety of human cancers including aerodigestive cancer, in which HIF-1α protein overexpression is associated with poor prognosis (18,42-47). Disruption of HIF-1α transcriptional activity has shown therapeutic activity in xenograft models of colon and breast cancers (8). SCH66336 suppressed HIF-1α protein levels at a concentration less than 5 μM, which is considerably below the concentration reported to be achievable *in vivo* (about 8 μM) in mice given a single oral dose of 25 mg/kg SCH66336 (35). Taken together, these data provide an important new rationale for the use of FTIs as an inhibitor of tumor angiogenesis in aerodigestive tract cancer, which depends in part on HIF-1 overexpression for tumor angiogenesis. Since FTIs are not specific for HIF-1α, their inhibition of HIF-1α and decrease in VEGF could be circumstantial and additional inhibitory pathways could be involved. Further investigations on the action mechanism of decrease in HIF-1α expression and their relatedness with VEGF production are required. In addition,

the role of other VEGF-inducing transcription factors in HIF-1α regulation by SCH66336 (9) needs to be studied.

References

1. Carmeliet P, Dor Y, Herbert JM, Fukumura D, Brusselmans K, Dewerchin M, et al. Role of HIF-1α in hypoxia-mediated apoptosis, cell proliferation and tumour angiogenesis. Nature 1998;394:485-90.
2. Coello MC, Luketich JD, Litle VR, Godfrey TE. Prognostic significance of micrometastasis in non-small-cell lung cancer. Clin Lung Cancer 2004;5:214-25.
3. Zetter BR. Angiogenesis and tumor metastasis. Ann Rev Med 1998;49:407-24.
4. Ferrara N. VEGF and the quest for tumour angiogenesis factors. Nat Rev Cancer 2002;2:795-803.
5. Rak J, Yu JL, Klement G, Kerbel RS. Oncogenes and angiogenesis: signaling three-dimensional tumor growth. J Dermatol Symp Proc 2000;5:24-33.
6. Jiang BH, Jiang G, Zheng JZ, Lu Z, Hunter T, Vogt PK. Phosphatidylinositol 3-kinase signaling controls levels of hypoxia-inducible factor 1. Cell Growth Differ 2001;12:363-9.
7. Fukuda R, Hirota K, Fan F, Jung YD, Ellis LM, Semenza GL. Insulin-like growth factor 1 induces hypoxia-inducible factor 1-mediated vascular endothelial cell growth factor expression, which is dependent on MAP kinase and PI-3-kinase signaling in colon cancer cells. J Biol Chem 2002;277:38205-11.
8. Jiang BH, Rue E, Wang GL, Roe R, Semenza GL. Dimerization, DNA binding, and transactivation properties of hypoxia-inducible factor 1. J Biol Chem 1996;271:17771-8.
9. Harris AL. Hypoxia – a key regulatory factor in tumour growth. Nat Rev Cancer 2002;2:38-47.
10. Ivan M, Kondo K, Yang H, Kim W, Valiando J, Ohh M, et al. HIFα targeted for VHL-mediated destruction by proline hydroxylation: implications for O_2 sensing. Science 2001;292:464-8.
11. Jaakkola P, Mole DR, Tian,YM, Wilson MI, Gielbert J, Gaskell SJ, et al. Targeting of HIF-α to the von Hippel-Lindau ubiquitylation complex by O_2-regulated prolyl hydroxylation. Science 2001;292:468-72.
12. Treins C, Giorgetti-Peraldi S, Murdaca J, Semenza GL, Van Obberghen E. Insulin stimulates hypoxia-inducible factor 1 through a phosphatidylinositol 3-kinase/target of rapamycin-dependent signaling pathway. J Biol Chem 2002;277:27975-81.
13. Zhong H, Chiles K, Feldser D, Laughner E, Hanrahan C, Georgescu MM, et al. Modulation of hypoxia-inducible factor 1alpha expression by the epidermal growth factor/phosphatidylinositol 3-kinase/PTEN/AKT/FRAP pathway in human prostate cancer cells: implications for tumor angiogenesis and therapeutics. Cancer Res 2000;60:1541-5.
14. Semenza, GL. Targeting HIF-1 for cancer therapy. Nat Rev Cancer 2003;3:721-32.
15. Isaacs JS, Jung Y-J, Mimnaugh EG, Martinez A, Cuttitta F, Neckers LM. Hsp90 regulates a von Hippel Lindau-independent hypoxia-inducible factor-1α-degradative pathway. J Biol Chem 2002;277:29936–44.
16. Lee H-Y, Chang YS, Chun K-H, Hassan K, Moon HJ, Cristiano R, et al. Apoptotic activity of NSCLC cells enhanced by synergy of IGFBP-3 with farnesyl transferase inhibitor

SCH66336. Accepted in JNCI 2004[AU: if you have publication info—volume, issue number, pages--please add it].
17. Hanahan D, Weinberg R. The hallmarks of cancer. Cell 2000;100:57-70.
18. Bueno OF, De Windt LJ, Tymitz KM, Witt SA, Kimball TR, Klevitsky R, et al. The MEK1–ERK1/2 signaling pathway promotes compensated cardiac hypertrophy in transgenic mice. EMBO J 2000;19:6341-50.
19. Chun K-H, Kosmeder JW, Sun S, Pezzuto JM, Lotan R, Hong WK, et al. Chemopreventive effects of deguelin, a naturally occurring PI3K/Akt inhibitor, during the malignant transformation of human bronchial epithelial cells. J Natl Cancer Inst 2003;95:291-302.
20. Fontana J, Fulton D, Chen Y, Fairchild TA, McCabe TJ, Fujita N, et al. Domain mapping studies reveal that the M domain of hsp90 serves as a molecular scaffold to regulate Akt-dependent phosphorylation of endothelial nitric oxide synthase and NO release. Circulation Res 2002;90(8):866-73.
21. Malinda KM, [AU:other authors?]et al. Identification of laminin alpha1 and beta1 chain peptides active for endothelial cell adhesion, tube formation, and aortic sprouting. Faseb J 1999;13:53-62.
22. Kim MS, Kwon HJ, Lee YM, Baek JH, Jang J-E, LeeS-W, et al. Histone deacetylases induce angiogenesis by negative regulation of tumor suppressor genes. Nat Med 2001;7(4):437-43.
23. Myers JN, Holsinger FC, Jasser SA, Bekele BN, Fidler IJ. An orthotopic nude mouse model of oral tongue squamous cell carcinoma. Clin Cancer Res 2002;8:293-8.
24. Ciechanover A. The ubiquitin-proteasome pathway: on protein death and cell life. EMBO J 1998;17:7151-60.
25. Wiesener MS, Munchenhagen PM, Berger I, Morgan NV, Roigas J, Schwiertz A, et al. Constitutive activation of hypoxia-inducible genes related to overexpression of hypoxia-inducible factor-1α in clear cell renal carcinomas. Cancer Res 2001;61:5215-22.
26. Benjamin LE, Keshet E. Conditional switching of vascular endothelial growth factor (VEGF) expression in tumors: induction of endothelial cell shedding and regression of hemangioblastoma-like vessels by VEGF withdrawal. Proc Natl Acad Sci USA 1997;94:8761-6.
27. Caplan AJ. Hsp90's secrets unfold: new insights from structural and functional studies. Trends Cell Biol 1999;9:262-8.
28. Minet E, Mottet D, Michel G, Roland I, Raes M, Remacle J, et al. Hypoxia-induced activation of HIF-1: role of HIF-1alpha-Hsp90 interaction. FEBS Lett 1999;460:251-6.
29. Folkman J. Fighting cancer by attacking its blood supply. Sci Am 1996;275:150-4.
30. Folkman J. Seminars in Medicine of the Beth Israel Hospital, Boston. Clinical applications of research on angiogenesis. N Engl J Med 1995;1757-63.
31. Laughner E, Taghavi P, Chiles K, Mahon PC, Semenza GL. HER2 (neu) signaling increases the rate of hypoxia-inducible factor 1α (HIF-1α) synthesis: novel mechanism for HIF-1-mediated vascular endothelial growth factor expression. Mol Cell Biol 2001;21:3995–4004.
32. Chan DA, Sutphin PD, Denko NC, Giaccia AJ. Role of prolyl hydroxylation in oncogenically stabilized hypoxia-inducible factor-1α. J Biol Chem 2002;277:40112–7.
33. Sebti SM, Hamilton AD. Farnesyltransferase and geranylgeranyltransferase I inhibitors and cancer therapy: lessons from mechanism and bench-to-bedside translational studies. [AU:journal?]2000;19(56):6584-93.

34. Lee H-Y, Chun K-H, Hassan K, Khuri FR, Hong WK, and Lotan R. Implication of protein kinase B/Akt and Bcl-2/Bcl-xl suppression by the farnesyl transferase inhibitor SCH66336 in apoptosis induction in squamous carcinoma cells. *Cancer Res 2003;*63:4796–4800.
35. Liu M, [Au: other authors?]et al. Antitumor activity of SCH 66336, an orally bioavailable tricyclic inhibitor of farnesyl protein transferase, in human tumor xenograft models and wap-ras transgenic mice. Cancer Res 1998;58:4947-56.
36. Suzuki H, Tomida A, Tsuruo T. Dephosphorylated hypoxia-inducible factor 1 of p53-dependent apoptosis during hypoxia. Oncogene 2001;20:5779-88.
37. Katschinski DM, Le L, Heinrich D, Wagner KF, Hofer T, Schindler SG, et al. Heat induction of the unphosphorylated form of hypoxia-inducible factor-1 alpha is dependent on heat shock protein-90 activity. J Biol Chem 2002;277:9262-7.
38. Connell P, Ballinger CA, Jiang J, Wu Y, Thompson LJ, Hohfeld J, et al. The co-chaperone CHIP regulates protein triage decisions mediated by heat-shock proteins. Nat Cell Biol 2001;3:93-6.
39. Melillo G, Taylor LS, Brooks A, Musso T, Cox GW, Varesio L. The co-chaperone CHIP regulates protein triage decisions mediated by heat-shock proteins. J Biol Chem 1997;272:12236-43.
40. Gradin K, McGuire J, Wenger RH, Kvietikova I, Fhitelaw ML, Toftgard R, et al. Functional interference between hypoxia and dioxin signal transduction pathways: competition for recruitment of the Arnt transcription factor. Mol Cell Biol 1996; 16:5221-31.
41. Kallio PJ, Okamoto K, O'Brien S, Carrero P, Makino Y, Tanaka H, et al. Signal transduction in hypoxic cells: inducible nuclear translocation and recruitment of the CBP/p300 coactivator by the hypoxia-inducible factor-1α. EMBO J 1998;176:[AU:OK?please check correct volume and page numbers]573-86.
42. Giatromanolaki A, Koukourakis MI, Sivridis E, Turley H, Talks K, Pezzella F, et al. Relation of hypoxia inducible factor 1α and 2α in operable non-small cell lung cancer to angiogenic/molecular profile of tumours and survival. Br J Cancer 2001;85:881-90.
43. Schindl M, Schoppmann SF, Samonigg H, Hausmaninger H, Kwasny W, Gnant[AU:name correct?] M, et al. Overexpression of hypoxia-inducible factor 1α is associated with an unfavorable prognosis in lymph node-positive breast cancer. Clin Cancer Res 2002;8:1831-7.
44. Birner P, Schindl M, Obermair A, Plank C, Breitenecker G, Oberhuber G. Overexpression of hypoxia-inducible factor 1α is a marker for an unfavorable prognosis in early-stage invasive cervical cancer. Cancer Res 2000;60:4693-6.
45. Aebersold DM, Burri P, Beer KT, Laissue J, Djonov V, Greiner RH, et al. Expression of hypoxia-inducible factor 1α: a novel predictive and prognostic parameter in the radiotherapy of oropharyngeal cancer. Cancer Res 2001;61:2911-6.
46. Koukourakis MI, Giatromanolaki A, Skarlatos J, Corti L, Blandamura S, Piazza M, et al. Hypoxia inducible factor (HIF-1α and HIF-2α) expression in early esophageal cancer and response to photodynamic therapy and radiotherapy. Cancer Res 2001;61:1830-2.
47. Kung AL, Wang S, Klco[AU??] JM, Kaelin WG, Livingston DM. Suppression of tumor growth through disruption of hypoxia-inducible transcription. Nat Med 2000;6:1335-40.

Figure Legends

Fig. 1. Antiangiogenic activities of SCH66336 in aerodigestive tract cancer. **A.** Matrigel plugs, which were mixed with EBM as a negative control or CM from SCH66336-treated or untreated UMSCC38 cells, were injected subcutaneously into mice. After a 7-day incubation, the Matrigel plugs were recovered. One representative experiments from two separate experiments was shown. **B.** Endothelial cell sprouting from chick aortic rings, incubated with CM from untreated or SCH66336-treated H1299 cells, was evaluated. Scoring of angiogenic activity was based on a scale of 0 to 4 units, and the results are expressed as means ± SD from six samples. The error bars represent 95% confidence intervals. **, $P<0.01$ compared with negative control. Shown is a representative group from each condition. Con, control. **C.** Angiogenic activities of CM from H1299 cells were tested by tube formation assay. HUVECs were seeded onto Matrigel-coated 12-well plates and treated with CM from H1299 cells treated with SCH66336 (5 μM) in hypoxia or normoxia. After 24 hours, images of capillary tube formation were captured, and tube formation was scored in one ×4 microscopic field as follows: one tube was designated as a three-branch point event. Data are shown as the means ± SD of two independent experiments with all of the samples in triplicate. ***, $P<0.001$ compared with control. **D.** HUVECs were allowed to grow in EBM (a negative control) or EBM containing CM from H1299 cells that were untreated or treated with 5uM of SCH66336 for 3 days, and then unstimulated or stimulated by hypoxia (1% O_2) or IGF-I (100ng/ml) for 4 hours. Cell proliferation was analyzed by MTT assay. Results are expressed as percentages ± SD. Independent experiments were repeated three times, and each value indicates the mean ± SD of eight samples. The error bars represent 95% confidence intervals. **, $P<0.01$; ***, $P<0.001$ compared with negative control.

Fig. 2. Role of HIF-1α in the angiogenic in the antiangiogenic activities of FTIs in aerodigestive tract cancer cells. **A.** Role of HIF-1α in the VEGF expression in NSCLC cells were examined. Immunoblot assays on HIF-1α and HIF-1β were performed in H1299 cells that were untransfected or transfected with indicated scrmbled (Scr) or HIF-1α siRNA and then incubated under normoxia or hypoxia for 2 d **(left)**. β–Actin protein was detected as loading control for western. The CM from these cells were used for the western blot analysis on VEGF expression. Equal amount of protein in each CM was confirmed by Panceau staining of the membrane after the transfer. **B.** Role of H-*ras* and hypoxia in the induction of HIF-1α expression in H1299 cells were examined. Semiquantitative RT-PCR analysis on H-*ras* and *GAPDH* mRNA expression and immunoblot assays on H-Ras, HIF-1α or HIF-1β, and β-Actin were performed in H1299 cells that were untransfected or transfected with Scr or H-*ras* siRNA and then incubated under normoxia or hypoxia for 2 d **(left)**. **C.** Kinetics of HIF-1α induction by IGF-I was tested in H1299 cell. Cells exposed to IGF-I (100ng/ml) for indicated time periods were harvestred and subjected to the western blot analysis on HIF-1a and HIF-1b. **D.** Effect of SCH66336 on HIF-1a and HI-1b expression in hypoxic-, normoxic IGF-stimulated, or unstimulated H1299 cells were tested by western blot analysis. H1299 cells were untreated or pretreated with 5 μM SCH66336 for indicated time periods or with 1 or 5 μM SCH66336 for 3 days in complete medium in normoxia. Otherwise cells were treated same way for 2 days in complete media and for 1 day in serum-free medium, and then exposed to 1% O_2 or IGF-1 for 4hours. Whole-cell extracts were subjected to immunoblot assays using antibodies specific for HIF-1α, HIF-1β, or β-Actin. **E,F.** H1299 cells (E) or UMSCC 38 cells (F) treated with SCH66336 or FTI-277 in complete medium for 3 days under normoxia or cells pretreated with FTI-277 (0.5-5 μM) for 2days in complete

medium and continuously for 1 day in serum free medium, and then exposed to 1% O_2 or 100ng/mL of IGF-I 4 hours. Whole-cell extracts were prepared and subjected to immunoblot assays using antibodies specific for HIF-1α and HIF-1β. **G.** Semiquantitative RT-PCR analysis on VEGF mRNA expression were performed in H1299 cells that were pretreated with 1 or 5 μM SCH66336 for 2 days in complete medium and 1 day in serum free medium and then exposed to 1% O_2 or IGF-1 (100 ng/ml) for 4 hours or in cells continuously treated with 5 μM SCH66336 in complete medium for 3 days.

Fig. 3. The effects of SCH66336 on HIF-1a and VEGF expression, tube formation,l proliferation of HUVECs were analyzed. **A.** HUVECs were pretreated with SCH66336 (5 μM) for 2 days in complete medium and 1 day in serum free medium and then exposed to 1% O_2 or IGF-1 (100 ng/ml) for 4 hours or continuously treated with SCH66336 in complete medium for 3 days. Whole-cell extracts were prepared and subjected to immunoblot assays using antibodies specific for HIF-1α and HIF-1β. **B.** HUVECs untreated or treated with SCH66336 (5 μM) for 1 d were seeded onto Matrigel-coated 12-well plates. After 6 hours, images of capillary tube formation were captured, and tube formation was scored in one ×4 microscopic field as follows: one tube was designated as a three-branch point event. Data are shown as the means ± SD of two independent experiments with all of the samples in triplicate. ***, $P<0.001$ compared with control. **C.** HUVECs were allowed to grow in complete medium containing indicated concentrations of SCH66336 in hypoxia (20% O_2) or in normoxia (1% O_2) for 3 days. Cell proliferation was analyzed by MTT assay. Results are expressed as percentages ± SD. Independent experiments were repeated three times, and each value indicates the mean ± SD of eight samples. The error bars represent 95% confidence intervals. **, $P<0.01$; ***, $P<0.001$ compared with negative control.

Fig. 4. Inhibition of HNSCC growth by SCH66336. **A:** Effect of SCH66336 on growth of orthotopic tongue tumors. Photograph of normal tongue from nude mice that were not inoculated with UMSCC38 cells is shown on the left. Orthotopic tongue tumors from control (middle) and SCH66336-treated (right) nude mice on day 28 after injection of UMSCC38 cells are shown. **B:** The results are expressed as the mean (±SD) tumor volumes (calculated from five mice) relative to the tumor volumes at the time of SCH66336 treatment (day 14). **, $P < 0.01$ compared with control (left). Changes in body weight during SCH66336 treatment was shown (middle). **C:** Immunohistochemical analysis by CD31 on VEGF and HIF-1α was performed in UMSCC38 orthotopic tongue tumor tissues from HPCD-treated control (Con) and SCH66336-treated nude mice on day 28 after injection of UMSCC38 cells.

Fig. 5. Effect of SCH66336 on the proteasomal degradation of hypoxia- or IGF-1-induced HIF-1α protein. **A.** Total cellular RNA was isolated and HIF-1α mRNA expression analyzed by semiquantitative RT-PCR. **B.** H1299 cells pretreated with 5 μM SCH66336 in complete medium for 2 and in serum free medium for 1 day were exposed to 1% O_2 or 100 ng/ml IGF-1 for 4 hours, and then cycloheximide (CHX) was added to a final concentration of 100 μM. Cells were harvested at the indicated time points, and whole-cell lysates were subject to immunoblot assay of HIF-1α and HIF-1β expression. Quantification of the autoradiographic HIF-1α signal was performed by densitometry (bottom). Values were normalized to the expression of HIF-1β and expressed as percentages relative to time 0. **C.** H1299 cells were untreated or treated with 5 μM

SCH66336 for 3 days and then incubated with or without MG132 (10 μM) or ALLN (50 μM) for 4 hours in hypoxic (1% O_2) and normoxic (100 ng/ml IGF-1) conditions. Whole-cell extracts were prepared and subjected to immunoblot assays using antibodies specific for HIF-1α or β-Actin. **D.** HIF-1α ubiquitination was analyzed by using whole-cell extracts from H1299 cells that were untreated or treated with 5 μM SCH66336 for 3 days and then incubated with or without MG132 (10 μM) for 4 hours in hypoxic (1% O_2) or normoxic (100 ng/ml IGF-1) conditions. The same amounts of whole-cell extracts were immunoprecipitated with an anti-HIF-1α antibody, and immunoprecipitates were washed and subjected to electrophoresis and western blot analysis using an anti-ubiquitin (Ub) antibody. Whole-cell extracts from MG132-treated cells in normoxic conditions were immunoprecipitated with preimmune rabbit serum (PS) and included as a negative control.

Fig. 6. Role of VHL, MAPK, PI3K/Akt in SCH66336-mediated inhibition of HIF-1α protein. **A.** Whole-cell extracts were prepared from H1299 cells that were untreated or treated with 5 μM SCH66336 for 3 days and then exposed to hypoxia or IGF-I(100ng/mL) for 4 hours or unstimulated, as described in the Materials and Methods. Whole cell lysates were collected and western blot analysis of VHL and β-Actin was performed. **B.** Western blot analysis was performed in H1299 cells that were transfected with Scr or *VHL* siRNA, incubated with 5 μM SCH66336 in complete medium for 2 d and in serum free medium for 1 day, and then exposed to 1% O_2 or 100 ng/ml IGF-1 for 4 hours under normoxia or in cells continuously treated with 5 μM SCH66336 in complete medium for 3d in normoxia. **C.** H1299 cells were incubated with 5 μM SCH66336 in complete medium for 2 d and in serum free medium for 1 day, and then exposed to 1% O_2 or 100 ng/ml IGF-1 for 4 hours under normoxia or in cells continuously treated with 5 μM SCH66336 in complete medium for 3d in normoxia. Whole-cell extracts were subjected to immunoblot assays using antibodies specific for unphosphorylated or phosphorylated p42/p44 MAP kinase and Akt. **D-F.** H1299 cells were infected with 50 pfu/cell of control adenovirus (EV), an adenoviral vector (Ad-HA-MyrAkt) that expresses constitutively active Akt (MyrAkt) with a hemagglutinin (HA) tag (upper panel), or an adenoviral vector that expresses constitutively active MEK1 (Ad-MEK1) (lower panel). Infected cells were treated with indicated concentrations of SCH66336 for 2 days in complete media and for 1 day in serum-free medium and then exposed to 1% O_2 (**D**) or 100 ng/ml IGF-1 (**E**) for 4 hours. Cells infected and treated with SCH66336 were also incubated in complete medium for 3 days (**F**). The expression levels of HIF-1α, phosphorylated glycogen synthase kinase (pGSK)-3β and unphosphorylated GSK-3β, HA, MEK1, unphosphorylated or phosphorylated p42/p44 MAP kinase, or β-Actin were analyzed by western blot analysis.

Fig.7. Effects of SCH66336 on Hsp90-mediated stabilization of HIF-1α. **A.** Effect of Ad-Hsp90 on HIF-1α protein level in SCH66336-treated H1299 cells was analyzed. After infection with EV or Ad-Hsp90-HA (50 pfu/cell), H1299 cells were untreated or treated with various concentrations of SCH66336 (1-5 μM) for 3 days. After exposure to 1% O_2 or 100 ng/ml IGF-1 for 4 hours, the expression levels of HA, HIF-1α, and β-Actin were analyzed by western blot analysis. **B.** Cells were pretreated for 3 days with 1 or 5 μM SCH66336 and then exposed to 1% O_2 or IGF-1 (100 ng/ml) for 4 hours. Whole-cell extracts were prepared and subjected to immunoblot assays using antibodies specific for Hsp90 and β-Actin. **C.** The effects of SCH66336 on the interaction between HIF-1α and Hsp90 in H1299 cells were analyzed. H1299

cells exposed to 1% O_2 or 100 ng/ml IGF-1 for 4 hours were treated with 5 μM SCH66336 for indicated time periods. Cells were harvested and whole-cell extracts were immunoprecipitated with an anti-Hsp90 antibody; western blot analysis was performed on immunoprecipitates using an anti-HIF-1α antibody. Whole-cell extracts from IGF-1-treated cells in normoxic conditions were immunoprecipitated with preimmune rabbit serum (PS) and included as a negative control. The position of HIF-1α was confirmed by western analysis on whole-cell extracts without immunoprecipitation. The same samples were used for western analysis of HIF-1α.

Fig. 8. Schematic representation of the cell signaling events leading to ubiquitin-mediated degradation of HIF-1α and inhibition of VEGF protein expression by SCH66336 in aerodigestive tract cancer cells. In normoxic conditions, a major portion of HIF-1α becomes hydroxylated by proline hydroxylase, binds to VHL, and then is subjected to ubiquitin-mediated proteasome degradation. However, a minor portion of HIF-1α, which is stabilized by binding to Hsp90, still translocalizes to the nucleus and combines with HIF-1β to form an active transcription factor. This heterodimer binds to the *VEGF* promoter and activates VEGF expression and secretion, and thus angiogenesis can be stimulated in normoxic conditions. SCH66336 also inhibits the interaction between HIF-1α and Hsp90 both in hypoxic condition and induces ubiquitin-mediated proteasome degradation, which results in a decrease in VEGF expression and inhibition of tumor angiogenesis.

Lymphocytic Expression of Nucleotide Excision Repair Proteins as a Marker for Cancer Susceptibility: A Pilot of Study of Squamous Cell Carcinoma of the Head and Neck[1]

Qingyi Wei[2] Li-E Wang, Erich M. Sturgis, Li Mao[2]

Departments of Epidemiology [Q. W., L-E. W., E. M. S.], Head and Neck Surgery [E. M. S.], and Thoracic and Head and Neck Medical Oncology [L. M.], The University of Texas M. D. Anderson Cancer Center, Houston, Texas 77030; The University of Graduate School of Biomedical Sciences at Houston [Q. W., E. M. S., L. M.], Texas 77030

[1] Supported by National Institutes of Health Grant R01 ES11740, CA 97007, PO1 CA106451, CA100264, and CA16672; Department of Defense Grant DAMD 17-02-1-0706.

[2] Correspondence to: Department of Epidemiology, Unit 189, The University of Texas M. D. Anderson Cancer Center, 1515 Holcombe Blvd., Houston, TX 77030. Telephone: 713-792-3020; Fax: 713-563-0999; (e-mail: qwei@mdanderson.org or lmao@mdanderson.org)

[3]Abbreviations: SCCHN, squamous cell carcinoma of the head and neck; NER, nucleotide excision repair; DRC, DNA repair capacity

Running head: Nucleotide excision repair protein expression and SCCHN risk

Keywords: Biomarker, DNA repair, genetic susceptibility, molecular epidemiology, proteomics

Abstract

Nucleotide excision repair (NER) plays a key role in maintaining genomic stability. In this pilot study, we quantified NER protein levels by a reverse-phase protein microarray in cultured lymphocytes transfected with damaged plasimids in 57 patients with newly diagnosed squamous cell carcinoma of head and neck (SCCHN) and 63 cancer-free controls. We tested the hypothesis that NER protein expression is associated with risk of SCCHN. We found that in 63 controls, the relative expression levels of the six core NER proteins were highly correlated ($P < 0.001$ for all). Compared with the controls, the cases had lower expression levels of all the NER proteins, particularly XPC and XPF, which had a greater than 25% reduction ($P < 0.01$). When we used the median expression levels of the NER proteins as the cut-off value, significantly increased risk of SCCHN was associated with low expression levels of XPA (odds ratio (OR) = 2.99; 95% confidence interval (CI) = 1.22-7.47), XPC (OR = 2.46; 95% CI=1.04-5.87), XPD (OR = 3.03; 95% CI=1.18-7.76) and XPF (OR = 5.29; 95% CI = 2.01-13.9) but not ERCC1 and XPG after adjustment for age, sex, ethnicity, smoking and alcohol use. When a multivariate logistic regression model included all NER proteins, only low expression level of XPF remained as a significant predictor for the risk of SCCHN (OR = 11.5; 95% CI = 2.32-56.6). These results suggest that this protein microarray assay may provide a useful tool for measuring protein markers for susceptibility to cancer.

Introduction

SCCHN, which includes cancers of the oral cavity, pharynx, and larynx, is a common malignancy with an estimated number of more than 500,000 new cases worldwide (1). In the United States, approximately 37,200 new SCCHN[3] cases and 11,000 SCCHN deaths occurred in 2003 (2). Many factors contribute to SCCHN, including tobacco smoking (3), alcohol use (4), viral infection (5,) and genetic factors (6). Although smoking and alcohol use play a major role in the etiology of SCCHN, only a fraction of smokers and drinkers develop SCCHN, suggesting that there is inter-individual variation in genetic susceptibility to SCCHN in the general population.

Cellular DNA is constantly bombarded by various endogenous and exogenous damaging agents, some of which are recognized carcinogens as contained in tobacco. During evolution, species of all living organisms developed sophisticated DNA repair pathways and mechanisms with which to battle genomic insults from these environmental hazards to maintain genomic integrity and thus to survive. Tobacco smoke contains numerous known compounds, many of which are mutagenic and carcinogenic. These carcinogens induce DNA adducts are repaired by nucleotide excision repair (NER), one of the most important pathways of DNA repair (7).

A number of critical genes,including seven so-called core factors (ERCC1, XPA, XPB, XPC, XPD, XPF and XPG) participate in NER activity (7), and functional mutations in any one of the seven genes can lead to abnormal NER and therefore increase susceptibility to cancer (8). NER abnormalities are present in several rare syndromes that are characteristic of deficient NER coupled with high ultraviolet (UV) light sensitivity and increased cancer risk (9). For example, xeroderma pigmentosum (XP) patients, who have mutations in at least one of seven XP (i.e.,

NER) genes, are extremely sensitive to sunlight-induced skin damage. Consequently, these patients have extremely high incidences of nonmelanoma skin cancer and melanoma as well as other solid tumors (9).

In previous studies, we demonstrated that reduced DRC as measured by the host-cell reactivation assay (10) and low reduced mRNA expression levels (11) of the NER genes in lymphocytes were associated with increased risk of SCCHN. In this report, we used a proteomic microarray assay to measure lymphocytic expression of the NER proteins in a pilot case-control study to test the hypothesis that reduced expression of NER proteins are associated with increased risk of SCCHN.

Materials and Methods

Subject recruitment and sample procurement. This was a pilot study that utilized previous cryopreserved viable peripheral blood lymphocyte samples from an ongoing case-control study of SCCHN. The samples collection started since years 2000. The selected samples were those whose lymphocytes were sufficient enough for cell culture and subsequent transfection of plasmids with and without damage induced by diol epoxide benzo[a]pyene (BPDE), an ultimate tobacco carcinogen we previously used for studying host-cell DRC (12). The blood sample processing, preparation of plasmids, and transfection have been described in detail previously (12). Briefly, lymphocytes were isolated from whole peripheral blood by Ficoll gradient centrifugation, cryopreserved within 24 h by using freezing medium, and then stored in a -80°C freezer in 1.5-ml aliquots until thawed for the assays.

Cell culture and protein preparation. The cryopreserved cells were thawed and cultured in T-25 flasks at 37°C in a 5% CO_2 atmosphere in regular RPMI 1640 (Life Technologies, Inc., Grand Island, NY) supplemented with 20% fetal bovine serum (Life Technologies, Inc.). The frozen cells in each vial (1.5 ml) were quickly thawed and mixed before the last trace of ice disappeared with 8.5 ml of thawing medium (50% fetal bovine serum, 40% RPMI 1640, and 10% dextrose; Sigma Chemical Co.), which ensured a cellular viability of >80% as tested by 0.4% trypan blue (Sigma Co., St. Louis, MO) exclusion test. After being washed with the thawing medium, the cells were incubated in RPMI 1640 supplemented with 20% fetal bovine serum and 56.25μg/ml phytohemagglutinin (Murex Diagnostics, Norcross, GA) for stimulation at 37°C for 72 h. Only stimulated lymphocytes will uptake the plasmids (13) and have active NER activities (14,15).

After harvesting, the cells (~1 x 10^6) were transfected with untreated plasmids (as the baseline for comparison) and duplicate transfections with BPDE-treated plasmids. The transfections were performed by the DEAE-dextran (Pharmacia Biotech Inc., Piscataway, NJ) method with ~0.25 μg of either untreated plasmids or plasmids treated with BPDE. In consistency with the protocol of the host-cell reactivation assay (12), the cells were harvested for protein extraction 40 hours after the transfections. This procedure is critical to ensure that the repair process was challenged by the presence of damaged plasmids transfected into the cells, which served as the substrate of repair enzymes. Thirty microlitter cell suspension (~1 x 10^5 cells) from each individual was mixed with 10 μl 4x SDS sample buffer containing 50 mM Tris-HCl (pH 8.0), 150 mM NaCl, 0.1% sodium dodecyl sulfate (SDS) and 1% Triton X-100 supplemented with a protease inhibitor cocktail (Roche Applied Science, Indianapolis, IN). The cell lysate was then boiled for 5 min and stored at –80° C until use.

Fabrication of reverse-protein microarrays. Proteins extracted from the cells were used to fabricate protein microarrays. The samples were serially diluted to 1, 2, and 4 by adding phosphate-buffered saline (PBS) buffer (pH 7.5) to final protein concentrations range from initial 1mg/ml reduced to 0.025mg/ml. The serial dilutions were transferred to 384-well plates and used to spot on FAST™ slides (Scheicher & schuell, Germany) by using SpotBot Arrayer (Telechem International, Cupertine, CA). Each sample was spotted in duplicate. Fabricated slides were either used immediately or stored at –20°C until use.

Quantitative analysis of protein levels using reverse-protein microarrays. Antibodies against XPD and XPG were purchased from Santa Cruz Biotechnology (Santa Cruz, CA): XPA, XPC, and XPF from Abcam (Cambridge, MA); ERCC1 from Novus biological (Littleton, Co); ß-Actin from Sigma (St. Louis, MO). No commercially available antibodies against XPB were specific enough for this study. Briefly, the fabricated slides were treated with Reblot (Chemicon, Temeula, CA) for 15 min and subsequently washed twice 10 min each with washing buffer containing 300 mM NaCL, 0.1% Tween 20, and 50mM Tris at pH7.6 (TBS). The protein arrays were then blocked using I-block (Applied Biosystem, Foscor city, Ca) for 30 min at room temperature. The primary antibodies were diluted based on their affinities tested in our preliminary testing (data not shown). The dilute ratios were 1:300 for XPA and ERCC1; 1:500 for XPC, XPD, XPF, and XPG; 1:100,000 for ß-Actin. The arrays were incubated with individual antibodies for 1 h at room temperature. Secondary antibodies (Vector Laboratories, Burlingame, CA) were biotin-labeled and diluted into 1:10,000 (anti-mouse, anti-goat, and anti-rabbit, respectively). The antibodies were added to the slides and incubated at room temperature for 30 min. DAKO catalyzed signal amplification system-CSA (DAKO Corporation, Carpinteria, CA) was used to enhance signals according to the manufacturer's protocol except the final step

by incubating with Cy5-conjugated streptavidin (1:1000 dilution) (Jackson Immuno Research Laboratories, West Grove, PA) for 30 min. The arrays were washed three times for 5 min each with TBS after each incubation step.

Statistical Analysis. Signals on the protein microarrays were scanned on a ScanArray Lite microarray scanner (Perkin-Elmer Life Sciences, Boston, MA). The signal intensity of each spot and its background signal were analyzed using ScanArray Express 2.0 microarray analysis system (Perkin-Elmer Life Sciences) "Run easy Quant " protocol. The final data were stored as tif. filef for further analysis. Any scan-reading value under 2000 was treated as missing data. The median value of the scan-reading data of each dot of a gene on the microarray was used for the calculation of the mean of the duplicates, and such scan-reading data of each gene relative to that of the β-actin gene were used as the relative expression levels of each gene. The Student *t* test was used to compare differences in mean values of readings for each gene between cases and controls. The control median expression value was used as the cut-off value for calculation of odds ratios (ORs) and their 95% confidence intervals (CIs). Multivariate logistic regression models were used to calculate the adjusted ORs and 95% CIs with adjustment for age (in years), sex (male vs female), ethnicity (non-Hispanic vs others) and sample storage time (in months). All statistical analyses were performed with SAS software (version 8.0e; SAS Institute Inc., Cary, NC).

Results

Protein microarray data. As shown in **Figure 1**, we plotted on the arrays with duplicate samples consecutively diluted twice for each subject. The average of the duplicate readings of the medians was used in calculation of the relative protein expression and for comparison.

Because of mechanical problems during the plotting, some protein spots were missed on the arrays. Therefore, some of the samples did not have valid readings for all the proteins examined. We first compared the sample readings for different dilutions and found that readings from spots with lower protein concentrations had a large variation, whereas the spots with higher protein concentration produced consistent, strong and readable signals; therefore the latter was used for calculating the relative expression levels. Then, we compared the relative expression levels of these samples between cells tranfected with undamaged plasmids and those transfected with damaged plasmids among the cases and controls. We found that the data from the samples transfected with damaged plasmids had a better prediction of the risk based on the comparisons (data not shown) although the two data sets were highly correlated with a coefficient ($P < 0.01$). Therefore, the following data presentation used the data derived from cells transfected with damaged plasmids that stimulated DNA repair activity.

Subject characteristics. This analysis included 57 patients with newly diagnosed SCCHN and 63 controls who were free of cancer, whose cryopreserved lymphocytes were available for culture, transfection, and protein extraction. The cases and controls were frequency matched on age, sex, and ethnicity. As shown in **Table 1**, the cases were slightly younger than the controls, and there were more males and non-Hispanic whites in the cases than in the controls, but these differences were not statistically significant. The mean age of the cases was 56.2 years compared with 57.2 years of the controls (**Table 2**). However, there were more smokers and alcohol drinkers in the cases than in the controls, and these differences were statistically significant ($P = 0.006$ and $P = 0.009$, respectively). Because the cases were recruited first and the controls were recruited later, the time period of lymphocytes storage was also statistically significantly different (17.7 months for the cases and 13.2 months for the controls; $P = 0.013$) (Table 2).

Therefore, all these variables were further adjusted for in the multivariate logistic regression analysis.

Difference in NER protein expression between the cases and controls. The differences in NER protein expression were evaluated by the Student *t* test between the cases and controls. As shown in **Table 2**, the expression of all seven NER proteins was lower among the cases than among the controls. For example, the relative expression of the XPC and XPF genes was reduced by 25% in the cases than in the controls, and the differences were statistically different (P = 0.003 and P = 0.004, respectively) (Table 2). The expression reduction of all NER proteins may reflect their association in the repair activities. Further correlation analysis revealed that the relative expression levels of these NER proteins were all highly correlated (P = or <0.001). For example, the expression of XPC was correlated with that of ERCC1 (r = 0.706), XPF (r = 0.505) and XPG (r = 0.715), whereas the expression of XPF was correlated with that of XPA (r = 0.695) and XPD (r = 0.541) and XPG (r = 0.781) (data not shown). Therefore, it was necessary to identify the expression of which protein that had played the most significant role in the increased risk of SCCHN.

Association between the protein expression levels and risk of SCCHN. When we used the median expression level of the controls as the cut-off value for calculating the ORs, significantly increased crude ORs were observed for XPA, XPC, XPD, XPF but not for ERCC1 and XPG, and the adjusted ORs were essentially unchanged after adjustment for age, sex, ethnicity, smoking, alcohol use, and sample storage time (**Table 3**). The highest adjusted OR was for XPF (OR = 5.29, 95% CI, 2.10-3.92) followed by XPD (OR = 3.02, 95% CI, 1.18-7.76) and XPA (OR = 2.99, 95% CI, 1.22-7.47). Because the relative expression levels of these NER proteins were

highly correlated, the relative expression levels of all proteins were further adjusted for each other simultaneously in a final multivariate logistic regression model containing age, sex, ethnicity, smoking, alcohol use, and sample storage time. As a result, the only significant multivariate adjusted OR was for XPF (OR = 11.5, 95% CI, 2.32-56.6) (Table 3).

Discussion

In this study, we have demonstrated that the relative expression levels of the six NER proteins (ERCC1, XPA, XPC, XPD, XPF and XPF) tested by the reverse protein assay were consistently significantly lower among the SCCHN cases than among the controls. Four NER proteins (XPA, XPC, XPD, XPF and XPG) out of the six tested were associated with significantly increased risk of SCCHN and the relative expression levels of the other two proteins (ERCC1 and XPG) were associated with borderline increased risk of SCCHN. These data are consistent with our previously published observation on the overall DRC for removing BPDE-induced DNA damage and subsequent study on the expression of these genes at mRNA levels in SCCHN (10,11). For example, in a previous study of 55 patients with newly diagnosed SCCHN and 61 healthy controls, we measured the DRC by the host-cell reactivation assay using a reporter gene damaged by BPDE (10). We found that the mean DRC was significantly lower in cases than it was in controls: those in the middle and lowest tertiles of DRC had greater than 2-fold and 4 fold increased risk, respectively, compared with the highest tertile of DRC (10).

To understand which NER genes may be underlying the reduced DRC, we measured the relative expression of five NER genes (*ERCC1, XPB/ERCC3, XPG/ERCC5, CSB/ERCC6,* and *XPC*) by a multiplex RT-PCT method (11). We found that the relative mRNA expression levels of *ERCC1, XPB/ERCC3, XPG/ERCC5,* and *CSB/ERCC6* were significantly lower in the cases than in the

controls and the risk associated with low expression of these genes ranged between 2- to 6-fold increased risk (11). In the later study, however, we were not able to measure the expression of *XPA, XPD,* and *XPF* because of either the sequences of the genes were unknown at that time or the presence of a high level of sequence homology in the genome for the primers chosen that made the assays failed.

It is interesting to note that by simultaneous adjustment for the expression levels of all the five proteins and other confounding factors, we found the relative expression level of XPF was the only independent risk factor with more than 11-fold increased risk of SCCHN. This finding suggests XPF plays a critical role in the repair of carcinogen damaged DNA. Because ERCC1 needs XPF to form a functional complex (7), it is possible that XPF acts as a rate limiting modulator for the function of the complex. Based on our data, ERCC1 expression level was the highest among the five proteins, whereas the XPF expression level was less than 70% of the ERCC1 level. It is possible that ERCC1 protein was in a saturated condition while the amount of XPF became critical to modulate the overall DNA DRC.

The present study is an extension of our previous studies in identifying the best biomarkers of DRC for predicting susceptibility to SCCHN. In the present study, we had successfully measured the relative expression levels of six out of the seven core NER proteins, although we did not find appropriate antibody for XPB. Our data further support the notion that altered NER capacity, either at cellular, mRNA or protein levels, may contribute to the risk of tobacco-induced SCCHN. More importantly, the relative protein expression measured by the protein microarray method appeared to be the most sensitive one compared to cellular DRC and the mRNA expression levels we have studied before.

The advantages of the protein microarray assay are several folds. First, compared with the host-cell reactivation assay (12), this microarray assay requires significantly fewer (3-fold less) viable lymphocytes that are needed for protein extraction; Second, compared with the RT-PCR assay, this microarray assay is highly sensitive and reproducible that is optimal for large scale screening at population level. Third, the assay has unlimited potential to test more proteins such as those involved in either NER or other repair pathways, which is important to elucidate the underlying molecular mechanisms of increased cancer risk. Finally, this microarray assay is rapid and cost-effective in producing a large quantity of data. With the availability of antibodies for specific protein post-translational modifications, the method may become a powerful tool to determine status of functional changes of the proteins. Nevertheless, more quality control issues of this microarray assay may need to be addressed before its application to large scale of population studies (16,17).

Acknowledgments

We thank Margaret Lung and Dr. Peggy Schuber for assistance in recruiting the subjects, Youhong Fan and Yawei Qiao for laboratory assistance, Betty J. Larson and Joanne Sider for manuscript preparation, and Rachel Williams for scientific editing.

References

1. Pisani, P., Parkin, D. M., Bray, F., and Ferlay, J. Estimates of the worldwide mortality from 25 cancers in 1990. Int J Cancer 1999; 83:18-29.
2. American Cancer Society Inc. Cancer Facts & Figures 2003. Atlanta: American Cancer Society; 2003.
3. Johnson N. Tobacco use and oral cancer: a global perspective. J Dent Educ 2001;65:328-39.
4. Casiglia J, Woo SB. A comprehensive review of oral cancer. Gen Dent 2001;49:72-82.
5. Dahlstrom, K. R., Adler-Storthz, K., Etzel, C. J., Liu, Z., Dillon, L., El-Naggar, A. K., Spitz, M. R., Schiller, J. T., Wei, Q., and Sturgis, E. M. Human papillomavirus type 16 infection and squamous cell carcinoma of the head and neck in never-smokers: a matched pair analysis. Clin Cancer Res 2003; 9:2620-2626.
6. Sturgis, E. M. and Wei, Q. Genetic susceptibility--molecular epidemiology of head and neck cancer. Curr Opin Oncol 2002;14:310-317.
7. Sancar A, Lindsey-Boltz LA, Unsal-Kacmaz K, Linn S. Molecular mechanisms of mammalian DNA repair and the DNA damage checkpoints. Annu Rev Biochem 2004;73:39-85.
8. Friedberg EC. How nucleotide excision repair protects against cancer. Nat Rev Cancer 2001;1:22-33.
9. Kraemer KH, Lee MM, Andrew AD, et al. The role of sunlight and DNA repair in melanoma and nonmelanoma skin cancer. Arch Dermatol 1994;130:1018-1021.
10. Cheng L, Eicher SA, Guo Z, Hong WK, Spitz MR, Wei Q. Reduced DNA repair capacity in head and neck cancer patients. Cancer Epidemiol Biomarkers Prev 1998;7:465-8.
11. Cheng L, Sturgis EM, Eicher SA, Spitz MR, Wei Q. Expression of nucleotide excision repair genes and the risk for squamous cell carcinoma of the head and neck. Cancer 2002;94:393-7.

12. Wei Q, Cheng L, Amos CI, Wang LE, Guo Z, Hong WK, Spitz MR. Repair of tobacco carcinogen-induced DNA adducts and lung cancer risk: a molecular epidemiologic study. J Natl Cancer Inst 2000;92:1764-72.

13. Cheng L, Wang LE, Spitz MR, Wei Q. Cryopreserving whole blood for functional assays using viable lymphocytes in molecular epidemiology studies. Cancer Lett 2001;166:155-63.

14. Athas AF, Hedayati M, Matanoski GM, Farmer ER, Grossman L. Development and field-test validation of an assay for DNA repair in circulating human lymphocytes. Cancer Res 1991;51:5786-93.

15. Barret J M, Calsou P, Salles B. Deficient nucleotide excision repair activity in protein extracts from normal human lymphocytes. Carcinogenesis 1995;16:1611-16.

16. Shivji MKK, Kenny MK, Wood R. Proliferating cell nuclear antigen is required for DNA excision repair. Cell 1992;69:367-74.

17. Cutler P. Protein arrays: the current state-of-the-art. Proteomics 2003;3:3-18.

Table 1. Demographic factors and exposures for SCCHN case and control subjects

Variable	Cases (No. = 57)		Controls (No. = 63)		*P* value[a]
	No.	%	No.	%	
Age					
≤ 55	24	42.1	25	39.7	
> 55	33	57.9	38	60.3	0.787
Sex					
Male	43	75.4	39	61.9	
Female	14	24.6	24	38.1	0.112
Ethnic group					
African-American	3	5.3	3	4.8	
Mexican-American	3	5.3	4	6.4	
Non-Hispanic white	51	89.5	56	88.9	0.962
Smoking status					
Yes	42	73.7	31	49.2	
No	15	26.3	32	50.8	0.006
Alcohol use					
Yes	43	75.4	33	52.4	
No	14	24.6	30	47.6	0.009

[a] Two-sided χ^2 test.

Table 2. Relative protein expression of nucleotide excision repair genes in SCCHN cases and controls

	No [a]	Mean ± SD [b]		Difference (%)	*P* value [c]
		Cases	Controls		
Age (years)	57/63	56.2 ± 9.7	57.2 ± 9.5		0.418
Storage time	57/63	17.7 ± 11.7	13.2 ± 6.8		0.013
Relative expression (%)[d]					
ERCC1	53/58	1.369 ± 0.401	1.696 ± 0.539	-19.3	<0.001
XPA	53/61	0.363 ± 0.111	0.424 ± 0.160	-14.4	0.017
XPC	54/62	1.326 ± 0.650	1.770 ± 0.923	- 25.1	0.003
XPD	52/59	0.947 ± 0.343	1.137 ± 0.584	- 19.0	0.037
XPF	56/62	0.966 ± 0.438	1.297 ± 0.764	- 25.5	0.004
XPG	55/60	1.206 ± 0.453	1.432 ± 0.628	- 15.8	0.028

[a] No: number of cases/controls.
[b] SD: standard deviation.
[c] Two-sided Student *t* test.
[d] The expression level relative to that of β-actin.

Table 3. Estimation of Risk (OR and 95% CI) for SCCHN associated with protein expression levels of nucleotide excision repair gene

Expression level [a]		Cases		Controls		Crude odds ratio (95% CI [b])	Adjusted odds ratio [c] (95% CI [b])	Mutivariate odds ratio [d] (95% CI [b])
		No.	%	No.	%			
ERCC1	High	17	32.1	29	50.0			
	Low	36	67.9	29	50.0	2.12 (0.98-4.59)	2.18 (0.91-5.24)	0.78 (0.21-2.85)
XPA	High	15	28.3	30	49.2			
	Low	38	71.7	31	50.8	2.45 (1.12-5.35)	2.99 (1.22-7.47)	2.01 (0.57-7.14)
XPC	High	13	24.1	31	50.0			
	Low	41	75.9	31	50.0	3.15 (1.42-7.01)	2.46 (1.04-5.87)	1.17 (0.31-4.41)
XPD	High	15	28.9	29	49.2			
	Low	37	71.1	30	50.8	2.38 (1.09-5.24)	3.02 (1.18-7.76)	1.88 (0.50-7.01)
XPF	High	13	23.2	31	50.0			
	Low	43	76.8	31	50.0	3.31 (1.49-7.33)	5.29 (2.01-13.9)	11.5 (2.32-56.6)
XPG	High	18	32.7	30	50.0			
	Low	37	67.3	30	50.0	2.06 (0.96-4.38)	1.56 (0.79-3.92)	0.48 (0.13-1.74)

[a] Dichotomized based on the median value of control subjects.
[b] CI: confidence interval.
[c] Obtained from the logistic regression model with adjustment for age, sex, race, smoking status, alcohol use and storage time.
[d] Obtained from the logistic regression model with adjustment for age, sex, race, smoking status, alcohol use, storage time and other genes.

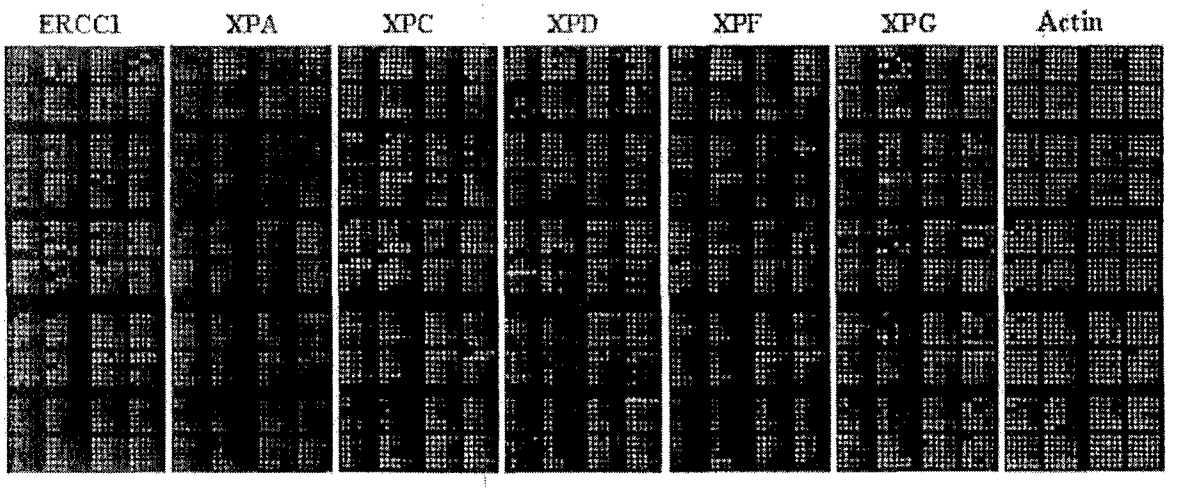


Figure 1. Protein microarrays fabricated using proteins extracted from activated peripheral T lymphocytes. Three dilutions were used for each sample in duplicate. Specific antibodies were used to detect levels of the corresponding proteins. The names of the proteins were shown on top of each microarray.

THE UNIVERSITY OF TEXAS
MD ANDERSON
CANCER CENTER

Department of Epidemiology - 189
Tel. (713) 792-3020

December 3, 2004

Dr. Frank J. Rauscher, III
Editor-in-Chief
CANCER RESEARCH Editorial Office
615 Chestnut St. 7th Floor
Philadelphia, PA, 19106

Dear Dr. Rauscher:

We are submitting an original article entitled "**Lymphocytic Expression of Nucleotide Excision Repair (NER) Proteins as a Marker for Cancer Susceptibility: A Pilot of Study of Squamous Cell Carcinoma of the Head and Neck**" to be considered for publication in the Advances of Brief in *Cancer Research.*

This article describes a molecular epidemiological case-control study of NER protein levels by a reverse-phase protein microarray in cultured lymphocytes transfected with damaged plasimids in 57 patients with newly diagnosed squamous cell carcinoma of head and neck (SCCHN) and 63 cancer-free controls. We found that in 63 controls, the relative expression levels of the six core NER proteins were highly correlated ($P < 0.001$ for all). Compared with the controls, the cases had lower expression levels of all the NER proteins, particularly XPC and XPF, which had a greater than 25% reduction ($P < 0.01$). When we used the median expression levels of the NER proteins as the cut-off value, significantly increased risk of SCCHN was associated with low expression levels of XPA (odds ratio (OR) = 2.99; 95% confidence interval (CI) = 1.22-7.47), XPC (OR = 2.46; 95% CI=1.04-5.87), XPD (OR = 3.03; 95% CI=1.18-7.76) and XPF (OR = 5.29; 95% CI = 2.01-13.9) but not ERCC1 and XPG after adjustment for age, sex, ethnicity, smoking and alcohol use. When a multivariate logistic regression model included all NER proteins, only low expression level of XPF remained as a significant predictor for the risk of SCCHN (OR = 11.5; 95% CI = 2.32-56.6). These results suggest that this protein microarray assay may provide a useful tool for measuring protein markers for susceptibility to cancer.

This manuscript has not been submitted to other journals for publication and has been reviewed and approved by all the authors. Please forward all comments to me at the address shown above. Thank you for your consideration.

Sincerely,

Qingyi Wei, M.D., Ph.D.
Professor of Epidemiology

Enclosures

Enhanced Growth Inhibition and Apoptosis Induction in NSCLC Cell Lines by Combination of Celecoxib and 4HPR at Clinically Relevant Concentrations

Shi-Yong Sun[1], Claudia P. Schroeder,Ping Yue, Dafna Lotan, Waun K. Hong, Reuben Lotan[2]

Department of Thoracic, Head and Neck Medical Oncology, The University of Texas M. D. Anderson Cancer Center, Houston, Texas 77030, USA.

[1]Present address:
Shi-Yong Sun, Winship Cancer Institute, Emory University. School of Medicine, 1365-C Clifton Road, Clinical Building C3088, Atlanta, GA 30322 USA. Tel: 404.778.2170; Fax: 404.778.5520; Email: shi-yong_sun@emoryhealthcare.org

[2]Correspondance to:
Reuben Lotan, University of Texas M. D. Anderson Cancer Center, 1515 Holcombe Blvd Box 432, Houston, TX 77030, USA. Tel: 713.792.8467; Fax: 713.745.5656; Email: rlotan@mdanderson.org or Dr. SY Sun as mentioned above.

RUNNING TITLE

INDUCTION OF APOPTOSIS BY CELECOXIB AND 4HPR

KEY WORDS

celecoxib, COX-2, fenretinide, 4HPR, growth inhibition, lung cancer cell lines

ACKNOWLEDGEMENTS

This study was supported by United States Public Health Service Grant PO1 CA98144 from the National Cancer Institute and by grant DAMD17-01-1-0689 from the Department of Defense. C.P. Schroeder was supported by a fellowship from the Deutsche Forschungsgemeinschaft (DFG, Germany). W. K. Hong is an American Cancer Society Clinical Research Professor. R. Lotan is the incumbent of the Irving and Nadine Mansfield and Robert David Levitt Cancer Research Chair.

ABBREVIATIONS

BHA	butylated hydroxyanisole
COX	cyclooxygenase
DMEM	Dulbecco's Modified Eagle's Minimal Essential Medium
DMSO	dimethyl sulfoxide
FBS	fetal bovine serum

FDA	U.S. Food and Drug Administration
4HPR	N-(4-hydroxyphenyl)retinamide
NAC	N-acetyl cysteine
NSAIDs	nonsteroidal anti-inflammatory drugs
NSCLC	non-small cell lung cancer
PARP	poly-(ADP-ribose) polymerase
PBS	phosphate-buffered saline
SRB	sulforhodamine B
TUNEL	terminal deoxynucleotidyl transferase-mediated nick end labeling

ABSTRACT

Celecoxib exhibits cancer preventive and therapeutic effects in animal models and clinical trials. It presumably acts through selective inhibition of cyclooxygenase-2 (COX-2) and subsequent reduction of prostaglandin (PG) synthesis. However, the concentrations of celecoxib required for growth inhibition and apoptosis induction in vitro are higher than those needed for suppression of PGs. Moreover, those concentrations are not achievable in humans raising a controversy regarding the clinical relevance of in vitro data. We investigated the activity of celecoxib alone and in combination with the pro-apoptotic retinoid *N*-(4-hydroxyphenyl)retinamide (4HPR) on growth and apoptosis of human non-small cell lung cancer (NSCLC) cell lines. Celecoxib inhibited growth of thirteen NSCLC cell lines with IC_{50} values ranging from 19 to 33 μM regardless of their COX-2 expression. Apoptosis was induced in cells with high (A549) as well as low (H1792) COX-2 levels but only at a concentration of 75 μM celecoxib. However, treatment with pharmacologically feasible concentrations of celecoxib (≤ 10 μM) in combination with 4HPR (≤ 2 μM) resulted in a marked suppression of NSCLC cell growth and colony formation. Apoptosis mediated by activation of caspase-3, cleavage of PARP and lamin A was suppressed by addition of antioxidants, suggesting that the generation of reactive oxygen species was partially involved. This study indicates, that celecoxib combined with 4HPR is more effective than treatment with either agent alone in inhibition of growth and induction of apoptosis in NSCLC cells. It suggests further investigations of this combination for lung cancer treatment.

INTRODUCTION

Lung cancer remains the leading cause of cancer mortality among both men and women in the United States. It has been estimated that 173,770 new cases and 160,440 deaths in 2004 will be attributed to lung cancer.[1] Unfortunately, the severe morbidity of lung cancer and the poor 5-year survival rate of approximately 15% have not been improved substantially by current treatment protocols during the last decade. Therefore, intense efforts are being mounted to find new agents and combinations for treatment and prevention of human lung cancer that may lead to the improvement in patients outcome. Nonsteroidal anti-inflammatory drugs (NSAIDs), such as the selective COX-2 inhibitor celecoxib, have gained much attention for their potential use as anticancer agents.[2,3]

The cyclooxygenase (COX) enzymes are responsible for the metabolic conversion of arachidonic acid to prostaglandins (PGs), which play a key role in diverse biological functions involving inflammation, immunological response, and development.[4] Several isoforms of COXs have been identified, which differ in their expression pattern and functions.[5] COX-1 is constitutively expressed in most human tissues and important for the maintenance of homeostatic functions. In contrast, COX-2 is inducible during pathological conditions such as inflammation and cancer in response to growth factors, mutagens, and cytokines. In fact, the up-regulation of COX-2 has been shown to promote cell growth, inhibit apoptosis, and enhance cell motility and angiogenesis in tumor tissues.[6-8] Lines of evidence have demonstrated that COX-2 is induced at almost all stages of non-small cell human lung cancer (NSCLC) progression relative to adjacent normal bronchial epithelial tissue.[9-11] Interestingly, among patients with stage I NSCLC, COX-2 overexpression was associated with a poor prognosis and a positive expression of RAR-β in their tumors as well.[12]

The selective COX-2 inhibitor celecoxib (celebrex®) has been approved by the FDA for treatment of rheumatoid arthritis and osteoarthritis in adults and for adjuvant treatment of patients with familial adenomatous polyposis.[13] It has been demonstrated, that celecoxib dose-dependently suppressed tumor growth, lung metastasis and angiogenesis in mice.[7,14-16] The ability of celecoxib to induce apoptosis has been confirmed in various types of cancer cells including lung but only at concentrations that exceeded maximum plasma level in humans ranging from 3.2 to 5.6 μM after administration of a single daily dose of 800 mg celecoxib.[15,17-19] Thus, a controversy has been raised concerning its presumed anti-tumor mechanisms.[14,20] Specifically, the concentrations of celecoxib needed to inhibit cell cycle progression and induce apoptosis in cancer cells are typically 10 to 100-fold higher than those required for suppression of PG synthesis.[15,21] Furthermore, significant anti-tumor effects have been observed in cancer cells irrespective of their COX-2 expression, suggesting that celecoxib may exert in part and/or cell type-specific therapeutic activity via pathways that are independent of selective inhibition of COX-2.[14,15,17-22] As a matter of fact, this assumption is not solely related to celecoxib as such discrepancy between high concentrations needed for anti-proliferative and pro-apoptotic effects compared to plasma levels which can be achieved in vivo have been reported for other NSAIDs.[15,22,23]

Interestingly, several reports have indicated that celecoxib interacts in additive and synergistic manners with conventional therapeutic regimens in patients with NSCLC.[3,24,25] In addition, various NSAIDs produced synergistic activity in combination with 13-*cis*-retinoic acid in NSCLC cell lines regardless of drug-resistance phenotype.[26] For the present study, we chose to evaluate the synthetic retinoid *N*-(4-hydroxyphenyl)retinamide (4HPR, fenretinide) in combination with celecoxib because it has been well established to exert potent pro-apoptotic effects on a variety of cancer

cells[27-30] and exhibits lower side effects compared to other retinoids in therapeutic and chemopreventive clinical trials including studies on NSCLC.[31-34]

Our results indicate, that celecoxib in combination with 4HPR exerted enhanced growth inhibitory and apoptosis-inducing effects in NSCLC cells at concentrations that are clinically relevant in humans. Thus, it may be useful in designing novel combination-therapeutic strategies for human lung cancer.

MATERIALS AND METHODS

Reagents. Dulbecco's Modified Eagle's Minimal Essential Medium (DMEM), penicillin, streptomycin, phosphate-buffered saline (PBS) and trypsin were purchased from Gibco™ Invitrogen Corporation (Carlsbad, CA). Fetal bovine serum (FBS) was from HyClone Laboratories, Inc. (Logan, UT) and celecoxib (celebrex®, 4-[5-(4-methylphenyl)-3-(trifluoromethyl)-1H-pyrazol-1-] benzene-sulfonamide) was obtained from GD Searle & Co (Chicago, IL). Dimethyl sulfoxide (DMSO), ethylene diamine tetra-acetic acid (EDTA), N-acetyl cystein (NAC), butylated hydroxyanisol (BHA), and sodium dodecyl sulfate (SDS) were purchased from Sigma Chemical Co. (St. Louis, MO).

Human NSCLC Cell Lines. The NSCLC cell lines H460, H292, A549, H157, H1299, H358, and H1792 were either obtained from Dr. A. Gadzar (The University of Texas Southwestern Medical Center, Dallas, TX) or purchased from the American Type Culture Collection (ATCC; Rockville, MD). These cells were grown in monolayer cultures in a mixture of DMEM/Ham's F12 medium (1:1, v/v) supplemented with 5% FBS at 37°C in a humidified atmosphere consisting of 5% CO_2 and 95% air. Celecoxib was dissolved in DMSO at a concentration of 0.05 M and stored at -80°C. 4HPR obtained from Dr. R. Lubet (National Cancer Institute, Bethesda, MD) was dissolved in DMSO at a concentration of 0.01 M and stored in the dark at -80°C. Stock solutions were diluted to desired concentrations with culture medium prior to use keeping the final concentration of DMSO less than 0.1%.

Growth Inhibition Assay. NSCLC cells were seeded in 96-well culture plates (BD Bioscience Labware, Bedford, MA), allowed to adhere overnight and treated with either celecoxib, 4HPR and their combinations in 5% FBS-containing medium for 3 days before estimation of cell number by sulforhodamine B (SRB) assay.[35] The absorbance was measured using an automated plate reader MR5000 (Dynatech Laboratories Inc., Chantilly, VA). The inhibition of cell growth was calculated from the equation, % inhibition = (1-A*t*/A*c*) x 100%, whereas A*t* and A*c* represent absorbencies of treated and control cultures, respectively. Concentration response curves were plotted and levels of celecoxib resulting in 50% growth inhibition (IC_{50}) were estimated. The results represent mean ± standard deviation (SD) of three independent experiments.

Colony Formation. Exponentially growing H292 cells were seeded in 6-well culture plates (Greiner Bio-One, Inc., Longwood, FL) and allowed to grow overnight before treatment with either celecoxib, 4HPR and their combinations. The culture medium was replaced with fresh medium containing the compounds every 3 days. After 14 days of incubation, the colonies were stained with crystal violet (0.5%) and examined under a microscope.

TUNEL Apoptosis Assay. Intranucleosomal DNA fragmentation was evaluated using an apoptosis detection kit (Phoenix Flow Systems, Inc., San Diego, CA) based on the TUNEL technique.[36] The reaction labels the 3'hydroxyl termini of DNA fragmented during apoptosis with fluorescein-isothiocyanate-conjugated dUTP. After treatment, the cells were harvested by trypsinization, pelleted by centrifugation, fixed with ice-cold ethanol (70%, v/v) and stained according to the protocol provided by the manufacturer. Cytofluorometric determinations and data analysis were performed on a Coulter XL flow cytometer (Coulter Corp., Miami, FL). Approximately 10,000 cells were evaluated for each sample.

Western Blot Analysis. Samples containing 50 µg of total cellular protein were electrophoretically separated through 10% sodium dodecyl sulfate (SDS)-polyacrylamide gels followed by transfer onto Hybond-ECL membranes (Amersham, Arlington Heights,

IL) as described previously.[20] After blocking with PBS containing 0.1% Tween 20 and 5% low-fat milk, the membranes were incubated with primary antibodies for COX-2 (Oxford Biomedical Research Inc., Oxford, MI), caspase-3 (clone 31A1067, Imgenex, San Diego, CA), PARP and lamin A (Cell Signaling Technology Inc., Beverly, MA), or β-actin (Sigma Chemical Co., St. Louis, MO) at appropriate dilutions. Antibody binding was detected with horseradish peroxidase-linked second antibody and enhanced chemiluminescence (Amersham Biosciences Corp., Piscataway, NJ).

RESULTS

Celecoxib Inhibits Growth of Human NSCLC cells independent of COX-2. To investigate, whether the sensitivity of several human NSCLC cell lines to celecoxib was associated with the target enzyme expression, we analyzed their constitutive COX-2 levels by Western immunoblotting. Figure 1 indicates, that A549, H358, and H292, H1944, and SK-MES-1 cells expressed COX-2 protein, whereas low or undetectable levels were found in other NSCLC cell lines examined. Apparently, some of the cell extracts exhibit a doublet of protein bands as a result of changes in the extent of COX-2 glycosylation. We then determined the concentration of celecoxib causing 50% growth inhibition (IC_{50}) from the dose-response curves of each cell line after 3 days of incubation. The IC_{50} values were in a range between 19 and 33 μM celecoxib (Fig. 1). However, NSCLC cell lines that expressed COX-2 exhibited similar sensitivity as cell lines with low or undetectable COX-2 levels.

Celecoxib Induces Apoptosis of Human NSCLC cells independent of COX-2. To study whether growth inhibition of NSCLC cells by celecoxib resulted from induction of apoptosis, we examined apoptotic events by the TUNEL method after treatment of H1792 (low COX-2 level), and A549 (high COX-2 level) cells with various concentrations of celecoxib. We observed no substantial induction of apoptosis with concentrations up to 50 μM celecoxib in both, COX-2 positive and COX-2 negative, NSCLC cell lines (Fig. 2). However, treatment with 75 μM celecoxib markedly increased the percentage of TUNEL-positive cells from less than 1% in control cultures to 60% in H1792 and 77% in A549 cells, respectively. Similarly to our findings on growth inhibition, the effects of celecoxib on induction of apoptosis appeared independent of COX-2 expression.

Celecoxib in Combination with 4HPR is More Potent in Growth Inhibition than Treatment with Either Agent Alone. Because the plasma levels of celecoxib feasible in humans are considerably lower than the concentrations found to be effective in vitro, we hypothesized that combinations of low doses of celecoxib with the pro-apoptotic retinoid 4HPR will be more potent in growth inhibition than each agent alone. To test this hypothesis, we treated A549, H1792, and H292 cell lines with celecoxib and 4HPR for 3 days. As shown in Figure 3, simultaneous treatment of celecoxib with 4HPR resulted in additive suppression of cell growth in a dose-dependent manner (Fig. 3A,B). However, the effects of various concentrations of 4HPR in addition to 10 μM celecoxib were less profound in H1792 cells than in the other two NSCLC cell lines (Fig. 3B).

The Celecoxib/4HPR Combination Reduces Colony Formation. Due to the modest effects of the celecoxib/4HPR combination on cell growth in monolayer culture, we asked whether colony formation, which allows a relatively longer treatment of tumor cells, would show greater activity. Thus, we estimated the effects of celecoxib and/or 4HPR on the ability of H292 cells to form colonies after 14 days of incubation. Celecoxib at 5 or 10 μM showed no discernible changes, while 4HPR was able to reduce the formation of H292 colonies in a dose-dependent manner (Fig. 4A,B). However, simultaneous treatment suppressed colony formation to a larger extent than 4HPR alone as illustrated in the photomicrographs (Fig. 4A).

Celecoxib in Combination with 4HPR is More Potent in Apoptosis Induction than Treatment with Either Agent Alone. To determine whether enhanced growth inhibition by celecoxib/4HPR combination resulted from induction of apoptosis, we compared apoptotic NSCLC cells incubated with either combinations or single treatment of the two agents. Celecoxib alone had no effect on induction of apoptosis up to a tested concentration of 20 μM, whereas treatment with 2 μM 4HPR resulted in 26% apoptosis.

In contrast, the combination of both agents exhibited more than 50% apoptotic cells (Fig. 5A,B).

Apoptosis Induced by Celecoxib/4HPR is Mediated by Caspase-3 Cascade and Suppressed by Antioxidants. To begin to understand the mechanism of the induction of apoptosis, we analyzed the effects of celecoxib and/or 4HPR on caspase-3 cascade. Western blot analysis revealed that combinations of 5 and 10 μM celecoxib, respectively with 2 μM 4HPR resulted in a greater activation of caspase-3 and cleavage of its substrates PARP and lamin A compared to each of the agents alone. In fact, celecoxib alone was inactive whereas 4HPR partially activated caspase-3 and cleavage of PARP and lamin A (Fig. 6A). According to studies, which have demonstrated that apoptosis induced by 4HPR can be suppressed by addition of antioxidants, we examined the effects of butylated hydroxyanisole (BHA) and N-acetyl cysteine (NAC) on apoptosis as well as cleavage of PARP and lamin A in NSCLC cells. Incubation of H1792 cells with 5 μM celecoxib in addition to 50 μM BHA or 5 mM NAC had no effect on apoptosis induction. However, treatment with 2 μM 4HPR alone compared to simultaneous incubation with 5 μM celecoxib increased the percentage of TUNEL-positive cells from 23% to 52%. Likewise, cleavage of the caspase-3 substrates PARP and lamin A was obtained after simultaneous incubation with celecoxib and 4HPR but partially prevented by co-treatment with the antioxidants BHA and NAC (Fig. 6B).

DISCUSSION

This in vitro study highlights the enhanced growth-inhibitory and apoptosis-inducing effects of celecoxib in combination with 4HPR at clinically relevant concentrations compared to single agent treatment alone in NSCLC cell lines. We have demonstrated that all NSCLC cell lines used in this study were susceptible to the growth-inhibitory activity of celecoxib with comparable IC_{50} values ranging from 19 to 33 μM. However, these effects appeared to be independent of COX-2 expression based on the fact that NSCLC cell lines exhibited variable levels of COX-2 protein ranging from high to very low. Moreover, the celecoxib concentrations required for growth inhibition were considerably higher than those required for suppression of COX-2 activity because we and others have shown that as little as 0.1 μM celecoxib was able to reduce PGE_2 levels in various tumor cell lines including lung cells.[3,17,21] In addition, our data indicate that induction of apoptosis by celecoxib concentration of ≥75 μM regardless of the COX-2 level in NSCLC cells. These findings are in agreement with studies reported by other investigators, which have demonstrated COX-2-independent responses to high doses of celecoxib in various types of cancer cell lines.[15,18,21] Noticeably, in vivo studies revealed significant suppression in tumor growth of COX-2-deficient colorectal cancer xenografts after treatment with celecoxib.[14,15] Recent reports highlighted several COX-2-independent mechanisms including activation of phosphatidylinositol 3-kinase (PI3K)/Akt,[8,19] modulation of NF-κB-dependent gene transcription[17] and peroxisome proliferator-activated receptors (PPARs)[37], alterations of cell-cycle regulatory proteins,[15] and induction of death receptor expression.[22] However, the discrepancy between using high concentrations of celecoxib to obtain apoptosis-inducing effects in cell culture (25 to 100 μM) and those pharmacologically achievable in humans raises questions regarding the clinical relevance of most of the in vitro data.[14,16,17] In fact, pharmacokinetic studies performed in humans revealed that plasma levels did not exceed 5.6 μM in individuals receiving up to 800 mg celecoxib per day.[17,36] At this low concentration, celecoxib neither inhibited cell growth nor induced apoptosis in any cancer cell line tested in vitro.[14,15,17,22] Consequently, we postulated that celecoxib's anti-cancer activity can be potentiated by combination with other pro-apoptotic agents.

We have selected the synthetic retinoid 4HPR as a partner for combination with celecoxib because this retinoid has been shown to induce apoptosis in several types of malignant cells including lung cancer cell lines.[27-30] In addition, it has been tested in several clinical trials for cancer chemoprevention and therapy with a favorable toxicity profile as compared with other retinoids.[31-34] For example, a very recent phase II study has demonstrated that the mean plasma concentration of 4HPR was 3.1 ± 0.7 μM in adults with recurrent gliomas given 900 mg/m^2 4HPR orally twice daily. This regimen was well tolerated.[34] In comparison, the clinical use of all-*trans*-retinoic acid is associated with the development of a potentially lethal syndrome when reaching peak plasma levels of 1 μM.[31] Moreover, combining celecoxib with retinoids has been previously suggested as protocol for preventing cancers of the upper aerodigestive tract.[2]

Here, we demonstrate that combinations of clinically achievable plasma levels but suboptimal in vitro-concentrations of celecoxib (2.5 to 10 μM) with 4HPR (0.5 to 3.0 μM) resulted in additive growth inhibition, induction of apoptosis and a more than additive suppression of colony formation in NSCLC cell lines. The mechanism of the interaction between celecoxib and 4HPR that results in potentiation of their effects on apoptosis remains to be elucidated fully. In this study, we have begun to understand some aspects of this mechanism. We found that the induction of apoptosis by the celecoxib/4HPR combination was mediated by activation of caspase-3 and cleavage of its substrates PARP and lamin A. Because as a single agent, 4HPR has been shown to

induce apoptosis by increasing endogenous ceramide levels and mitochondrial reactive oxygen species (ROS)[27-30] we asked whether ROS generation may also be important in the action of the celecoxib/4HPR combination. Indeed, we found that antioxidants blocked the celecoxib/4HPR-induced apoptosis implicating ROS in their effect. Clearly, additional investigations are needed to fully elucidate the molecular mechanisms underlying the increased efficacy of the combination of these agents. Nonetheless, our demonstration of the more than additive effects of the celecoxib 4HPR combination at pharmacologically achievable concentrations warrants further testing of this regimen in in vivo models and potentially also in clinical trials.

References

1. Surveillance Research. Lung and bronchus. In: Cancer Facts & Figures 2004. American Cancer Society, Atlanta, GA, USA 2004, No:5008-04.
2. Mestre JR, Chan G, Zhang F, Yang EK, Sacks PG, Boyle JO et al. Inhibition of cyclooxygenase-2 expression. An approach to preventing head and neck cancer. Ann N Y Acad Sci 1999; 889:62-71.
3. Sandler AB, Dubinett SM. COX-2 inhibition and lung cancer. Semin Oncol 2004; 31 (suppl 7):45-52.
4. Williams CS, Mann M, Du Bois RN. The role of cyclooxygenases in inflammation, cancer, and development. Oncogene 1999; 18:7908-7916.
5. Cao Y, Prescott SM. Many actions of cyclooxygenase-2 in cellular dynamics and in cancer. J Cell Physiol 2002; 190:279-286.
6. Tsujii M, Du Bois RN. Alterations in cellular adhesion and apoptosis in epithelial cells overexpressing prostaglandin endoperoxide synthase-2. Cell 1995; 83:493-501.
7. Masferrer JL, Leahy KM, Koki AT, Zweifel BS, Settle SL, Woerner BM, et al. Antiangiogenic and antitumor activities of cyclooxygenase-2 inhibitors. Cancer Res 2000; 60:1306-1311.
8. Lin MT, Lee RC, Yang PC, Ho FM, Kuo ML: Cyclooxygenase-2 inducing mcl-1 dependent survival mechanism in human lung adenocarcinoma cells. J Biol Chem 2001; 276:48997-49002.
9. Hida T, Yatabe Y, Achiwa H, Muramatsu H, Kozaki K, Nakamura S, et al. Increased expression of cyclooxygenase 2 occurs frequently in human lung cancers, specifically in adenocarcinomas. Cancer Res 1998; 58:3761-3764.
10. Hosomi Y, Yokose T, Hirose Y, Nakajima R, Nagai K, Nishiwaki Y, et al. Increased cyclooxygenase 2 (COX-2) expression occurs frequently in precursor lesions of human adenocarcinoma of the lung. Lung Cancer 2000; 30:73-81.
11. Riedl K, Krysan K, Põld M, Dalwadi H, Heuze-Vourc'h N, Dohadwala M, et al. Multifaceted roles of cyclooxygenase-2 in lung cancer. Drug Resist Updat 2004; 7:169-184.
12. Khuri FR, Wu H, Lee JJ, Kemp BL, Lotan R, Lippman SM, et al. Cyclooxygenase-2 overexpression is a marker of poor prognosis in stage I non-small cell lung cancer. Clin Cancer Res 2001; 7:861-867.
13. Steinbach G, Lynch PM, Phillips RK, Wallace MH, Hawk E, Gordon GB, et al. The effect of celecoxib, a cyclooxygenase-2 inhibitor, in familial adenomatous polyposis. N Engl J Med 2000; 342:1946-1952.
14. Williams CS, Watson AJ, Sheng H, Helou R, Shao J, DuBois RN. Celecoxib prevents tumor growth in vivo without toxicity to normal gut: lack of correlation between in vitro and in vivo models. Cancer Res 2000; 60:6045-6051.
15. Groesch S, Tegeder I, Niederberger E, Brautigam L, Geisslinger G. COX-2 independent induction of cell cycle arrest and apoptosis in colon cancer cells by the selective COX-2 inhibitor celecoxib. FASEB J 2001; 15:2742-2744.
16. Zhang S, Lawson KA, Simmons-Menchaca M, Sun LZ, Sanders BG, Kline K. Vitamin E analog α-TEA and celecoxib alone and together reduce human MDA-MB-435-FL-GFP breast cancer burden and metastasis in nude mice. Breast Cancer Res Treat 2004; 87:111-121.
17. Niederberger E, Tegeder I, Vetter G, Schmidtko A, Schmidt H, Euchenhofer C, et al. Celecoxib loses its anti-inflammatory efficacy at high doses through activation of NF-κB. FASEB J 2001; 15:1622-1624.
18. Waskewich C, Blumenthal RD, Li H, Stein R, Goldenberg DM, Burton J. Celecoxib exhibits the greatest potency amongst cyclooxygenase (COX) inhibitors for growth

inhibition of COX-2-negative hematopoietic and epithelial cell lines. Cancer Res 2002, 62:2029-2033.
19. Zhang Z, Lai GH, Sirica AE. Celecoxib-induced apoptosis in rat cholangiocarcinoma cells mediated by akt inactivation and bax translocation. Hepatology 2004, 39:1028-1037.
20. Raz A. Is inhibition of cyclooxygenase required for the anti-tumorigenic effects of nonsteroidal, anti-inflammatory drugs (NSAIDs)? In vitro versus in vivo results and the relevance for the prevention and treatment of cancer. Biochem Pharmacol 2002; 63:343-347.
21. Schroeder CP, Yang P, Newman RA, Lotan R. Eicosanoid metabolism in squamous cell carcinoma cell lines derived from primary and metastatic head and neck cancer and its modulation my celecoxib. Cancer Biol & Ther 2004; 9:29-34.
22. Liu X, Yue P, Zhou Z, Khuri FR, Sun SY. Death receptor regulation and celecoxib-induced apoptosis in human lung cancer cells. J Natl Cancer Inst. 2004; 96:1769-1780.
23. Aggarwal S, Taneja N, Lin L, Orringer MB, Rehemtulla A, Beer DG. Indomethacin-induced apoptosis in esophageal adenocarcinoma cells involves upregulation of bax and translocation of mitochondrial cytochrome c independent of COX-2 expression. Neoplasia 2000; 2: 346-356.
24. Carbone D, Choy H, Csiki I, Dang T, Campbell N, Garcia B, et al. Serum/plasma VEGF level changes with cyclooxygenase-2 (COX-2) inhibition in combined modality therapy in state III non-small cell lung cancer (NSCLC): preliminary results of a phase II trial (THO-0059). Proc Am Soc Clin Oncol 2002; 21:1270.
25. Altorki NK, Keresztes RS, Port JL, Libby DM, Korst RJ, Flieder DB, et al. Celecoxib, a selective cyclooxygenase-2 inhibitor, enhances the response to preoperative paclitaxel and carboplatin in early-stage non-small-cell lung cancer. J Clin Oncol 2003; 21:2645-2650.
26. Soriano AF, Helfrich B, Chan DC, Heasley LE, Bunn PA Jr, Chou TC. Synergistic effects of new chemopreventive agents and conventional cytotoxic agents against human lung cancer cell lines. Cancer Res 1999; 59:6178-6184.
27. Oridate N, Suzuki S, Higuchi M, Mitchell MF, Hong WK, Lotan R. Involvement of reactive oxygen species in N-(4-hydroxyphenyl)retinamide-induced apoptosis in cervical carcinoma cells. J Natl Cancer Inst 1997; 89:1191-1198.
28. Sun SY, Li W, Yue P, Lippman SM, Hong WK, Lotan R. Mediation of N-(4-hydroxyphenyl)retinamide induced apoptosis in human cancer cells by different mechanisms. Cancer Res 1999; 59:2493-2498.
29. Suzuki S, Higuchi M, Proske RJ, Oridate N, Hong WK, Lotan R. Implication of mitochondria-derived reactive oxygen species, cytochrome C and caspase-3 in N-(4-hydroxyphenyl)retinamide-induced apoptosis in cervical carcinoma cells. Oncogene 1999; 18:6380-6387.
30. Hail N Jr, Lotan R. Mitochondrial respiration is uniquely associated with the pro-oxidant and apoptotic effects of N-(4-hydroxyphenyl)retinamide. J Biol Chem 2001; 276:45614-45621.
31. Frankel SR, Eardley A, Lauwers G, Weiss M, Warrell R. The 'retinoic acid syndrome' in acute promyelocytic leukemia. Ann Intern Med 1992; 117:292-296.
32. Lotan R. Retinoids and apoptosis: implications for cancer chemoprevention and therapy. J Natl Cancer Inst 1995; 87:1655-1657.
33. Ulukaya E, Wood EJ. Fenretinide and its relation to cancer. Cancer Treat Rev 1999; 25:229-235.

34. Puduvalli VK, Yung WKA, Hess KR, Kuhn JG, Groves MD, Levin VA et al. Phase II study of fenretinide (NSC 374551) in adults with recurrent malignant gliomas: a north American brain tumor consortium study. J Clin Oncol 2004; 22:4282-4289.
35. Skehan P, Storeng R, Scudiero D, Monks A, McMahon J, Vistica D, et al. New colorimetric cytotoxicity assay for anticancer-drug screening. J Natl Cancer Inst 1990; 82:1107-1112.
36. Li X, Traganos F, Melamed MR, Darzynkiewicz Z. Single-step procedure for labeling DNA strand breaks with fluorescein-or BODIPY-conjugated deoxynucleotides: detection of apoptosis and bromodeoxyuridine incorporation. Cytometry 1995; 20:172-180.
37. Levine L. Stimulated release of arachidonic acid by agonists of the peroxisome proliferator-activated receptor and retinoic acid receptors. Prostaglandins Leukot Essent Fatty Acids. 2001; 65:229-232.
38. Chow SHH, Anavy N, Salazar D, Frank DH, Alberts DS. Determination of celecoxib in human plasma using solid-phase extraction and high-performance liquid chromatography. J Pharm Biomed Anal 2004; 34:167-174.

Figure legends

Figure 1. Expression of COX-2 in human NSCLC cell lines and their relation to growth inhibition by celecoxib as indicated as IC_{50} values (μM) presented under each lane. Cultures of thirteen cell lines were grown to approximately 80% confluence before harvested and separated through 10% SDS-PAGE gel electrophoresis followed by Western immunoblotting as described under Materials and Methods. The effects of celecoxib on NSCLC cell growth were determined using SRB assay[35] after 3 days of incubation.

Figure 2. Effects of celecoxib on induction of apoptosis in NSCLC cell lines. H1792 (low COX-2 level) and A549 (high COX-2 level) cell lines were treated with different concentrations of celecoxib for 24 hours before harvested and subjected to apoptosis detection kit based on the TUNEL technique.[36] The percentages of TUNEL-positive cells are presented inside each histogram.

Figure 3. Effects of different concentrations of celecoxib, 4HPR and their combinations on growth of human A549, H292, and H1792 lung cancer cell lines. NSCLC cells were treated with 4HPR (1 μM) or celecoxib (2.5, 5 or 10 μM) and their combinations for 3 days (A). NSCLC cells were incubated with celecoxib (10 μM), or 4HPR (1, 2 or 3 μM) and their combinations for 3 days (B). Cell numbers were estimated by SRB assay.[35] The data represent mean values (bars, SE) of four replicate wells of one of two independent experiments, which yielded similar results.

Figure 4. Effects of celecoxib and/or 4HPR on colony formation of H292 lung cancer cells. H292 cells were treated with celecoxib (5 or 10 μM) and/or 4HPR (0.5 or 1.0 μM) for 14 days before staining and examination under the microscope as described under Materials and Methods. Colony-forming ability of H292 lung cancer cells was markedly suppressed by combined treatment of celecoxib and 4HPR as compared with each of the single agents or cultures treated with DMSO alone.

Figure 5. Enhanced induction of apoptosis in H1792 lung cancer cells by combinations of celecoxib and 4HPR. The apoptotic events were examined after 48 hours in the presence or absence of the two drugs as single or combination using TUNEL technique.[36] Dual parameter flow cytometric analysis measuring FITC-labeled DNA fragments (*ordinate*) and cellular DNA content (*abscissa*) in H1792 cells (A). Effects of celecoxib in combination with 4HPR on induction of apoptosis represented as percentage TUNEL-positive nuclei (B).

Figure 6. Suppression of apoptosis induced by celecoxib in combination with 4HPR by antioxidants in H1792 cells. Regulation of apoptosis-related proteins by celecoxib and/or 4HPR using Western immunoblot analysis. β-Actin served as loading control (A). Partial suppression of the induction of apoptosis after simultaneous treatment of celecoxib (5 μM) and 4HPR (2 μM) preincubated with 50 μM butylated hydroxyanisole (BHA) or 5 mM N-acetyl cysteine (NAC) for 30 min. The cells were harvested after 24 hours and processed for analysis by TUNEL technique (B) or Western immunoblotting as described under Materials and Methods (C).

Fig. 1

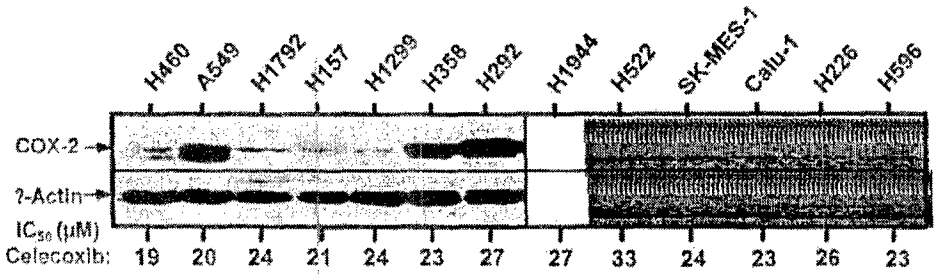

H460
A549
H1792
H157
H1299
H358
H292
H1944
H522
SK-MES-1
Calu-1
H226
H596
COX-2
?-Actin
IC50 (μM)
Celecoxib: 19 20 24 21 24 23 27 27 33 24 23 26 23

Fig. 2

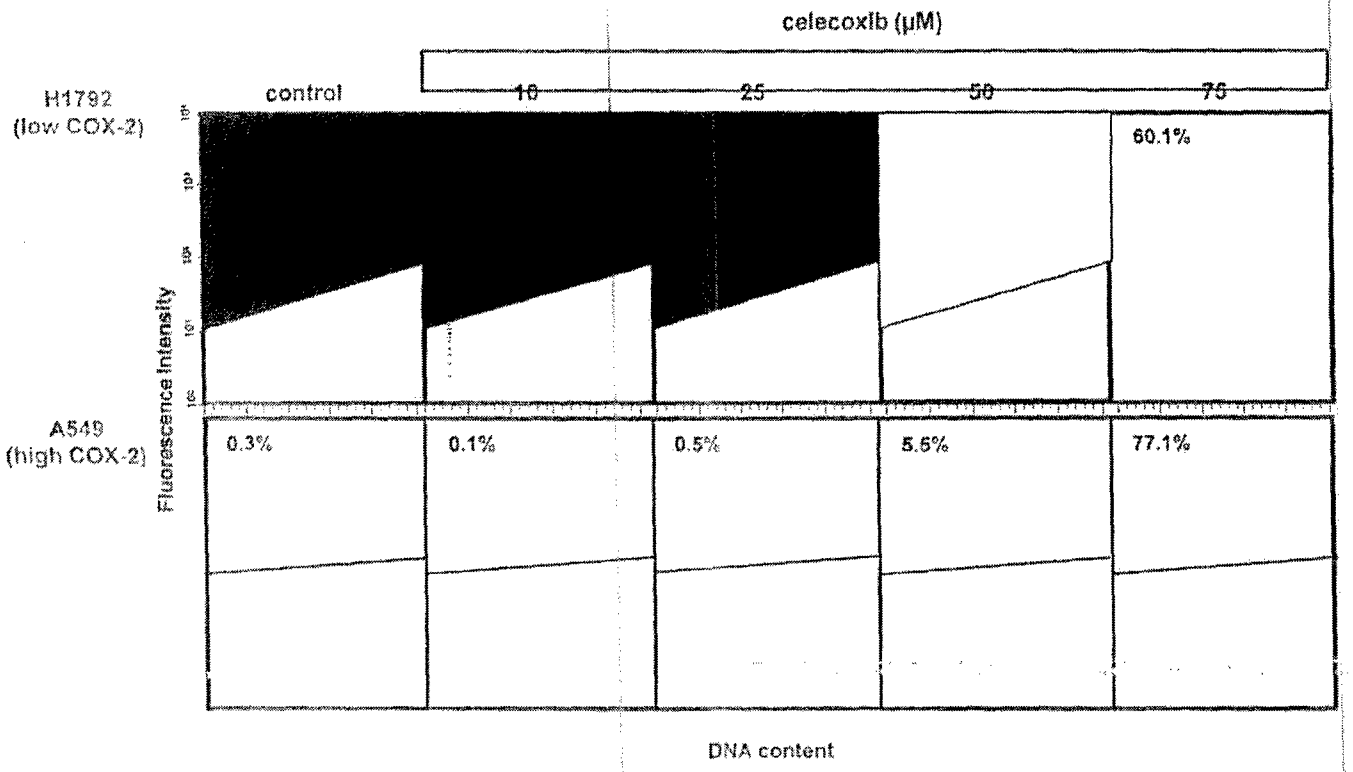

celecoxib (μM)
control
10
25
50
75
H1792
(low COX-2)
60.1%
A549
(high COX-2)
0.3%
0.1%
0.5%
5.6%
77.1%
Fluorescence Intensity
DNA content

Fig. 3

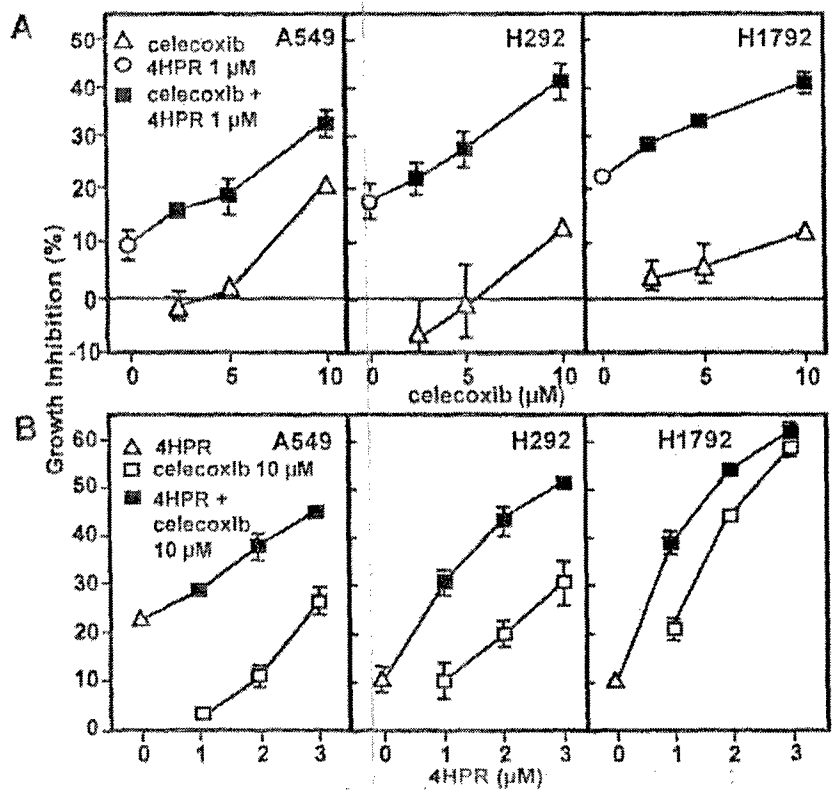

A
B
A549
H292
H1792
celecoxib
4HPR 1 μM
celecoxib + 4HPR 1 μM
4HPR
celecoxib 10 μM
4HPR + celecoxib 10 μM
Growth Inhibition (%)
celecoxib (μM)
4HPR (μM)

Fig. 4

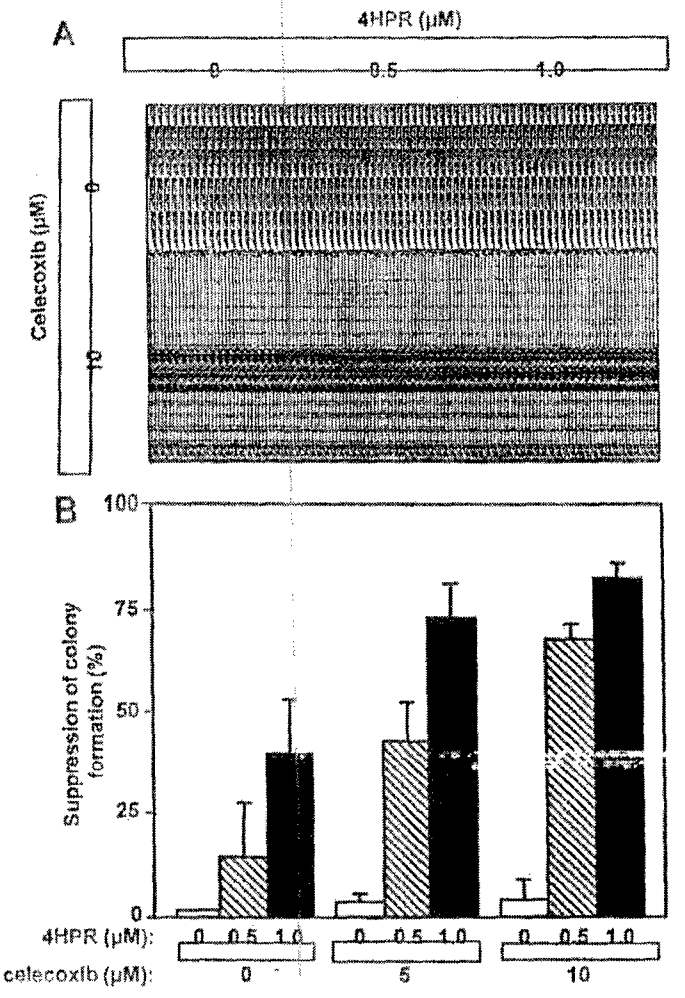

A
4HPR (μM)
0
0.5
1.0
Celecoxib (μM)
0
10
B
100
75
50
25
0
Suppression of colony formation (%)
4HPR (μM):
0 0.5 1.0
0 0.5 1.0
0 0.5 1.0
celecoxib (μM):
0
5
10

Fig. 5

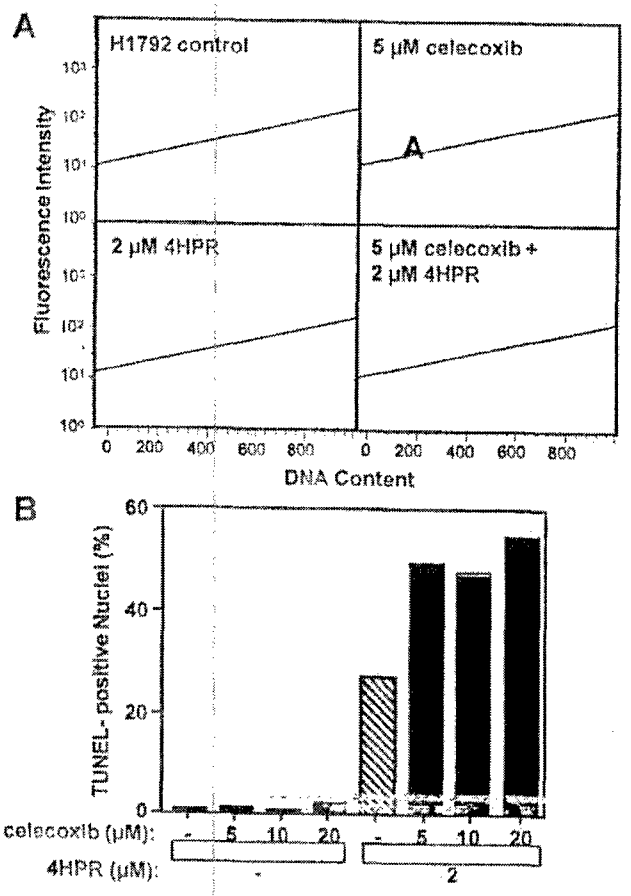
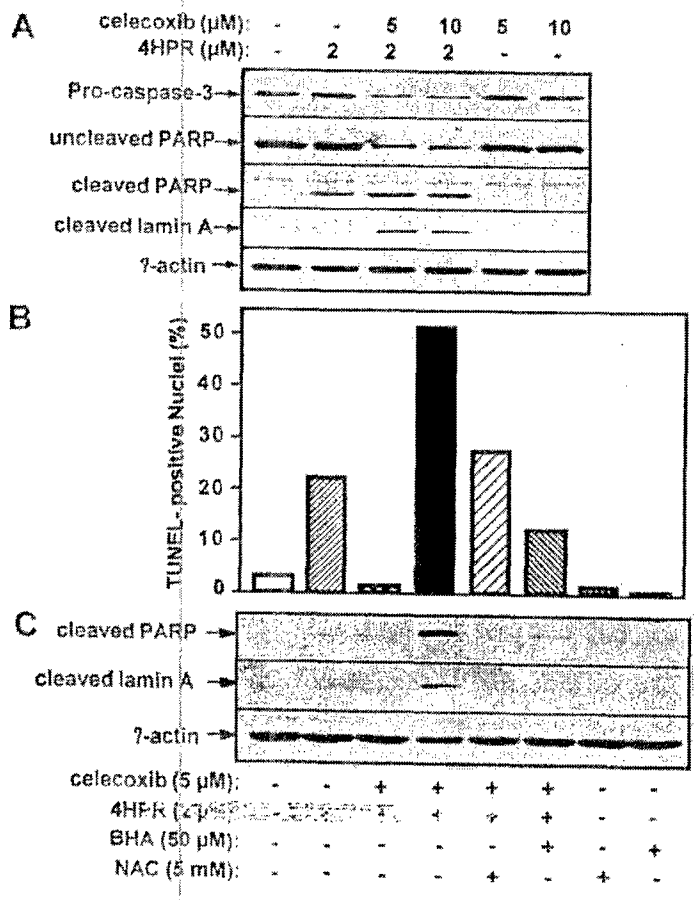

A
H1792 control
5 μM celecoxib
A
2 μM 4HPR
5 μM celecoxib +
2 μM 4HPR
Fluorescence Intensity
DNA Content
B
TUNEL- positive Nuclei (%)
celecoxib (μM):
4HPR (μM):

Fig. 6


A
celecoxib (μM): - - 5 10 5 10
4HPR (μM): - 2 2 2 - -
Pro-caspase-3
uncleaved PARP
cleaved PARP
cleaved lamin A
?-actin
B
TUNEL-positive Nuclei (%)
0
10
20
30
40
50
C
cleaved PARP
cleaved lamin A
?-actin
celecoxib (5 μM): - - + + + + - -
4HPR (2 μM): - - - + + + - -
BHA (50 μM): - - - - - + - +
NAC (5 mM): - - - - + - + -

The synergistic combination of the FT inhibitor Lonafarnib and Paclitaxel enhances tubulin acetylation and requires a functional tubulin deacetylase

Adam I. Marcus, [1] Jun Zhou, [1] Aurora O'Brate, [1], Ernest Hamel, [2] Jason Wong, [3] Michael Nivens, [1] Adel El-Naggar,[4] Tso-Pang Yao,[5] Fadlo R. Khuri, [1]and Paraskevi Giannakakou, [1,6].

[1]Winship Cancer Institute, Emory University School of Medicine, Atlanta, GA 30322

[2]Screening Technologies Branch, Developmental Therapeutic Program, Division of Cancer Treatment and Diagnosis, National Cancer Institute, National Institutes of Health, Frederick, MD 21702

[3] Harvard University, Cambridge, Massachusetts 02138

[4] The University of Texas M. D. Anderson Cancer Center, Houston, TX 77030

[5] Department of Pharmacology and Cancer Biology, Duke University, Durham, NC 27710

[6]To whom correspondence should be addressed: pgianna@emory.edu

Abstract

Farnesyl transferase inhibitors (FTIs) are anti-cancer agents developed to target oncogenic Ras proteins by inhibiting Ras farnesylation. FTIs potently synergize with paclitaxel and other microtubule-stabilizing drugs; however, the mechanistic basis underlying this synergistic interaction remains elusive. Here we show that the FTI, lonafarnib (LNF), affects the microtubule cytoskeleton resulting in microtubule bundle formation, increased microtubule stabilization and acetylation, and suppression of microtubule dynamics. Notably, treatment with the combination of low doses of LNF with paclitaxel markedly enhanced tubulin acetylation (a marker of microtubule stability) as compared to either drug alone. This synergistic effect correlated with farnesyl transferase (FT) inhibition and was accompanied by a synergistic increase in mitotic arrest and cell death. Mechanistically, we show that the combination of LNF and paclitaxel, inhibits the *in vitro* deacetylating activity of the only known tubulin deacetylase, HDAC6. In addition, the LNF/taxane combination is synergistic only in cells lines expressing the wild-type tubulin deacetylase, HDAC6, but not a catalytic-mutant HDAC6, revealing that functional HDAC6 is required for the synergy of LNF with the taxanes. Furthermore, tubacin, a specific HDAC6 inhibitor, synergistically enhanced tubulin acetylation in combination with paclitaxel, similar to the combination of LNF and paclitaxel. Taken together, these data suggest a relationship between FT inhibition, HDAC6 function, and cell death, providing insight into the putative molecular basis of the LNF/taxane synergistic anti-proliferative combination.

Introduction:

Farnesyl transferase inhibitors (FTIs) are a novel class of anti-neoplastic agents that have high anti-tumor activity and are currently in clinical trials (1-3). These agents inhibit the farnesyl transferase (FT) enzyme, whose function is to post-translationally modify proteins by the addition of a 15-carbon farnesyl group. The initial driving force behind FTI development was based on the finding that oncogenic Ras, a low molecular weight GTPase, induces malignant transformation upon the addition of a farnesyl group to its C-terminus by the FTase. This in turn allows it to localize to the plasma membrane and act as a relay switch by transducing biological information from extracellular signals to the nucleus (for review see (4)).

Since Ras farnesylation is required for Ras membrane localization, FTase became an attractive target for new anti-cancer agents (5-7). Furthermore, based on the finding that oncogenic Ras mutations are found in 30% of all human cancers (8, 9), it was hypothesized that tumor growth could be inhibited by preventing Ras farnesylation. Thus, FTIs were developed as targeted agents against Ras and were shown to inhibit Ras function (10), as well as possess potent anti-tumor activity in multiple cancer cell lines and animal models. Despite the initial hypothesis that FTIs inhibit tumor growth by inhibiting Ras farnesylation, it was later shown that FTIs demonstrate anti-tumor activity independent of Ras status (11-13), suggesting that the mechanism of FTI activity extends beyond the inhibition of Ras farnesylation (14).

To probe the molecular mechanisms of FTI action, some previous works have focused on the relationship between FTIs and microtubule-targeting agents. Microtubules are dynamic polymers, composed of α- and β-tubulin subunits that elongate and shorten. In the cell, they function in a variety of processes including cell division, cell signaling, and intracellular trafficking (reviewed in 15). Since microtubules are essential components of the cell division machinery, they are attractive and validated targets for anti-cancer therapy (16, 17) as evidenced by the clinical success of microtubule-targeting drugs such as the taxanes (18-20). More recently, epothilones, a new class of microtubule-targeting drugs, are in clinical development and show very positive preliminary results (21). Notably, FTIs in combination with paclitaxel or epotholines act synergistically to inhibit cell growth in numerous human cancer cell lines and xenograft models (14, 22-24) . In addition, a combination clinical study of the FTI, lonafarnib (SCH66336 or sarasar; LNF) with paclitaxel yielded impressive preliminary results, with partial responses in eight of twenty evaluable patients, including patients whose disease had previously progressed while on taxanes alone (25). Despite these promising results, the molecular mechanism of the synergistic interaction of FTIs with taxanes is unknown.

The synergy between taxanes and FTIs, suggests that there may be a link between microtubules and the mechanism of FTI action. This is further supported by studies showing that FTI-2153 inhibited normal bipolar microtubule spindle formation, suggesting that spindle microtubules may have been affected by this treatment (26-28). These FTI-treated cells were arrested in early mitosis and this effect was independent of p53 and Ras status. Nevertheless, the effects of FTI treatment on interphase microtubules have not been examined.

Here we investigated the effects of LNF (29), on interphase microtubules in lung and breast cancer cells. Our results demonstrate that exposure to LNF resulted in microtubule bundle formation, stabilized interphase microtubules, and suppressed microtubule dynamics. Moreover, we show that the combination of LNF and paclitaxel for16 hr synergistically enhanced tubulin acetylation, mitotic arrest, and cell death; furthermore this effect correlated with FT inhibition. In addition, the combination of LNF and paclitaxel inhibits the deacetylating activity of HDAC6 *in vitro*, whereas either drug alone does not. Importantly, we show that the LNF/taxane combination is synergistic only in cells lines expressing the wild-type tubulin deacetylase, HDAC6, but not a catalytic-mutant HDAC6, revealing that functional HDAC6 is required for the synergy of LNF with taxanes. Taken together, these data suggest a relationship between FT inhibition, HDAC6 function, enhanced tubulin acetylation and cell death, providing a putative molecular basis for the LNF/taxane anti-proliferative combination.

Results:

Lonafarnib treatment alters microtubule structure

To examine the effects of LNF on interphase microtubules, we performed live cell microtubule imaging using MCF-7 breast cancer cells stably expressing GFP:α-tubulin. This cell line allows for the visualization of microtubules in living cells and eliminates the possibility of artifacts associated with fixed tissue analyses. Cells were treated for 48 hrs with 5 and 10 μM LNF (mean 72 hr IC_{50} of LNF was 8 μM in seven cancer cell lines tested; data not shown) and microtubules were observed using live-cell epi-fluorescence microscopy (Fig. 1A). Nearly all untreated control cells observed had an extensive, fine, and organized microtubule network. In contrast, LNF treatment led to a dose-dependent increase in microtubule bundling compared to control cells ($p < 0.05$; Fig. 1B). Treatment with 5 μM and 10 μM LNF led to nearly 10% and 25% of cells harboring extensive microtubule bundling, respectively. Similar microtubule bundles were observed in nearly 60% of cells treated with paclitaxel, while cells treated under the same condition with the non-microtubule targeting, DNA-intercalating agent, adriamycin (ADR) had identical microtubule morphologies as control cells.

To examine whether these effects were cell-line specific we performed immunofluorescence microscopy with an anti α-tubulin antibody on A549 and H1299 human lung cancer cells treated with LNF. Representative data from this experiment are shown in Figure S1-A depicting a dose-dependent increase in microtubule bundling following LNF treatment for 48 hr.

Lonafarnib treatment increases tubulin acetylation and microtubule stability

The appearance of microtubule bundles after LNF treatment in A549, H1299, and MCF-7 cells raises the possibility that LNF can affect microtubule stability in a manner similar to paclitaxel. To validate this hypothesis, indirect immunofluorescence using an antibody against acetylated α-tubulin was performed. Acetylation of α-tubulin at lysine 40 is an established marker of microtubule stability (30). Thus, the amount of acetylated tubulin is thought to be proportional to the stability of the microtubule. As shown in Figure 1C, LNF treatment for 48 hr resulted in a marked dose-dependent increase in acetylated α-tubulin, in contrast to the low basal levels of acetylated tubulin in untreated cells. This effect was similar to paclitaxel-induced tubulin acetylation, suggesting that LNF may also affect microtubule stability similar to paclitaxel.

To further probe the effects of LNF treatment on microtubule stabilization, a cell-based tubulin polymerization assay was performed (31, 32). This quantitative tubulin polymerization assay is based on the fact that drug-stabilized microtubule polymers remain detergent-insoluble when extracted in a hypotonic buffer, and therefore, remain in the pellet after centrifugation. Conversely, the pool of soluble tubulin dimers remains in the supernatant. LNF treatment resulted in a dose-dependent increase in tubulin polymerization, as shown by the increase in the percentage of tubulin found in the pellet fraction, as compared with untreated control cells (Fig. 1D). Specifically, untreated cells contain almost no stabilized tubulin (0% tubulin in the pellet) under our experimental conditions, whereas LNF treatment (5-20 μM) led to a dose-dependent increase in tubulin polymerization (25-60% of total tubulin in the pellet fraction). Similarly, treatment with 5

nM paclitaxel resulted in about 80% tubulin polymerization. The same blot was re-probed with an antibody against acetylated α-tubulin. A similar dose-dependent increase in acetylated α-tubulin in the pellet was observed upon LNF treatment and this shift of acetylated-tubulin towards the polymerized (P) fraction was greater than total tubulin. Thus, the majority of tubulin polymers in the pellet fraction represent stabilized acetylated microtubules rather than random microtubules trapped in this fraction.

Transmission electron microscopy confirms microtubule bundles in LNF-treated cells
To obtain high-resolution analysis of LNF-induced changes of the microtubule architecture, we performed transmission electron microscopy (TEM; 33). In contrast to control cells, which had individual microtubules throughout the cell's cytoplasm, LNF treatment induced the formation of microtubule bundles, similar to the bundles observed with paclitaxel (Fig 2S-B). Interestingly, LNF treatment mainly led to the formation of loose microtubule clusters that were longer in length but not as tightly packed as paclitaxel-induced microtubule bundles, suggesting that LNF-induced bundles may differ morphologically from paclitaxel-induced bundles (Fig. 2S-B, insets).

LNF suppresses microtubule dynamics in MCF-7 cells
Drugs that target microtubules, potently suppress microtubule dynamics at relatively low concentrations (16, 34) and this function is essential for their activity. Our results show LNF targets cellular microtubules, therefore, we investigated whether LNF also affects microtubule dynamics, similar to other microtubule-targeting drugs. To test this hypothesis, we measured microtubule dynamics in living MCF7-GFP:tubulin breast cancer cells using live-cell fluorescence microscopy. Time-lapse sequences of microtubule movements were generated, from untreated and LNF treated cells. Representative time frames show microtubule growth (white arrows), shortening (black arrows), and pause (white dashed arrows) in untreated control cells (Fig. 2A). In order to quantitate LNF's effects on microtubule dynamics, we tracked microtubule movements in cells treated with 10 μM LNF and untreated control cells. Individual microtubule life history plots, depicting changes in microtubule length over time were generated (Fig. 2B).

From these life history plots various parameters of microtubule dynamics were measured, comparing the dynamicity of microtubules in control cells and LNF-treated cells (Table I). These data show that there is a significant difference (p-value < 0.05) in the mean rate (μm/min) of microtubule growth and shortening with a decrease of 31% and 41%, respectively, when LNF-treated cells (10 μM for 48 hrs) are compared to control cells. Consequently, mean growth and shortening length (μm) also decreased by 34% and 42%, respectively. When the percentage of total time that microtubules spent in growth, shortening and pause states was determined, the growth time dropped from 30 to 17%, shortening time from 17 to 8.8%, and paused time increased from 53 to 74.2%; whereas the rescue and catastrophe frequencies per micrometer increased 31 and 12%, respectively (see methods for definition). The overall dynamicity of microtubules, which represents the total tubulin length change/min after LNF (10 μM) treatment, decreased by 63%. At 20 μM LNF microtubules were almost completely stabilized and most cells had few if any dynamic microtubules.

Combination of LNF with paclitaxel synergistically increases acetylated tubulin, mitotic arrest, and cell death

FTIs have been shown to synergize with microtubule stabilizing drugs in numerous preclinical models as well as in a phase 1 clinical trial (25). These observations were confirmed in our laboratory by performing combination index analysis assays of 10 different human cancer cell lines treated with paclitaxel and LNF. These assays revealed a marked synergy (CI = 0.2-0.7) between the two drugs (data not shown) and is consistent with previous findings. Our results, together with the reported literature, prompted us to hypothesize that the synergy of LNF with taxanes may in part be due to their combined effects on cellular microtubule acetylation and stability.

To test this hypothesis we quantitated acetylated tubulin levels using flow cytometry in cells treated for 16 hr (unlike the 48 hr treatment in Fig.1B) with LNF and paclitaxel, both alone and in combination. As shown in Figure 4A there was not a significant difference in acetylated tubulin levels between control untreated cells and cells treated for only 16 hr with LNF (1, 5, and 10 μM) or paclitaxel(2, 5 and 10 nM) alone. In contrast, the combination of 1, 5, and 10 μM LNF with as low as 2 nM paclitaxel resulted in a marked increase of acetylated tubulin similar to that observed with 100 nM of paclitaxel alone (Fig. 3A). Notably, non-microtubule-targeting chemotherapy drugs, such as adriamycin (DNA-intercalating antibiotic) and U89 (anti-metabolite) had no effect on acetylated tubulin levels; whereas, the microtubule-destabilizing drug vincristine led to a slight decrease of acetylated tubulin levels compared to untreated cells (Figure 3A).

To further explore the synergistic combination of LNF with paclitaxel, immunofluorescence analysis of acetylated tubulin at two different time points was performed (Fig. 3B). This analysis confirmed the marked increase in acetylated tubulin levels after 16 hr when low doses of LNF (at 0.5, 1, and 5 μM) were combined with low doses of 2nM paclitaxel. At 32 hr of treatment similar effects on acetylated tubulin were observed, suggesting that this effect is maintained for at least 32 hr.

Since tubulin acetylation is associated with microtubule stability, we examined whether the increased levels of acetylated tubulin observed with the combination of LNF and paclitaxel resulted in increased mitotic arrest and cell death. Flow cytometry analysis of DNA content revealed that the combination of LNF and paclitaxel led to a synergistic increase in G_2/M arrest as compared to each drug alone (Fig. 3C). Specifically, 16 hr treatment with as low as LNF 0.5 μM + PTX 2 nM resulted in a dramatic increase in G_2/M arrested cells as compared to untreated cells or cells treated with each drug alone. Longer treatment (32 hr) with the same drug combinations resulted in a dose-dependent increase in apoptotic cell death that is likely due to cells previously arrested in mitosis becoming apoptotic (Fig. 3C). The percentage of apoptotic cells in the combination treatments was similar to that achieved with PTX at 100 nM, whereas either drug alone at low dose produced minimal apoptotic cells. Overall, these results show that the LNF/paclitaxel-mediated increase in tubulin acetylation correlates with a synergistic increase in mitotic arrest and cell death.

The synergistic increase in tubulin acetylation correlates with farnesyl transferase inhibition

Since LNF inhibits the farnesyl transferase enzyme, we wanted to determine if the increase in tubulin acetylation observed with the combination of LNF and paclitaxel correlates with farnesyl transferase inhibition in cells. If so, it would suggest that the observed increase in tubulin acetylation may be a consequence of FTase inhibition. To do this, HDJ-2 was used as a readout for farnesyl transferase inhibition, since FTI treatment inhibits HDJ-2 farnesylation resulting in the appearance of a slower-migrating non-farnesylated HDJ-2 form. As shown in Fig. 4A, 1μM LNF alone and in combination with paclitaxel inhibited HDJ-2 farnesylation in a time-dependent manner, as assessed by the increase of the non-farnesylated (upper band) and concomitant decrease of the farnesylated HDJ-2 band (lower band). As expected, paclitaxel alone had no effect on HDJ-2 farnesylation. When the same blots were reprobed for acetylated α-tubulin, we observed a correlation between inhibition of HDJ-2 farnesylation and tubulin acetylation beginning at 3 hr treatment with the LNF/paclitaxel combination. In contrast, minimal effect on tubulin acetylation was observed with either drug alone. Taken together, these results show a positive temporal correlation between farnesyl transferase inhibition and tubulin acetylation, when LNF and paclitaxel are combined.

Next, we wanted to determine if there is also a correlation between tubulin acetylation and mitotic arrest. Therefore, in parallel with the time course experiment described above, we quantitated the percentage of cells in mitosis after treatment with the combination of LNF and paclitaxel. This result is represented in the bar graph in Figure 4B showing that there is about a 3 hr delay between the increase in microtubule acetylation (starting at 3 hr) and the first indication of mitotic arrest (at 6hr). Furthermore, the percentage of cells in mitosis increased with longer exposures to the combination of the two drugs, peaking at 12 hr of treatment. Overall, this result shows that when LNF and paclitaxel are combined, microtubule acetylation occurs prior to mitotic arrest and suggests that there is a correlation between tubulin acetylation/stability and mitotic arrest.

LNF in combination with paclitaxel inhibits the tubulin deacetylating activity of HDAC6

Our observation that LNF and paclitaxel synergistically enhance tubulin acetylation (Figure 3) prompted us to explore the possibility that this effect is due to the functional inhibition of the only known tubulin specific deacetylase (35), histone deacetylase 6 (HDAC6). To determine the effect of LNF on HDAC6 function we transfected A549 cells with FLAG-tagged HDAC6 (wild-type or catalytic subunit mutant) and these proteins were immunoprecipitated with an anti-FLAG antibody (see Material and Methods). The tubulin deacetylase activity of HDAC6 in the presence of LNF and paclitaxel was assayed *in vitro* by co-incubating the immunoprecipitants with purified bovine brain microtubule protein. Western blot analyses of acetylated tubulin levels were used as a read-out for HDAC6 activity (Fig.5A), such that HDAC6 functionality is evidenced by tubulin deacetylation. As a positive control we used trichostatin A (TSA), which inhibits the function of all HDACs including HDAC6. As expected bovine brain tubulin is heavily acetylated (lane 1) and co-incubation with wt-HDAC6 almost completely deacetylated tubulin (lane 3). In contrast, co-incubation with the catalytically

inactive mutant HDAC6 had no effect on tubulin acetylation (last lane). The addition of LNF or paclitaxel alone to the purified wild-type HDAC6-tubulin complex had no effect on HDAC6 activity, since tubulin was heavily deacetylated indicating normal HDAC6 activity. In contrast, when LNF (variable doses) and paclitaxel (kept constant at 10 μM) were combined *in vitro*, there was a dose-dependent increase of tubulin acetylation, suggesting that the combination of these agents inhibits tubulin deacetylating HDAC6 activity. Paclitaxel alone had no effect on HDAC6 activity even at 100 μM. We also tested the microtubule depolymerizing agent colchicine for HDAC6 inhibitory activity, and like paclitaxel, it did not inhibit HDAC6 function.

Since our results suggest that the combination of lonafarnib and paclitaxel synergistically inhibit HDAC6 function, we wanted to determine if these drugs also affect the function of other HDACs. Thus, we treated A549 cells with lonafarnib, alone and in combination with paclitaxel for 16 hr, and probed for acetylated histone 3 (H3). TSA (a pan-HDAC inhibitor) was included as a positive control. As expected, treatment with TSA resulted in increased levels of acetylated H3. In contrast, no effect on acetylated H3 was observed with LNF treatment either alone or in combination with paclitaxel (Fig. S2), suggesting that LNF and/or paclitaxel do not affect the function of other HDACs.

To probe the importance of HDAC6 inhibition in the mechanism of synergy between LNF and paclitaxel, we combined the specific HDAC6 inhibitor, tubacin, with paclitaxel. This experiment allows us to determine whether the combination of a specific HDAC6 inhibitor with paclitaxel leads to a synergistic increase in tubulin acetylation, similar to the LNF/paclitaxel combination. Western blot analysis of A549 cells treated with the combination of tubacin and paclitaxel at low doses (beginning at 0.3 μM tubacin and 1 nM paclitaxel) led to a synergistic increase in acetylated tubulin, as compared to either drug alone (Fig 5B). These findings were confirmed with acetylated tubulin immunofluorescence (data not shown). Thus, specific inhibition of HDAC6 (e.g., with tubacin) in combination with paclitaxel leads to a synergistic increase in acetylated tubulin, further suggesting that the LNF/paclitaxel inhibition of HDAC6 activity provides a mechanistic basis for the enhanced tubulin acetylation. Furthermore, the addition of 3 and 10 μM tubacin (IC_{50} > 1mM) to PTX (IC_{50} 7.7 ± 1.7 μM) decreased the IC_{50} of PTX, 20.8 and 31.5%, respectively (Table S1). Similar results were also observed when tubacin was combined with docetaxel (Table S1), suggesting that although tubacin as a single agent is not cytotoxic, its affect on tubulin acetylation can enhance the cytotoxicity of PTX.

To further explore the functional importance of HDAC6 in the synergy between LNF and paclitaxel we tested this drug combination in a pair of cell lines engineered to stably express either wild-type HDAC6 (HDAC6-wt) or a catalytic mutant HDAC6 (HDAC6-mut). These cells lines will allow us to determine if a functional HDAC6 protein is required for the observed effects on acetylated tubulin. In agreement with previously published data (35), HDAC6-wt cells had lower baseline levels of acetylated tubulin relative to HDAC6-mut cells, consistent with the presence of a functional *versus* a non-functional HDAC6 (Figure 5C, untreated). Upon treatment with the LNF/paclitaxel combination, there was a synergistic increase in acetylated tubulin in HDAC6-wt cells as

expected; however the LNF/paclitaxel combination had no effect on tubulin acetylation in the HDAC6-mut cells. This results indicates that the synergistic increase in acetylated tubulin induced by the LNF/paclitaxel combination is dependent upon the presence of a functional HDAC6. To extend these observations, we used another taxane, docetaxel (DTX), in combination with LNF.

Next, we wanted to determine if functional HDAC6 is required not only for the synergistic increase in acetylated tubulin with the LNF/taxane combination (Figure 5C), but also for the synergistic anti-proliferative activity of the drugs. Thus, we performed cytotoxicity assays employing the routinely used combination index analysis to assess synergy between the two drugs against cells with HDAC6-wt and HDAC6-mut genetic background. Our results show that the combination of LNF with DTX resulted in a robust synergistic anti-proliferative effect in HDAC6-wt cells (mean CI=0.4 indicating strong synergy; Figure 5D). In stark contrast, the combination of LNF and DTX was antagonistic in the HDAC6-mut cells (mean CI=2.5), suggesting that the lack of functional HDAC6 in these cells not only precludes increased levels of acetylated tubulin with this drug combination but also abolishes their anti-proliferative synergy. To confirm that the combination of DTX with LNF inhibits the tubulin deacetylase activity of HDAC6 *in vitro,* similar to our previous results with paclitaxel (Figure 5A), we used cells stably expressing wild-type HDAC6 to immunoprecipitate HDAC6, and performed another *in vitro* tubulin deacetylase assay. Our data show that the combination of 10 μM LNF with 10 μM DTX resulted in a synergistic inhibition of HDAC6 function, as evidenced by the appearance of acetylated tubulin, whereas either drug alone had no effect on HDAC6 functionality (Figure 5E). Collectively, these data provide a mechanistic link between HDAC6 inhibition, tubulin acetylation and the synergistic interaction of these drugs.

Discussion:

Analyzing the effects of LNF as a single agent on microtubules

The farnesyl transferase inhibitors were developed as targeted therapies against cancers with oncogenic Ras mutations, however, FTIs were shown to retain their activity independently of Ras status(11-13). Here we examined the effects of the FTI, lonafarnib (LNF), on interphase microtubules in human cancer cells. Our results demonstrate that prolonged exposure (48 hr) to LNF alone leads to microtubule stabilization as evidenced by increased tubulin acetylation, suppression of microtubule dynamics, and bundle formation (Figs. 1-2, Table I). Since tubulin acetylation is an established marker of microtubule stability (30), we believe that the LNF-induced microtubule stabilization may contribute to its anti-proliferative effects, similar to the taxanes and epothilones. However, it is important to note that the microtubule-stabilizing capacity of LNF is weak relative to other established microtubule stabilizing agents, which stabilize microtubules at low nanomolar concentrations. This suggests that the mechanism by which LNF induces microtubule stabilization may differ from traditional microtubule-stabilizing agents (e.g. the taxanes). Further supporting this hypothesis, is our electron microscopy analysis (Figure 1S-B), which show that LNF-induced microtubule bundles are longer and not as tightly clustered as paclitaxel-induced bundles, suggesting that their differing

morphologies may stem from alternative mechanisms of bundle formation Thus, we propose that LNF is a microtubule-stabilizing agent, however its mechanism of microtubule stabilization likely varies from established microtubule-stabilizing agents.

Microtubule acetylation and the mechanism of synergy between LNF and the taxanes
Previous reports have shown that FTIs synergize with taxanes and epothilones in a variety of human cancer cell lines *in vitro* and *in vivo* (22, 24); however, the mechanism underlying this synergy is unknown. Our results show that the combination of low doses of LNF (beginning at 0.5 μM) and paclitaxel (2nM) resulted in a dramatic increase in tubulin acetylation (Figure 3A-C), compared to untreated cells or each drug treatment alone. Importantly, the mean C_{max} of LNF achieved in patients dosed twice daily with 200 mg of LNF is 4.4 μM (unpublished) and therefore the doses (LNF beginning at 0.5 μM) at which we observed synergistic enhancement of acetylated tubulin are within the C_{max}. Furthermore, the effect of LNF/PTX on acetylated tubulin was observed in as little as 3 hr of drug treatment (Fig 4A) and preceded the synergistic increase in mitotic arrest (Fig. 3C, 4B), suggesting that increased microtubule acetylation/stability is associated with aberrant mitotic arrest and cell death. Nevertheless, it remains unclear if LNF/PTX induced microtubule acetylation only serves as marker for cell death or instead is the catalyst, and therefore studies are underway addressing this issue.

Mechanistically, we show that the synergistic increase in microtubule acetylation is due to the effect of the combination of LNF and paclitaxel on the tubulin deacetylase HDAC6 (Fig. 5). We propose that the enhanced tubulin acetylation we observe is due to the inhibition of HDAC6 function. We provide four lines of evidence to support this claim. First, we show that the combination of LNF and paclitaxel inhibit HDAC6 tubulin deacetylating activity *in vitro,* whereas either drug alone had no effect (Fig 5A). Second, we can reproduce the LNF/paclitaxel-induced increase in tubulin acetylation by using tubacin, a specific HDAC6 inhibitor, in combination with paclitaxel (Figure 5B). This suggests that pharmacologic inhibition of HDAC6 in combination with paclitaxel synergistically increases tubulin acetylation. Third, cells expressing a catalytically inactive HDAC6 (HDAC6-mt) fail to show an increase in acetylated tubulin when LNF and paclitaxel are combined (Figure 5C), suggesting that this drug combination requires functional HDAC6 to retain efficacy. Fourth, the robust cytotoxic synergy of LNF and docetaxel is lost in these cells expressing mutant HDAC6, whereas potent synergy remains in their wild type HDAC6 counterparts (Figure 5D). This observation provides evidence that the deacetylating activity of HDAC6 is required for the LNF/taxane synergy, providing a mechanistic link between functional HDAC6, tubulin acetylation and cell death. However, it is still unknown whether the effect of the LNF/taxane combination on HDAC6 function is due to direct binding of these drugs to this enzyme or due to their effects on microtubule stability, which in turns alters the affinity of HDAC6 for the microtubule. We favor the latter scenario, since either drug alone does not alter HDAC6 function, reducing the likelihood that these drugs bind HDAC6 directly.

Is there a biological link between FTase inhibition and microtubule acetylation?

Since all FTIs tested to date synergize with paclitaxel, it is likely that they share a common mechanism of synergy related to farnesyl transferase inhibition. In Fig. 4A, we show that the increase in tubulin acetylation observed with the low dose LNF/paclitaxel combination, correlates with farnesyl transferase inhibition. This result suggests that inhibition of farnesyl transferase may be biologically linked with enhanced tubulin acetylation. Currently, there are no reports of a link between the FTase enzyme and interphase microtubules. Preliminary data from our laboratory in 50 human cancer cell lines used in the NCI Anticancer Drug Screen (http://dtp.nci.nih.gov) have revealed that acetylated tubulin protein levels negatively correlated with FTase gene expression and protein levels (COMPARE analysis http://itbwork.nci.nih.gov/CompareServer/CompareServer; unpublished data). Thus, it may be possible that proteins regulating microtubule stability are farnesylated by FTase; consequently, inhibition of FTase by LNF may in turn affect microtubule stability. In fact it is already known that the mitotic microtubule associated protein, CENP-E, is farnesylated and its association with microtubules during mitosis is altered in mitotic cells (27). Thus, further investigation of a putative link between FTase and interphase microtubules is warranted.

Overall, our data show that treatment with LNF alone causes microtubule bundling, increased microtubule acetylation and stabilization, and suppression of microtubule dynamics. This result is consistent with LNF being, in addition to its role as an FTI, a microtubule-stabilizing agent. Importantly, our data also show that functional HDAC6 is required for the synergy between LNF and the taxanes and suggest that there is a link between FTase and tubulin acetylation. As there are ongoing phase II and III trials testing the efficacy of this drug combination, elucidating the molecular mechanism(s) of synergy can provide insight into the design of future combination cancer therapies.

Materials and Methods

Cell Culture

The human non-small cell lung cancer cell lines, A549 and H1299, were maintained in RPMI 1640 supplemented with 5% fetal calf serum, nonessential amino acids and 0.1% penicillin/streptomycin at 37°C in 5% CO_2. Live cell microscopy was performed with MCF-7 breast cancer cells stably transfected with GFP:α-tubulin and maintained in DMEM supplemented with 5% fetal calf serum, nonessential amino acids and 0.1% penicillin/streptomycin.. All lines were cultured at 37°C in a humidified atmosphere with 5% CO_2. NIH-3T3 cells expressing various HDAC6 constructs were previously generated (35) and were cultured in DMEM medium under the same conditions.

Immunofluorescence analysis

Immunofluorescence microscopy was performed as previously described (36). Cells were fixed in PHEMO buffer (68 mM PIPES, 25 mM HEPES, 15 mM EGTA, 3 mM $MgCl_2$, 10% DMSO) with 3.7% formaldehyde, 0.05% glutaraldehyde, 0.5% Triton X-100. Cells were washed in PBS 3 times for 5 minutes then blocked in 10% goat serum for 15 minutes. The following primary antibodies were used: α-tubulin (Chemicon International, MAB1864; 1:500 dilution) and acetylated tubulin (Sigma T-6793, dilution 1:1000) with incubation times of 1 hr. The secondary antibodies used were Alexa 563

conjugated goat anti-rat IgG (1:500); Alexa 488 conjugated goat anti-mouse IgG antibody (1:500), both from Molecular probes. Cells were imaged using a Zeiss LSM 510 Meta (Thornwood, NY) confocal microscope using a either a 63X (N.A. 1.4) or 100X (N.A. 1.4) Apochromat objective. To stain DNA for mitotic cell counting, we fixed cells as described above, and added Sytox Green (Molecular Probes; #S7020) to the Gel Mount mounting media (Biomeda Corp; Foster City, CA). All images were acquired using Zeiss LSM 510 software and processed in Adobe Photoshop 7.0

Cell tubulin polymerization assay

Quantitative drug-induced tubulin polymerization was performed as previously described(31, 32). The percent pellet (%P) is calculated as the amount of polymerized tubulin (P), over the total amount of polymerized and soluble tubulin (P+S) times 100 {P/(P+S) x 100} based upon densitometric analysis.

Electron Microscopy

A549 cells were seeded on Thermanox cover slips (Electron Microscopy Sciences #72280) in 24 well plates and grown overnight to 60% confluency. Cells were then treated with 10 μM LNF for 48 hrs and fixed using a protocol described in Vanier et al (33). Cells were then fixed in 2% glutaraldelhyde for 4 hours at room temperature, rinsed in distilled water twice, post-fixed in 1% OsO_4 in 0.1M sodium cacodylate buffer (pH 7.4) at 4°C for 1 hour and finally rinsed in distilled water as above. Samples were then dehydrated through an ethanol series (30, 50, 60, 80, 90, 100, 100%) followed by 2 changes of propylene oxide (PPO; 10 minutes each). Then samples were infiltrated with Embed 812 (Electron Microscopy Sciences) for 3 days according to the manufacturer's instructions. Each block was cut at 1mm x 1mm using a diamond knife and RMC MT-7000 ultramicrotome, and thin sections were made and collected onto 200 mesh copper grids. Grids were post stained with 10% uranyl acetate in distilled water and then 2% lead citrate in distilled water for 20 minutes in each treatment.

FLOW cytometry analysis

To determine acetylated tubulin levels, cells were plated and on the following day treated with different concentrations of the drugs for 16 hr. After drug treatment, cells were fixed with PHEMO buffer for 10 minutes as previously described (36) and stained with an antibody against acetylated tubulin (1:500; Sigma T-6793) followed by secondary Alexa 488 goat anti-mouse IgG antibody (1:500). Finally, cells were scraped into 1 ml of PBS, and FLOW cytometry analysis was performed on a Becton Dickinson FLOW cytometer.

For cell cycle analysis, cells were scraped from plates, centrifuged at 1000 rpm for 5 minutes, and propidium iodide buffer containing 0.1 mg/ml propidium iodide and NP-40 (0.6%) in water was used to resuspend cells. Cell were incubated in this buffer for 30 minutes at room temperature in the dark, then passed through a filter to remove cell clumps and finally read in a Becton Dickinson FLOW cytometer

Microtubule dynamics assays

Experiments were performed using a MCF-7 breast cancer cell line stably expressing a GFP-α-tubulin microtubule reporter protein (kind gift of Dr. Mary Ann Jordan). Cells were plated and analyzed as previously described (34). Images were taken using a Hamamatsu Orca ER camera (Middlesex, NJ) every four seconds for two minutes (250-400 s exposure) on a Zeiss Axiovert (Thornwood, NJ) epi-fluorescence microscope equipped with 100X Apochromat (N.A.=1.4) oil lens and adjustable mercury arc lamp (set at 100% intensity). A stage heater as well as Zeiss heating chamber were used to maintain the temperature at 37 ±0.5°C. Microtubules ends at the lamellar edge of interphase cells were imaged and subsequently tracked using the "track points" feature on Metamorph image analysis software (Universal Imaging, Downingtown, PA). The coordinates generated from this tracking feature were used to determine the distance individual microtubule ends changed from a fixed point. These values were transferred to a Microsoft Excel spreadsheet and used to generate life history plots of individual microtubules. From these graphs, the various parameters shown in Table 1 were calculated. All p-values were calculated using the Student's T-test.

Microtubule dynamicity is defined as the total length grown and shortened during the life (measured in min.) of an individual microtubule. A catastrophe is defined as a transition into microtubule shortening while a rescue is a transition from shortening to growth or pause. To calculate catastrophe frequency per unit time or per unit length the number of catastrophes was divided by the total time in growth and pause or the total distance grown, respectively. Conversely, the rescue frequency was calculated by dividing the number of rescues by the total time spent shortening or distance shortened.

In vitro acetylated tubulin assay

A549 cells were transiently transfected with Flag-tagged pBJ5-HDAC6 expression plasmids using FuGene (Roche) following the manufacturer's guidelines. Untransfected cells or cells transfected with an empty vector were used as controls. In Figure 6F, we used NIH-3t3 cells stably expressing FLAG tagged HDAC6-wt and HDAC6-mt proteins and therefore cells did not have to be transfected. Cell lysates were prepared 48 hours after transfection and then immunoprecipitated with anti-Flag M2 agarose beads (Sigma-FLAGIPT1). Tubulin acetylation assays were performed by incubating the immunoprecipitates with preformed MAP-stabilized microtubules at 37 °C, along with the appropriate drug, for 2 hours as described previously (35). Reactions were then placed on ice for 15 minutes and centrifuged briefly at 14, 000 rpm to separate the supernatant from the agarose beads. The supernatant was analyzed by Western blotting with antibodies against acetylated α-tubulin and against α-tubulin (as described below) and the beads were analyzed with an antibody against Flag M2 (Sigma- F3165; 1:1000).

Western blotting

Cells were plated in 6-well plates at 50% confluency and treated the next day with the appropriate drug and time interval. Cells were lysed, centrifuged at 15,000 rpm for 15 min, and electrophoresed on a 7.5% SDS-PAGE gel (BCA assay was used to determine protein concentration in a spectrophotometer). Proteins were transferred to a PVDF membrane (100V for 1 hr) using a Bio-Rad transfer apparatus and blotted with antibodies against acetylated tubulin (Sigma T6793; 1:1000), total tubulin (Sigma DM1α, 1:1000),

HDJ-2, acetylated histone H3 (Cell Signaling; at 1:1000), actin, and HDAC6 (1:1000; Cell Signaling #2162).

Cell survival and Synergy Assays (Combination Index Analysis)

Cells were plated in a 96-well plate at 2,000 cells/well and allowed to attach overnight. Cells were then treated with serial dilutions (1:3) of either LNF alone, PTX alone, or the combination of LNF and PTX for 72 hr. Cell were then fixed with 50% tri-chloro acetic acid (TCA) for 30 min, washed 3 times with water, dried, and stained with 0.4% sulfurhodamine B (SRB; protein stain) for 30 min. Cell were then washed with 0.1% acetic acid, air dried, and the bound SRB was dissolved with 10mM unbuffered TRIS-base (pH= 10.5). The plates were read in a microplate reader (OD_{564}) and synergy was determined using CalcuSyn software, which calculates the combination index (CI) based upon the percent cell survival at vary doses of the drug treatments, both alone and in combination. A CI greater than 1 indicates antagonism, equal to 1 is additivity, and less than 1 is synergism.

Acknowledgements

We would like to thank Drs. Mary Ann Jordan and Kathy Kamath (UCSB, Santa Barbara, CA) for providing us with the MCF-7 cells stably expressing GFP:α-tubulin as well as sharing their invaluable experience on performing the live-cell microtubule dynamic assays. We would also like to thank Dr. Stuart Schreiber (Harvard University, Boston, MA) for providing us with tubacin and the FLAG-HDAC6 constructs, and for providing guidance to Jason Wong (gm38627, awarded to s.l.s.). We gratefully acknowledge Dr. W. Robert Bishop for his invaluable insight and for providing us with Lonafarnib (Schering-Plough Research Institute). We wish to thank Dr. Robert Apkarian, director of the electron microscope core facility at Emory University, for his help with TEM,a nd Cindy Giver for her help with flow cytometry. Lastly, we would like to thank the WCI Cancer Imaging and Microscop Core for their support and service. This work was supported in part by NIH 1R01 CA100202, Aventis Pharmaceuticals, and Department of Defense Grant DAMD 17-02-1-0706.

References

1. Brunner TB, Hahn SM, Gupta AK, *et al.* Farnesyltransferase inhibitors: an overview of the results of preclinical and clinical investigations. Cancer Res 2003;63:5656-68.
2. Adjei AA. Blocking oncogenic Ras signaling for cancer therapy. J Natl Cancer Inst 2001;93:1062-74.
3. Hahn SM, Bernhard E, and McKenna WG. Farnesyltransferase inhibitors. Semin Oncol 2001;28:86-93.
4. McCormick F. Ras-related proteins in signal transduction and growth control. Mol Reprod Dev 1995;42:500-6.
5. Jackson JH, Cochrane CG, Bourne JR, *et al.* Farnesyl modification of Kirsten-ras exon 4B protein is essential for transformation. Proc Natl Acad Sci U S A 1990;87:3042-6.
6. Kato K, Cox AD, Hisaka MM, *et al.* Isoprenoid addition to Ras protein is the critical modification for its membrane association and transforming activity. Proc Natl Acad Sci U S A 1992;89:6403-7.
7. Willumsen BM, Christensen A, Hubbert NL, Papageorge AG, and Lowy DR. The p21 ras C-terminus is required for transformation and membrane association. Nature 1984;310:583-6.
8. Barbacid M. ras genes. Annu Rev Biochem 1987;56:779-827.
9. Bos JL. ras oncogenes in human cancer: a review. Cancer Res 1989;49:4682-9.
10. Li T and Sparano JA. Inhibiting Ras signaling in the therapy of breast cancer. Clin Breast Cancer 2003;3:405-16; discussion 17-20.
11. End DW, Smets G, Todd AV, *et al.* Characterization of the antitumor effects of the selective farnesyl protein transferase inhibitor R115777 in vivo and in vitro. Cancer Res 2001;61:131-7.
12. Nagasu T, Yoshimatsu K, Rowell C, Lewis MD, and Garcia AM. Inhibition of human tumor xenograft growth by treatment with the farnesyl transferase inhibitor B956. Cancer Res 1995;55:5310-4.
13. Sepp-Lorenzino L, Ma Z, Rands E, *et al.* A peptidomimetic inhibitor of farnesyl:protein transferase blocks the anchorage-dependent and -independent growth of human tumor cell lines. Cancer Res 1995;55:5302-9.
14. Moasser MM and Rosen N. The use of molecular markers in farnesyltransferase inhibitor (FTI) therapy of breast cancer. Breast Cancer Res Treat 2002;73:135-44.
15. Nogales E. Structural insights into microtubule function. Annu Rev Biochem 2000;69:277-302.
16. Jordan MA. Mechanism of action of antitumor drugs that interact with microtubules and tubulin. Curr Med Chem Anti-Canc Agents. 2002;2:1-17.
17. Jordan MA and Wilson L. Microtubules as a target for anticancer drugs. Nat Rev Cancer 2004;4:253-65.
18. Drukman S and Kavallaris M. Microtubule alterations and resistance to tubulin-binding agents (review). Int J Oncol 2002;21:621-8.
19. Rowinsky EK. The development and clinical utility of the taxane class of antimicrotubule chemotherapy agents. Annu Rev Med 1997;48:353-74.

20. Checchi PM, Nettles JH, Zhou J, Snyder JP, and Joshi HC. Microtubule-interacting drugs for cancer treatment. Trends Pharmacol Sci 2003;24:361-5.
21. Wartmann M and Altmann KH. The biology and medicinal chemistry of epothilones. Curr Med Chem Anti-Canc Agents 2002;2:123-48.
22. Moasser MM, Sepp-Lorenzino L, Kohl NE, *et al.* Farnesyl transferase inhibitors cause enhanced mitotic sensitivity to taxol and epothilones. Proc Natl Acad Sci U S A 1998;95:1369-74.
23. Sun J, Blaskovich MA, Knowles D, *et al.* Antitumor efficacy of a novel class of non-thiol-containing peptidomimetic inhibitors of farnesyltransferase and geranylgeranyltransferase I: combination therapy with the cytotoxic agents cisplatin, Taxol, and gemcitabine. Cancer Res 1999;59:4919-26.
24. Shi B, Yaremko B, Hajian G, *et al.* The farnesyl protein transferase inhibitor SCH66336 synergizes with taxanes in vitro and enhances their antitumor activity in vivo. Cancer Chemother Pharmacol 2000;46:387-93.
25. Khuri FR, Glisson BS, Kim ES, *et al.* Phase I study of the farnesyltransferase inhibitor lonafarnib with paclitaxel in solid tumors. Clin Cancer Res 2004;10:2968-76.
26. Crespo NC, Ohkanda J, Yen TJ, Hamilton AD, and Sebti SM. The farnesyltransferase inhibitor, FTI-2153, blocks bipolar spindle formation and chromosome alignment and causes prometaphase accumulation during mitosis of human lung cancer cells. J Biol Chem 2001;276:16161-7.
27. Crespo NC, Delarue F, Ohkanda J, *et al.* The farnesyltransferase inhibitor, FTI-2153, inhibits bipolar spindle formation during mitosis independently of transformation and Ras and p53 mutation status. Cell Death Differ 2002;9:702-9.
28. Ashar HR, James L, Gray K, *et al.* Farnesyl transferase inhibitors block the farnesylation of CENP-E and CENP-F and alter the association of CENP-E with the microtubules. J Biol Chem 2000;275:30451-7.
29. Taveras AG, Kirschmeier P, and Baum CM. Sch-66336 (sarasar) and other benzocycloheptapyridyl farnesyl protein transferase inhibitors: discovery, biology and clinical observations. Curr Top Med Chem 2003;3:1103-14.
30. Piperno G, LeDizet M, and Chang XJ. Microtubules containing acetylated alpha-tubulin in mammalian cells in culture. J Cell Biol 1987;104:289-302.
31. Giannakakou P, Sackett DL, Kang YK, *et al.* Paclitaxel-resistant human ovarian cancer cells have mutant beta-tubulins that exhibit impaired paclitaxel-driven polymerization. J Biol Chem 1997;272:17118-25.
32. Giannakakou P, Villalba L, Li H, Poruchynsky M, and Fojo T. Combinations of paclitaxel and vinblastine and their effects on tubulin polymerization and cellular cytotoxicity: characterization of a synergistic schedule. Int J Cancer 1998;75:57-63.
33. Vanier MT, Neuville P, Michalik L, and Launay JF. Expression of specific tau exons in normal and tumoral pancreatic acinar cells. J Cell Sci 1998;111 (Pt 10):1419-32.
34. Kamath K and Jordan MA. Suppression of microtubule dynamics by epothilone B is associated with mitotic arrest. Cancer Res 2003;63:6026-31.
35. Hubbert C, Guardiola A, Shao R, *et al.* HDAC6 is a microtubule-associated deacetylase. Nature 2002;417:455-8.

36. Mabjeesh NJ, Escuin D, LaVallee TM, *et al.* 2ME2 inhibits tumor growth and angiogenesis by disrupting microtubules and dysregulating HIF. Cancer Cell 2003;3:363-75.

Table I Analysis of *in vivo* microtubule dynamics in the presence and absence of LNF.

Parameter		Control	LNF 10 μM	Percent Change
Growth				
	rate (μm/min)	11.2 ± 2.1	**7.7 ± 3.8**	-31%
	length (μm)	2.9 ± 1.6	**1.9 ± 0.9**	-34%
	time (min)	0.3 ± 0.08	0.28 ± 0.07	-7%
Shortening				
	rate (μm/min)	17.1 4.0	**9.9 ± 3.3**	-41%
	length (μm)	5.3 ± 1.9	**3.1 ± 1.6**	-42%
	time (min)	0.34 ± 0.11	0.33 ± 0.1	-3%
Pause				
	time (min)	0.36 ± 0.23	0.40 ± 0.2	-11%
Percentage time spent				
	Growth	30	**17**	
	Shortening	17	**8.8**	
	Pause	53	**74.2**	
Dynamicity (μm/min)		8.1 ± 4.0	**3.0 ± 1.9**	-63%
Rescue frequency (events/min)		4.1 ± 2.6	4.0 ± 2.5	-2%
Catastrophe frequency (events/min)		0.9 ± 0.8	0.88 ± 0.75	-2%
Rescue frequency (events/μm)		0.19 ± 0.15	**0.25 ± 0.21**	31%
Catastrophe frequency (events/μm)		0.33 ± 0.29	0.37 ± 0.31	12%
Number of cells		21	23	
Number of MTs		81	69	

Values in bold type differ significantly from control values at > 99% confidence interval as determined by Student's t-test
Values are mean ± SD

Figure legends

Figure 1. LNF treatment alters microtubule structure and increases tubulin acetylation. (A) MCF-7 breast cancer cells stably expressing GFP:α-tubulin were observed using live-cell fluorescence microscopy following the indicated drug treatments for 48 hrs. Microtubule bundling is indicated with solid arrows. Bottom row displays higher magnification of microtubules shown in the top row. Scale bars are at 10 μm. **(B).** A bar graph depicting the number of cells containing microtubule bundles following drug treatments shown in A. Asterisks denote a significant difference in the percentage of cells having microtubule bundles compared to control ($p<0.05$). Error bars are standard deviation **(C)** A549 cells were treated with LNF for 48 hrs and microtubules were visualized by immunofluorescence labeling using an antibody against acetylated α-tubulin. Treatment with PTX is included as a positive control. Scale bars are at 10 μm. **(D)** Western blot analysis against total α-tubulin (top row) and acetylated tubulin (bottom row) on the polymerized (P) and soluble (S) fraction of protein lysates from A549 cells treated with the indicated drug concentrations for 48 hrs. The relative percentage of polymerized tubulin for each drug treatment is denoted as (%P).

Figure 2. LNF treatment suppresses microtubule dynamics in living MCF-7 cells. (A) Time lapse sequences of microtubules in untreated living MCF-7 cells stably expressing GFP:α-tubulin. Arrows depict dynamic microtubules that change length over the course of 16s. Black arrows: microtubule shortening, white arrows: microtubule growth, dashed arrows: paused microtubules. Scale bars are 5 μm. **(B)** Individual microtubule life-history plots from control untreated cells or cells treated with 10 μM LNF for 48 hrs. Growth events are seen as an increase in distance from a fixed-point (y-axis) over time (x-axis) and shortening events show a decrease in distance over time.

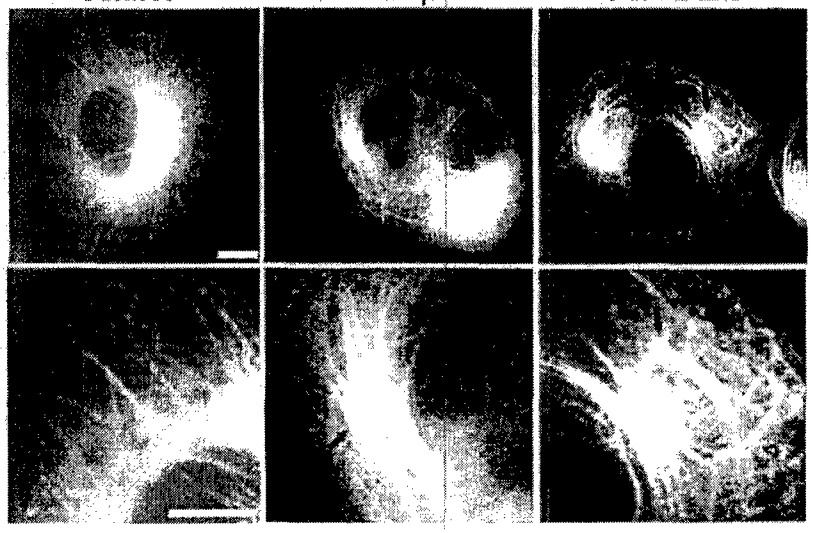
Figure 3. LNF and PTX synergistically increase acetylated tubulin, mitotic arrest and apoptosis. (A) Flow cytometry was performed with an acetylated tubulin antibody in A549 cells treated with the indicated drugs. Bar graph representation of acetylated tubulin levels by after 16 hr of drug treatment. Each bar represents the mean fluorescence for acetylated tubulin relative to that of control untreated cells (FTI=lonafarnib). **(B)** Acetylated tubulin immunofluorescence of cells treated with LNF and PTX, both alone and in combination, for 16 hr and 32 hr. **(C)** A bar graph showing cell cycle analysis for 16 and 32 hr of treatment with the combination of LNF and PTX.

Figure 4. The synergistic increase in acetylated tubulin caused by LNF and PTX treatment correlate with farnesyl transferase inhibition and mitotic arrest
(A) Western blot analysis for acetylated tubulin, HDJ-2 (N= non-farnesylated band, F= farnesylated band), and total tubulin following LNF and/or PTX treatment over time. **(B)** Bar graph representation of percent mitosis assessed by DNA staining, performed in parallel and with the same drug treatments over time as in A. Error bars are standard deviation.

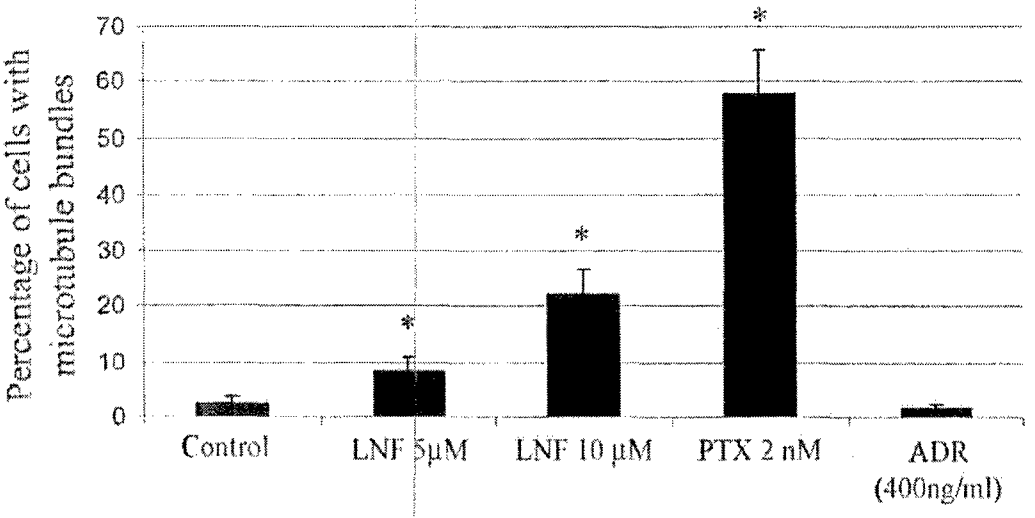
Figure 5. The synergistic combination of LNF and a taxane prevents HDAC6 tubulin deacetylation *in vitro* and is dependent on HDAC6 functionality

(A) Representative western blots of acetylated-α-tubulin, total-tubulin and Flag, following immunoprecipitation (IP) from A549 cells transfected with either Flag-HDAC6-WT or Flag-HDAC6-mut. Prior to western blotting the Flag-IP complexes were incubated *in vitro* with pre-assembled purified bovine brain microtubule protein in the presence of the various drugs, to determine the tubulin deacetylase activity of HDAC6 (left hand blot). (**B**) Western blotting of acetylated tubulin after treatment with tubacin, a specific HDAC6 inhibitor, both alone and in combination with PTX. TSA was used as additional positive control for pan-HDAC inhibition. As a control for total tubulin levels, blots were reprobed for α-tubulin. (**C**) Immunofluorescence analyses of acetylated tubulin in NIH-3T3 cells stably expressing either HDAC6-wt (wild-type) or HDAC-mut (catalytically inactive mutant), following 16 hr drug treatments as indicated. (**D**) A bar graph assessing synergy between LNF and docetaxel in HDAC6-wt and HDAC6-mut using combination index analysis. The LNF/docetaxel combination is synergistic in HDAC6-wt (CI <1) but is antagonistic in HDAC6-mt cells (CI >1). Error bars are standard deviation. (**E**) Representative western Blots of acetylated-α-tubulin, total-tubulin and HDAC6 following immunoprecipitation (IP) from NIH-3T3 cells stably expressing Flag-HDAC6-WT. Prior to western blotting the Flag-IP complexes were incubated *in vitro* with pre-assembled purified bovine brain microtubule protein in the presence of the various drugs, to determine the tubulin deacetylase activity of HDAC6. The *in vitro* effects of TSA (pan-HDAC inhibitor), LNF, and docetaxel (DTX) on acetylated α-tubulin are shown.

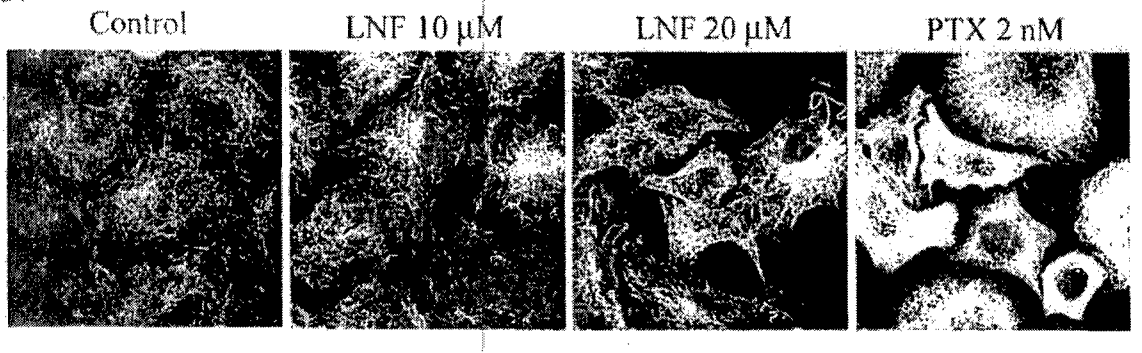
A.


Control
LNF 10 μM
PTX 2 nM

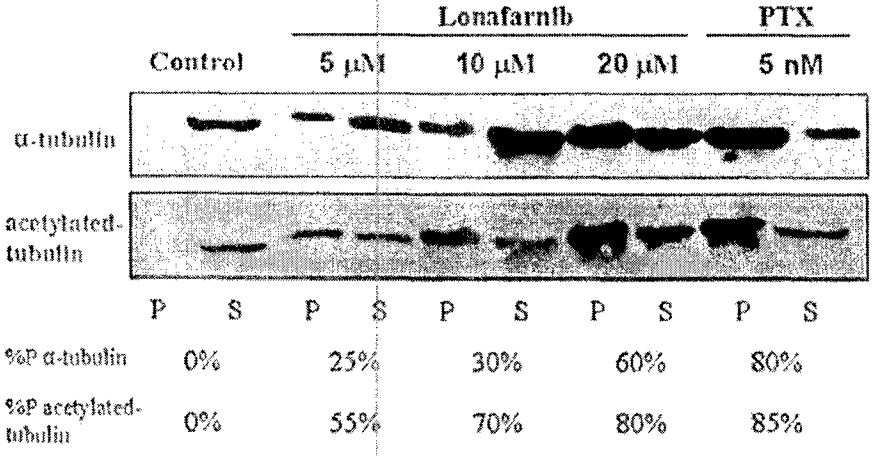
B.


Percentage of cells with microtubule bundles
70
60
50
40
30
20
10
0
*
*
*
Control
LNF 5μM
LNF 10 μM
PTX 2 nM
ADR (400ng/ml)

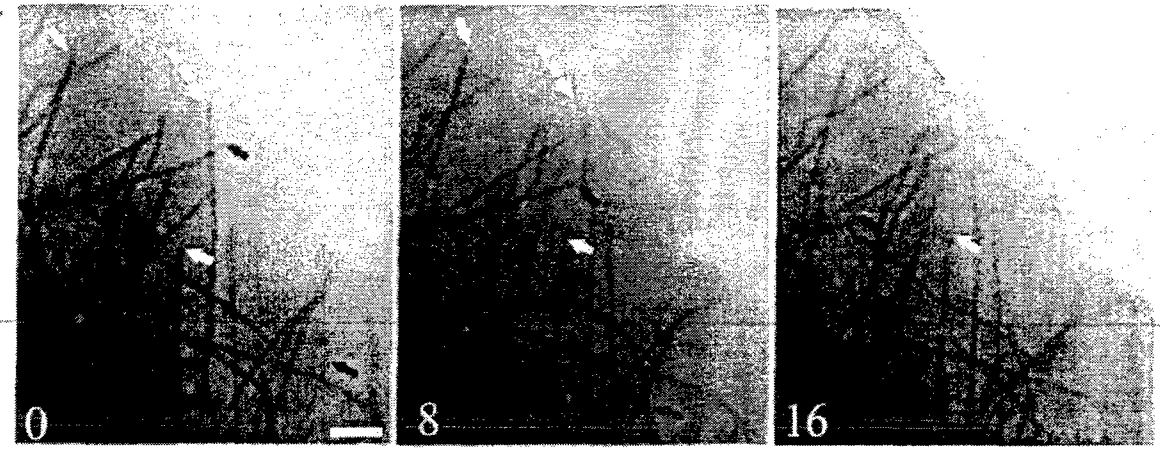
C.


Control
LNF 10 μM
LNF 20 μM
PTX 2 nM

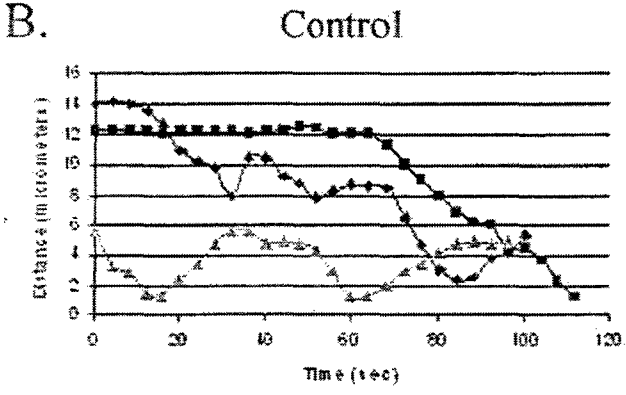
D.

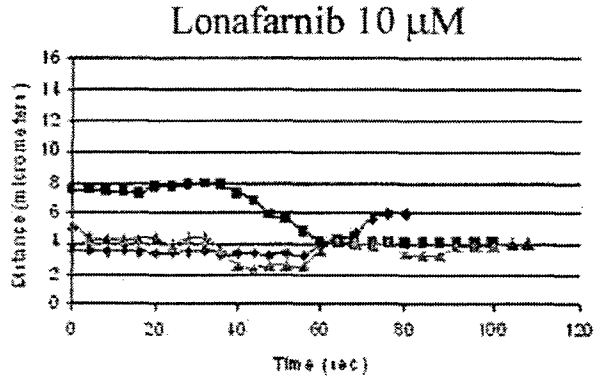

Lonafarnib
PTX
Control
5 μM
10 μM
20 μM
5 nM
α-tubulin
acetylated-tubulin
P S P S P S P S P S
%P α-tubulin 0% 25% 30% 60% 80%
%P acetylated-tubulin 0% 55% 70% 80% 85%

A.

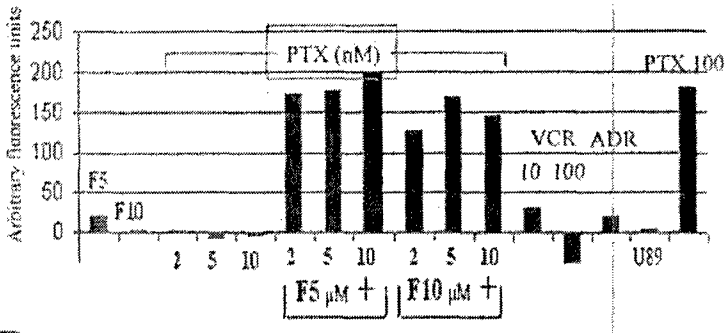

0
8
16

B.


Control
Distance (micrometers)
Time (sec)

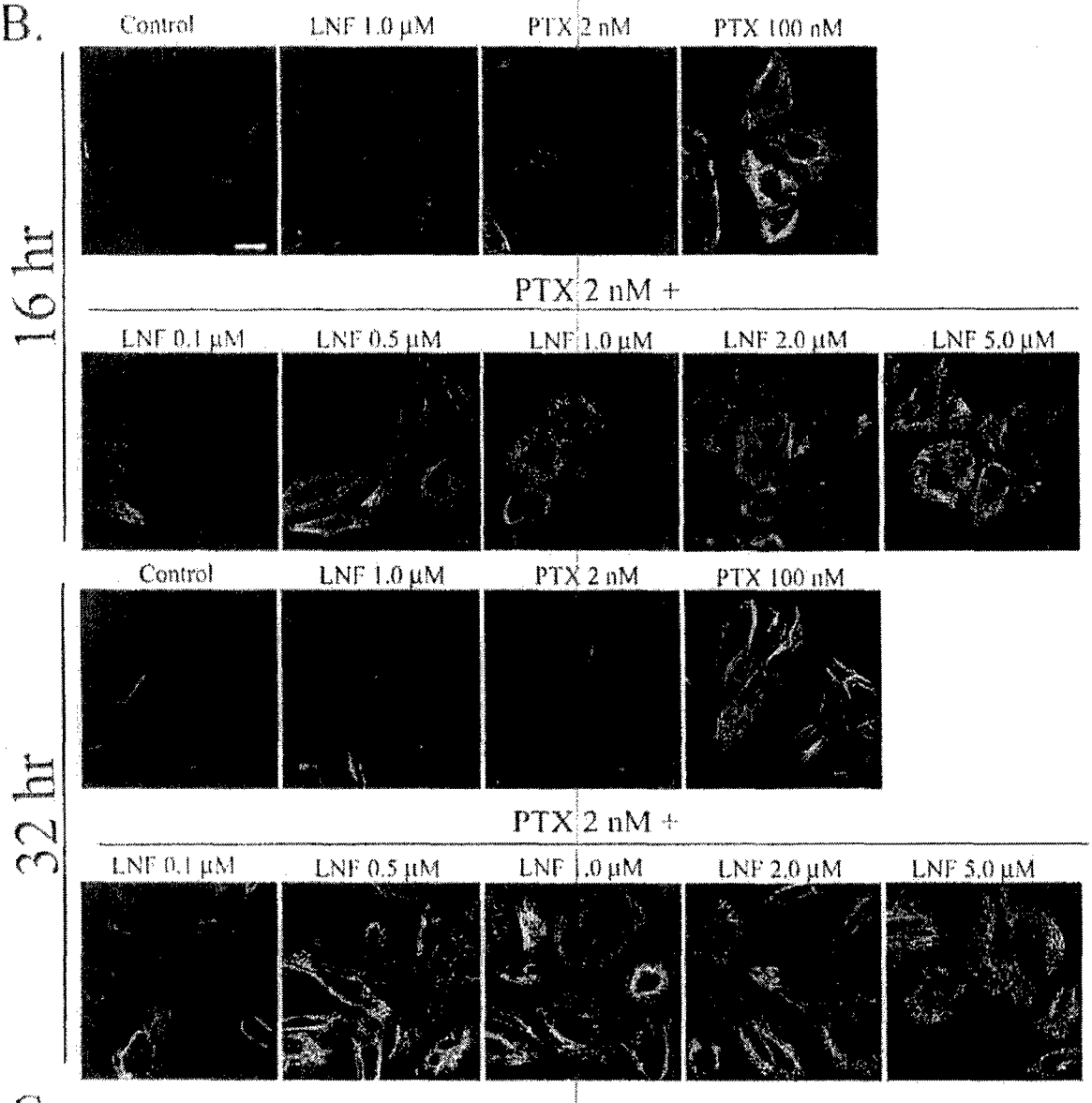

Lonafarnib 10 µM
Distance (micrometers)
Time (sec)

A.

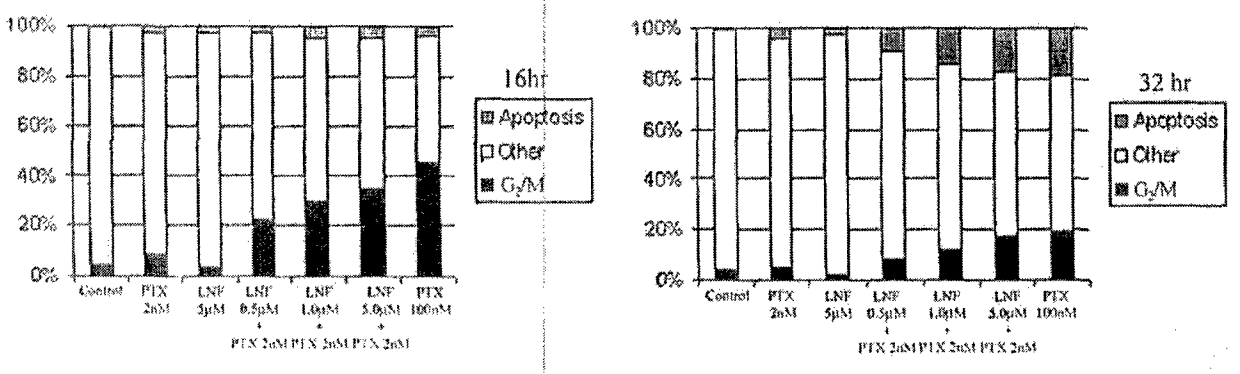


Sample	Drug
1	FTI 5 μM
2	FTI 10 μM
3	PTX 2 nM
4	PTX 5 nM
5	PTX 10 nM
6	FTI 5 μM + PTX 2 nM
7	FTI 5 μM + PTX 5 nM
8	FTI 5 μM + PTX 10 nM
9	FTI 10 μM + PTX 2 nM
10	FTI 10 μM + PTX 5 nM
11	FTI 10 μM + PTX 10 nM
12	VCR 10 nM
13	VCR 100 nM
14	ADR 400 ng/ml
15	U89
16	PTX 100 nM

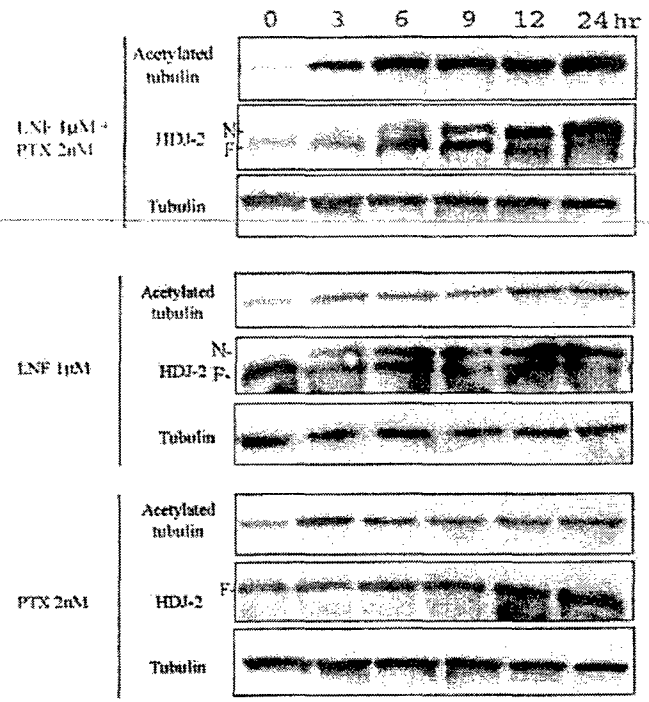
B.



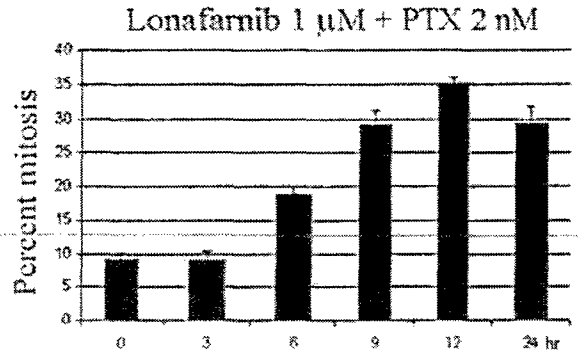
C.

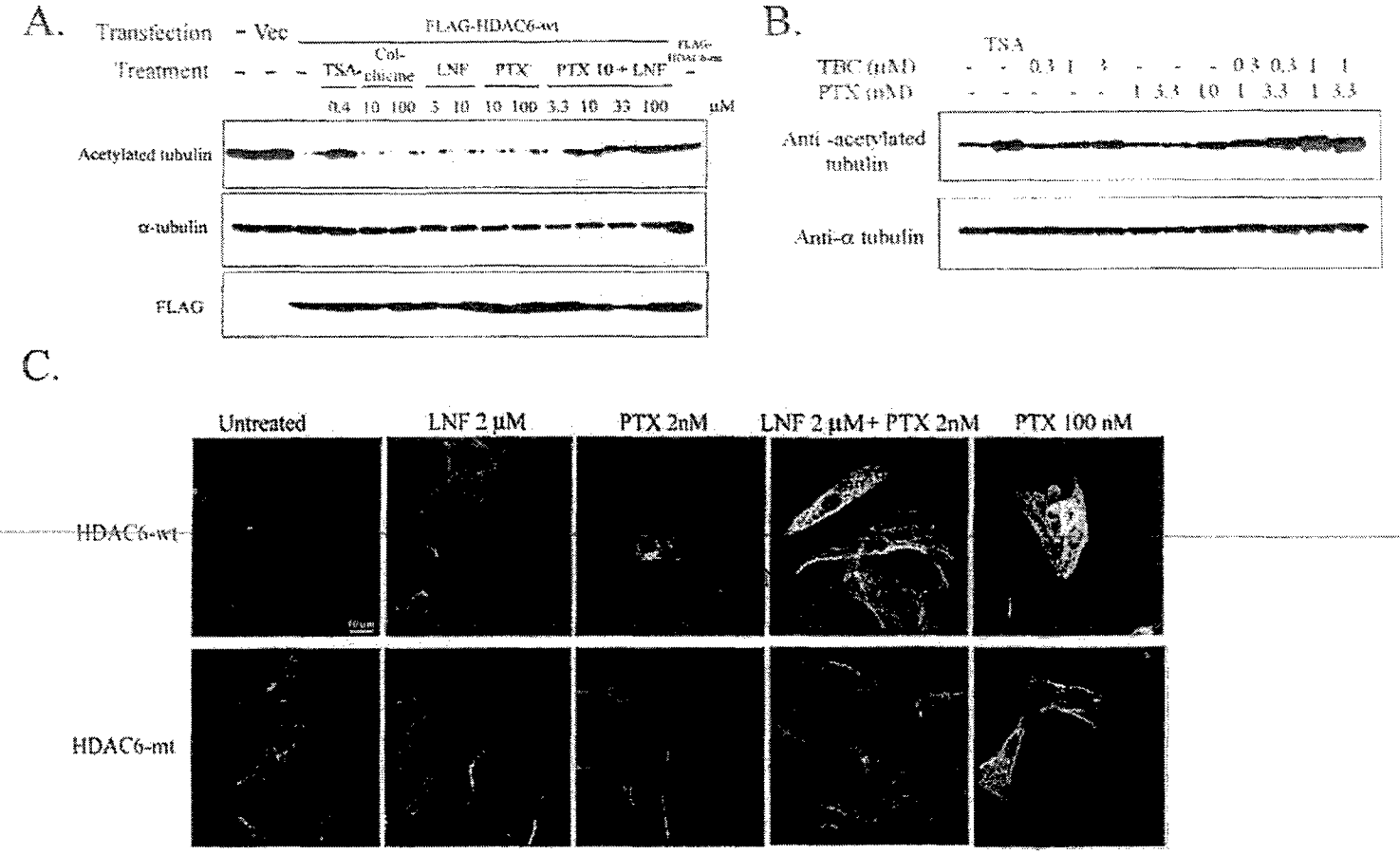


A.


0 3 6 9 12 24 hr
LNF 1μM + PTX 2nM
Acetylated tubulin
HDJ-2 N- F-
Tubulin
LNF 1μM
Acetylated tubulin
HDJ-2 N- F-
Tubulin
PTX 2nM
Acetylated tubulin
HDJ-2 F-
Tubulin

B.


Lonafarnib 1 μM + PTX 2 nM
Percent mitosis
40
35
30
25
20
15
10
5
0
0
3
6
9
12
24 hr


A.
Transfection
- Vec
FLAG-HDAC6-wt
Treatment
TSA
Col-chicine
LNF
PTX
PTX 10 + LNF
0.4 10 100 5 10 10 100 3.3 10 33 100 μM
Acetylated tubulin
α-tubulin
FLAG
B.
TSA
TBC (nM)
PTX (nM)
Anti -acetylated tubulin
Anti-α tubulin
C.
Untreated
LNF 2 μM
PTX 2nM
LNF 2 μM + PTX 2nM
PTX 100 nM
HDAC6-wt
HDAC6-mt
D.
LNF + Taxotere
Combination Index
3.5
3
2.5
2
1.5
1
0.5
0
Antagonism
Synergy
HDAC6-wt
HDAC6-mut
E.
Control
TSA 0.4
LNF 10
DTX 10
DTX + LNF
Acetylated α-Tubulin
α-Tubulin
HDAC6